Water Technology and Sciences

• Mexican Index of Scientific and Technological Research Journals, Consejo Nacional de Ciencia y Tecnología (Conacyt)

Included in Thomson Reuters Science Citation Index® (ISI) • Expanded Thomson Reuters Research Alert® (ISI) • EBSCO • ProQuest • Elsevier • Redalyc

Vol. VII, No. 1, January-February, 2016

Water Technology and Sciences

Edit Board

Editorial coordination and careful editing: Helena Rivas- López • **Editorial assistance and editorial layout**: Luisa Guadalupe Ramírez-Martínez • **Figures design**: Luisa Guadalupe Ramírez-Martínez and Rosario Castro-Rivera • **Coordination arbitration**: Elizabeth Peña and Bibiana Bahena • **Proofreading English**: Ellen Weiss • **Logo design and cover**: Oscar Alonso-Barrón • **Design format**: Gema Alín Martínez-Ocampo • **Marketing**: Carlos Ramón Peña Montiel.

Editorial Committee

©***Water Technology and Sciences.*** Vol. VII, No. 1, January-February, 2016, is a bimonthly publication edited by the Instituto Mexicano de Tecnología del Agua, Paseo Cuauhnáhuac 8532, Colonia Progreso, Jiutepec, Morelos, C.P. 62550, telephone +52 (777) 3 29 36 00, extension 474, www.imta.gob.mx/tyca, fsalinas@tlaloc.imta.mx. Responsible editor, Nahún Hamed García Villanueva; Copyright No. 04-2013-121014514100-203, granted by the Instituto Nacional de Derechos de Autor. ISSN pending. Responsible for the latest update of this issue: Sub-Department of Dissemination and Circulation, Francisco José Salinas Estrada, Paseo Cuauhnáhuac 8532, Colonia Progreso, Jiutepec, Morelos, C.P. 62550.

Water Technology and Sciences is the traslation of *Tecnología y Ciencias del Agua*, which is the continuation of the following journals: *Irrigación en México* (1930-1946); *Ingeniería hidráulica en México* (1947-1971); *Recursos hidráulicos* (1972-1978), and *Ingeniería hidráulica en México*, second period (1985-2009).

Water Technology and Sciences

Vol. VII, No. 1, January-February, 2016

For subscriptions, click here

Coordination for editorial comments, click here give

Cover: sunset in the brook La Azotea, system of the river Paraná, province of Entre Ríos, Argentina. The photograph was taken in the Pre-Delta National Park and can be observed some plants of *Eichhornia crassipes* (camalote or hyacinth of water), a species of floating free macrophyte characteristic of these environments. Due to the ability to accumulate contaminants in their tissues, the wetland plants of the Parana River system are used in wetlands built for effluent treatment. See the article "Wetlands built for treatment of effluents from the metallurgical industries in Santa Fe, Argentina" by María Alejandra Maine *et al*. (pp. 5-16).

Photo: Hernán R. Hadad.

Waterfall of the Chorillos, Province of Cordoba, Argentina (2014).

Photo: Antoine Patalano.

Contents

Technical articles

Contenido

Artículos técnicos

Constructed Wetlands to Treat Effluents from Metallurgy Industries in Santa Fe, Argentina

• María Alejandra Maine* •
Universidad Nacional del Litoral, Argentina
Consejo Nacional de Investigaciones Científicas y Técnicas, Argentina
*Autor de correspondencia

• Gabriela Cristina Sánchez •
Universidad Nacional del Litoral, Argentina

• Hernán Ricardo Hadad •
Universidad Nacional del Litoral
Consejo Nacional de Investigaciones Científicas y Técnicas, Argentina

• Sandra Ester Caffaratti •María del Carmen Pedro •
Universidad Nacional del Litoral, Argentina

• Gisela Alfonsina Di Luca • María de las Mercedes Mufarrege •
Consejo Nacional de Investigaciones Científicas y Técnicas, Argentina

Abstract

Maine, M. A., Sánchez, G. C., Hadad, H. R., Caffaratti, S. E., Pedro, M. C., Di Luca, G. A., & Mufarrege, M. M. (January-February, 2016). Constructed Wetlands to Treat Effluents from Metallurgy Industries in Santa Fe, Argentina. *Water Technology and Sciences* (in Spanish), 7(1), 5-16.

The use of constructed wetlands in Argentina to treat effluents is still limited, even though ideal conditions exist for their implementation (large availability of low-cost marginal land, temperate climate with mild winters and large availability of macrophytes that are adapted to the climate). The objective of this work was to evaluate the efficiency of two constructed wetlands (CW1 and CW2) to treat effluents from metallurgy industries and determine whether the sediments or plants retain the pollutants. This knowledge is key to correctly managing the wetland. Both wetlands treated sewage along with industrial waste containing metals. Since the volumes to be treated and the chemical composition of the effluents were different, the constructed wetlands presented distinct design characteristics. CW1 has been in operation for 12 years and CW2 for 5 years. Both function efficiently, with satisfactory removal efficiencies for SRP, total phosphorus, nitrogen species, COD, BOD, sulfate and metals. Typha domingensis (cattail), the dominant species in both cases, had a high capacity to retain metals, especially by its root zone, which demonstrates its phytostabilization capacity. The concentration of metals and phosphorus increased in the sediment in the inlet area, in chemically stable fractions which are not released into the water if the environmental conditions are maintained. Typha domingensis detritus accumulated high concentrations of metals and can be easily removed for final disposal.

Keywords: Effluents, depuration, metals, sediment, macrophytes, wetlands, Argentina.

Resumen

Maine, M. A., Sánchez, G. C., Hadad, H. R., Caffaratti, S. E., Pedro, M. C., Di Luca, G. A., & Mufarrege, M. M. (enero-febrero, 2016). Humedales construidos para tratamiento de efluentes de industrias metalúrgicas en Santa Fe, Argentina. Tecnología y Ciencias del Agua, *7(1), 5-16.*

En Argentina, el uso de humedales construidos para tratamiento de efluentes es aún limitado, a pesar de que las condiciones para su implementación son ideales (gran disponibilidad de terrenos marginales de bajo costo, clima templado con inviernos poco rigurosos y gran disponibilidad de macrófitas adaptadas al clima). El objetivo de este trabajo fue evaluar la eficiencia de dos humedales construidos (HC1 y HC2) para el tratamiento de efluentes de industrias metalúrgicas y determinar si los contaminantes son retenidos por el sedimento o por la plantas, conocimientos clave para llevar a cabo un correcto manejo del humedal. En ambos humedales se trata el efluente cloacal junto con el industrial que contiene metales. Como los volúmenes a tratar y la composición química de los efluentes es diferente, los humedales construidos presentan distintas características de diseño. HC1 está en operación desde hace 12 años y HC2 desde hace cinco años. Ambos humedales funcionaron de manera eficiente, mostrando eficiencias de remoción satisfactorias para PRS, P total, especies nitrogenadas, DQO, DBO, sulfato, y metales. Typha domingensis (totora), especie dominante en ambos casos, presentó alta capacidad de retención de metales, en especial en su zona radicular, lo que demuestra su capacidad de fitoestabilización. Las concentraciones de metales y P aumentaron en el sedimento de la zona de entrada en fracciones químicamente estables, que no los liberarán al agua si se mantienen las condiciones ambientales. Los detritos de Typha domingensis acumularon altas concentraciones de metales. Estos detritos pueden ser removidos con facilidad para su disposición final.

Palabras clave: *efluentes, depuración, metales, sedimento, macrófitas, humedales, Argentina.*

Received: 08/04/2015
Accepted: 18/08/2015

Introduction

Natural wetlands have been used as wastewater receptors since long ago. In the 20th century, humans constructed wetlands that were designed to optimize processes that are naturally produced in the wetlands' vegetation, sediments and substrate, as well as the associated microorganisms. The purpose was to improve the system's efficiency for purifying water. This technology began to be implemented in the 1970s and, given its efficiency and low installation and maintenance cost, its use has increased since then. While constructed wetlands have been the subject of many studies (Maine, Suñé, Hadad, Sánchez, & Bonetto, 2006, 2007; Maine, Hadad, Sánchez, Caffaratti,& Bonetto, 2009; Kadlec & Wallace, 2009; Vymazal, 2011; Zhang *et al*., 2014), most of the investigations have been related to the treatment of household effluents from small communities, single family homes and hotels, as well as runoff, in which the pollutants to be eliminated are phosphorous (P) and nitrogen (N). Hundreds of these wetlands are functioning, particularly in countries such as Germany, France, the United Kingdom, Spain, Italy, Denmark, Australia and the United States. In Latin America, countries such as Mexico, Colombia, Peru and Bolivia have widely implemented this technology to treat sanitary effluents from small towns, resort complexes, university campuses, etc. (García, Paredes, & Cubillos, 2013; Rivas-Hernández, Barceló-Quintal, & Moeller-Chávez, 2014). In Argentina, the use of constructed wetlands to treat effluents is still limited, even though the conditions for its implementation are ideal (large availability of marginal, low-cost land, temperate climate with mild winters and macrophytes that have adapted to the climate).

According to experiences by various specialists, which were presented at the recent international conferences on constructed wetlands, companies in Argentina and other countries in Latin America are working in the area of constructed wetlands without the necessary prior studies or posterior monitoring to control and optimize the systems. This results in the inadequate functioning of the systems or their being taken out of operation, contributing to the idea that this technology is inefficient. Therefore, it is important to conduct prior studies that are specific to each case and monitor the systems over time, not only to understand the purification mechanisms but also to optimize the functioning of the system.

Wetlands also function efficiently when treating industrial wastes (Dunbabin & Bowmer, 1992; Chen, Kao, Yeh, Chien, & Chao, 2006; Khan, Ahmad, Shah, Rehman, & Khaliq, 2009; Kadlec & Wallace, 2009). Two metallurgy industries in the study zone use constructed wetlands as final treatment for their effluents. Since the volumes that are treated and their chemical compositions are different, the constructed wetlands have different design characteristics. The objective of this work was to compare the efficiency of two constructed wetlands (CW1 and CW2) and determine whether the pollutants were retained by the sediment or by the plants, knowledge which is key to correctly managing the wetlands.

Methodology

Description of the Wetlands

The two wetlands studied had superficial flow. They were built as final treatment for effluents from two metallurgy industries. Both CW1 and CW2 treated combined sanitary and industrial waste from industries. Before entering the wetlands, both effluents received primary treatment. Since studies of greenhouses have corroborated the hypothesis that enriching the effluent with nutrients may improve the plants' tolerance to metals (Hadad, Maine, Natale, & Bonetto, 2007), it was decided to treat the sanitary and industrial wastes together, for both industries.

CW1 has been operating for 12 years. It is 50 m long by 40 m wide with a depth of 0.3 – 0.6 m. A center brick divider forces the effluent to flow twice the distance to obtain a length:width ration of 5:1, which is favorable to the hydraulics of the system. It was sealed with six layers of compact bentonite (reaching a hydraulic conductivity of 10-7 m/s). One meter of earth was placed on top, where the plants were rooted. Various species common to the zone were initially transplanted, of which *Eichhornia crassipes* and *Typha domingensis* had the largest coverage. A total of 100 000 l/day were treated (industrial effluent with a high pH and salinity, and containing Fe, Cr, Ni and Zn along with the sanitary effluent). The residence time was between 7 and 12 days. After passing through the wetland, the effluent followed a canal to a 1.5 ha lagoon located on the same property (Figure 1).

CW2 has been operating for 5 years. It is 7 m x 20 m (a length:width ratio of 3:1) with a depth of 0.5 m. It was sealed with a 1.5 mm thick high-density polyethylene (HDP) geomembrane. A 1.50 m layer of earth was placed on top of this which served as a substrate for the rooting of the plants. Based on the experience with CW1, *Typha domingensis* was the species selected for this wetland. Plants growing in the lagoon located on the company's property were transplanted to ensure the adaptation of the plants to the location. They were cut to an approximate height of 30 cm, preserving the rhizomes, and were planted at a density of 3 per m^2. To aid the development of the plants in the deepest zone and increase the flow of the effluent through the wetland, 0.5 m-wide slopes were built transverse to the direction of the water flow, on which the vegetation was planted. The water level above the plants was 0.30 to 0.40 m. In other zones, the depth was between 0.5 and 0.7 m. The wetland was operated with sanitary waste (previously subject to primary treatment), pluvial effluent and effluent from the cooling circuit for one year. The industrial waste (from chrome plating) began to be added later and both the industrial and sanitary wastes underwent primary treatment. These flowed together, along with the cooling circuit and pluvial effluents, into an equalizing chamber, after which it entered the lagoon. The daily volume that entered the wetland was roughly 10 m^3. The minimum residence time was 7 days, after which the purified effluent exited the wetland through an outlet canal, dropping in a waterfall into a 4 m x 2m concrete basin

Figure 1. Satellite photography of constructed wetland 1 (CW1), the lagoon (a) and the company's facilities (b).

with a depth of 40 cm. The treated effluent samples were taken at this point to monitor the system. The treated effluent then exited the basin through an overflow waterfall and entered a canal in an adjacent lagoon on the same property (Figure 2).

Sampling and Analytical Determinations

Samples were collected monthly of the effluent, sediments and vegetation in the inlet and outlet areas of both constructed wetlands.

The analytical determinations of the water were performed according to APHA (1998). The conductivity of the water was measured with a YSI conductivity meter, model 33, and pH with an Orion pH meter. Dissolved oxygen (DO) was measured using a Hanna HI 91-46 oxygen meter and total phosphorous(TP), soluble reactive phosphorous (SRP) and nitrites were determined using colorimetric techniques with a Perkin Elmer Lambda 20 UV-VIS spectrophotometer. Nitrate and ammonium concentrations in the water were estimated using potentiometry, with an Orion Ion plus 93-07 and Orion 9512 BN electrode, respectively. Chemical oxygen demand (COD) was determined with the open reflux method and biological oxygen demand (BOD) with the 5-day test. Alkalinity and hardness were determined using titration and sulfate was estimated by turbidimetry. The determinations of Fe, Cr, Ni and Zn in water were performed with atomic absorption spectrophotometry (flame or electrothermal atomization depending on the concentration of the sample, Perkin Elmer AAnalyst 200). The concentrations of phosphorus (P) and the metals chrome (Cr), nickel (Ni) and zinc (Zn) were determined in sediments and macrophytes (leaves and roots) using atomic absorption spectrophotometry after digestion with an acid mixture of $HCl:HNO_3:HClO_4$ (5:3:2). TP was determined with these same digestions using the Murphy and Riley (1962) colorimetric technique. To evaluate the quantities and chemical forms in which these pollutants accumulated in the sediment, chemical fractionation of Cr, Ni and Zn was also performed with the Tessier, Campbell and Bisson (1979) method. This method uses successive sequential extractions with acidic, alkaline or complexing solutions in order to dissolve the salts and oxides and extract their corresponding metals.

A paired t-test was used to verify whether a statistical difference existed between the concentrations at the inlet and outlet of the wetland ($p < 0.05$).

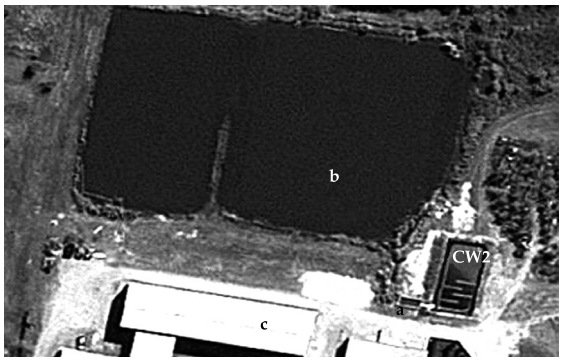

Figure 2. Satellite photography of constructed wetland 2 (CW2), the outlet basin (a), the lagoon (b) and the company's facilities (c).

Results and Discussion

Figure 3a shows the coverage of the macrophytes in CW1 since it began operating. As can be seen, *Eichhornia crassipes* quickly developed and was dominant, covering roughly 80% of the water surface after 2 years, but the coverage began to decrease thereafter. In October 2005, the water level in the wetland fell and sediment slopes were added perpendicular to the flow direction to aid the development of the rooted *Typha domingensis species*. Coverage then increased and this species became dominant over the last 10 years, with a mean coverage of 80%. Reductions in its coverage were due to periodic

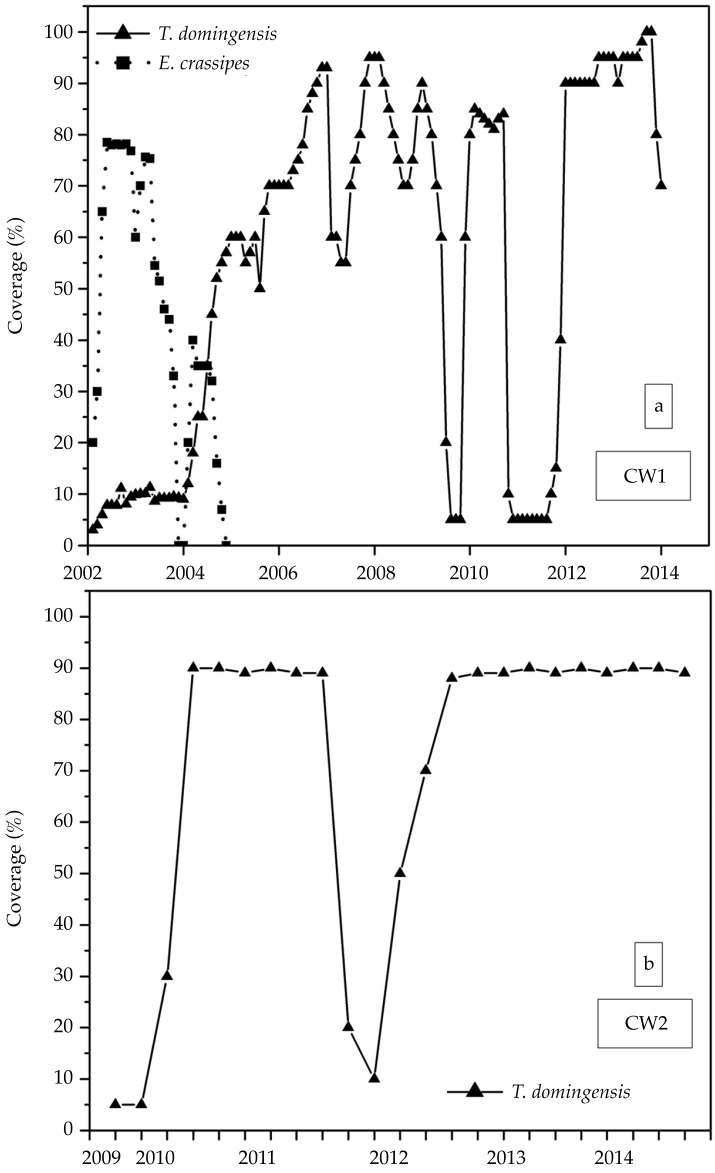

Figure 3. Vegetation coverage registered over the study period in CW1 (a) and CW2 (b).

trimming to contribute to its growth. During the years 2009 and 2011, a notable decrease was seen in the coverage due to capybaras (Hydrochoerus hydrochaeris) which fed on the plants. The wetland came to resemble a lagoon with little vegetation because of the destruction of the aerial portion of the vegetation by the animals. Nevertheless, the roots and rhizomes of the emergent plants were not damaged (Maine *et al.*, 2013) and the plants recovered after erecting a fence around the perimeter to prevent the animals from entering the wetland.

Figure 3b shows the coverage of *Typha domingensis* in CW2, which reached 90% after a few months. A decrease in coverage was seen during the first months of 2012 due to the accidental spilling of effluent that was

not properly treated. Nevertheless, a rapid recuperation in the plants was registered. It is worth noting that the environment was preserved because the pollutants were retained in the wetland, which fulfilled one of the functions for which it was built. As was mentioned, decreases in plant coverage occurred in both constructed wetlands because of different events, but they were able to recover, demonstrating the robustness of these systems.

Both wetlands functioned efficiently, presenting high percentages of pollutant removal, with a decrease not only in mean values but also in variability, in spite of the high heterogeneity of the effluent at the inlet (Tables 1 and 2). Even though the pH of the two effluents were different at the inlets, the values at the outlets were not significantly different. The effluent in CW1 had lower DO and higher conductivity than CW2. Concentrations of nitrate and nitrite satisfactorily decreased in HC1, while ammonium, SRP and TP presented low removal percentages, probably due to low DO concentrations. The aerobic conditions favored the retention of P in the sediments. In terms of ammonium, the low oxygen concentrations were not favorable to nitrification. In CW2, ammonium had the highest removal percentage, and nitrite increased at the outlet of the wetland due to the nitrification process which occurs under aerobic conditions. Nevertheless, it is worth highlighting that the nitrite concentrations measured were low and within the values required by current legislation (Law 11220/94,

Table 1. Mean concentrations of the parameters measured in the effluent at the inlet and outlet of CW1. (*) indicates statistically significant differences between the value of the parameter measured before and after it flowed through the wetland.

Parameters	Inlet		Outlet		Removal %
	Mean	Range	Mean	Range	
pH	10.8	10.4-11.5	8.3*	7.9-9.3	-
Temperature	19.5	14-23.9	17.6	12.5-23	-
DO (mg l^{-1})	3.40	0-6.2	2.12*	0.3-5.2	-
Conductivity (umho/cm)	5 113.3	3 890-7 700	1 955.6*	1 400-2 500	-
Hardness (mg $CaCO_3$ l^{-1})	219.6	92.3-305.2	81.3*	51.1-101.2	61.7
Alkalinity	553.2	114.6-750.4	224.1*	156.8-332.3	36.5
SO_4^{2-} (mg l^{-1})	1 872.9	991.4-2 316.1	626.4*	412.1-884.1	66.5
NO_3^- (mg l^{-1})	50.6	15.4-98.2	9.9*	3.6-24.2	80.4
NO_2^- (mg l^{-1})	2.221	0.258-6.22	0.352*	0.017-0.766	84.1
NH_4^+ (mg l^{-1})	0.88	0.154-2.67	0.77*	0.05-2.14	11.8
PRS (mg l^{-1})	0.030	0.005-0.079	0.026	0.005-0.334	13.3
PT (mg l^{-1})	0.396	0.064-1.38	0.309	0.129-0.696	22.0
Fe (mg l^{-1})	0.824	0.05-2.54	0.087*	0.05-0.230	89.4
Cr (mg l^{-1})	0.092	0.023-0.204	0.014*	0.002-0.033	84. 7
Zn (mg l^{-1})	0.041	0.022-0.070	0.020*	0.015-0.050	51.2
Ni (mg l^{-1})	0.048	0.004-0.101	0.023*	0.004-0.082	69.5
COD (mg l^{-1})	85.0	27.9-154.0	37.1*	13.9-42.9	74.6
BOD (mg l^{-1})	31.3	9.8-30.9	9.97*	3.0-20.1	73.2

Cuadro 2. Concentraciones medias de los parámetros medidos en el efluente de entrada y salida del HC2. (*) indica diferencia estadísticamente significativa entre el valor del parámetro medido antes y después de atravesar el humedal.

Parameters	Inlet		Outlet		Removal %
	Mean	Range	Mean	Range	
pH	7.9	7.4-8.3	8.0	8.0-8.1	-
Temperature	22	19-23	16	15-18	-
Oxygen (mg l^{-1})	6.0	3.2-7.4	6.4	4.2-7.8	-
Conductivity (umho/cm)	3 213.0	975-10 060	1 203.6*	1 058-1 358	-
Hardness (mg $CaCO_3$ l^{-1})	90.5	76.8-120.0	65.2*	48-88.8	36.9
Alkalinity	690.0	101.7-1 647.0	283.0*	167.9-378.2	63.2
SO_4^{2-} (mg l^{-1})	1 428.8	56.3-2 781	133.7*	75.3-181.3	90.6
NO_3^- (mg l^{-1})	0.745	0.271-1.28	0.564*	0.158-1.084	24.4
NO_2^- (mg l^{-1})	0.012	0.004-0.023	0.040*	0.030-0.053	-
NH_4^+ (mg l^{-1})	6.15	0.957-15.6	2.08*	0.722-3.89	66.1
PRS (mg l^{-1})	0.692	0.247-0.903	0.307*	0.291-0.350	58.1
PT (mg l^{-1})	0.889	0.642-1.322	0.425*	0.398-0.442	52.8
Fe (mg l^{-1})	0.350	0.151-0.561	0.110*	0.061-0.173	70.4
Cr (mg l^{-1})	0.310	0.012-1.45	0.022*	0.019-0.025	92.9
Zn (mg l^{-1})	0.072	0.006-0.145	0.031*	0.003-0.067	51.7
Ni (mg l^{-1})	0.018	0.003-0.082	0.004*	0.004-0.004	77.5
COD (mg l^{-1})	57.1	21.3-160	12.4*	< 6-27	78.2
BOD (mg l^{-1})	45.3	10.2-55.5	8.6*	3.2- 17.6	82.5

Resolution 1089, Province of Santa Fe, Argentina). In general, ammonium is removed from aquatic systems through sedimentation, nitrification, absorption by plants or volatilization. The decrease in NO_3^- is primarily due to the process of denitrification and absorption by plants (Saunders & Kalff, 2001). This process requires energy, which is obtained from the oxidation of the organic matter present in the anaerobic zones of the sediment. The macrophytes can improve the denitrification conditions since they supply organic C which can be directly used by denitrification bacteria, or can indirectly stimulate denitrification, contributing to decreasing the redox potential (Weisner, Eriksson, Granéli, & Leonardson, 1994). The COD and BOD values were significantly lower at the wetland's outlet than at its inlet. A large reduction in sulfate was also observed, which is used in primary treatment and therefore enters the wetlands in high concentrations. The concentrations of Cr and Zn in the effluent at the inlets were significantly higher in CW2, and Fe and Ni were higher in CW1. The removal of these metals was satisfactory in both of the wetlands.

Typha domingensis was efficient for retaining metals, especially in the root zones, which demonstrates its phytostabilization capacity (Table 3). This is a desirable condition in which the metals become immobilized in the wetlands' sediments. In both wetlands, the metal and P concentrations in the tissue were significantly higher in the plants located in the inlet areas than those at the outlets, since the effluent becomes more purified as it circulates.

Table 3. Concentrations of P, Cr, Ni and Z in the tissue of Typha domingensis. (*) indicates statistically significant differences between the concentrations in the vegetation tissue at the inlet and outlet areas.

CW1								
Sample	Cr (mg g^{-1})		Ni (mg g^{-1})		Zn (mg g^{-1})		P (mg g^{-1})	
	Leaves	Roots	Leaves	Roots	Leaves	Roots	Leaves	Roots
Inlet area	0.023*	0.356*	0.014*	0.199*	0.034	0.090	2.24*	1.84*
Outlet area	0.010	0.034	0.006	0.030	0.035	0.086	1.16	1.02
CW2								
Sample	Cr (mg g^{-1})		Ni (mg g^{-1})		Zn (mg g^{-1})		P (mg g^{-1})	
	Leaves	Roots	Leaves	Roots	Leaves	Roots	Leaves	Roots
Inlet area	0.053*	0.764*	0.009	0.019	0.034*	0.199*	2.48*	1.87*
Outlet area	0.033	0.195	0.007	0.013	0.014	0.054	1.76	1.29
Detritos (*T. domingensis*)	2.29		0.013		0.206		1.09	

There was a high concentration of Cr in the roots of *Typha domingensis* at both the inlet and the outlet of CW2. This was due to a spill with high concentrations of Cr. Even though CW1 had been operating for a longer period of time, the Cr concentrations in the tissues were significantly lower.

The concentration of Ni in the tissue was higher in CW1 because of the presence of this metal in the effluent treated. The concentrations of Zn in the plants in the inlet of CW2 were higher than in CW1 because of a higher concentration of Zn in the effluent treated by CW2. It is important to mention that the bio-geochemical cycles of the sediments are affected by the accumulation of emergent macrophytes and pollutants in the tissues, due to effects on the redox potential, given its capacity to transport oxygen from the roots to the rhizosphere (Barko, Gunnison, & Carpenter, 1991; Sorrell & Boon, 1992). Quantitatively, this oxygenated layer can be seen by the red color associated with oxidized forms of iron on the surface of the roots and the surrounding sediment.

Typha domingensis detritus accumulated in the inlet area of CW2, where high concentrations of retained metals were found. These detritus were primarily composed of dry leaves that remained after winter, which is part of the annual cycle of the macrophytes. The macrophytes do not only absorb pollutants when they are alive. At the laboratory scale, Schneider and Rubio (1999) demonstrated that dry biomass from three floating macrophytes (*Potamogeton lucens, Salvinia herzogii* and *Eichhornia crassipes*) were excellent bio-absorbers of heavy metals. Miretzky, Saralegui and Fernandez-Cirelli (2006) reported similar results when they worked with dead biomass from *Spirodela intermedia*, *Lemna minor* and *Pistia stratiotes* with a multi-metal solution (Cu^{2+}, Pb^{2+}, Cd^{2+}, Ni^{2+} and Zn^{2+}). This would be significantly beneficial to the management of constructed wetlands since the plants slowly decompose after they die and thus the metals continue to be retained in the wetland (Hammerly, Leguizamon, Maine, & Schiver, 1989), as has been experimentally determined. These detritus can be easily removed from the wetland for their final disposal, if necessary.

Although the plants retained metals in their tissue, most of the P and metals accumulated in the sediments, when considering not only the concentration but also mass. Sorption by sediments is the primary mechanism for the long-term accumulation of pollutants

(Machemer, Reynolds, Laudon, & Wildeman, 1993; Wood & Shelley, 1999; Maine *et al*., 2009). In both wetlands, the concentrations of Cr, Ni, Zn and P in the sediments near the inlets were significantly greater than in the sediments near the outlets (Table 4).

The concentrations near the outlets were not significantly different than those measured at the beginning of the study, which would indicate that the pollutants were retained by the sediments in the inlet area. The concentrations of Cr in the sediments in the inlet areas of the two wetlands were not significantly different, in spite of the different lengths of time they had been operating. Ni accumulated near the inlet of CW1, which was not observed in the sediments in CW2 given that the effluent did not contain Ni. In the case of Zn, CW1 had higher concentrations in the sediments near the inlet as well as the outlet. Nevertheless, the sediments can release the pollutants if the environmental conditions change (Boström, Ahlgren, & Bell, 1985). In order to determine the durability of the retention of pollutants in the wetlands' sediments, a sequential extraction was performed in order to evaluate which chemical compositions of the sediment retained the pollutants. In both wetlands, there was a significantly higher accumulation of Cr in the Fe-Mn oxide fraction and in organic matter (Table 5).

Organic matter can complex and adsorb cations because of the presence of negatively charged groups (Laveuf & Cornu, 2009). The low Eh reduced Cr(VI) to Cr(III), which precipitates as Cr(OH)n (mostly $Cr(OH)_3$) (Guo, Delaune, & Patrick, 1997) or co-precipitates with Fe and Mn oxides. The low concentrations of Ni in different fractions of the sediments in CW2 corroborates the low concentrations of this metal in the effluent, indicating that it did not accumulate in the sediment.

The accumulation of Ni in CW1 was significantly higher when bonded to carbonate and Fe-Mn oxides and in the residual fraction, as was the case for Zn in both wetlands.

Table 4. Concentrations of P, Cr, Ni and Zn in sediments at the end of the study period. (*) indicates statistically significant differences between concentrations in the sediment with respect to initial values.

Sample	CW1				CW2			
	Cr (mg g^{-1})	Ni (mg g^{-1})	Zn (mg g^{-1})	P (mg g^{-1})	Cr (mg g^{-1})	Ni (mg g^{-1})	Zn (mg g^{-1})	P (mg g^{-1})
Inlet area	0.811*	0.453*	0.096*	0.896*	0.865*	0.017	0.056*	0.496*
Outlet area	0.057	0.060	0.063	0.379	0.026	0.011	0.025	0.388
Initial	0.038	0.028	0.060	0.378	0.016	0.011	0.024	0.392

Table 5. Cr, Ni and Zn fractionation performed in sedmients at the end of the study period in CW1 and CW2.

Fraction		Exchangeable	Carbonate bonding	Fe-Mn oxide bonding	organic matter bonding	Residual
Cr	CW1	**0.003**	**0.034**	**0.285**	**0.280**	**0.209**
	CW2	0.008	0.024	0.509	0.314	0.011
Ni	CW1	**0.032**	**0.134**	**0.120**	**0.072**	**0.117**
	CW2	0.0004	0.004	0.004	0.005	0.003
Zn	CW1	**0.002**	**0.039**	**0.022**	**0.011**	**0.022**
	CW2	0.001	0.014	0.018	0.004	0.019

The precipitation of carbonate is favored by thermodynamics, and Ni and Zn can co-precipitate with it. Fe-Mn oxides represent heavy metal sinks. The residual fraction indicates lithogenic forms of strong bonds with metals, such as with clay crystalline structures (Di Luca *et al.*, 2011).

The extraction sequence can be seen as an inverse scale of the relative availability of the metals. The concentrations of the exchangeable fraction of the three metals, which is the most labile and bio-available, were significantly lower than the other concentrations, in all cases. In addition, it is very unlikely that the metals from the other two more labile fractions (bonded with carbonates and with Fe-Mn oxides) would be released into the water, since the effluents provide the conditions (high pH, alkalinity, Fe, Ca and ionic concentrations) for the sediment to continue retaining Cr, Ni and Zn.

Conclusions

In both constructed wetlands, the pollutant removal efficiencies were satisfactory since the wetlands decreased not only the mean value—which enabled complying with law 11220/94 of the Province of Santa Fe, Argentina— but also the variability in the concentration of the pollutants in the effluents, regardless o9f the high heterogeneity of the influent in the inlets.

The metals and P were efficiently removed in both wetlands, with retention in both the sediments and the vegetation tissues located in the inlet areas.

Typha domingensis was tolerant to the effluents and efficiently retained the metals.

Typha domingensis detritus accumulated high concentrations of metals. These detritus can be easily removed for final disposal.

The wetlands studied would be highly efficient for retaining the three metals, since they bond to fractions that are not released into the water, as long as the chemical and environmental conditions of the system are maintained.

Acknowledgements

The authors thank the National Council for Scientific and Technical Investigations ((Conicet), Consejo Nacional de Investigaciones Científicas y Técnicas), the CAI+D Project of the National Litoral University (Universidad Nacional del Litoral (UNL)) and the Agency for the Promotion of Science and Technology (Agencia de Promoción Científica y Tecnológica) for providing the funds needed to perform this work.

References

APHA (1998). *Standard Methods for the Examination of Water and Wastewater* (pp. 1268). New York: American Public Health Association/American Water Works Association/Water Environment Federation.

Barko, J. W., Gunnison, D., & Carpenter, S. R. (1991). Sediment Interactions with Submersed Macrophyte Growth and Community Dynamics. *Aquat. Bot.*, *41*, 41-65.

Boström, B., Ahlgren, L., & Bell, R. (1985). Internal Nutrient Loading in a Eutrophic Lake, Reflected in Seasonal Variations of Some Sediment Parameters. *Verhandlungen*, *44*(22), 3335-3339.

Chen, T. Y., Kao, C. M., Yeh, T. Y., Chien, H. Y., & Chao, A. C. (2006). Application of a Constructed Wetland for Industrial Wastewater Treatment: A Pilot-Scale Study. *Chemosphere*, *64*, 497-502.

Di Luca, G. A., Maine, M. A., Mufarrege, M. M., Hadad, H. R., Sánchez, G. C., & Bonetto, C. A. (2011). Metal Retention and Distribution in the Sediment of a Constructed Wetland for Industrial Wastewater Treatment. *Ecol. Eng.*, *37*, 1267-1275.

Dunbabin, J., & Bowmer, K. (1992). Potential Use of Constructed Wetlands for Treatment of Industrial Wastewaters. *Containing Metals. Sci. Tot. Environ.*, *111*, 151-168.

García, J. A., Paredes, D., & Cubillos, J. A. (2013). Effect of Plants and the Combination of Wetland Treatment Type Systems on Pathogen Removal in Tropical Climate Conditions. *Ecol. Eng.*, *58*(6), 57-62.

Guo, T., Delaune, R., & Patrick, W. (1997). The Effect of Sediment Redox Chemistry on Solubility/Chemically Active Forms of Selected Metals in Bottom Sediment Receiving Produced Water Discharge. *Spill. Sci. Technol.*, *4*, 165-175.

Hadad, H. R., Maine, M. A., Natale, G. S., & Bonetto, C. (2007). The Effect of Nutrient Addition on Metal Tolerance in *Salvinia herzogii*. *Ecol. Eng.*, *31*(2), 122-131.

Hammerly, J., Leguizamon, M., Maine, M. A. & Schiver, D. (1989). Decomposition Rate of Plant Material in the Parana Medio River (Argentina). *Hydrobiologia*, *183*, 179-184.

Kadlec, R. H., & Wallace, S. D. (2009). Treatment Wetlands (2nd. ed.). Boca Raton, Florida: RC Press.

Khan, S., Ahmad, I., Shah, M. T., Rehman, S. & Khaliq, A. (2009). Use of a Constructed Wetland for the Removal of Heavy Metals from Industrial Wastewater. J. Environ. Manag., *90*, 3451-3457.

Laveuf, C., & Cornu, S. (2009). A Review on Potentiality of Rare Earth Elements to Trace Pedogenetic Processes. *Geoderma*, *154*, 1-12.

Machemer, S., Reynolds, J., Laudon, L., & Wildeman, T. (1993). Balance of S in a Constructed Wetland Built to Treat Acid Mine Drainage, Idaho Springs, Colorado, USA. *Appl. Geochem*., *8*, 587-603.

Maine, M. A., Suñé, N., Hadad, H. R., Sánchez, G., & Bonetto, C. (2006). Nutrient and Metal Removal in a Constructed Wetland for Waste-Water Treatment from a Metallurgic Industry. *Ecol. Eng*., *26*, 341-347.

Maine, M. A., Suñé, N., Hadad, H. R., Sánchez, G., & Bonetto, C. (2007). Removal Efficiency of a Constructed Wetland for Wastewater Treatment According to Vegetation Dominance. *Chemosphere*, *68*, 1105-1113.

Maine, M.A., Hadad, H. R., Sánchez, G., Caffaratti, S., & Bonetto, C. (2009). Influence of Vegetation on the Removal of Heavy Metals and Nutrients in a Constructed Wetland. *J. Environ. Manag*., *90*, 355-363.

Maine, M. A., Hadad, H. R., Sánchez, G. C., Mufarrege, M. M., Di Luca, G. A., Caffaratti, S. E., & Pedro, M. C. (2013). Sustainability of a Constructed Wetland Faced with a Depredation Event. *J. Environ. Manag*., *128*, 1-6.

Miretzky, P., Saralegui, A., & Fernandez-Cirelli, A. (2006). Simultaneous Heavy Metal Removal Mechanism by Dead Macrophytes. *Chemosphere*, *66*(2), 247-254.

Murphy, J., & Riley, J. (1962). A Modified Single Solution Method for Determination of Phosphate in Natural Waters. *Anal. Chim. Acta*., *27*, 31-36.

Rivas-Hernández, A., Barceló-Quintal, I. D., & Moeller-Chávez, G. E. (2014). Importancia de las constantes cinéticas para el diseño de humedales de tratamiento bajo una condición climática en México (147-151 pp.). En A. Rivas-Hernández, & D. Paredes-Cuervo (Eds.). Sistemas de humedales para el manejo, tratamiento y mejoramiento de la calidad del agua. *Memorias de la Segunda Conferencia Panamericana en Sistemas de Humedales para el Manejo, Tratamiento y Mejoramiento de la Calidad del Agua*, Morelia, Michoacán, México.

Saunders, D. L., & Kalff, J. (2001). Nitrogen Retention in Wetlands, Lakes and Rivers. *Hydrobiologia*, *443*(1), 205-212.

Schneider, I., & Rubio, J. (1999). Sorption of Heavy Metal Ions by the Nonliving Biomass of Freshwater Macrophytes. *Environ. Sci. Technol*., *33*, 2213-2217.

Sorrell, B. K., & Boon, P. L. (1992). Biogeochemistry of Billabong Sediments II. Seasonal Variations in Methane Production. *Freshwater Biol*., *27*, 435-445.

Tessier, A., Campbell, P., & Bisson, M. (1979). Sequential Extraction Procedure for the Speciation of Particulate Trace Metals. *Anal. Chem*., *51*(7), 844-851.

Vymazal, J. (2011). Constructed Wetlands for wastewater Treatment: Five Decades of Experience. *Environ. Sci. Technol*., *45*, 61-69.

Weisner, S., Eriksson, P., Granéli, W., & Leonardson, L. (1994). Influence of Macrophytes on Nitrate Removal in Wetlands. *Ambio*, *23*(6), 363-366.

Wood, T., & Shelley, M.A. (1999). Dynamic Model of Bioavailability of Metals in Constructed Wetland Sediments. *Ecol. Eng*., *12*, 231-252.

Zhang, D. Q., Jinadasa, K. B., Richard, M. G., Liu, Y., Ng, W. J., & Tan, S. K. (2014). Application of Constructed Wetlands for Wastewater Treatment in Developing Countries: A Review of Recent Developments (2000-2013). *J. Environ. Manag*., *141*, 116-131.

Institutional Address of the Authors

Dra. María Alejandra Maine

Universidad Nacional del Litoral
Facultad de Ingeniería Química
Consejo Nacional de Investigaciones Científicas y Técnicas, Argentina
Santiago del Estero 2829
3000 Santa Fe, Argentina
Consejo Nacional de Investigaciones Científicas y Técnicas (Conicet)
Teléfono: +549 (0342) 4571 164, extensión 2515
amaine@fiq.unl.edu.ar

M.C. Gabriela Cristina Sánchez

Universidad Nacional del Litoral
Facultad de Ingeniería Química
Santiago del Estero 2829
3000 Santa Fe, Argentina
Teléfono: +549 (0342) 4571 164, extensión 2515
gsanchez@fiq.unl.edu.ar

Dr. Hernán Ricardo Hadad

Universidad Nacional del Litoral
Facultad de Ingeniería Química
Consejo Nacional de Investigaciones Científicas y Técnicas (Conicet)
Santiago del Estero 2829
3000 Santa Fe, Argentina
Teléfono: +549 (0342) 4571 164, extensión 2515
hhadad@fiq.unl.edu.ar

M.C. Sandra Ester Caffaratti

Universidad Nacional del Litoral
Facultad de Ingeniería Química
Santiago del Estero 2829
3000 Santa Fe, Argentina
Teléfono: +549 (0342) 4571 164, extensión 2515
cafarati@fiq.unl.edu.ar

M.C. María del Carmen Pedro

Universidad Nacional del Litoral
Facultad de Ingeniería Química
Santiago del Estero 2829
3000 Santa Fe, Argentina
Teléfono: +549 (0342) 4571 164, extensión 2515
maritapv@yahoo.com.ar

Dra. Gisela Alfonsina Di Luca

Universidad Nacional del Litoral
Facultad de Ingeniería Química
Consejo Nacional de Investigaciones Científicas y Técnicas (Conicet)
Santiago del Estero 2829
3000 Santa Fe, Argentina
Teléfono: +549 (0342) 4571 164, extensión 2515
gdiluca@fiq.unl.edu.ar

Dra. María de las Mercedes Mufarrege

Universidad Nacional del Litoral
Facultad de Ingeniería Química
Consejo Nacional de Investigaciones Científicas y Técnicas (Conicet)
Santiago del Estero 2829
3000 Santa Fe, Argentina
Teléfono: +549 (0342) 4571 164, extensión 2515
mmufarrege@fiq.unl.edu.ar

Click here to write the autor

Coagulation-Flocculation, Filtration and Ozonation of Wastewater for Reuse in Crop Irrigation

• Eliet Veliz* •
Centro Nacional de Investigaciones Científicas, Cuba
*Autor de correspondencia

• José Guadalupe Llanes •
Universidad Autónoma de Sinaloa, México

• Lidia Asela Fernández • Mayra Bataller •
Centro Nacional de Investigaciones Científicas, Cuba

Abstract

Veli, E., Llanes, J. G., Fernández, L. A., & Bataller, M. (January-February, 2016). Coagulation-Flocculation, Filtration and Ozonation of Wastewater for Reuse in Crop Irrigation. *Water Technology and Sciences* (in Spanish), 7(1), 17-34.

The aim of this work was to perform a bench-scale evaluation of coagulation-flocculation, filtration and ozonation processes (each one separately and all combined) for the treatment of municipal wastewater for reuse in crop irrigation. Three coagulants (aluminum sulfate, ferric sulfate and aluminum polychloride), two stirring speeds and three pH values were evaluated. Three filter medias were used (silica sand, anthracite and mixed media bed) with four filtration speeds. For ozonation, a 2^3 experimental design was performed with two ozone gas concentrations (20 and 40 mg/l), two gas flows (30 and 60 L/h) and two contact times (15 and 30 min). The pollutants evaluated were treated as response variables. Ozone doses between 37 and 300 mg/l were applied. The most efficient coagulants were aluminum polychloride and aluminum sulfate. The best results were obtained with faster stirring speeds (278 G-S-1) for rapid mixing, and the coagulant doses were reduced (50-66%). Silica sand was the filter medium selected since it had the best efficiency. During the ozonation stage, statistical models were obtained to predict the reduction levels of the pollutants evaluated. A minimum dose of 40 mg/l is proposed. With the treatment scheme presented, reduction efficiencies of 84-98% were obtained for the physiochemical parameters and 99.98-100% for microbiological parameters, which enables complying with the norms for reuse in crop irrigation.

Keywords: Coagulation-flocculation, filtration, ozonation, wastewater treatment, reuse.

Resumen

Veli, E., Llanes, J. G., Fernández, L. A., & Bataller, M. (enero-febrero, 2016). Coagulación-floculación, filtración y ozonización de agua residual para reutilización en riego agrícola. Tecnología y Ciencias del Agua, *7(1), 17-34.*

El objetivo del trabajo fue la evaluación a escala de banco de los procesos de coagulación-floculación, filtración y ozonización (cada uno por separado y con la combinación de todos) en el tratamiento de agua residual municipal para su reutilización en riego agrícola. Se evaluaron tres coagulantes: sulfato de aluminio, sulfato férrico y policloruro de aluminio, dos gradientes de velocidad de agitación y tres valores de pH. Para la filtración se utilizaron tres medios filtrantes: arena sílice, antracita y lecho mixto, para cuatro velocidades de filtración. En la ozonización se realizó un diseño experimental 2^3 para dos concentración de ozono en el gas (20 y 40 mg/l), dos flujo de gas (30 y 60 l/h) y dos tiempos de contacto (15 y 30 min): como variable respuesta se consideraron los contaminantes evaluados, se aplicaron dosis de ozono entre 37 y 300 mg/l. Los coagulantes más eficientes fueron policloruro de aluminio y sulfato de aluminio. Se obtienen mejores resultados con el aumento de la velocidad de agitación en la mezcla rápida (278 G-S^{-1}) y se reducen las dosis de coagulante (50-66%). Se seleccionó la arena sílice por su mejor eficiencia como medio filtrante. En la etapa de ozonización se obtuvieron modelos estadísticos para predecir los niveles de reducción de los contaminantes evaluados, se propone una dosis mínima de ozono de 40 mg/l. Con el esquema de tratamiento propuesto se logran eficiencias de reducción de los parámetros físico-químicos (84-98%) y microbiológicos (99.98-100%), que permiten cumplir con las normas para reutilización en riego agrícola.

***Palabras clave**: coagulación-floculación, filtración, ozonización, tratamiento de agua residual, reutilización.*

Received: 28/03/2014
Accepted: 09/09/2015

Introduction

Agricultural activity has been seriously affected by water scarcity and many countries have chosen to use only untreated wastewater for irrigation. In Latin America, over 500 000 ha of farmland are irrigated directly with untreated wastewater (IDRC OPS/HEP/CEPIS, 2002). In other regions of the world, China stands out with 1 300 000 ha and Pakistan with roughly 26% of national vegetable production irrigated with wastewater (Ensink, Mehmood, Vand der Hoeck, Raschid-Sally, & Amerasinghe, 2004), in addition to Ghana with approximately 11 500 ha (Keraita & Drechsel, 2004).

Wastewater has been used for over 200 years, and its high nutrient contents for plants has increased the productivity of land. Examples of this are shown in studies by Miralles de Imperial *et al*. (2003), Zamora, Rodríguez, Torres and Yendis (2008), Simonete, Kiehl and Andrade (2003), Andrade, Marcet, Reyzábal and Montero (2000), Nascimento, Barros, Melo and Oliveira (2004) and Rodríguez, Arruda, Cleidson, Machado and Arnaldo (2006), which report an increase of 67% to 150% in the yield of crops irrigated with wastewater, including corn, barley, tomato, oats for foraging, alfalfa, chili peppers, wheat and beans, among others.

Meanwhile, other authors (Cifuentes *et al*., 2000) have demonstrated a considerable increase in gastrointestinal illnesses, particularly among children, as a consequence of the pathogens contained in wastewater, which has raised public health concerns. Other studies suggest that roughly 40% of the urban population contracts infectious diseases associated with water, thus this problem urgently needs to be addressed (Moscoso & Egocheaga, 2003; Angelakis, Bontoux, & Lazarova, 2003). Untreated wastewater can contain dangerous chemical substances that come from industrial sources — primarily heavy metals, active hormonal substances and antibiotics (Yuan, 1998; Kuo, Zappi, & Chen, 2000; Joss *et al*., 2005; Snyder, Wert, Rexing, Zegers, & Dnury, 2006; Nakonechny, Ikekata, & Gamal-El-Din, 2008). The risks associated with these substances may represent the greatest long-term threat to health and may be more difficult to manage than the risk created by excreted pathogenic agents (Yuan, 1998; Kuo *et al*., 2000; Joss *et al*., 2005; Snyder *et al*., 2006; Nakonechny *et al*., 2008). It is estimated that one-tenth of the global population consumes agricultural products that are irrigated with wastewater (RUAF Foundation, 2002).

Many countries have their own regulations for the reuse of wastewater, which can be made stricter. For instance, the U.S. Environmental Protection Agency regulation (US-EPA, 1992) limits fecal coliforms to 0- 200 in 100 ml, depending on the type of crop, BOD5 to between 10 and 30 mg/l and suspended solids to 30 mg/l. Other countries follow guidelines by international organizations such as the World Health Organization (WHO, 2006) which proposes a maximum of 1 000 fecal coliforms per 100 ml. Most of the guidelines coincide with the need to eliminate intestinal nematodes to less than one helminth egg per liter of treated water.

The treatment technologies needed to comply with these regulations require the development of more efficient treatment processes and disinfection techniques for the proper reuse of treated wastewater, in order to ensure safe agricultural products for consumers and workers. This will also minimize the environmental impact, at a reasonable cost.

Advanced primary treatment (APT) uses a combination of coagulation-flocculation-sedimentation and filtration processes. Reductions in total solids of 70 to 90% have been achieved, which is better than conventional primary treatment and slightly inferior to secondary treatment. This combination can also result in a BOD5 in the effluent of 30 to 40 mg/l (Santiago, 2002).

The efficiency of ozone gas as an oxidizing agent and disinfectant is well known. It

inactivates germs that are highly resistant to chlorine with relative ease (Roustan, Stambolieva, Duguet, Wable, & Mallevialle, 1991; Lezcano, Perez-Rey, Baluja, & Sanchez, 1999; Liberti, Notarnicola, & Lopez, 2000; Finch, Haas, Oppenheimer, Gordon, & Trussel, 2001; Orta-de-Velásquez, Rojas- Valencia, & Vaca-Mier, 2002; Pei-Xu, Janex, Savoye, Cockx, & Lazarova, 2002; Thompson & Leong, 2007; Zhang, Huck, Anderson, & Stubley, 2007). The same is true for the inactivation of viruses, parasitic protozoa such as Giardia lambia and Cryptosporidium parvum and various amoebic species (Hertemann, Block, Joret, Foliguet, & Richard, 1983; Vaughn, Chen, Lindburg, & Morales, 1987; Herbold, Flehming, & Botzenhart, 1989; Janex *et al*., 2000; Finch *et al*., 2001; Rojas-Valencia, 2004).

Because of its high oxidizing power, ozone is used to oxidize a large number of organic substances, obtain oxygenated compounds, treat organic compound mixtures for increasing biodegradation and decrease chemical pollutants in industrial and domestic wastewater (Haapea, Coronen, & Tunkanen, 2002; Beltrán, 2004; Snyder *et al*., 2006; Ried, Mielckle, & Wieland, 2007; Yasunaga & Hirotsuji, 2008). It is also used to oxidize compounds that are not easily oxidized by conventional methods (Ried, Mielckle, & Kampmann, 2003; Haapea *et al*., 2002; Wang, Gamal El-Din, & Smith, 2004; Zinder, Pert, & Rexing, 2006; Naghashkar & Gamal-El-Din, 2005; Bataller *et al*., 2005; Hernández *et al*., 2008; Fernández *et al*., 2010).

The objective of the present work was to perform a bench-scale analysis of the combination of coagulation-flocculation, filtration and ozonation processes (each one separately and all combined) to treat municipal wastewater for reuse in crop irrigation.

Materials and Methods

This study was performed in the Ozone Treatment Technology Laboratory, at the National Center for Scientific Research, Cuba, in collaboration with specialists from the Autonomous University of Sinaloa, Mexico. The wastewater was collected at the inlet of a stabilization lagoon in Reparto San Agustin, municipality of La Lisa, province of Havana, Cuba. Point sampling was performed on a random day of each month, over one year (September 2011 to August 2012), for a total of 12 samples during all seasons in this tropical region. The water was collected in plastic 20-liter tanks for immediate use in the experiments. When necessary, the samples were stored for 24 hours in refrigeration at 4 to 8°C (277 to 281 K).

The coagulation-flocculation, filtration and ozonation processes were studied independently to test each one's effectiveness in reducing pollutants. All the treatment processes were then combined in a continuous treatment scheme. The work was performed at a bench-scale level.

Coagulation-Flocculation (C-F) Process

A jar-test was used containing six 0.5 m-diameter stirrers and 2-liter beakers with a diameter of 0.12 m, resulting in a stirrer/beaker diameter ratio *($d_{stirrer}/d_{beaker}$) of 0.41.*

Three coagulants were evaluated: AnalaR brand aluminum sulfate ($Al_2(SO_4)_3.16H_2O$) and ferric sulfate ($Fe_2(SO_4)_3.5H_2O$), and Prosifloc brand coagulant (aluminum polychloride powder). The three coagulants were studied with doses ranging from 50 to 400 mg/l.

The entire study was performed using two stirring speed gradients (100 and 200 rpm (72 and 278 $G\text{-}S^{-1}$) for 1 min.) in order to evaluate the influence of rapid mixing on the dissolution of the reagent and the efficiency of the process. In both cases, slow mixing was at 50 rpm (30 $G\text{-}S^{-1}$) for 20 min and sedimentation was 30 min.

Using the best coagulant, doses and speed gradient, the coagulation flocculation processes was evaluated with three pH values (5, 7, 9). A HANNA brand pH meter was used.

Lastly, the process was performed in a 40-l tank with an internal diameter of 0.3 m using the best coagulant, dose, pH and speed gradient obtained from the previous experiment. A mechanical stirrer (model RW20DZM, Janke&Kunkel brand) with a diameter of 0.10 m ($d_{stirrer}/d_{beaker}$ of 0.33) was used. After the process was completed and the sludge had settled, the treated wastewater was separated by overflow, for its use in the filtration study.

Filtration Process

Three filtration media were evaluated: silica sand, anthracite and mixed media bed. The effective size was determined to be 0.3 mm for silica sand and 0.66 for anthracite. The uniformity coefficients were 1.32 and 2.50, respectively. The mixed bed was composed of 70% anthracite on the top and 30% silica sand on the bottom (Maldonado, 2000). A rapid pressure filter with a cross-section area of 43.56 cm^2 (0.004356 m^2) was used to study filtration speeds of 44, 66, 132 and 209 $m^3/m^2/d$, which corresponded to filtration flows of 8, 12, 24 and 38 l/h, depending on the area of the filter. These speeds were chosen in order to conduct the study with values that were above and below the operating values recommended by the literature for rapid pressure filters (120-150 $m^3/m^2/d$) (Maldonado, 2000).

Ozonation Process

The wastewater used was that which had been coagulated-flocculated and filtered under the best operating conditions obtained by the previous experiments. Ozonation was performed in a 5-liter column with a diameter of 0.10m, which contained a porous silica boron diffuser on top and a valve for taking samples located in the middle of the column of liquid. On the top of the column, at the gas outlet, a foam collection system was connected before the residual ozone destruct unit.

A 2^3 experimental design was conducted to determine the best operating conditions, with semi-continuous experiments.

The experimental conditions were:

- Ozone concentration in gas $C(O_3)_g$: 20 and 40 mg/l.
- Gas flow (Q_g): 30 and 60 l/h (0.5 y 1.0 l/min).
- Contact times (t_c): 15 and 30 minutes.

The pollutants evaluated were treated as the response variable.

The combination of these experimental conditions made it possible to calculate the ozone doses to be applied based on the following expression:

$$D_a(O_3) = \frac{C(O_3)g(inl) * Q_g}{V} * tc$$

Where:

$D_a(O_3)$: ozone doses applied (mg/l).
$C(O_3)g_{(ent)}$: concentration of ozone in the gas at the column inlet (mg/l).
Q_g: flow of the gas (l/h).
V: volume of the residual (l).
t_c: contact time (h).

This design involved the application of 37 to 300 mg/l of ozone and running the experiment 24 times in three random blocks.

Determination of Ozone Doses at the bench-scale level

Ozonation was performed continuously using a 3^2 experimental design, with the ozone concentration in gas and the flow of gas as independent variables. The measurement parameter was the concentration of dissolved ozone in the liquid for a contact time of 20 minutes. The experimental conditions were:

- Concentration of ozone in gas $C(O_3)_g$: 20, 30 and 40 mg/l.
- Flow of gas (Q_g): 30, 60 and 90 l/h (0.5; 1.0 and 1.5 l/min).

The acceptance criteria was the minimal doses required to detect a minimum of 0.1 mg/l of dissolved ozone concentrations in the water. This residual ozone concentration indicates that the majority of the reactions with the pollutants had been completed, primarily microbiological reactions (Paraskeva, Lambert, & Graham, 1998; Janex *et al*., 2000).

The complete treatment schemed is shown in Figure 1.

Physical-Chemical and Microbiological Determinations

The following analyses were performed using the techniques described in the Standard Methods (APHA 2005, ed. 21): pH, turbidity (2130-A), color (2120-C), chemical oxygen demand (COD (5220-D), total suspended solids (TSS) (2540-D). The following were also measured:

- Absorbance at 254 nm, measuring the majority of the polycyclic aromatic and unsaturated compounds, precursors of trihalomethanes and organochlorines, as well as phenolic compounds (Beltrán, 2004).
- Ozone gas concentration: this was measured using a Pharmacia brand Ultrospec III spectrophotometer to directly measure ozone at a wavelength of 256 nm, using a 1 mm flow bucket.
- Concentration of ozone in the liquid: this was measured continuously throughout the ozonation process using direct ozone measurement equipment with a selective electrode (Dulcometer brand, from the Prominent company), calibrated using the indigo trisulfonate method.

Fecal coliform microorganisms were determined given that they are the fecal contamination indicators stipulated by regulations related to the discharge or reuse of wastewater. This was determined by fermentation in several tubes (9221-C). *Pseudomona* sp. and *Salmonella*/*Shigella* microorganisms were also quantified, directly sown in the different culture media (9260-E). Helminth eggs were quantified using a sedimentation procedure described by the World Health Organization (WHO, 1996).

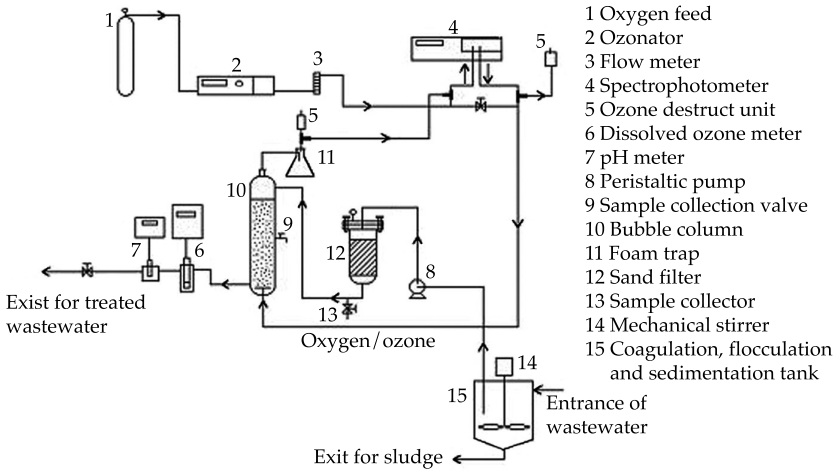

Figure 1: Flow diagram of the bench-scale test used.

Statistic Analysis

The processing of the results and the optimization analysis were performed using the computer program *Statgraphics Plus*, version 5.0. The mean and standard deviation of all the data groups were determined using the analysis of variance (Anova) at a 95% confidence level. To determine whether significant differences existed among the groups, a multiple range test (Duncan) was conducted, also at a 95% confidence level. Each experiment was performed in triplicate ($n = 3$).

Results

Table 1 presents the average values and their respective standard deviations, as well as the minimum and maximum values of the physical-chemical and microbiological parameters of the wastewater during the study period. An analysis of these values indicates that the majority of the pollution was due to suspended particles and colloids that increased the water's turbidity and apparent color and contributed to a considerable presence of pathogenic organisms.

The average COD obtained indicates a medium level of pollution in the water which could be associated with surfactant compounds (detergents), greases and oils, and general organic compounds, among others. All of these are characteristic of water such as that used in this study, which was primarily from domestic sources. The average BOD_5/COD was 0.56, which indicates good biodegradability of these substances (Menéndez & Pérez, 2007). The concentrations of the heavy metals evaluated were very low and their presence in the water did not represent a risk, even without treatment. As can be seen, this wastewater had a high concentrations of nutrients which in this case were favorable as organic fertilizers for crops.

Given the variability observed in all the parameters, the use of initial collector tanks is suggested as part of the treatment technology in order to homogenize the wastewater that enters the treatment system. These initial tanks also serve as primary settlers to retain the thickest solids that settle most easily.

Table 1. Characterization of wastewater over the study period (September 2011 - August 2012): $n = 12$.

Parameters	Units	Average	Min-max
pH	-	7.35	6.57 - 7.55
Turbidity	NTU	201 ± 101	82 - 458
TDS	mg/l	221 ± 66.7	90 - 435
Color	U Pt-Co	990 ± 380	310 - 2 140
Absorbance at 254 nm	nm	0.98 ± 0.27	0.447 -1.381
COD	mg/l	431.4 ± 186.8	115 - 946
Total coliform	MPN/100 ml	$(1.45 \pm 0.87) \times 10^7$	$(1.1 - 3.2) \times 10^7$
Fecal coliform	MPN/100 ml	$(6.18 \pm 3.46) \times 10^6$	$(0.24 - 1.2) \times 10^7$
Helminth eggs	HE/1	4.3 ± 1.2	1 - 6
Pseudomona sp.	CFU/ml	$(6.02 \pm 1.65) \times 10^3$	$(3.8 - 8.1) \times 10^3$
Shigella/Salmonella	CFU/ml	$(8.2 \pm 3.2) \times 10^3$	$(0.45 - 1.3) \times 10^4$

NTU: Nephelometric turbidity units; U Pt-Co: platinum-cobalt units.
MPN: Most probable number; HE: helminth eggs.
CFU: Colony forming units.

Coagulation-Flocculation Process

Obtaining the best coagulant, operating doses and stirring gradient

Figure 2 shows the results from the experimental conditions evaluated with stirring speed gradient 1. Since the other stages that were performed after this one further decreased the turbidity of the water, the minimum dose chosen for each coagulant was under 25 nephelometric turbidity units (NTU). The initial samples (0), for the samples performed with their replicates, were considered to be homogeneous.

Figures 3a and 3b statistically compare the average turbidity values of the three coagulants for each dose and the doses for each coagulant, for gradient 1.

As can be seen in Figure 3a, the best turbidity reduction efficiencies were obtained with aluminum sulfate and aluminum polychloride (APC), with no significant differences between the two for the doses evaluated. The results in the case of ferric sulfate were statistically different than those obtained with the other two coagulants.

In Figure 3b, when statistically comparing the doses for each coagulant and considering a value of 25 NTU, the doses that met the established criteria were:

APC = 100 mg/l,
aluminum sulfate = 150 mg/l,
ferric sulfate = 300 mg/l.

Figures 4 and 5 (a and b) present the results from this same analysis with stirring speed gradient 2.

Figure 5b shows that, with the lowest dose studied, APC resulted in turbidity values under 25 NTU, which was significantly different than the other two coagulants. With doses of at least 100mg/l, aluminum sulfate met the criteria established and was statistically equal to the selection criteria of 200 mg/l or over, though significantly different than the other two coagulants.

Based on this analysis, the following doses were chosen for this gradient:

APC = 50 mg/l, aluminum sulfate = 100 mg/l, ferric sulfate = 200 mg/l.

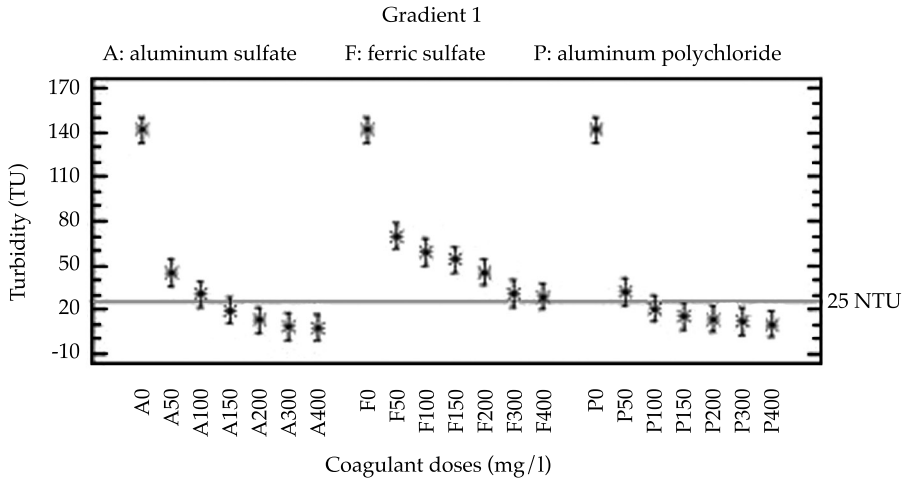

Figure 2. Comparison of the three coagulants for the six doses applied and with gradient 1.

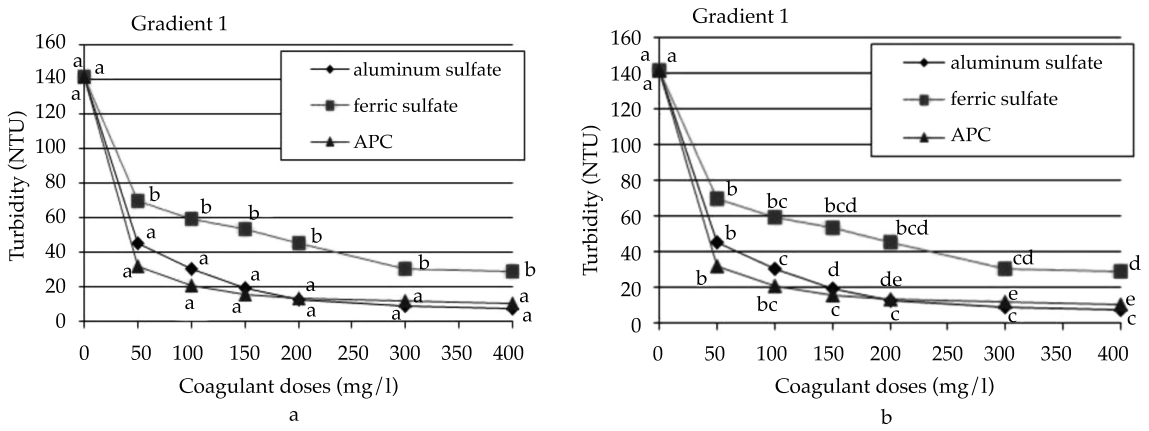

Figura 3. Comparación estadística para el gradiente 1: a) comparación entre coagulantes para cada dosis; b) comparación entre dosis para cada coagulante.

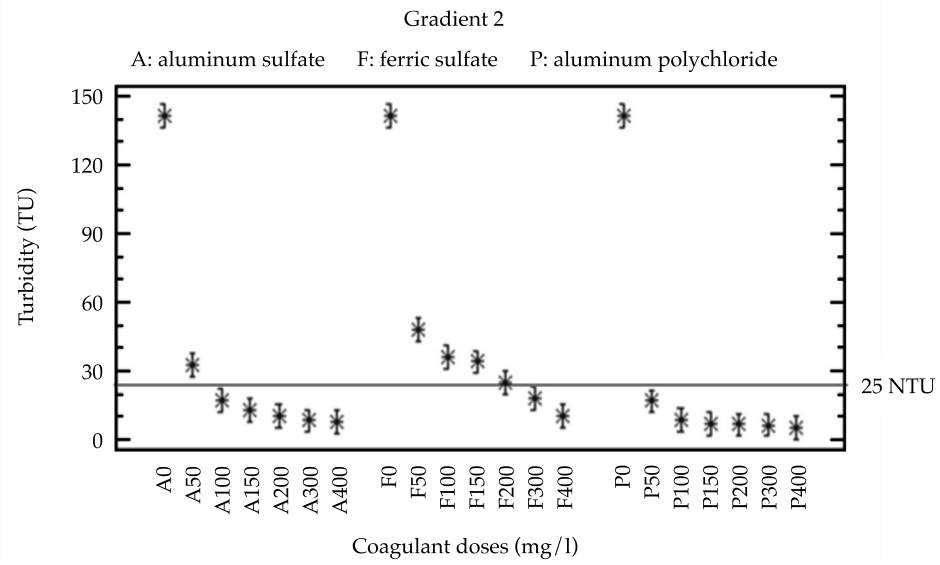

Figure 4. Comparison of three coagulants for the six doses applied and and gradient 2. A: aluminum sulfate; F: ferric sulfate; P: aluminum polychloride

These doses were similar to those reported for wastewater by other investigations (Durán, González, & Ramirez, 2001; Jubersay & Gilceira, 2011; Ramírez & Sierra, 2014). And although other works have reported lower doses, in the majority of the cases the use of the coagulant was followed by the application of a flocculant product to aid in the process, thereby contributing to the reduction of the coagulant doses evaluated by these cases (Tsukamoto, 2002).

When statistically comparing both stirring speed gradients, significant differences were found between the two gradients for all the

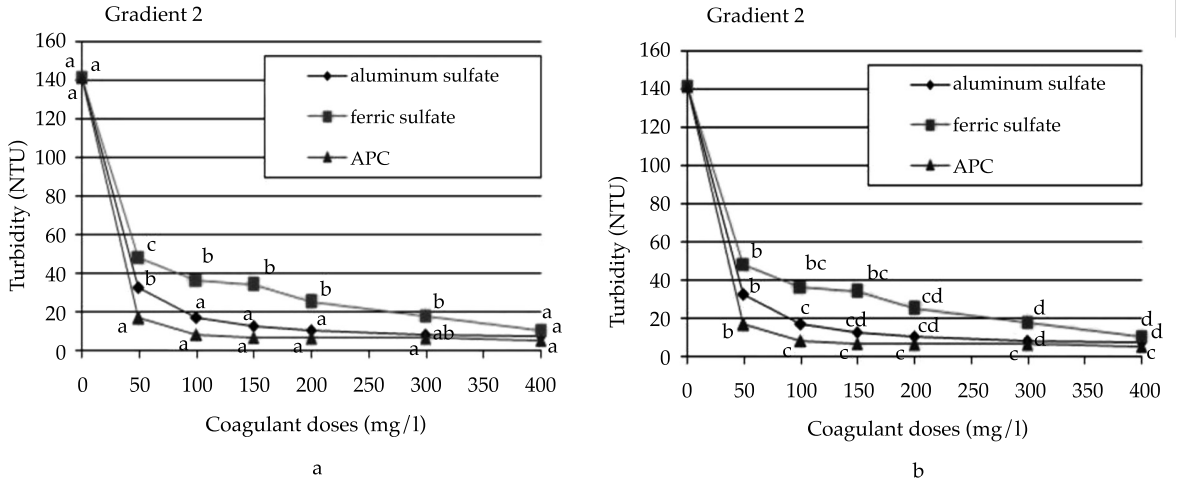

Figure 5. Statistical comparison of for gradient 2: a) comparison among coagulants for each doses; b) comparison among dose for each coagulant.

coagulants, with doses of 50 and 100 mg/l. Meanwhile, no significant differences were found between the two gradients for higher doses.

Taking into account this positive influence of increased stirring speed on rapid mixing with the lowest doses, it is recommended that industrial scale systems increase mixing efficiency and the dissolving of the coagulants with the water to be treated. This will later increase the number and size of flocs that form.

Influence of pH on the Coagulation-Flocculation Process

To study the possible influence of the variability in the pH of the wastewater on the coagulation-flocculation process, experiments were performed with three pH levels (5, 7, 9) using aluminum sulfate as a coagulant, with a dose of 100 mg/l and stirring speed gradient 2.

The most unfavorable condition was pH = 9, due to the formation of aluminates ($Al_2O_3^{3-}$), which given their negative charge repel each other and the colloids present in the wastewater, which are also negatively charged. Therefore, the formation of micro-flocs increases, which remain in suspension and do not settle, making the water more turbid and significantly decreasing the efficiency of the process.

Figures 6a and 6b show the influence of pH on reducing turbidity and organic matter measured at 254 nm, with five experiments performed using highly polluted wastewater, with an initial turbidity value over 120 NTU and an absorbance over 1.0 at 254 nm.

The statistical analysis of these results is presented in Figure 7. No significant differences were seen in average turbidity values between water with a pH of 6 versus 7. The same was true for water with pH values of 7 and 9. Nevertheless, significant differences in turbidity were observed between pH values of 5 and 9.

Given that the pH range of the wastewater studied was between 6.5 and 7.8, and since the turbidity values were under 25 NTU (adjusted for a pH = 7) and were not significantly different than the values obtained with a a pH = 5, it can be suggested that systems that adjust for pH are not necessary.

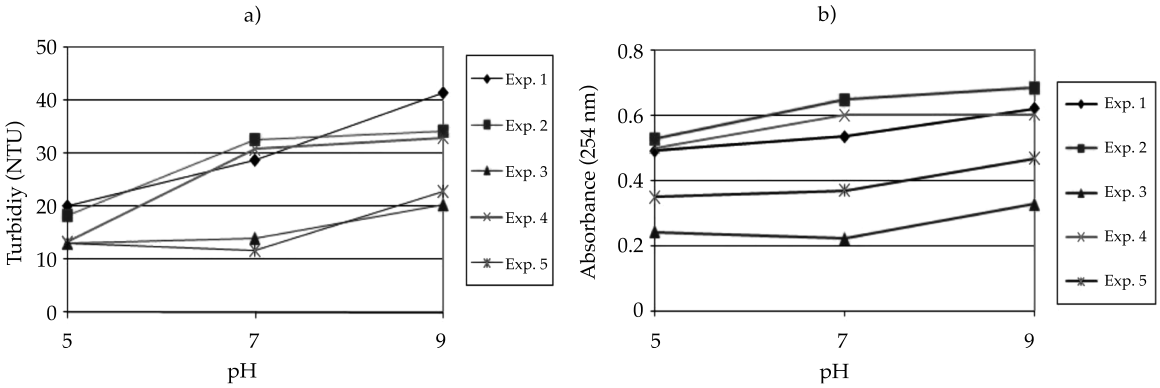

Figure 6. Influence of pH on reducing turbidity (a) and organic matter measured at 254 nm (b); n = 5.

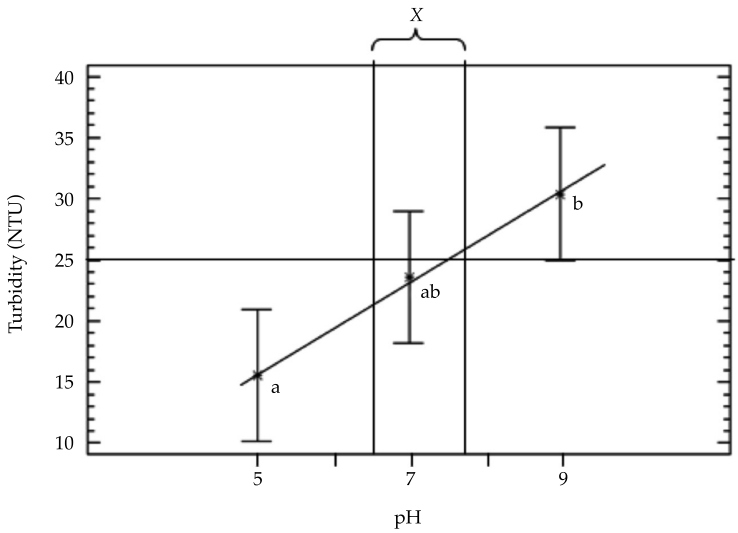

Figure 7. Statistical comparison among the pH values evaluated: n=5.
X- pH range of the wastewater studied.

Filtration process

Figure 8 (a and b) shows the influence of the three filtration media (a) and the filtration flows (b) evaluated on the retention of particles that increase the water's turbidity. Reductions in turbidity were observed with all the experimental conditions, with significant differences with respect to the initial sample. Therefore, this is considered to be a good stage to ensure the retention of particles that do not settle in the coagulation-flocculation process. In the case of slower filtration flows (8 and 12 l/h), sand filtration provided the best reduction in turbidity, with significant differences with respect to the other filtration

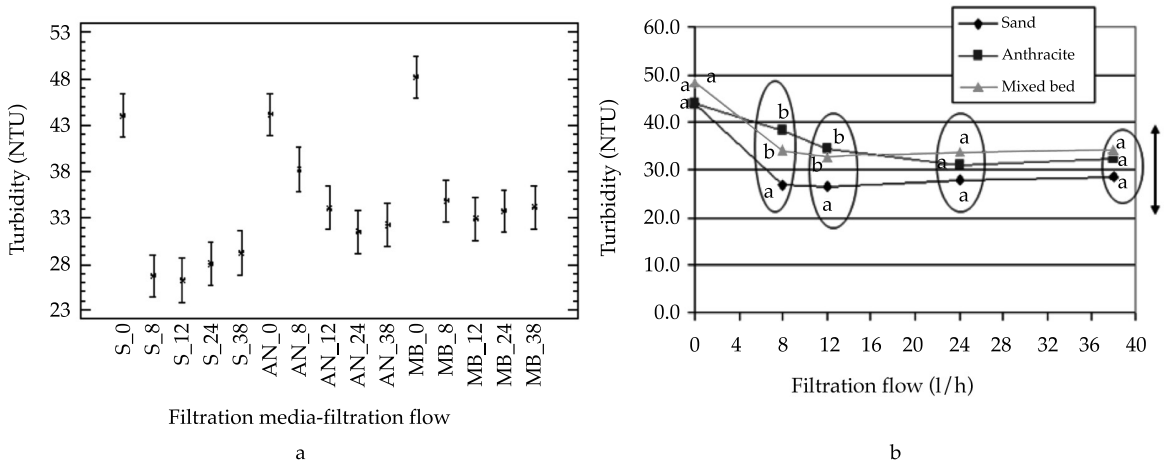

Figure 8. Statistical comparison among the three filtration media (a) for each filtration flow (b). S: sand, AN: anthracite, MB: Mixed bed.

media. This difference is important to choosing the filtration media when a slow gravity filter is used.

For filtration flows of 24 l/h (132 $m^3/m^2/d$) and 38 l/h (209 $m^3/m^2/d$), turbidity was reduced by the three filtration media without any significant differences among them. This indicates that any of the filtration media evaluated can be used with rapid pressure filters and function with the recommended filtration flows (120-150 $m^3/m^2/d$).

This study also tested transparent acrylic filters and demonstrated that higher backwash flows and pressures can be used for the backwashing of filters (cleaning against the current of the filtration material), given that sand has a heavier specific weight than anthracite (1.7 times heavier). This improves the cleaning of the filtration material without losing the finer particles, which improve filtration and do not form grooves in the filtration material. In the case of anthracite, when increasing the backwash pressure to expand the filtration layer, the finer heavier particles are dragged by the backwash water to the outlet at the top of the filter.

Silica sand was selected as a filtering medium for treatment at larger scales, given the above results and it is one of the least expensive and most common materials used to filter water, and functions best. Authors such as McNeilla, Almasrib and Mizyed (2009), and Bakopoulou, Emmanouil and Kungolos (2011) mention the use of silica sand for filtration in the treatment of wastewater. Jimenez (2002) also proposed the use of this filtration medium to retain particles from the coagulation flocculation stage, as well as to retain helminth eggs.

Ozonation Process

Based on the experimental conditions evaluated, statistical models of several physical-chemical and microbiological pollutants were obtained, with an ozone dose range between 37 and 300 mg/l. The analysis of these models makes it possible to know which of the operating parameters have more influence on the efficiency of this treatment stage. The models obtained with the parameters evaluated are presented below.

– **Turbidity (NTU) = 34.6 - 0.481 * $C(O_3)_g$ - 0.229 * Q_g**

R^2 = 78.4%; p-value = ($C(O_3)_g$: 0.009; Q_g: 0.0083)

– **Color (UPt-Co) = 126 - 3.16 * $C(O_3)_g$ - 2.01 * Q_g + 0.05 * $C(O_3)_g$ * Q_g**

R^2 = 78.0%; p-value = ($C(O_3)_g$: 0.0026; Q_g: 0.0076; $C(O_3)_g$ * Q_g: 0.0076)

– **Abs 254 nm = 0.711 - 0.00693 * $C(O_3)_g$ - 0.00265 * Q_g - 0.00536 * t_c**

R^2 = 83.5%; p-value = ($C(O_3)_g$: 0.0001; Q_g: 0.0069; t_c: 0.0065)

– **COD (mgO_2/L) = 335.98 - 2.411 * $C(O_3)_g$ - 1.797 * Q_g**

R^2 = 75.3%; p-value = ($C(O_3)_g$: 0.0388; Q_g: 0.0235)

– **Fecal coloforms (MPN/100 ml) = 9 965.0 - 246.75 * $C(O_3)_g$ - 162.392 * Q_g + 4.023* $C(O_3)_g$ * Q_g**

R^2 = 82.0%; p-value = ($C(O_3)_g$: 0.0015; Q_g: 0.0022; $C(O_3)_g$ * Q_g: 0.0028)

– ***Salmonella and Shigella* (CFU/ml) = 189.0 - 4.725 * $C(O_3)_g$ - 3.083 * Q_g + 0.077 * $C(O_3)_g$ * Q_g**

R^2 = 81.2%, p-value = ($C(O_3)_g$: 0.0017; Q_g: 0.0029; $C(O_3)_g$ * Q_g: 0.0029)

Overall, the ozone concentration in gas ($C(O_3)_g$) and the flow of gas (Q_g) were found to be the parameters that most influenced the reduction of pollutants.

The importance of the flow of gas and the concentration of ozone is shown in Table 2, which presents the results from the local optimization of ozonation factors, with a minimization criteria for each pollutant in the process. As can be seen, to reduce these pollutants to a minimum, it is necessary to apply the highest gas concentration and flow, while contact time required only 15 minutes of ozonation in several cases. The latter is important since most of the pollutants that reach this treatment stage are pathogenic microorganisms, which according to the results obtained are eliminated with less ozonation time, making it possible to reduce the ozone dose and treatment costs.

Determination of Ozone Dose for Subsequent Scales

Table 3 presents the average dissolved ozone concentrations obtained for each ozone dose applied, in accordance with the experimental design developed. The shaded dose values correspond to dissolved ozone concentra-

Table 2. Local optimization of ozonation factors for the physical-chemical and microbiological pollutants evaluated.

Parameter	Factors			Optimal value of the minimized parameter
	$CO_{3\,g}$ (mg/l)	Q_g (l/h)	t_c (min)	
Turbidity	40.0	60.0	30.0	1.59 NTU
Color	40.0	60.0	15.0	0.0 (U Pt-Co)
Abs. 254 nm	40.0	60.0	30.0	0.114
SAAM	40.0	60.0	30.0	0.1 mg/l
COD	40.0	60.0	15.0	131.7 mg/l
Fecal coliform	40.0	60.0	15.0	8.5 MPN/100 ml
Salmonella/Shigella	40.0	60.0	15.0	0.0 CFU/ml

tions ($C(O_3)_L$) equal to or over 0.1 mg/l. This value was chosen as a selection criterion since research has demonstrated that low ozone concentrations in liquid are sufficient for obtaining high efficiencies in the inactivation of microorganisms (Paraskeva et al., 1998; Janex et al., 2000). In addition, with this dissolved oxygen concentration and a contact time between 20 to 30 minutes, a CT value between 2 and 3 mg/l-min would be applied, sufficient enough to achieve the needed disinfection (Janex *et al*., 2000). Likewise, measuring the treated water for residual concentrations of the disinfectant being applied indicates that the initial demand for this was satisfied and the majority of reactions with the pollutants was completed.

The minimum ozone dose that met the selection criterion mentioned previously is 80 mg/l. This corresponds to the combination of the highest concentration of ozone in gas and the lowest gas flow. In addition, a positive influence of the increased gas flow can be seen for the lowest ozone concentration in gas.

Based on the analysis in this experimental design, the following statistical model was obtained:

$$\mathbf{CO_{3\ liquid}}\ (\mathrm{mg/l}) = \mathbf{-\ 0.1775 + 0.0139}\ (\boldsymbol{Q_g} \cdot \mathbf{CO_{3\ g}})\quad R^2 = 90\%,\ N = 27$$

This model enables estimating the average dissolved oxygen concentrations that would be obtained by applying the combination of gas flow and ozone concentration in gas, for this type of wastewater with prior treatment using coagulation-flocculation and filtration processes. This estimation can also be performed based on the graph in Figure 9, with a 95% confidence leveL.

Study of the Combination of Continuous Processes

Table 4 shows the statistical comparison of the results obtained from applying three ozone doses (40, 80 and 160 mg/l) to reduce the physical-chemical and microbiological pollutants present after the coagulation-flocculation and filtration processes.

With continuous operations of the treatment scheme, the first treatment stages (C-F+F) were demonstrated to be very efficient in reducing turbidity, TDS and color, with removal levels between 83 and 91%, and with statistically significant differences in concentrations with respect to the initial wastewater. Ozonation lowered the TDS to under 30 mg/l, the value stipulated by regulations for reuse in agricultural irrigation in the United States (US-EPA, 1992). Many local regulations do not include this parameter, neglecting the importance of ensuring low water turbidity to avoid clogging and obstructing sprinkler or nozzle irrigation systems.

In the case of the compounds measured at 254 nm, it was verified that the pollutants that contribute to COD values were

Table 3. Average concentrations of dissolved ozone for the ozone doses evaluated

$C(O_3)_g$ (mg/l)	Q_g (l/min)					
	0.5		1.0		1.5	
	Doses (mg/l)	$C(O_3)_L$ (mg/l) ± SD	Doses (mg/l)	$C(O_3)_L$ (mg/l) ± SD	Doses (mg/l)	$C(O_3)_L$ (mg/l) ± SD
20	40	0.05 ± 0.04	80	0.07 ± 0.05	**120**	**0.18 ± 0.09**
30	60	0.06 ± 0.04	**120**	**0.16 ± 0.02**	**180**	**0.46 ± 0.06**
40	**80**	**0.16 ± 0.06**	**160**	**0.38 ± 0.11**	**240**	**0.84 ± 0.22**

$C(O_3)_g$: ozone concentration in gas; Q_g: flow of gas.
$C(O_3)_L$: ozone concentration in liquid; SD: standard deviation

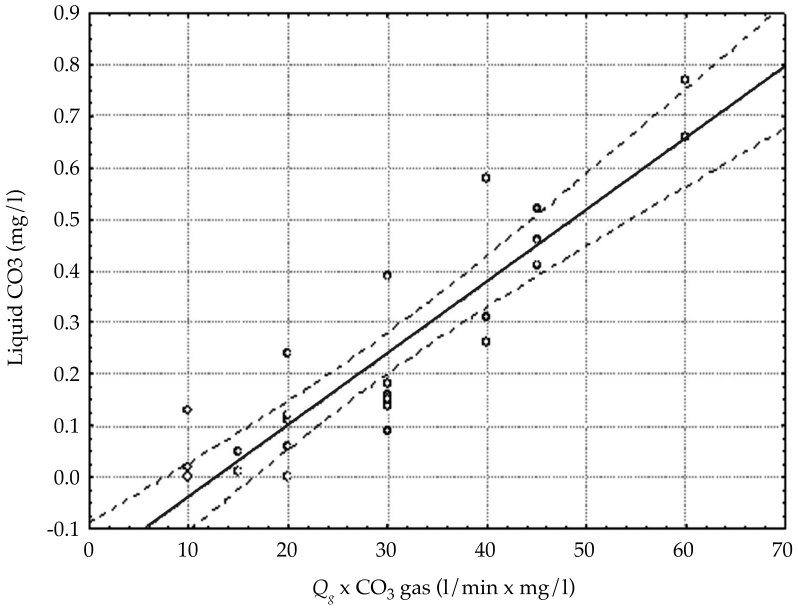

Figure 9. Graphic to estimate average levels of dissolved ozone

Table 4. Average values and percentages in the reduction for each process and totals for the entire treatment scheme at a bench-scale level. Comparison among ozone doses.

Stages/parameters		RW	C - F + F	Ozonation. O_3 doses (mg/l)			TE (%)
				40	80	160	
Turbidity	UNT ± DE	312.7 ± 21.2^{a}	28.2 ± 8.4^{b}	5.7 ± 1.1^{c}	5.2 ± 0.8^{c}	5.0 ± 1.0^{c}	98
	TDS	-	91	80	82	82	
SST	mg/l ± DE	283.0 ± 19.3^{a}	33.6 ± 8.2^{b}	10.2 ± 2.8^{c}	9.2 ± 1.1^{c}	8.8 ± 0.7^{c}	96
	R (%)	-	88	70	73	74	
Color	U Pt-Co ± DE	1 270.0 ± 90.6^{a}	215.2 ± 18.3^{b}	56.5 ± 5.6^{c}	51.5 ± 3.6^{c}	28.6 ± 4.2^{d}	96
	R (%)	-	83	74	76	87	
Abs. 254 nm	Abs. ± DE	0.988 ± 0.103^{a}	0.543 ± 0.09^{b}	0.155 ± 0.01^{c}	0.137 ± 0.01^{c}	0.111 ± 0.01^{d}	84
	R (%)	-	45	71	75	80	
COD	mg O_2/L ± DE	281.3 ± 10.7^{a}	74.9 ± 14.6^{b}	41.2 ± 9.1^{c}	27.3 ± 6.9^{c}	15.6 ± 1.5^{d}	85
	R (%)	-	73	45	64	79	
Fecal coliform	NMP/100 ml ± DE	8.10 ± 0.15 x 10^{6a}	1.22 ± 0.50 x 10^{5b}	830 ± 35^{c}	110 ± 25.0^{d}	0^{e}	99.98
	R (%)	-	98.49	99.32	99.91	100	
Helminth eggs	HH/L	4.3 ± 1.2^{a}	2.2 ± 0.8^{b}	0^{c}	0^{c}	0^{c}	100

SD: standard deviation.
RW: raw untreated water. Initial sample.
C-F+F: Wastewater treated with coagulation-flocculation using aluminum sulfate, dose of 100 mg/l, followed by filtration with silica sand.
O_3 doses: ozone doses applied during the ozonation stage (mg/l).
R (%): porcentaje de reducción parcial, al compararse los valores obtenidos en cada etapa con respecto a la muestra en la etapa anterior.
ET (%): percentage in total efficiency between RW and the ozone dose of 80 mg/l.
Same letters in the superscript (for each parameter): no statistically significant differences in relation to the value of the previous sample.
Different letters in the superscript (for each parameter): statistically significant differences exist in relation to the value of the previous sample.

eliminated in the first treatment stages, including a significant portion of those which were fundamentally related to non-soluble compounds (45 and 73%, respectively). The soluble compounds also decreased after the ozonation stage. The statistical comparison between the values obtained with the three ozone doses and the previous stage indicates significant removal levels with the 40 mg/l dose.

In terms of the removal of fecal coliforms, the first treatment stages (C-F+F) resulted in a decrease of more than one logarithmic unit, with a 98.49% efficiency, but was insufficient for attaining the microbiological quality required by regulations related to crop irrigation (WHO, 2006; US-EPA, 1992).

The ozonation process was very effective for eliminating fecal coliforms. The lowest dose evaluated (40 mg/l) resulted in reductions over 99% and enabled meeting the WHO regulations for reuse of wastewater for crop irrigation (< 1 000 MPN/100 ml of fecal coliforms). Nevertheless, the ozone dose would need to be increased to 80 mg/l in order to comply with the strictest regulations established by states and countries (< 200 MPN/100 ml of fecal coliforms) (US-EPA, 1992). Furthermore, an ozone dose of 160 mg/l would be needed if the objective of disinfection were to eliminate 100% of the fecal coliform.

The statistical analysis showed significant differences between the ozone doses that were applied and all the doses with respect to the initial sample. The decision to recommend an ozone dose of 40 or 80 mg/l depends on the requirements of each country, their regulations for reuse and the financing available to acquire high-capacity ozone equipment. In the case of Cuba, fecal coliform regulations are the same as those recommended by the WHO, and therefore an ozone dose of 40 mg/l is recommended.

Table 4 shows the efficiency (49%) of the first treatment stages in retaining helminth eggs, and the ability of ozone to completely destroy them (100% efficiency), even with the lowest ozone dose. This is very important when considering that these parasites are strictly controlled by regulations related to the reuse of domestic wastewater, especially for food products that are consumed raw.

With the combined treatment scheme, total efficiencies in reducing the physical-chemical parameters were between 84 and 98%, and between 99.98 and 100% for the microbiological pollutants, using the lowest ozone dose evaluated.

Conclusions

The efficiency of the coagulants were aluminum polychloride > aluminum sulfate > ferric sulfate. Turbidity removal was best when increasing the stirring speeds (from 72 to 278 G-S-1) for rapid mixing, which enabled decreasing the coagulant doses between 33 and 50%. Aluminum sulfate (100 mg/l) was selected as the recommended coagulant for larger treatment scales, since it is less expensive and easier to use than aluminum polychloride.

Silica sand was selected because of its efficiency as a filtration medium and its low cost and durability, as compared to other options, in addition to providing better filtration and backwash operations.

The ozonation process was very effective for disinfecting municipal wastewater. An ozone dose between 40 and 80 mg/l is recommended.

The proposed treatment scheme produced treated effluents with the physical-chemical and microbiological quality required by the USA Environmental Protection Agency (US-EPA, 1992) and the World Health Organization (WHO, 2006) for reuse in crop irrigation. Many countries use these regulations as their main reference for local regulations.

References

Andrade, M. L., Marcet, P., Reyzábal, M. L., & Montero, M. J. (2000). Contenido, evolución de nutrientes y productividad en un suelo tratado con lodos residuales urbanos. *Edafología*, *7*(3), 21-29.

Angelakis, A. N., Bontoux, L., & Lazarova, V. (2003). Challenges and Prospectives for Water Recycling and Reuse in EU Countries. *Water Sci. Technol. Water Supply*, *3*(4), 59-68.

Bakopoulou, S., Emmanouil, C., & Kungolos, A. (February, 2011). Assessment of Wastewater Effluent Quality in Thessaly Region, Greece, for Determining its Irrigation Reuse Potential. *Ecotoxicol. Environ. Saf.*, *74*(2), 188-194, doi: 10.1016/j.ecoenv.2010.06.022. Epub 2010 Aug 16.

Bataller, M., Hernández, C., Fernandez, L. A., Lopez, A., Veliz, E., & Alvarez, C. (2005). Effect of O_3/H_2O_2 Molar Concentration Ratio Different pH Values on Cyclophosphamide Degradation. *Journal of Water Supply Research and Technology, AQUA*, *54*, 403-410.

Beltrán, F. J. (2004). *Ozone Reaction Kinetics for Water and Wastewater Systems* (pp. 7-26). Florida: Lewis Publishers.

Cifuentes, E., Gómez, M., Blumental, U., Tellez-Rojo, M., Romieu, I., Ruiz-Palacios, G., & Ruiz-Velazco, S. (2000). Risk Factors for *Giardia intestinalis* Infection in Agricultural Villages Practicing Wastewater Irrigation in Mexico. *Am. J. Trop. Med. Hyg.*, *62*(3), 388-392.

Durán, A., González, E., & Ramirez, R. M. (2001). Comparación de dos procesos fisicoquímicos para el pretratamiento de aguas residuales. *Tecnol. Ciencia Ed.* (IMIQ), *16*(1), 28-41.

Ensink, H. H., Mehmood, T., Vand der Hoeck, W., Raschid-Sally, L., & Amerasinghe, F. P. (2004). A Nation-Wide Assessment of Wastewater Use in Pakistan: An Obscure Activity or a Vitally Important One? *Water Policy*, *6*, 197-206.

Fernández, L. A., Hernández, C., Bataller, M., Veliz, E., Lopez, A., Ledea, O., & Padron, S. (2010). Cyclophosphamide Degradation by Advanced Oxidation Processes. *Water and Environmental Journal*, *24*(3), 174-180.

Finch, G. R., Haas, C. N., Oppenheimer, J. A., Gordon, G., & Trussel, R. R. (2001). Design Criteria for Inactivation of *Cryptosporidium* by Ozone in Drinking Water. *Ozone Science and Engineering*, *23*(4), 259-284.

Haapea, P., Coronen, S., & Tunkanen, T. (2002). Treatment of Industrial Leachates by Chemical and Biological Methods; Ozonation, Ozonation + Hydrogen Peroxide, Hydrogen Peroxide and Biological Post-Treatment for Ozonated Water. *Ozone Science & Engineering*, *24*, 369.

Herbold, K., Flehming, B., & Botzenhart, K. (1989). Comparision of Ozone Inactivation in Flowing Water of Hepatitis A Virus, Poliovirus 1, and Indicator Organism. *Applied and Environmental Microbiology*, 2949-2953.

Hernández, C., Ramos, Y., Fernandez, L. A., Ledea, O., Bataller, M., Veliz, E., Besada, V., & Rosado, A. (2008). Ozonation of Cisplatin in Aqueous Solution at pH 9. *Ozone Science and Engineering*, *30*, 189-196.

Hertemann, P. H., Block, J. C., Joret, J. C., Foliguet, J. M., & Richard, Y. (1983). Virological Study of Drinking and Wastewater Disinfection by Ozonation. *Water Science and Technology*, *15*, 145-154.

IDRC-OPS/HEP/CEPIS (2002). *Sistemas integrados de tratamiento y uso de aguas residuales en américa latina: realidad y potencial. Resumen ejecutivo, 2000-2002*. Recuperado de http://www.bvsde.paho.org/bvsaar/e/proyecto/rejecutivo.pdf.

Janex, M. L., Savoye, P., Roustan, M., Do-Quang, Z., Lainé, J. M., & Lazarova, V. (2000). Wastewater Disinfection by Ozone: Influence of Water Quality and Kinetics Modeling. *Ozone Science & Engineering*, *22*, 113-121.

Jiménez, B. (Octubre, 2002). *Riego agrícola con agua residual y sus implicaciones en la salud. Caso práctico*. XVIII Congreso Interamericano de Ingeniería Sanitaria y Ambiental, Cancún, México.

Joss, A., Keller, E., Alder, A. C., Gobel, A., McArdell, C. S., Ternes, T., & Siegrest, H. (2005). Removal of Pharmaceuticals and Fragrances in Biological Wastewater Treatment. *Water Resource*, *39*(3), 39-52.

Jubersay, C., & Gilceira, G. (2011). *Procesos de tratamiento de aguas. Coagulación y floculación*. Santa Ana de Coro, Venezuela: Programa Ciencias Ambientales, Universidad Nacional Experimental Francisco de Miranda.

Keraita, B. N., & Drechsel, P. (2004). Agricultural Use of Untreated Urban Wastewater in Ghana. In C. A. Scott, N. I. Faruqui, & L. Raschid-Sally, *Wastewater Use in Irrigated Agriculture*. Wallingford, UK: CABI Publishing.

Kuo, C. H., Zappi, M. E., & Chen, S. M. (2000). Peroxone Oxidation of Toluene and 2, 4, 6 Trinitrotoluene. *Ozone Science & Engineering*, *22*, 519.

Lezcano, I., Perez-Rey, R., Baluja, C., & Sanchez, E. (1999). Ozone Inactivation of *Pseudomonas aeruginosa, Escherichia coli, Shigella sonnei* and *Salmonella thyphimurium* in Water. *Ozone Science & Engineering*, *21*(3), 293.

Liberti, L., Notarnicola, M., & Lopez, A. (2000). Advanced Treatment for Municipal Wastewater Reuse in Agriculture. III-Ozone Disinfection. *Ozone Science & Engineering*, *22*, 151-166.

Maldonado, V. (2000). Capítulo 9: Filtración (pp. 83-152). En *Manual de tratamiento de agua*. CEPIS/OPS.

Mcneilla, L. S., Almasrib, M. N., & Mizyed, N. (2009). A Sustainable Approach for Reusing Treated Wastewater in Agricultural Irrigation in the West Bank-Palestine, ScienceDirect. *Desalination*, *24*(8), 315-321.

Menéndez, C., & Pérez, J. M. (2007). *Procesos para el tratamiento biológico de aguas residuales industriales*. La Habana: Editorial Félix Varela.

Miralles-de-Imperial, R., Ma. Beltrán, E., Angel, M., Beringola, Ma. Luisa., Valero, J., Calvo, R., Delgado, & Del Mar, M. (2003). Disponibilidad de nutrientes por el aporte de tres tipos de lodos de estaciones depuradoras. *Revista*

Internacional de Contaminación Ambiental, *19*(3).

Moscoso, J., & Egocheaga, L. (2003). Sistemas Integrados de tratamiento y reuso de aguas residuales en América Latina. Realidad y potencial. *Revista Agricultura Urbana*, *8*. Recuperado de http://www.ipes.org/images/agriculturaUrbana/documents/revEsp8/ruaf8p7.pdf.

Naghashkar, N. J., & Gamal-El-Din, M. (2005). *Aqueos Pharmaceutical Degradation by Advanced Oxidation Processes: A Review (Part II)*. IOA 17th World Ozone Congress. Strasbourg, France.

Nakonechny, M., Ikekata, K., & Gamal-El-Din, M. (2008). Kinetics of Estione Ozone/Hydrogen Peroxide Advanced Oxidation Treatment. *Ozone Science & Engineering*, *30*, 249-255.

Nascimento, C., Barros, A., Melo, D., & Oliveira, A. (2004). Alterações químicas em solos e crescimento de milho e feijoeiro após aplicação de lodo de esgoto. *Revista Brasileira de Ciência de Solo*, *28*(2), 385-392.

OMS (Marzo 1996). *Directrices sanitarias sobre el uso de aguas residuales en agricultura y acuicultura*. Ginebra: OMS (1989) (pp. 40-64). Serie de informes técnicos. Reproducido en *Repindex*, *57*.

Orta-de-Velásquez, M. A. T., Rojas-Valencia, M. A. N., & Vaca-Mier, M. (2002). Destruction of Helminth Eggs (*Ascaris suum*) by Ozone: Second Stage. *Water Science and Technology: Water Supply*, IWA Publishing, 2(3), 227-233.

Paraskeva, P., Lambert, S. D., & Graham, N. J. (1998). Influence of Ozonation Conditions on the Treatability of Secondary Effluents. *Ozone Science & Engineering*, *20*(2), 134.

Pei-Xu, H., Janex, M. L., Savoye, P.H., Cockx, A., & Lazarova, V. (2002). Wastewater Disinfection by Ozone: Main Parameters for Process Design. *Water Research*, *36*, 1043-1055.

Ramírez, L. F., & Sierra, L. F. (2014). Evaluación de coagulantes como alternativa de remoción de fósforo en el pulimiento del efluente del sistema lagunar salguero de Valledupar. *Revista Ambiental*, *5*(1).

Ried, A., Mielckle, J., & Kampmann, M. (2003). Ozone and UV Processes for Additional Wastewater Treatment to Meet Existing and Future Limits Regarding Disinfection, Pharmaceuticals and Endocrine Disrupters. *Proceedings IOA 16th World Congress*, Las Vegas, USA.

Ried, A., Mielcke, J., & Wieland, A. (2007). Ozonation of municipal Waste Water Effluents: A Tool for the Removal of Pharmaceuticals, EDCs and Pathogens. *Proceedings IOA IUVA 18th World Congress*, Los Angeles, USA.

Rodríguez, T., Arruda, S., Cleidson, F., Machado, F., & Arnaldo, L. (2006). Produtividade de milho e de feijão consorciados adubados con diferentes formas de lodo de esgoto. *Revista de la Ciencia del Solo y Nutrición Vegetal*, *6*(1), 52-63.

Rojas-Valencia, M.N. (2004). *Tratamiento avanzado de desinfección con ozono para eliminar* Vibrio cholerae, Salmonella typhi, *amebas y huevos de helmintos en aguas residuales tratadas para reúso*. Doctorado en Ciencias e Ingeniería Ambiental. México, DF: Universidad Autónoma Metropolitana.

Roustan, M., Stambolieva, Z., Duguet, J. P., Wable, O., & Mallevialle, J. (1991). Research Note: Influence of Hydrodynamics on *Giardia* Cyst Inactivation by Ozone. Study by Kinetics and by "CT" Approach. *Ozone Science & Engineering*, *13*(4), 451.

RUAF Foundation (2002). *El uso agrícola de aguas residuales urbanas no tratadas en países de bajos ingresos*. Conferencia electrónica, 24 junio-5 julio, 2002. Recuperado de http://www.ruaf.org.

Santiago, J. F. (2002). *Estrategias de tratamiento de residuales y reúso de aguas tratadas como alternativa de solución ante los eventos de sequía*. II Seminario Internacional del Uso Integral del Agua, Centro de Hidrología y Calidad de las Aguas, La Habana, Cuba.

Simonete, M., Kiehl, J., & Andrade, T. (2003). Efeito do lodo de esgoto em um Argissolo e no crescimento e nutrição de milho. *Pesquisa Agropecuária Brasileira*, *38*(10), 1187-1195.

Snyder, S., Wert, E., Rexing, D., Zegers, R., & Dnury, D.D. (2006). Ozone Oxidation of Endocrine Disruptors and Pharmaceuticals in Surface Water and Wastewater. *Ozone Science & Engineering*, *28*, 445-460.

Thompson, C., & Leong, L. Y. C. (February, 2007). *30 Years of Experience Using Ozone in the United States Disinfecting Wastewater. Current Practice and Future Trends in Disinfection: Water, Wastewater, Stormwater, Water Reuse, and Biosolids*. WEF Specialty Conference Series, Pittsburgh, PA, USA.

Tsukamoto, R. Y. (2002). Tratamiento primario avanzado: el paradigma moderno del tratamiento de aguas residuales sanitarias, 2da parte. *Revista Agua Latinoamérica*, *2*(2). Recuperado de http://www.agualatinoamerica.com/docs/pdf/5-6-02int.pdf.

US-EPA (1992). Environmental Protection Agency/US Agency for International Development. Guidelines for water reuse. Office of Wastewater Enforcement and Compliance, Technical report No. EPA/625/R-92/004, Washington, DC, USA.

Vaughn, J. M., Chen, Y. S., Lindburg, K., & Morales, D. (1987). Inactivation of Human and Simian Rotaviruses by Ozone. *Applied and Environmental Microbiology*, 2218-2221.

Wang, F., Gamal El-Din, M., & Smith, D. W. (2004). Oxidation of Aged Raw Landfill Leachate with O_3 only and O_3/H_2O_2: Treatment Efficiency and Molecular Size Distribution Analysis. *Ozone Science and Engineering*, *26*, 287.

WHO (2006). *Guidelines for the Safe Use of Wastewater, Excreta and Greywater. 2: Wastewater Use in Agriculture*. World Health Organization. Recuperado de http://www.who.int.

Yasunaga, N., & Hirotsuji, H. (2008). Efficient Decomposition of Trichloroethylene (TCE) in Groundwater by Ozone-Hydrogen Peroxide Treatment. *Ozone Science & Engineering*, *30*(2), 127-135.

Yuan, Y. (1998). Etiological Study of High Stomach Cancer Incidence among Residents in Wastewater Irrigated Areas. In: World Resources Institute. A Guide to the Global Environment: Environmental Change and Human Health, Oxford University Press, New York. *Environmental Protection Science*, *19*(1), 70-73.

Zamora, F., Rodríguez, N., Torres, D., & Yendis, H. (2008). Efecto del riego con aguas residuales sobre propiedades químicas de suelos de la planicie de Coro, Estado Falcón. *Bioagro*, *20*(3).

Zhang, J., Huck, P. M., Anderson, W. B., & Stubley, G. (2007). A Computational Fluid Dynamics based Integrated Disinfection Design Approach for Improvement of Full-Scale Ozone Contactor Performance. *Ozone Science & Engineering*, *29*(6), 451-460.

Zinder, A., Pert, E. C., & Rexing, D. J. (2006). Ozone Oxidation of Endocrine Disruptors and Pharmaceuticals in Surface Water and Wastewaters. *Ozone Science & Engineering*, *28*(6) 43.

Institutional Address of the Authors

Eliet Veliz
Lidia Asela Fernández
Mayra Bataller

Centro Nacional de Investigaciones Científicas
Dirección de Medio Ambiente
Avenida 25 y 158, Cubanacán, Playa
La Habana, Cuba
eliet.veliz@cnic.edu.cu
asela.fernandez@cnic.edu.cu

José Guadalupe Llanes

Universidad Autónoma de Sinaloa
Facultad de Física y Matemática
Ciudad Universitaria
Blvd. de las Américas y Blvd. Universitarios, s/n, Col Universitaria
Culiacán, Sinaloa, México
Teléfono: +52 (667) 7581 403
fisicomatematicas@live.com.mx

Click here to write the autor

Patrones temporales de flujo del río en las cuencas del norte de México

• José Návar* •
Tecnológico Nacional de México/Instituto Tecnológico de Ciudad Victoria
*Autor de correspondencia

• Liliana Lizárraga-Mendiola •
Universidad Autónoma del Estado de Hidalgo, México

Resumen

Navar, J., & Lizárraga-Mendiola, L. (enero-febrero, 2016). Patrones temporales de flujo del río en las cuencas del norte de México. *Tecnología y Ciencias del Agua*, 7(1), 35-44.

En las cuencas áridas del norte de México, las preocupaciones por los ríos se centran en las variaciones estacionales y de largo tiempo en la descarga de los ríos que pudiera ser atribuida al cambio climático porque controla el suministro de agua para los usos domésticos, industriales, públicos y agrícolas. El objetivo de esta investigación fue separar los componentes del caudal diario y entender los patrones de 172 series de tiempo de cinco ríos del norte de México. Los ríos San Pedro, Sinaloa, Nazas-Aguanaval, San Juan y San Fernando-Soto La Marina nacen en las montañas de las Sierras Madre Oriental y Occidental, y fluyen a través de las planicies del océano Pacífico, el Golfo de México y la Mesa Central del norte de México, proveyendo con más de 90% del suministro de agua para todos los usos. El programa de cómputo Rora separó los flujos base y directo del total. La prueba de Mann-Kendall y el método del Seno S evaluaron las tendencias y magnitud del cambio de la descarga anual, mensual, desviación estándar mensual, y mínimo y máximo diario para los flujos total, directo y base. Los resultados mostraron que los flujos base y directo se encuentran en equilibrio para la mayoría de los ríos, pero más de 40% de las estaciones hidrométricas tuvieron tendencias estadísticamente significativas en cada una de las variables analizadas. Más de 26% de la estaciones mostraron un reducción consistente del caudal en tiempo. Aunque se necesita de investigación adicional para aislar de modo cuantitativo las potenciales fuentes de variación que explican las tendencias temporales, éstas pueden ser preliminarmente atribuidas a la variabilidad climática, en combinación con las prácticas de recursos naturales, pero el efecto del potencial cambio climático no puede ser excluido de estos patrones.

Palabras clave: tendencia negativa, magnificación de la sequía, caudal base, directo y total.

Abstract

Navar, J., & Lizárraga-Mendiola, L. (January-February, 2016). Temporal Patterns in River Flows in Basins in Northern Mexico. Water Technology and Sciences *(in Spanish), 7(1), 35-44.*

In the dry basins in northern Mexico, concern about rivers is focused on seasonal and long-term variations in river flows that may be attributable to climate change, since it affects the water supply for domestic, industrial, public and agricultural uses. The objective of this research was to separate daily flow components and understand the patterns in 172 time-series corresponding to five rivers in northern Mexico. The headwaters of the San Pedro, Sinaloa, Nazas-Aguanaval, San Juan and San Fernando-Soto La Marina rivers are located in the Sierra Madre Occidental and Oriental, and flow through the plains into the Pacific Ocean, the Gulf of Mexico and the Central Plateau in northern Mexico, providing over 90% of the water supply for all uses. The Rora computer program isolated the base and direct flows from the total. The Mann-Kendall test and the Seno S method evaluated the trends and magnitudes of the changes in annual and monthly flow, monthly standard deviation, and daily maximums and minimums for total, direct and base flows. The results found that the base and direct flows were in equilibrium for most of the rivers. Meanwhile, each one of the variables analyzed had statistically significant trends at 40% of the hydrometric stations. Over 26% of the stations showed a consistent reduction in flow over time. Although additional investigations are needed to quantitatively isolate the potential sources of the variations to explain the temporal trends, the causes can preliminarily be attributed to climate variability in combination with natural resource management practices. The effect of potential climate change cannot be excluded from these patterns.

Keywords: *Negative discharge tendency, drought magnification, base flow, direct flow and total discharge.*

Recibido: 02/09/2014
Aceptado: 22/08/2015

Introducción

Las prácticas de gestión convencionales de los recursos hídricos no pueden satisfacer las demandas futuras de agua para el desarrollo en países de zonas áridas, semiáridas y subtropicales (CNUAD, 1992; Postel, 2000; Secretaría de Evaluación Integral, 2006). Las cuencas hidrográficas del norte de México abarcan los cinturones áridos y semiáridos de América del Norte del hemisferio boreal, donde el caudal del río se caracteriza por la descarga temporal y espacial errática y variable (Ward, 1998; Návar-Cháidez, 2012). Además, la agricultura, la población, la industria, el comercio y los servicios, entre otros, confían en el caudal del río para satisfacer las demandas de agua convencionales (Conagua, 2012). En las zonas áridas del norte de México, estos sectores económicos han crecido constantemente en los últimos 60 años debido a (a) el crecimiento de la población y (b) el desarrollo económico por el aumento de los tratados comerciales con otras naciones.

La variabilidad del clima, junto con el aumento creciente de las desviaciones de agua modifica el caudal del río y tiene un peaje en los ecosistemas de humedales (Postel, 2000; Návar-Cháidez y Lizárraga-Mendiola, 2013). La perturbación del caudal del río requiere entonces nuevas estrategias para hacer frente a las demandas de agua convencional y ambiental, creando un circuito de retroalimentación positiva entre el aumento de perturbación del río y la necesidad de adaptación. Para varias cuencas hidrográficas, durante los episodios agudos secos, el caudal del río no cumple con las exigencias convencionales y por lo tanto la sociedad se basa actualmente en la perforación profunda y la transferencia de agua entre cuencas (Conagua, 2012). En paralelo a las transferencias de agua entre cuencas, varias prácticas sustentables de los recursos hidrológicos se están produciendo (Conagua, 2005). Sin embargo, las prácticas no sustentables permanecen en estas cuencas hidrográficas, tales como el alto volumen de irrigación contra la baja productividad de varios distritos de riego, por debajo de la valoración de los recursos hídricos, y el flujo altamente regular de la mayoría de los ríos (Pereyra, Oweis, y Zairi, 2002; Secretaría de Evaluación Integral, 2006). En algunos casos, la eficiencia del uso del agua ha aumentado, lo que resulta en duplicar la productividad con la misma cantidad de agua. Además, la extracción de agua de uso doméstico (a veces referido como el agua gris) está siendo tratada adicionalmente para el riego de campos agrícolas, junto con otras prácticas sustentables (Postel, 2000).

La variabilidad del clima es responsable de episodios de mucha lluvia erráticos y poco frecuentes y anomalías de caudal del río que por lo general comienzan o terminan en largos episodios de sequía, una característica común de norte de México, así como de la mayoría de las tierras secas semiáridas de la misma región. Huracanes y ciclones que entran en el noreste de México tienen un período de frecuencia de cerca de 15 años (Návar-CHAIDEZ, 2012). Estos fenómenos climáticos restauran acuíferos y el almacenamiento de embalses, así como los componentes del flujo de ríos. En los períodos de sequía, el almacenamiento se agota con frecuencia. Los episodios de sequía de varias escalas temporales, interanual, 3-7 años, 9-12 años y 60-80 años han sido bien documentados en la región y se han correlacionado con fenómenos climáticos de gran escala, tales como El Niño/Oscilación del Sur, la Oscilación Decenal del Pacífico, Oscilación Multidecadal del Atlántico, o por una combinación de cualquiera de estos eventos climáticos de escala sinóptica (Cavazos y Hastenrath, 1990; Comrie y Glenn, 1998). El cambio climático también puede a su vez contribuir a ampliar la variabilidad del caudal de los ríos de la mayoría de las cuencas hidrográficas áridas y semiáridas. De acuerdo con Mulholland et al. (1997), cuyas proyecciones se basan en los modelos de circulación global, el norte de México probablemente recibirán entre 5 a 20% menos de precipitaciones y entre el 5 y el 25% menos de caudal con la continuación de la tendencia de calentamiento global.

Las sequias de las décadas de los años de 1950 y de 1990, y las sequías interanuales de de 2010 han llevado a renovar rápidamente los esfuerzos para cuantificar el almacenamiento de

agua y la longitud de los patrones temporales de sequía. Por lo tanto, este informe se enfoca en si los componentes del caudal de los ríos de 172 estaciones de medición de cinco ríos muestran patrones monótonos temporales en las regiones hidrológicas de Sinaloa (RH10), Presidio-San Pedro (RH 11), Nazas-Aguanaval (RH 36), San Juan (RH 37) y San Fernando-Soto La Marina (RH 25). La hipótesis de trabajo fue que no hay ningún cambio consistente en cualquiera de los parámetros o componentes del caudal a lo largo del tiempo y, por lo tanto, ningún cambio en la magnitud de la descarga.

Materiales y métodos

El área de estudio

El área de estudio abarca las cuencas de Sinaloa, Presidio-San Pedro, Nazas-Aguanaval, San Fernando-Soto La Marina y el río San Juan. Estas cuencas hidrográficas abarcan los estados del norte de México de Sinaloa, Nayarit, Durango, Chihuahua, Zacatecas, Coahuila, Nuevo León y Tamaulipas.

La información demográfica presente y futura en cada cuenca hidrográfica se presenta en el cuadro 1.

Una gran diversidad de climas caracteriza al norte de México (Conagua, 2005). El clima frío es típico de los picos más altos y las tierras altas de las cordilleras montañosas. Los climas templados caracterizan los valles centrales y las mesas de las cordilleras. Los climas subtropicales y tropicales encaran los bajos rangos de las llanuras del océano Pacífico y el Golfo de México. Los climas secos son típicos en el desierto Central de Chihuahua y el sur de las Grandes Llanuras de América del Norte.

El pino, el roble y una mezcla de los bosques de pino-encino cubren extensas zonas altas de las cordilleras de la sierras madre del este y oeste. Los bosques montañosos, dominadas por arbustos espinosos y, árboles de hojas anchas, se distribuyen ampliamente en los paisajes de los altiplanos de las principales cadenas montañosas. La flora tropical y subtropical se distribuyen en las llanuras y tierras bajas de los altiplanos que se ubican frente a los océanos. La cubierta de, plantas xerofíticas, seca y de chaparral es típica en el centro de Desierto de Chihuahua y el sur de las grandes llanuras de América del Norte. Los bosques tamaulipecos de matorral espinoso, acacias y mezquite se extienden hacia las tierras bajas del océano Pacífico, el Golfo de México septentrional y las Grandes Llanuras de América del Norte (Rzedowskii, 1980).

Los litosoles poco profundos son típicos de las principales cadenas montañosas. Los regosoles xerosoles y yermosoles profundos, caracterizan el paisaje del centro del desierto de Chihuahua. Los vertisoles profundos se distribuyen en las llanuras de las tierras bajas del océano Pacífico y el norte del Golfo de México.

Metodología

Se seleccionó un total de 172 estaciones hidrométricas situadas en los cinco principales ríos de caudal para separar los componentes del caudal y probar las series de tiempo para patrones temporales monótonos (Figura 1). El número de estaciones hidrométricas analizadas por cuenca se describe en la Tabla 2.

Tabla 1. Crecimiento demográfico de cinco cuencas hidrográficas del norte de México (Fuente: Conapo, 2000).

Cuenca hidrográfica	Habitantes		
	2006	2015	2030
1. Sinaloa (RH 10)	2 279 975	2 431 372	2 612 141
2. Presidio-San Pedro (RH 11)	771 164	782 424	781 339
3. Nazas-Aguanaval (RH 36)	1 766 811	1 868 697	1 977 106
4. San Juan (RH 37)	4 651 828	5 242 335	6 069 918
5. San Fernando-Soto La Marina (RH 25)	682 033	727 322	781 397
Total	10 151 811	11 052 150	12 221 901

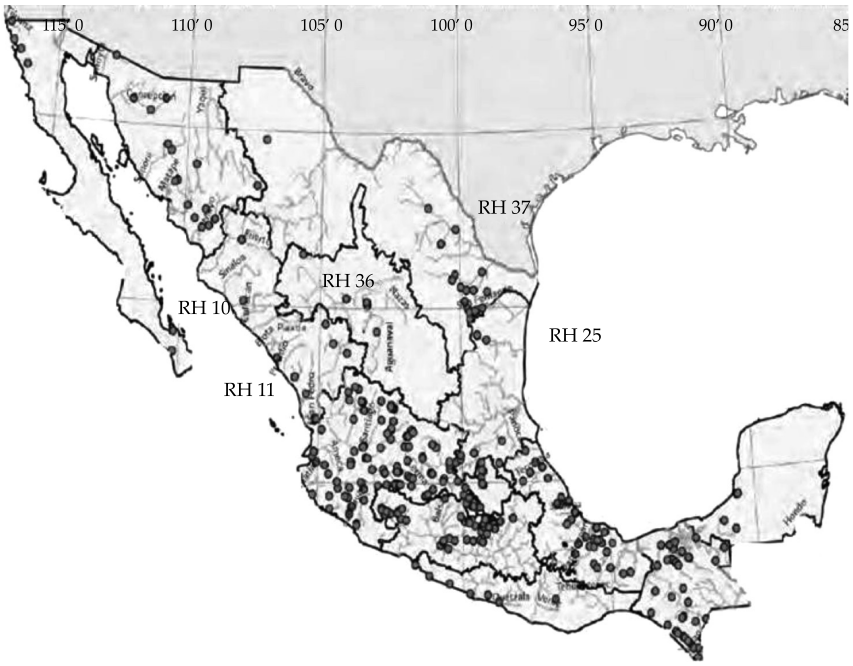

Figura 1. Mapa que muestra varias estaciones hidrométricas de cinco cuencas hidrográficas en el norte de México.

Tabla 2. El número de estaciones hidrométricas analizadas en los patrones temporales y la magnitud de la descarga del río en cinco cuencas en el norte de México.

Cuenca hidrográfica	Estación hidrométrica	Periodo de registro promedio
1. Sinaloa (RH 10)	58	1960-1999
2. Presidio-San Pedro (RH 11)	15	1970-1998
3. Nazas-Aguanaval (RH 36)	33	1940-1999
4. San Juan (RH 37)	30	1955-1999
5. San Fernando-Soto La Marina (RH 25)	36	1970-1999

Datos analizados de registros de Conagua (2005).

Análisis de separación hidrográfica

La separación de múltiples hidrográficas de río en el caudal de base y directo es una tarea difícil. Para simplificar esta tarea para las series temporales del caudal del río a largo plazo, la descarga diaria total se dividió en el caudal de base y directo o rápido usando las técnicas de separación hidrográfica de RORA (Rutledge, 1998). Antes de que los datos de descargas diarias se introdujeran en el programa de cómputo RORA, se comprobó: a) la presencia de largos períodos de recesión y b) la ausencia de datos faltantes intermedios. Screen, un programa de cómputo, comprueba los datos de recesión y continuidad. El índice de la recesión se requiere con el fin de definir la curva maestra. Una vez que se desarrolla la curva maestra, PART se utiliza como un módulo de RORA para separar el caudal base y directo.

La descarga mensual total, la desviación estándar de descarga diaria (dentro de un mes determinado), la descarga anual, el flujo de base anual, y el flujo directo anual o flujo rápido son

los parámetros y componentes derivados de los datos de descargas diarias. La estadística no paramétrica de Mann-Kendall se probó para de tendencias monótonas temporales sobre los datos de series de tiempo del caudal del río. Esta prueba revela la presencia o ausencia de patrones monótonos temporales crecientes o decrecientes.

El método no paramétrico de Sen cuantificó la magnitud del cambio de pendiente en las cinco variables de descarga. El coeficiente de la pendiente describe un cambio de la variable por unidad de tiempo (escala de tiempo anual). El método de Sen asume una tendencia monótona en la serie de tiempo.

Los datos sobre los cambios de uso del suelo fueron compilados por varios ecosistemas del norte de México. Además, también se evaluaron los cambios en los parámetros de las precipitaciones y la temperatura para varias estaciones climáticas. Las correlaciones entre los parámetros del caudal de los ríos y los fenómenos climáticos de gran escala [El Niño / Oscilación del Sur (ENSO), Oscilación Decenal el Pacífico (ODP), y la Oscilación Multidecadal del Atlántico (AMO)] reportadas anteriormente ayudaron a entender las fuentes de variabilidad del caudal del río. Esta información, además del crecimiento de la población, se vinculó a los posibles patrones temporales potenciales y sutiles de caudal del río..

Resultados

La tabla 3 muestra las estadísticas de los componentes de caudal de río para las cinco cuencas hidrográficas estudiadas. El flujo base y el directo son estadísticamente similares para todas las cuencas. Es decir, en promedio, 50% de la descarga es el caudal base bajo extendido que se levanta desde poca profundidad (tierras altas de la cordillera) y acuíferos de tierra baja de poca profundidad. El restante 50% de la descarga es de flujo directo producido durante

Tabla 3. Caudal base y estadísticass de flujos rápidos para varios rios de cinco cuencas hidrográficas del norte de México..

Cuenca hidrográfica	Variables de descarga	
	Flujo base (± intervalos de confianza) (%)	Flujo rápido (± intervalos de confianza) (%)
1. Sinaloa (RH 10)	0.52 (± 0.08)	0.48 (± 0.08)
2. Presidio-San Pedro (RH 11)	0.52 (± 0.08)	0.48 (± 0.08)
3. Nazas-Aguanaval (RH 36)	0.56 (± 0.09)	0.44 (± 0.09)
4. San Juan (RH 37)	0.57 (± 0.08)	0.43 (± 0.09)
5. San Fernando-Soto La Marina (RH 25)	0.50 (± 0.06)	0.50 (± 0.08)

Tabla 4. Número de estaciones de medición con patrones monótonos temporales estadísticamente significativos de varios parámetros del caudal de río.

	Parámetros del caudal del río				
Cuenca hidrográfica	Anual	Mensual	Desv. est.	Caudal base	Caudal directo
Sinaloa	25(-4, +21)	26(-5, +21)	28(-17, +11)	28(-3, +25)	27(-16, +11)
San Pedro	6(-4, +2)	5(-3, +2)	6(-6, +0)	2(-0, +2)	6(-6, +0)
Nazas	18(-15, +3)	18(-15, +3)	19(-16, +3)	11(-7, +4)	18(-15, +3)
San Juan	13(-11, +2)	14(-12, +2)	12(-9, +3)	12(-8, +4)	12(-8, +4)
San Fernando	12(-9, +3)	12(-9, +3)	8(-7, +1)	18(-14, +4)	8(-7, +1)
Total	74(-43, +31)	75(-44, +31)	73(-55, +18)	71(-32, +39)	71(-52, +19)
Ratio (%)	43(25, 18)	44(26, 18)	42(32, 10)	41(19, 22)	41(30, 11)

Desv. est. = Desviación estándar de la descarga mensual. La última fila se estimó de la razón entre el número de estaciones de medición con significancia estadística y el número total de estaciones de medición analizadas.

e inmediatamente después de la temporada de lluvias que se extiende de junio a septiembre. El flujo hortoniano superficial y el subsuperficial rápido controlan el caudal directo. Las cuencas hidrográficas que desembocan en el océano Pacífico (RH10 y RH11) y en el interior de la Meseta Central (HR 036) tienen un tipo de precipitación unimodal-monzónico, con un pico principal en julio. Por otro lado, las cuencas hidrográficas que desembocan en el Golfo de México presentan un tipo bimodal de la distribución de precipitaciones con dos picos, el primero durante mayo-junio y el último en septiembre-octubre.

La tabla 4 muestra el número y porcentaje de estaciones de medición con tendencias monótonas temporales negativa (-) y positiva (+) estadísticamente significativas.

En general, más de 40% de cada parámetro analizado del caudal del río mostraron tendencias temporales monótonas estadísticamente significativas. Es decir, las series de tiempo del caudal del río no son estacionarias en el primer momentum.

Sin embargo, del total, en promedio, 26% tenían una tendencia negativa y el restante 16% tenía una tendencia positiva. Los parámetros total anuales y totales mensuales del caudal de los ríos están disminuyendo de manera constante en las cuencas hidrográficas de San Pedro, Nazas, San Juan, y San Fernando, pero está aumentando en la mayoría de estaciones de medición a lo largo de los ríos de Sinaloa.

La mayoría de las estaciones de medición con patrones temporales en declive del caudal del río se extienden en las cuencas hidrográficas áridas, semiáridas y subtropicales RH11, RH36, RH37 y RH25, caracterizadas por tener un área importante en los valles interiores del desierto de Chihuahua y las Grandes Llanuras del sur de Norte América. En estas regiones fisiográficas, pérdidas monzónica erráticas, de precipitaciones poco frecuentes y de elevadas evapotranspiración controlan el ciclo hidrológico. El dominio humano sobre el caudal del río es de menor importancia en estas cuencas y por lo tanto el caudal del río no está tan regulado como lo es, por ejemplo, en el RH10.

La mayoría de las estaciones de medición con tendencias monótonas temporales positivas en el caudal del río total anual y total mensual se distribuyen a lo largo de la cuenca de Sinaloa (RH10), una cuenca hidrográfica con la mayoría de las estaciones hidrométricas colocadas a lo largo de las tierras bajas del océano Pacífico. La mayoría de las estaciones de medición se colocaron por debajo de los distritos de riego, embalses y centros urbanos, donde el control humano ejercido sobre los recursos hídricos (aumento de las desviaciones de los embalses de las tierras altas, así como en los recursos de aguas subterráneas profundas y descarga del exceso de agua en otros lugares) puede explicar la tendencia temporal positiva de la descarga de los ríos. Por lo tanto, el aumento de los patrones del caudal de los ríos en el tiempo puede explicarse en parte por las prácticas de gestión de los recursos de agua. Este efecto enmascara en el corto plazo los cambios potenciales sutiles en las variables locales hidroclimáticas de las tierras bajas del océano Pacífico.

Los caudales directos reducidos y los caudales base incrementados en el tiempo podrían explicarse por el efecto del caudal regulado por los embalses artificiales, que reducen la variación de descarga de la mayor parte de las estaciones de medición debajo de los embalses cuando los ríos se usan como cuencas para transportar agua a los distritos de riego. Varias secciones del río están experimentando la presencia de caudales directos más pequeños y caudales base más grandes. La descarga constante de los alcantarillados municipales y el exceso de riego en arroyos puede explicar parcialmente estas observaciones.

El caudal base está aumentando en la mayoría de las estaciones de medición a lo largo de las cuencas de Sinaloa y San Pedro, pero está disminuyendo en la mayoría de las estaciones de medición restantes en las cuencas de Nazas, San Juan y San Fernando. El exceso de riego, el vertido municipal y el aumento de desviaciones de los acuíferos profundos de las cuencas hidrográficas interiores explican en parte esta tendencia. Los cambios sutiles en la frecuencia de las precipitaciones, la profundidad y la inten-

Tabla 5. La pendiente media (e intervalos de confianza) para cinco parámetros de descarga con tendencia temporal negativa de 172 estaciones de medición situadas en cinco cuencas hidrográficas en el norte de México.

	Parámetros del caudal del río (Mm^3 $año^{-1}$)				
	Anual	**Mensual**	**Desv. est.**	**Caudal base**	**Caudal directo**
Sinaloa	-3.66(2.19)	-0.82(1.06)	-0.32(0.41)	-1.91(0.51)	-9.69(6.25)
San Pedro	-0.11(0.12)	-2.05(0.94)	-2.52(4.89)	-1.02(0.77)	0(0)
Nazas	-4.74(3.98)	-0.40(0.31)	-0.50(0.28)	-1.31(0.92)	-1.28(0.80)
San Juan	-0.84(1.11)	-2.10(0.92)	-0.01(0.01)	-1.58(0.61)	-2.73(3.30)
San Fernando	-16.47(8.17)	-2.56(2.03)	-2.53(1.02)	-0.12(0.10)	-10.01(2.61)
Promedio	-5.16(3.11)	-1.59(1.05)	-1.18(1.32)	-1.19(0.58)	-4.74(2.59)

Desv. est. = Desviación estándar de la descarga mensual.

sidad también pueden estar contribuyendo al aumento de la recarga de acuíferos, que pueden a su vez controlar la descarga del caudal base. En varias cuencas hidrográficas, los cambios en la frecuencia y la profundidad de las precipitaciones, junto con el aumento de la temperatura media anual pueden, a su vez, contribuir para modificar los parámetros de la descarga de los ríos.

Los flujos directos también están disminuyendo en la mayoría de las estaciones de medición de todas las cuencas hidrográficas. La mayor capacidad de almacenamiento de embalses artificiales por encima de 30 000 Mm^3 en zonas áridas, semiáridas y subtropicales puede explicar en parte el control que ejerce el exceso de precipitación en el caudal de los ríos. La velocidad de cambio de los parámetros de descarga se presenta en el cuadro 5.

La mayoría de los valores de pendiente estadísticamente se desvían de cero destacando la significación estadística de la disminución de la descarga directa en el tiempo. Para la descarga anual total, las cuencas de San Fernando (-16.47 Mm3 al año), Nazas (-4.74 Mm^3 al año) y Sinaloa (-3.66 Mm^3 al año) tienen las mayores reducciones de la descarga total anual en el tiempo. El resto de las cuencas presentan una descarga total anual de menos de -1.00 Mm^3 al año. Para el caudal mensual de río, las reducciones de descarga son más importantes en las cuencas de San Pedro (-2.05 Mm3 al año), San Juan (-2.10 Mm3 al año) y San Fernando (-2.56 Mm^3 al año).

Los patrones temporales de los caudales pico se habían modificado notablemente (con una reducción en promedio de 4.7 m^3 por segundo) en contraste con la pequeña reducción del caudal base (reducción o 1.4 m^3 por segundo) para todas las cuencas. Las cuencas de Sinaloa y San Fernando presentan el mayor control humano sobre el caudal del río y por lo tanto en los caudales máximos. Esto, a su vez, se correlaciona bien con el número de embalses artificiales. Aunque el caudal base se ha modificado poco en contraste con el caudal máximo, su importancia está fuera de cuestión en los climas áridos durante la estación seca.

La población está aumentando en la región a una tasa anual media de 1% para las cinco cuencas. hidrográficas. En la actualidad, existen más de 10 M de habitantes en estas cuencas y se espera que superarán los 12 M para el año 2030. Este nuevo escenario prevé un incremento en la demanda de agua de más de 20% para el suministro municipal y, potencialmente, para suministros industriales y de riego, ya que estos sectores de la economía están ligados al crecimiento demográfico.

Discusión

La regulación del caudal del río por la construcción de embalses, la explotación de los recursos de aguas subterráneas profundas, el vertido municipal, y el exceso de riego en arroyos se observó consistentemente por el efecto contras-

tante del caudal base aumentado y los caudales directos reducidos de 7% de las estaciones hidrométricas estudiadas. Los grandes embalses se habían construido con una huella importante sobre el caudal del río. La capacidad de almacenamiento ha aumentado exponencialmente en las últimas cuatro décadas y en la actualidad el norte de México tiene una capacidad de almacenamiento normal por encima de 30 000 Mm^3, ubicada en 10 embalses principales, cada uno con una capacidad máxima de almacenamiento normal de más de 1 000 Mm^3 en las cinco cuencas.

La gestión de los recursos naturales contribuye parcialmente a perturbar también el caudal del río. Un efecto acoplado de una mayor caudal directo y un caudal base reducido se observó en varias estaciones de medición. A pesar de que debe haber otras causas que explican este efecto de contraste, la deforestación y la degradación de los recursos de suelos parecen jugar un papel importante en la promoción de procesos que conducen a los caudales base reducidos (recarga de aguas subterráneas) y a los caudales directos incrementados (infiltración reducida y aumento de los escurrimientos superficiales hortonianos). Los cambios en el uso de la tierra de bosques nativos a agricultura o pastizales conducen a tasas mayores de escurrimiento superficial y erosión del suelo (Návar y Synnott, 2000a; 2000b). Por lo tanto, la desaparición de los bosques de matorral espinoso tamaulipecos que se correlaciona bien con la expansión de la agricultura y la minería intensivas en las llanuras del noreste de México pueden reducir a su vez la recarga de aguas subterráneas.

La deforestación modifica los componentes del ciclo hidrológico y la descarga del río muestra claramente su huella. La tasa anual de deforestación de los ecosistemas del noreste de México se aproxima a 1.7%, causada principalmente por la agricultura y la minería de gas intensivas (Návar-Cháidez, 2008). La tasa de deforestación se acerca a 1.70% en las llanuras costeras del océano Pacífico, en el RH 10 y 11, de acuerdo con los estudios de cambio de uso del suelo realizados sobre bosques secos tropicales. Los bosques templados se distribuyen en altas cordilleras y tienen una tasa media anual de deforestación de 0.50% (Ramos-Juárez, 2005). En estos ecosistemas, las prácticas de deforestación incluyen sobrepastoreo, incendios forestales, plagas y enfermedades, la extracción de madera ilegal, construcción no planificada de caminos forestales, entre otros. La capacidad de carga ganadera a veces es entre 2 a 5 veces mayor que la recomendada (Manzano y Návar, 2000; Manzano, Návar, Pando, y Martínez, 2000).

Las prácticas de deforestación también pueden aumentar aún más las anomalías de los regímenes de caudal del río en un futuro próximo, ya que las proyecciones en escenarios convencionales del área, previamente cubiertas por matorral espinoso tamaulipecos hasta 80 490 km2 en la década de 1950 (Návar-CHAIDEZ, 2008), se reducirían a 22 000 km2 en el año 2020 y a 4 974 km2 para el año 2100. Los bosques templados se reducirían 10% para el año 2020 y 40% para el año 2100 con respecto al área boscosa total medida en el año 2000. Se espera que las prácticas de desforestación reduzcan aún más el flujo base y aumenten los flujos directo y pico de la mayoría de las cuencas de tierras altas.

El cambio climático también puede magnificar parcialmente oscilaciones del caudal de río. Sin embargo, este control de la variabilidad de la descarga de los ríos no puede cuantificarse de manera apropiada y se debe confiar en las proyecciones ordinarias. Utilizando modelos de circulación global, Mulholland et al. (1997) y el IPCC (2014) predijeron que el noreste de México podría recibir potencialmente menos lluvia (entre -5 a -20%) y producir menos caudal de los ríos (entre 5-25% menos de descarga) debido al aumento de las temperaturas globales. Méndez-González, Návar-Cháidez y González-Ontiveros (2008) han observado evidencia estadística de que el número de días de lluvia y la precipitación total anual han estado disminuyendo de manera constante en las últimas cuatro décadas en varias estaciones climáticas en el noreste de México.

En la actualidad, la variabilidad del clima es la fuente más importante de anomalías de caudal de los ríos, ya que los parámetros del mismo se correlacionan bien con los fenómenos

climáticos de gran escala. Návar-Cháidez y Lizárraga-Mendiola (2013) asociaron fenómenos climáticos de gran escala con variables de descarga en una cuenca hidrográfica boscosa del norte de México; por ejemplo, el Índice de Oscilación del Sur, IOS, se correlacionó negativamente, la DOP se correlacionó positivamente y la AMO se correlacionó negativamente con la descarga de los ríos.

Dado este estado de entendimiento, el fortalecimiento de las prácticas de manejo sustentables de los recursos hídricos debe abordarse en paralelo a la explotación de nuevas fuentes del caudal de los ríos en las cuencas hidrográficas con descarga errática de ríos, población alta y crecimiento industrial. Los ríos, lagos y acuíferos deben suministrar toda el agua convencional (pública, doméstica, agrícola e industrial) y ambiental (caudal ambiental para ecosistemas). Debido a la frecuencia errática de los sucesos climáticos como huracanes, ciclones y depresiones tropicales, el almacenamiento en los embalses construidos debe aumentarse para recoger y almacenar la mayor parte del caudal de los río en épocas de alta disponibilidad. En las cuencas hidrográficas caracterizadas por períodos de sequía de largo plazo y tasas importantes de desarrollo regional, cuando se agote el almacenamiento, deben explotarse de forma sustentable otras fuentes de suministro de agua, tales como la transferencia entre cuencas. El caudal de los ríos y la recarga de agua subterránea también deben protegerse en las cuencas hidrográficas receptoras y donantes (Postel, 2000; Schmandt et al, 2000) y el caudal ambiental debe planificarse, transportarse y forzarse en los ríos regulados (Návar-Cháidez, 2014).

La productividad también debe duplicarse por cada gota de agua que se desvía de los embalses, arroyos y acuíferos con el fin de cumplir con el suministro convencional, así como para conservar el caudal del río para cumplir con la conservación ambiental (Postel, 2000). La situación actual y el futuro probable consideren escenarios que prevén la necesidad de la implementación de las siguientes prácticas sustentables principales para mejorar la gestión sustentable de los recursos hídricos: (a) aumentar el almacenamiento mediante la construcción de embalses, el manejo adecuado de acuíferos, y otras estrategias tales como la implementación del régimen del caudal ambiental de ríos regulados, (b) la reducción del uso de agua per cápita, (c) el aumento de la eficiencia del uso del agua en los municipios, industrias y el sector agrícola, (d) tratar las aguas residuales antes de que se vierten en ríos y embalses, con el objetivo de evitar el deterioro de otras fuentes de abastecimiento de agua y para ser reutilizado sin recurrir a la cuenca hidrográfica, (e) valorar correctamente los recursos hídricos.

Conclusiones

El caudal de los ríos está en transición en varias de las cuencas hidrográficas del norte de México. Actualmente, el caudal base y el directo constituyen aproximadamente 50% cada uno del total de la descarga de ríos diaria. Un poco más del 40% de cada uno de los cinco parámetros del caudal de los ríos presentan las tendencias temporales con significación estadística para el período de 1940 a 1999. En promedio 26% de cada uno de los cinco parámetros evaluados tenía una tendencia negativa que forzaba a la disminución del caudal del río a través del tiempo. La variabilidad del clima, la regulación de caudal de los ríos, la deforestación, la degradación de la tierra, y los cambios climáticos potencialmente sutiles parecen explicar las tendencias temporales monótonas a la baja. Es importante fortalecer las prácticas de gestión sustentables de caudal de los ríos, en paralelo a la explotación de nuevas fuentes sustentables del caudal de los ríos para cumplir con el suministro convencional, así como con el ambiental, en cuencas hidrográficas con alto crecimiento demográfico y económico regionales, con el objetivo de duplicar la productividad de cada gota de agua desviada de arroyos, lagos y acuíferos.

Referencias

Cavazos, T., & Hastenrath, S. (1990). Convection and Rainfall over Mexico and their Modulation by the Southern Oscillation. *International Journal of Climatology*, *10*, 377-386.

Conagua (2005). *Estadísticas del agua en México*. México, DF: Comisión Nacional del Agua, Secretaría de Medio Ambiente y Recursos Naturales.

Conagua (2012). *Estadísticas del agua en México*. México, DF: Comisión Nacional del Agua, Secretaría de Medio Ambiente y Recursos Naturales.

Conapo (2000). *Estimaciones de la población en México*. México, DF: Consejo Nacional de Población.

Comprehensive Assessment Secretariat (2006). *Insights from the Comprehensive Assessment of Water Management in Agriculture*. Stockholm: World Water Week.

Comrie, A. C., & Glenn, E. C. (1998). Principal Components-Based Regionalization of Precipitation Regimes across the Southwest United State and Northern Mexico, with Application to Monsoon Precipitation Variability. *Climate Research*, *10*, 201-215.

IPCC (2014). *Impacts, Adaptation, and Vulnerability. Summary for Policy Makers*. Cambridge, UK: Intergovernmental Panel on Climate Change, Cambridge University Press.

Manzano, M., & Návar, J. 2000. Desertification Processes Associated to Overgrazing Practices in Tamaulipan Thorn Scrub of Linares, N. L., Mexico. *Journal of Arid Environments*, *44*, 1-17.

Manzano, M., Návar, J., Pando, M., & Martínez, A. (2000). Overgrazing and Desertification in México: Highlights on the Northeastern Region. *Annals of Arid Zone*, *39*, 285-304.

Méndez-González, J., Návar-Cháidez, J. J., & González-Ontiveros, V. (2008). Análisis de tendencias de precipitación (1920-2004) en México. *Investigaciones Geográficas*, *65*, 38-55.

Mulholland, P. J., Best, G. R., Coutant, C. C., Hornberger, G. M, Meyer, J. L., Robinson P. J., Stemberg, J. R., Turner, R. E., Vera-Herrera, F., & Wetzel, R. G. (1997). Effects of Climate Change on Freshwater Ecosystems of United States and the Gulf of Mexico. *Hydrological Processes*, *11*, 949-970.

Návar, J. & Synnott, T. 2000a. Soil erosion and land use in Northeastern Mexico. *Terra* 18 (3): 247-253.

Návar, J. and Synnott, T. 2000b. Soil infiltration and land use in Northeastern Mexico. *Terra* 18 (3). 255-262.

Návar, J. (2008). Reconstrucción de las sequías en los últimos 10 mil años en el norte de México. *Agrofaz*, *8*, 41- 53.

Návar-Chaidez, J. J. (2008). Carbon Fluxes Resulting from Land Use Changes in the Tamaulipan Thorn Scrub of Northeastern Mexico. *Carbon Balance and Management*, doi: 10.1186/1750-0680-3:6: 1-11.

Návar, J. (2013). Modeling the Water Balance Components for the Management of the Watershed 'La Rosilla', Durango, Mexico. *Agrofaz*, *13*(1), 91-103.

Návar-Chaidez, J. J. (2011). Water Scarcity and Land Degradation in the Rio San Juan Watershed of Northeastern Mexico. *Frontera Norte*, *23*(46): 125-150.

Návar-Cháidez, J. J., & Lizárraga-Mendiola, L. G. (2013). Hydro-Climatic Variability and Forest Fires in Mexico's Northern Temperate Forests. *Geofísica Internacional*, *52*, 5-20.

Pereyra, L. S., Oweis, T., & Zairi, A. (2002). Irrigation Management under Water Scarcity. *Agricultural and Water Management*, *57*, 175-206.

Postel, L. S. (2000). Entering an Era of Water Scarcity: The Challenges Ahead. *Ecological Applications*, *10*(4): 941-948.

Ramos-Juárez, S. (2005). *Cambios de uso del suelo en la cuenca del río San Pedro*. Tesis de Licenciatura. Durango, México: Facultad de Ciencias Forestales, Universidad Juárez del Estado de Durango.

Rutledge, A. T. (1998). *Computer Programs for Describing the Recession of Ground-Water Discharge and for Estimating Mean Ground-Water Recharge and Discharge from Streamflow Data-Update* (43 pp.). Washington, DC: U.S. Geological Survey Water-Resources Investigations Report 98-4148.

Rzedowskii, J. (1980). *La vegetación de México*. México, DF: Editorial Limusa.

Schmandt, J., Aguilar, I, Armstrong, N., Chapa, L. Contreras, S., Edwards, R., Hazelton, J., Mathis, M. Návar, J., Vogel, E., & Ward, G. (March 31, 2000). *Water and Sustainable Development. Executive Summary*. EPA Research Agreement R 824799-01-0.

UNCED (1992). *United Nations Conference on Environment and Development. Agenda 21, Chapter 18, sections 8 and 9*. Rio de Janeiro: UNCED.

Ward, G. (1998). *Water Supply in the US Side of the Lower Rio Bravo/Rio Grande Watershed. HARC-ITESM Joint Research Project on Water and Sustainable Development in the Binational Lower Rio Grande/Rio Bravo Basin*. Monterrey, Mexico: ITESM.

Dirección institucional de los autores

Dr. José Návar

Tecnológico Nacional de México/Instituto Tecnológico de Ciudad Victoria
Blvd. Emilio Portes Gil 1301 Pte.
87010 Ciudad Victoria, Tamaulipas, México
Teléfono: +52 (834) 1532 000, extensión 330
jnavar5978@gmail.com

Dra. Liliana Lizárraga-Mendiola

Universidad Autónoma del Estado de Hidalgo
Área Académica de Ingeniería
Mineral de la Reforma
Carr. Pachuca-Tulancingo km 4.5
Col. Carboneras, Mineral de la Reforma
42184, México
lililga.lm@gmail.com

Click here to write the autor

Validation of a Model to Estimate the Wet Bulb Dimensions in Drip Irrigation

• Fidencio Cruz-Bautista* •
Universidad de Sonora, México
*Corresponding Author

• Alejandro Zermeño-González • Vicente Álvarez-Reyna • Pedro Cano-Ríos •
Universidad Autónoma Agraria Antonio Narro, México

• Miguel Rivera-González •
Centro Nacional de Investigación Disciplinaria en Relación Agua, Suelo, Planta, Atmosfera, México

• Mario Siller-González •
Centro de Investigación y de Estudios Avanzados del Instituto Politécnico Nacional, México

Abstract

Cruz-Bautista, F., Zermeño-González, A., Álvarez-Reyna, V., Cano-Ríos, P., Rivera-González, M., & Siller-González, M. (January-February, 2016). Validation of a Model to Estimate the Wet Bulb Dimensions in Drip Irrigation. *Water Technology and Sciences* (in Spanish), 7(1), 45-55.

The ability of an experimental model to simulate the advance of water in the wet bulb was evaluated. The aim was to verify its reliability for use in the design and operations of drip irrigation systems. Models used as a reference included Schwartzman and Zur, Amin and Ekhmaj, Kandelous and Liaghat and Abbasi. Field measurements were taken for evaluation purposes. A statistical comparison was preformed with coefficients of determination (R2) and the root mean square error (RMSE). R2 indicates the correlation between the modeled results and the field measurements, and the RMSE shows the capacity of the models to simulate the advance of water in the wet bulb. These statistical comparisons indicate that the experimental model simulates the lateral and vertical advance of water in the wet bulb with a reliability of 91 and 96%, with an estimated standard error of 2.7 and 3%, respectively. The R2 and the RMSE also showed that the experimental model that used clay loam soil with emitter flows of 2 and 4 liters per hour resulted in the modeled data and the field observations having the most similar values in terms of the advance of the wet bulb.

Keywords: Simulation, mathematical model, wetted soil volume, drip irrigation, wetting-pattern.

Resumen

Cruz-Bautista, F., Zermeño-González, A., Álvarez-Reyna, V., Cano-Ríos, P., Rivera-González, M., & Siller-González, M. (enero-febrero, 2016). Validación de un modelo para estimar la extensión del bulbo de humedecimiento del suelo con riego por goteo. Tecnología y Ciencias del Agua, *7(1), 45-55.*

Se evaluó la capacidad de un modelo experimental para simular el avance del agua en el bulbo de humedecimiento. La finalidad fue verificar su confiabilidad para su uso en el diseño y operación de los sistemas de riego por goteo. Como referencia se emplearon los modelos de Schwartzman y Zur, Amin y Ekhmaj, Kandelous, Liaghat y Abbasi, y para la evaluación se realizaron mediciones de campo. La comparación estadística se hizo con los coeficientes de determinación (R^2) y la raíz del error cuadrático medio (RECM); donde R^2 indica la correlación que existe entre los resultados modelados y las mediciones realizadas en campo y RECM muestra la capacidad de los modelos para simular el avance del agua en el bulbo de humedecimiento. Estos estadísticos de comparación indicaron que el modelo experimental simula el avance lateral y vertical del agua en el bulbo de humedecimiento con una confiabilidad de 91 y 96%, con un error estándar de estimación de 2.7 y 3%. El R^2 y la RECM también mostraron que la mejor aproximación entre los datos modelados y los observados en campo respecto al avance del agua en el bulbo húmedo se obtuvo con el modelo experimental para un suelo franco arcilloso a descargas de emisor de 2 y 4 litros por hora.

Palabras clave: *simulación, modelo matemático, volumen de suelo mojado, riego por goteo, patrón de humedecimiento.*

Received: 18/07/2012
Accepted: 11/09/2015

Introduction

The water distribution pattern in the soil is a characteristic that significantly influences the design and operations of local irrigation systems, given that its extension, depth and diameter should coincide with the plants' root systems and the spacing between emitters and irrigation lines. The distribution of water under the emitter can be determined using three methods: a) direct field measurements of the volume of wet soil, b) use of sensors to measure changes in the water content of the soil and c) models to simulate the movement of water in the soil (Gil-Marín, 2001; Arbat, Barragán, Puig, Poch, & Ramírezde- Cartagena, 2003; Ainechee, Baroomand- Nasab, & Behzad, 2009). Several studies have been performed to determine the wetting pattern of water in the soil using empirical, analytical and numerical models derived from experimental observations and by solving the Richards equations (Dasberg & Or, 1999; Cook, Fitch, Thorburn, Charlesworth, & Bristow, 2006;Kandelous & Simunek, 2010). Although the calculations of many of these models incorporate prediction variables such as the emitter flow, applied water volume and hydraulic properties of the soil, many are not validated or tested under field conditions (Kandelous & Simunek, 2010; Nafchi, Mosavi, & Parvanak, 2011). In addition, none of the models consider the different physical and hydraulic properties of the different strata in the soil profile. Furthermore, most of the analytical and numerical models are not directly applicable to the design and management of local irrigation systems and are based on solutions that have large restrictions (Ramírez-de-Cartagena & Sáinz-Sánchez, 1997). Meanwhile, empirical models have typically been developed through regression analyses of observational or field data (Ramírez-de-Cartagena & Sáinz-Sánchez, 1997; Kandelous & Simunek, 2010). For example, Schwartzman and Zur (1986) developed an empirical model derived from experimental observations and a dimensional analysis to estimate the vertical and horizontal advance of the wetting front. Amin and Ekhmaj (2006) evaluated the Schwartzman and Zur (1986) model using experimental data and included the saturated water content of the soil as an additional prediction parameter. Later, Ainechee, Baroomand-Nasab and Behzad (2009) and Nafchi, Mosavi and Parvanak (2011) also analyzed this model in the laboratory with three types of soil and reported having obtained good fits between the simulated and observed values. Nevertheless, these equations have not yet been fully validated under field conditions with different soil characteristics. Therefore, the objective of this work was to evaluate the ability of a proposed experimental model to simulate the water advance in a wet bulb. To this end, field measurements were quantitatively compared to the results from the experimental model and the models proposed by Schwartzman and Zur (1986), Amin and Ekhmaj (2006) and Kandelous, Liaghat and Abbasi (2008), in order to verify the reliability of the model for use in the design and operations of drip irrigation systems.

Materials and Methods

Comparison Models

Experimental Models

Equations (1) and (2) were derived, presenting the relation among the explanatory variables for the water advance in wet bulbs. The resulting non-linear relationship among these variables is expressed as:

$$r = 0.14\ V^{0.353} K_s^{-0.110} \theta_v^{-0.387} \quad (1)$$

$$Z = 7.906\ V^{0.458} Q^{-0.152} \theta_v^{0.386} \theta_r^{0.349} L_i^{-0.421} \quad (2)$$

where r = lateral advance (m); Z = vertical advance (m); Q = emitter flow ($m^3\ s^{-1}$); V

= applied water volume (m^3); K_s = saturated hydraulic conductivity (m s^{-1}); θ_v = initial soil moisture content (m^3 m^{-3}); θ_r = residual moisture content of the soil (m^3 m^{-3}); L_i = silt content (%).

These equations are based on a study of water distribution patterns in the wet bulb in three soil textures, with variables selected based on the Stepwise method and the models introduced by Shwartzman and Zur (1986) and Amin and Ekhmaj (2006).

The study of the water distribution pattern in the wet bulb was performed using three soil textures —silty loam, clay loam and sandy loam— located in the lagoon region of Coahuila, Mexico.

Three wetting tests were performed with each texture and the wetting pattern of the bulbs that formed under the emitters was evaluated. The tests consisted of applying different volumes of water to the soil using surface drip irrigation equipment. The first test used emitters with a nominal flow of 2 liters per hour (lph) and irrigation times of 0.5, 1.0, 1.5, 2.25, 3.0, 4.0, 5.0, 6.5 and 8.0 hours. The other two tests used the same procedure with emitters with a nominal flow of 4 and 8 lph.

The variables in equations (1) and (2) were significant for a total of nine variables that were considered to be explanatory of the lateral and vertical advance (r and Z) of the water in the bulbs. These variables presented a correlation coefficient of 0.90 for (r) and 0.94 for (Z).

Schwartzman and Zur (1986) Model

Schwartzman and Zur (1986) developed an empirical model from experimental observations and a dimensional analysis to estimate the wetting pattern in soil resulting from a surface emitter. They assumed that the geometry (width and depth) of the wet zone after irrigation depended on the type of soil and was represented by the saturated hydraulic conductivity, discharge from the emitter and total applied water volume. The model was developed with results from silty soil and sandy loam, with a saturated hydraulic conductivity of 2.49 X 10-6 and 2.49 X 10-5 m s-1, and emitter discharges of 4.3 and 20 lph. The simplified Schwartzman and Zur (1986) model used to determine the geometry of the wet volume of the soil is:

$$w = 1.82\left(V\right)^{0.22}\left(\frac{K_s}{Q}\right)^{-0.17} \quad (3)$$

$$z = 2.54\left(V\right)^{0.63}\left(\frac{K_s}{Q}\right)^{0.45} \quad (4)$$

where w and z are the horizontal and vertical dimensions of the wet bulb in the soil profile (m); V is the total applied water volume (m^3); K_s is the saturated hydraulic conductivity (m s-1) and Q is the discharge flow from the emitter (m^3 s^{-1}).

Amin and Ekhmaj Model (2006)

Amin and Ekhmaj (2006) developed equations (5) and (6) to estimate the horizontal and vertical advances in the wetting front in soil based on a non-linear regression analysis. The experimental data were derived from four types of soil to which water was applied using surface emitters and discharge flows of 2 to 8 lph:

$$R = 0.2476\ \Delta\theta^{-0.562}V^{0.268}Q^{-0.0028}K_s^{-0.034} \quad (5)$$

$$Z = 2.0336\ \Delta\theta^{-0.383}V^{0.365}Q^{-0.101}K_s^{0.195} \quad (6)$$

where R and Z are the horizontal and vertical dimensions of the wetting pattern (m); $\Delta\theta$, is the average volumetric water content behind the wetting front ($\Delta\theta = \theta_s/2$, where θ_s is the saturated moisture content); V, is the total

applied water volume (m^3); Q, is the emitter discharge flow ($m^3\ s^{-1}$), and Ks is the saturated hydraulic conductivity of the soil ($m\ s^{-1}$).

Kandelous Liaghat and Abbasi Model (2008)

Based on the dimensional analysis method, Kandelous, Liaghat and Abbasi (2008) developed equations (7) and (8) to estimate the horizontal and vertical advances of a wetting front in soil for a sub-surface emitter. These equations were derived from experimental data obtained in clay soil with sub-surface drip irrigation and an emitter discharge of 1 lph:

$$w = 4.244\left(V\right)^{0.526}\left(\frac{K_s}{Q\ z}\right)^{0.026} \tag{7}$$

$$Z- = 0.66\left(V\right)^{0.333}\left(\frac{K_s}{Q\ z}\right)^{-0.167} \tag{8}$$

where w and Z- are the horizontal and vertical dimensions of the wetting pattern (m); V is the applied water volume that infiltrates the soil (m^3), K_s is the saturated hydraulic conductivity of the soil (m s-1), Q is the emitter discharge ($m^3\ s^{-1}$), and z is the depth of the emitter installation (m).

Statistical analysis

The predictive capacities of the experimental model and the Schwartzman and Zur (1986), Amin and Ekhmaj (2006) and Kandelous, Liaghat and Abbasi (2008) models were compared to the field measurements. The coefficients of determination (R2) and the root mean square error (RMSE) were estimated for each model in accordance with the methodology reported by Siyal and Skaggs (2009), Nafchi et al., (2011) and Kandelous, Simunek, Van Genuchten and Malek (2011):

$$R^2 = 1 - \frac{\sum_{i=1}^{n}\left(P_i - O_i\right)^2}{\sum_{i=1}^{n}\left(O_i - \overline{O}\right)^2} \tag{9}$$

$$\text{RMSE} = \sqrt{\frac{\sum_{i=1}^{n}\left(P_i - O_i\right)^2}{n}} \tag{10}$$

where P_i are simulated data; O_i, are observed field data; $\bar{O}$, is the mean of the observed data and n is the number of data.

Field tests

Physical and hydraulic soil parameters

The hydrometer method by Bouyoucos was used to determine the proportion of sand, silt and clay for the three types of soils used to test the wet bulbs. The texture was classified based on the texture triangle. The moisture contents of the soils were also determined, using the gravimetric method before each depth test, as shown in Table 1. The saturated hydraulic conductivity of the soil was determined in situ with a Guelph permeameter, using loads of 5 and 10 cm, according to the procedure described by Reynolds and Elrick (1985) and Reynolds et al. (2002). The parameters of the water retention curve and saturated hydraulic conductivity for the three soil textures were modeled with the Rosetta program, version 1.2 (Schaap, Leij, &Van Genuchten, 2001). This program uses the constitutive equations by Van Genuchten (1980) and Mualem (1976) in its estimations (Skaggs, Trout, Simunek, & Shouse, 2004; Kandelous & Simunek, 2010) (Table 2).

Bulb Wetting Pattern

Three tests of the wetting of the soil were performed for each soil texture to obtain the wetting patterns in the bulbs that formed under the emitters. The tests consisted of applying different water volumes to the soil using surface drip irrigation equipment. The irrigation equipment was constructed with a water container, irrigation head and irrigation

Table 1. Physical and hydraulic properties of the soils with which field tests of the wetting patterns of the bulbs were performed.

Texture	Depth	Clay	Silt	Sand	Apparent density	Initial moisture	Saturated hydraulic conductivity
	(cm)	(%)	(%)	(%)	(g cm^{-3})	(cm^3 cm^{-3})	(cm h^{-1})
Silty loam	0-20	28	46	26	1.146	0.098	2.050
	Sandy loam	24	54	22	1.154	0.105	
	40-60	30	52	18	1.241	0.127	
Clay loam	0-20	26	22	52	1.139	0.066	3.283
	20-40	36	32	32	1.113	0.075	
	40-60	44	30	26	1.362	0.103	
Sandy loam	0-20	11	12	77	1.468	0.030	2.803
	20-40	11	9	80	1.538	0.048	
	40-60	8	8	84	1.526	0.063	

Table 2. Hydraulic parameters of the soils with which the wetting pattern tests were conducted, botained using the Rosetta program, version 1.2 (Schaap et al., 2001)

Texture	Depth (cm)	θ_r (cm^3 cm^{-3})	θ_s (cm^3 cm^{-3})	K_s cm h^{-1}	α cm^{-1}	*n*	*L*
Silty loam	0-20	0.071	0.495	1.928	0.013	1.351	-0.357
	20-40	0.062	0.480	2.210	0.009	1.413	0.207
	40-60	0.075	0.482	1.173	0.008	1.384	-0.046
Clay loam	0-20	0.071	0.507	3.944	0.034	1.294	-1.611
	20-40	0.087	0.531	2.183	0.022	1.271	-1.472
	40-60	0.081	0.483	0.434	0.014	1.227	-1.439
Sandy loam	0-20	0.041	0.401	5.152	0.050	1.416	-1.337
	20-40	0.043	0.386	4.797	0.051	1.435	-1.359
	40-60	0.037	0.386	7.336	0.056	1.499	-1.212

θ_s and θ_r represent the saturated and residual water contents; k_s, the saturated hydraulic conductivity; α, the inverse relation of the entrance of air in the soil; *n*, the measurement of the distribution of the sizes of the soil pores, and *L* the connectivity among pores. These are the parameters that influence water retention.

line. The first test was performed with nominal flow emitters of 2 liters per hour (lph) and applications times of 0.5, 1.0, 1.5, 2.25, 3.0, 4.0, 5.0, 6.5 and 8.0 hours. The other two tests were performed using the same procedure using emitters with a nominal flow of 4 and 8 lph.

The wetting pattern, lateral and vertical advance of the water in the soil, was obtained based on direct measurements of the wetting front immediately after irrigation, according to the procedure below.

a) The wet area of the soil under the emitter was measured once irrigation ended as indicated by the times mentioned above.
b) A quarter-circle was dug out of the wet soil area until reaching the wetting front, and a grid was drawn with coordinates (*x*,

z) and (*y*, *z*) centered at the emitter source (Figure 1).

c) After drawing the grid, the distance of the wetting front was measured in the horizontal and vertical directions.

Results

Tables 3 and 4 show the coefficients of determination (R^2), the root mean squared error (RMSE) and the standard error of estimation for the capacity of the models to predict the field measurements of the water advance in the wet bulbs. Figure 2 shows the distance of the water advance in the bulbs as calculated by the modeled data and the field measurements, with respect to the applied water volume ($m^3\ h^{-1}$) for each soil texture.

Discussion

The coefficient of determination (R^2) and the RMSE show that the experimental model proposed simulated the lateral and vertical advance of the water in the wet bulb with a reliability of 91 and 96%, and a standard error of estimation of 2.7 and 3%. That is, there is a margin of error of 3 and 4 cm between the modeled data and the field measurements for the three soil textures (Tables 3 and 4). According to these indices, the experimental model's predictions of both the horizontal and vertical advance of water were best with clay loam soil and emitter discharges of 2 and 4 lph (Table 3). And when using an emitter discharge of 8 lph, the best prediction was obtained with sandy loam soil, followed by clay loam.

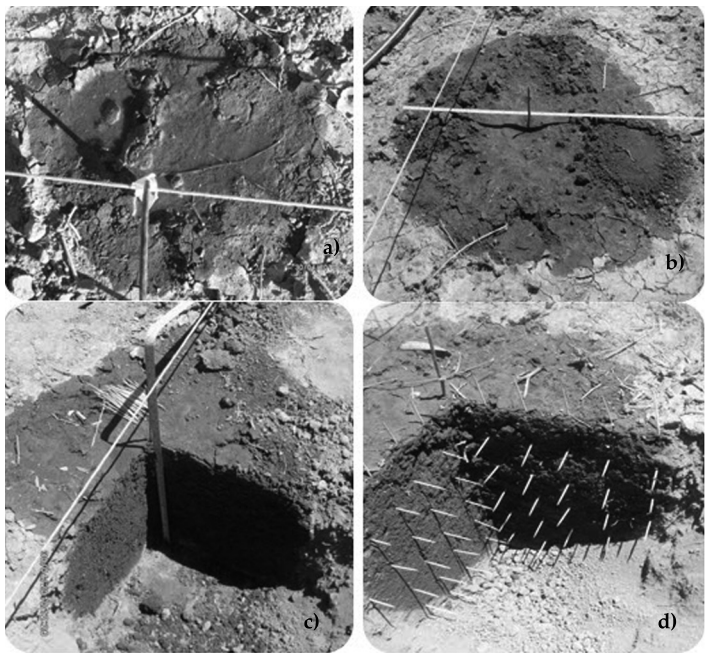

Figure 1. Shape and dimensions of the wet bulb of the soil under the emitter: a) application of water by the emitter; b) surface of the wet soil; c) profile of the wet soil; d) dimension of the wet soil (grid on the *x*, *y*, *z*, coordinates with 5 cm seperation) centered at the application source.

Table 3. Coefficients of determination in relation to the length of the advance of water in the wet bulb in function of the emitter flow and soil texture.

Discharge	Soil	Model	Indices			
			R^2		RMSE (m)	
emisor (lph)			Lateral Adv.	Vertical Adv.	Lateral Adv.	Vertical Adv.
2	Silt loam	Experimental model	0.87	0.93	0.022	0.024
		Schwartzman & Zur (1986)	0.87	0.94	0.025	0.118
		Amin & Ekhmaj (2006)	0.87	0.97	0.022	0.016
		Kandelous *et al*. (2008)	0.85	0.96	0.055	0.150
	Clay loam	Experimental model	0.93	0.95	0.020	0.020
		Schwartzman & Zur (1986)	0.93	0.93	0.053	0.093
		Amin & Ekhmaj (2006)	0.94	0.94	0.039	0.045
		Kandelous *et al*. (2008)	0.94	0.94	0.075	0.182
	Sandy loam	Experimental model	0.90	0.91	0.039	0.041
		Schwartzman & Zur (1986)	0.89	0.80	0.112	0.258
		Amin & Ekhmaj (2006)	0.82	0.87	0.044	0.046
		Kandelous *et al*. (2008)	0.72	0.94	0.118	0.233
4	Silt loam	Experimental model	0.88	0.95	0.024	0.026
		Schwartzman & Zur (1986)	0.84	0.72	0.043	0.064
		Amin & Ekhmaj (2006)	0.86	0.78	0.025	0.040
		Kandelous *et al*. (2008)	0.88	0.95	0.049	0.149
	Clay loam	Experimental model	0.98	0.93	0.024	0.033
		Schwartzman & Zur (1986)	0.90	0.30	0.074	0.187
		Amin & Ekhmaj (2006)	0.97	0.75	0.052	0.122
		Kandelous *et al*. (2008)	0.98	0.85	0.098	0.207
	Sandy loam	Experimental model	0.79	0.99	0.031	0.039
		Schwartzman & Zur (1986)	0.92	0.97	0.125	0.055
		Amin & Ekhmaj (2006)	0.94	0.99	0.032	0.056
		Kandelous *et al*. (2008)	0.92	0.93	0.098	0.221
8	Silt loam	Experimental model	0.93	0.98	0.041	0.041
		Schwartzman & Zur (1986)	0.94	0.80	0.044	0.079
		Amin & Ekhmaj (2006)	0.94	0.83	0.053	0.112
		Kandelous *et al*. (2008)	0.93	0.97	0.046	0.210
	Sandy loam	Experimental model	0.93	0.99	0.029	0.059
		Schwartzman & Zur (1986)	0.90	0.98	0.078	0.178
		Amin & Ekhmaj (2006)	0.92	0.99	0.027	0.085
		Kandelous *et al*. (2008)	0.96	0.98	0.049	0.380

Table 4. Coefficient of determination and estimation of error of the models for the advance of water in the wet bulb.

Model	Multiple coefficient of determination (R^2)		Standard error of estimation (%)	
	Lateral adv.	Vertical adv.	Lateral adv.	Vertical adv.
Experimental model	0.91	0.96	2.7	3.0
Amin & Ekhmaj (2006)	0.86	0.82	2.9	4.6
Kandelous *et al*. (2008)	0.85	0.66	2.8	4.3
Schwartzman & Zur (1986)	0.70	0.66	4.4	13.9

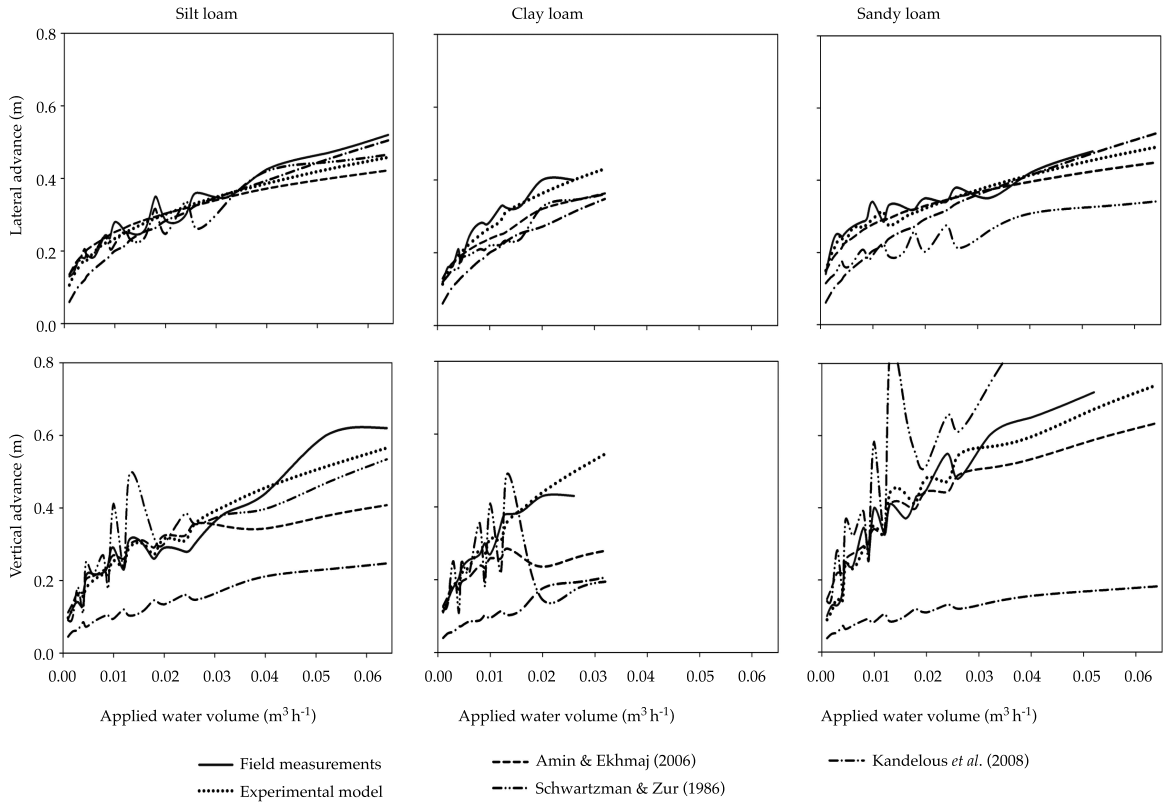

Figure 2. Simulation of the advance of water in the wet bulb in function of the applied volume.

The goodness of fit of the experimental model with the best predictions of the water advance in the wet bulb is due to the inclusion of the initial and residual moisture contents of the soil (θ_v and θ_r), as proposed by Kandelous and Simunek (2010) and Nafchi *et al*. (2011). It also incorporated the silt content (L_i) as another variable that influences the water advance in the wet bulb, in addition to the proposals in the models by Schwartzman and Zur (1986), Amin and Ekhmaj (2006) and Kandelous *et al*. (2008). The simulation also took into account differences in the physical and hydraulic properties of the soil profile, as suggested by Ramírez-de-Cartagena and Sáinz-Sánchez (1997).

The R^2 and RMSE also demonstrated that the best calculation resulting from the four models, in terms of the modeled versus observed field data corresponding to the water advance in the wet bulb, was obtained with clay loam soil and emitter flows of 2 lph, as shown in Table 4. And although the models by Amin and Ekhmaj (2006), Kandelous et al. (2008) and Schwartzman and Zur (1986) were performed with silty, sandy and sandy loam soil with emitter flows of 1, 2, 4.3, 8 and 20 lph, they present a good approximation with the soil texture and emitter flows mentioned.

The models with the best approximation of the lateral or radial water advance in the wet bulbs were those with clay loam soil and emitter flows of 2 and 4 lph. In the case of vertical advance, the best approximation was obtained with sandy loam soil and emitter flows of 8 lph. Nevertheless, the differences

in the physical and hydraulic properties of the soil profiles need to be considered separately, as indicated by Ramírez-de-Cartagena and Sáinz, (1997), taking into account the applied water volume —that is, irrigation time, emitter flow, saturated hydraulic conductivity, initial and residual moisture content and the silt content of the soil, as suggested by Amin and Ekhmaj, (2006), Kandelous and Simunek (2010) and Nafchi *et al*. (2011).

One of the variables that contributes most to the movement of water in wet bulbs is the volume of the water applied (V), as observed in Figure 2. Thus, the experimental model simulates the dimensions of the water advance with a high degree of accuracy. Meanwhile, the models by Amin and Ekhmaj (2006), Kandelous *et al*. (2008) and Schwartzman and Zur (1986) tend to underestimate or overestimate the advance, particularly in the vertical direction, with respect to the field measurements. The ability of the experimental model to better simulate the water advance in the wet bulb with any applied water volume, as compared to the other models, is due to the inclusion of the initial and residual moisture contents of the soil at different strata, as mentioned.

Overall, the results indicate that the calculation of the lateral or radial advance of the water in the wet bulb was better with the four models, in the order shown in Table 4. Whereas in the vertical direction, since the physical and hydraulic properties of the soils have a certain degree of homogeneity in their horizons, these characteristics varied with the depth, and given filtration which occurs vertically. Therefore, when the emitter applies water to the soil, the dimensions of the bulbs increase until the water absorption capacity equals the supply velocity. Initially, the velocity of the vertical advance is quicker because the soil is dry. But if water continues to be applied and as the porous spaces fill and the clay expands, a point is reached at which the speed of penetration stabilizes. Then, the lateral or radial advance in the bulb increases. Nevertheless, if the application time of the water (that is, the applied water volume) continues to increase then the vertical advance will increase again.

Conclusion

According to the results obtained in this work, the experimental model proposed is a viable option to model the advance of water in a wet bulb with drip irrigation systems. In particular, when designing and determining the separation between emitters and irrigation lines, the coefficients of determination (R^2) and the root mean square error (RMSE) show that the model simulates the lateral and vertical advance of water in the wet bulb with a reliability of 91 and 96%, and a standard error of estimation of 2.7 and 3%.

The model can also be used to determine the volume of water to be applied —that is, the irrigation time for the different soil textures that are present where the local irrigation systems are used— in function of the emitter discharge flows.

Even though the model presents a good approximation of the water advance in wet bulbs with the soils studied —in particular for clay loam soil with emitter flows of 2 and 4 lph— it is important to fully validate the models for soil textures and emitter flows other than those used in this study.

References

Ainechee, G., Baroomand-Nasab, S., & Behzad, M. (2009). Simulation of Soil Wetting Pattern under Point Source Trickle Irrigation. *Journal of Applied Sciences*, *9*(6), 1170-1174.

Amin, M. S. M., & Ekhmaj, A. I. M. (2006). *DIPAC-Drip Irrigation Water Distribution Pattern Calculator*. 7th International Micro Irrigation Congress, 10-16 Sept., Pwtc, Kuala Lumpur, Malaysia.

Arbat, G., Barragán, J., Puig, J., Poch, R., & Ramírez-de-Cartagena, B. F. (2003). Evaluación de los modelos numéricos de flujo de agua en el suelo Hydrus-2D y SIMDAS en riego localizado. En J. Álvarez-Benedí / P.

Marinero. Estudios de la zona no saturada del suelo. *Actas de las VI Jornadas sobre Investigación de la Zona no Saturada de Suelo*, *6*, 279-288.

Cook, F. J., Fitch, P., Thorburn, P., Charlesworth, P. B., & Bristow, K. L. (2006). Modelling Trickle Irrigation: Comparison of Analytical and Numerical Models for Estimation of Wetting Front Position with Time. *Environmental Modelling & Software*, *21*(9), 1353-1359.

Dasberg, S., & Or, D. (1999). *Drip irrigation* (162 pp). New York: Springer-Verlag.

Gil-Marín, J. A. (2001). Forma y dimensiones del bulbo húmedo con fines de diseño de riego por goteo en dos suelos típicos de sabana. *Revista UDO Agrícola*, *1*(1), 42-47.

Kandelous, M. M. K., & Simunek, J. (2010). Comparison of Numerical, Analytical, and Empirical Models to Estimate Wetting Patterns for Surface and Subsurface Drip Irrigation. *Irrig. Sci.*, *28*, 435-444.

Kandelous, M. M., Liaghat, A., & Abbasi, F. (2008). Estimation of Soil Moisture Pattern in Subsurface Drip Irrigation Using Dimensional Analysis Method. *J. Agri Sci.*, *39*(2), 371-378.

Kandelous, M. M., Simunek, J., Van Genuchten, M. Th., & Malek, K. (2011). Soil Water Content Distributions between Two Emitters of a Subsurface Drip Irrigation System. *Soil Sci. Soc. Am. J.*, *75*(2), 488-497.

Mualem, Y. (1976). A New Model for Predicting the Hydraulic Conductivity of Unsaturated Porous Media. *Water Resour. Res.*, *12*, 513-522.

Nafchi, R. F., Mosavi, F., & Parvanak, K. (2011). Experimental Study of Shape and Volume of Wetted Soil in Trickle Irrigation Method. *African Journal of Agricultural Research*, *6*(2), 458-466.

Ramírez-de-Cartagena, B. F., & Sáinz-Sánchez, M. A. (1997). Modelo de distribución de agua en suelo regado por goteo. *Ingeniería del Agua*, *4*(1), 57-70.

Reynolds, W. D., & Elrick, D. E. (1985). Measurement of field-saturated hydraulic conductivity, sorptivity and the conductivity-pressure head relationship using the "Guelph Permeameter". *Proc. National Water Well Association Conference on Characterization and Monitoring of the Vadose (Unsaturated) Zone*, Denver, Co., USA.

Reynolds, W. D., Elrick, D. E., Youngs, E. G., Amoozegar, A., Booltink, H. W. G., & Bouma, J. (2002). Saturated and Field-Saturated Water Flow Parameters (pp. 797-878). In *Methods of Soil Analysis, Part 4-Physical Methods*. Madison, USA: Soil Science Society of America.

Schaap, M. G., Leij, F. J., & Van Genuchten, M. Th. (2001). Rosetta: A Computer Program for Estimating Soil Hydraulic Parameters with Hierarchical Pedotransfer Functions. *Journal of Hydrology*, *251*, 163-176.

Schwartzman, M., & Zur, B. (1986). Emitter Spacing and Geometry of Wetted Soil Volume. *J. Irrig. Drain. Eng.*, *112*(3), 242-253.

Siyal, A. A., & Skaggs, T. H. (2009). Measured and Simulated Soil Wetting Patterns under Porous Clay Pipe Sub-Surface Irrigation. *Agricultural Water Management*, *96*, 893-904.

Skaggs, T. H., Trout, T. J., Simunek, J., & Shouse, P. J. (2004). Comparison of HYDRUS-2D Simulations of Drip Irrigation with Experimental Observations. *Journal of Irrigation and Drainage Engineering*, *130*(4), 304-310.

Van Genuchten, M.Th. (1980). A Closed-Form Equation for Predicting the Hydraulic Conductivity of Unsaturated Soils. *Soil Sci. Am. J.*, *44*, 892-898.

Institutional Address of the Authors

Dr. Fidencio Cruz-Bautista

Universidad de Sonora
Departamento de Agricultura y Ganadería
Blvd. Luis Encinas y Rosales S/N.
Col. Centro, 83000, Hermosillo, Sonora, México
Teléfonos: +52 (662) 259 2100 y 259 2200
fidencio.cruz@guayacan.uson.mx

Dr. Alejandro Zermeño-González

Universidad Autónoma Agraria Antonio Narro
Calz. Antonio Narro 1923
Buenavista, 25084, Saltillo, Coahuila, México
Teléfonos: +52 (844) 417 2474 y 411 0200
azermeno@uaaan.mx

Dr. Vicente Álvarez-Reyna
Dr. Pedro Cano-Ríos

Universidad Autónoma Agraria Antonio Narro Unidad Laguna
Periférico Raúl López Sánchez s/n
Col. Valle Verde
27059 Torreón, Coahuila, México
Teléfonos: +52 (871) 729 7613, 729 7614 y 729 7610
Fax: +52 (871) 733 3490
vicpaal@hotmail.com
canorp49@hotmail.com

M.C. Miguel Rivera-González

Centro Nacional de Investigación Disciplinaria en Relación Agua, Suelo, Planta, Atmosfera (CENID RASPA-INIFAP)
Km. 6.5 margen derecha canal Sacramento
35140 Gómez Palacio, Durango, México
Teléfonos: +52 (871) 159 0104, 05 o 07
rivera.miguel@inifap.gob.mx

Dr. Mario Ángel Siller González Pico

Centro de Investigación y de Estudios Avanzados del
Instituto Politécnico Nacional (Cinvestav-IPN)
Unidad Guadalajara
Av. Científica 1145, Col. El Bajío
45019 Zapopan, Jalisco, México
Teléfono: +52 (33) 3777 3600
mario_siller@gdl.cinvestav.mx

Click here to write the autor

Test of an intake and exhaust valve.

Photo: Pedro L. Iglesias.

Characterization of Commercial Air Intake and Exhaust Valves

• Pedro L. Iglesias-Rey* • Vicente S. Fuertes-Miquel
• Francisco J. García-Mares • F. Javier Martínez-Solano •
Universitat Politècnica de València, España
*Corresponding Author

Abstract

Iglesias-Rey, P. L., Fuertes-Miquel, V. S., García-Mares, F. J., & Martínez-Solano, F. J. (January-February, 2016). Characterization of Commercial Air Intake and Exhaust Valves. *Water Technology and Sciences* (In Spanish), 7(1), 57-68.

The objective of this work was to perform a detailed study of the actual behavior of different valves (air intake and exhaust). The first part of the work describes the different experimental techniques used to characterize the valves. The second part uses an air valve bench test developed by Bermad CS at its Evron factory, Israel, to perform statistical studies with different commercial valves. Lastly, a comparative analysis is described of the behavior of the different models analyzed, including an analysis of the best coefficients for the mathematical characterization of these devices.

Keywords: Air valves, test bench entrapped air, air flow curves, laboratory.

Resumen

Iglesias-Rey, P. L., Fuertes-Miquel, V. S., García-Mares, F. J., & Martínez-Solano, F. J. (enero-febrero, 2016). Caracterización de válvulas de admisión y expulsión de aire comerciales. Tecnología y Ciencias del Agua, *7(1), 57-68.*

El objetivo del trabajo es estudiar en detalle el comportamiento real de diferentes ventosas (válvulas de admisión y expulsión de aire). La primera parte del trabajo describe las diferentes técnicas experimentales de caracterización de ventosas. En la segunda parte se utiliza el banco de pruebas de válvulas de aire construido por Bermad CS en su fábrica de Evron, Israel, para realizar los ensayos de caracterización estática a diferentes ventosas comerciales. Finalmente se realiza un estudio comparativo del comportamiento de los diferentes modelos analizados, analizando los coeficientes más adecuados para la caracterización matemática de estos elementos.

***Palabras clave**: válvulas de aire, bancos de prueba, aire atrapado, curvas de flujo de aire, laboratorio.*

Received: 14/01/2015
Accepted: 29/07/2015

Introduction

Trapped air is one of the main problems involved in the technical management of water distribution networks. Air pockets trapped inside piping can create numerous problems during the normal operations of a network (Fuertes, 2001), including: reductions in the cross-section of the pipe, losses in additional loads, decreased pump performance, noise and vibration problems, internal corrosion of the pipes from the oxygen in the air, loss in the efficiency of some types of filters and significant errors in meters that are not specifically designed to carry biphasic flow.

The air inside the pipes comes from three clearly distinct sources. The first is the amount of dissolved air in the water. These small amounts of air are released throughout the piping and tend to collect at the high points in the installation. This process can be easily controlled with manual or automated purging systems. Nevertheless, the main problem with the air in the piping occurs when there is a

significant amount of air. These large volumes of air come from two clearly different sources: the introduction of air in the piping to control depressions during transient events in the water distribution system and filling and draining processes in the pipes (Cabrera-Béjar & Tzatchkov, 2012).

Significant depressions can occur during transient events such as starting and stopping a group of pumps (Carmona & Aguilar, 1987; Carmona, 1987; Vázquez & Aguirre, 1986). Cavitations inside the pipes are created when these depressions reach the vapor pressure value (Cervantes- Osornio, Arteaga-Ramírez, Vázquez-Peña, Ojeda-Bustamante, & Quevedo-Nolasco, 2013). One of the strategies often used to control depressions during transient events it to introduce air into these depressions (Boulos, Karney, Wood, & Lingireddy, 2005).

The study of the problem of filling pipes is not new. Authors such as Zhou, Hicks and Steffler (2002) and Fuertes (2001) proposed mathematical models to study the behavior of air during these processes. In all these studies, one of the key aspects is the mathematical representation of the behavior of the valves during the process. The presence of air inside the water pipes definitely creates significant difficulties for processes related to starting and stopping the system as well as for transient events (Lingireddy, Wood, & Zloczower, 2004). The air trapped in the pipes has a high compression capacity and, therefore, the acceleration or deceleration of the flow generates transients that can cause overpressure. On occasion, these pressures can greatly exceed those generated by transient events without the presence of air, such as failures in the supply of electricity to pumps or the rapid closing valves.

Air valves are installed in water distribution networks to prevent the problems caused by air entering and leaving the system. Once installed they become part of the system, interacting with other components therein, such as piping, other valves and pumps. Given this set of interactions, it is not possible to analyze their behavior without taking into account the system in which they are installed.

The design and selection of valves requires knowledge about their behavior, which is characterized by the air intake and exhaust capacity in function of the existing differential pressure. But this characterization does not end with the valve's ventilation capacity, it is also necessary to know its operating limits.

One of the main problems related to the functioning of these devices is called "kinetic closure." This occurs when the floater is dragged by the air current instead of by the effect of its floating on top of the water. This closure results from excessive differential pressure in the valve, which causes a velocity rapid enough to generate a drag on the floater that exceeds its weight. Under these circumstances, the valve closes before the water reaches it, leaving part of the air trapped inside the pipe. This closure definitely should be studied in detail since it can create large transient events that can damage water distribution systems.

A general practice by some engineers is to consider the nominal size of the air valve as its characteristic parameter. Therefore, it is common to find projects with specifications that only indicate the nominal diameter of the air valve without in any way specifying design conditions (intake flow, exhaust flow or differential pressure). United States norms (AWWA, 2004) established that the smallest section throughout the length of an air valve should be at least equal to its intake section. That is, it is not possible to reduce the intake cross-section over the length of the body of the valve. Therefore, many manufacturers around the world take this restriction into account when designing their valves. In Europe, the reference standard is regulation EN 1074-4, defined by the CEN (2001).

Therefore, the main objective of this work was to perform a comparative study of the behavior of different valves. First, different mathematical models representing the behavior of a valve were analyzed. Then, the different techniques to test existing valves were studied. Using one of these techniques, extensive experiments were conducted with a wide range of commercial valves having the same diameter. Based on the results, a comparative analysis was performed of the characteristic curves for the different models studied. The validation of the capacity of the different mathematical models to represent the behavior of the valves was also studied throughout this work.

Mathematical Characterization of the Behavior of Valves

The use of mathematical models to represent the behavior of air trapped inside piping is not new. The inclusion of certain behaviors of air through a valve can be found in some classical texts such as Chaudhry (1987) or Wylie and Streeter (1993), as well as in more recent studies such as Lingireddy *et al*. (2004).

In each case, the characterization of a valve consists of determining the relationship between air intake and exhaust capacities and the existing differential pressure. The most general equation used to represent the behavior of valves is obtained according to convergent-divergent flow in an isentropic nozzle. Thus, the mass flow that can exit the nozzle (Cambell & Jennings, 1967) in subsonic flow conditions is:

$$G = \frac{C_d A}{\sqrt{1-\left(\frac{p_2^*}{p_1^*}\right)^{2/k}\left(\frac{A_2}{A_1}\right)^2}} \sqrt{\frac{2k}{k-1} p_1^* \rho_1 \left[\left(\frac{p_2^*}{p_1^*}\right)^{2/k} - \left(\frac{p_2^*}{p_1^*}\right)^{(k+1)/k}\right]} \qquad (1)$$

In the above equation, p_1^* and p_2^* are the absolute pressure in the intake and outlet of the nozzle, respectively; A_1 and A_2, lare the corresponding cross-sections at the same points and C_d is a coefficient representing the fact that the energy conversion between pressure and velocity is not perfect. In addition, k represents the adiabatic exponent of the behavior of the fluid, which for air is 1.4.

This equation is used later by Chaudhry (1987) and Wylie and Streeter (1993) to formulate the characteristic equations for the valve. The only simplification introduced by these authors is to consider that the pipe intake, A_1, is much larger than the valve's outlet section, A_2. In addition, for air exhaust, points 1 and 2 are identified as the inside of the pipe and outside atmospheric pressure, and the opposite for intake. Thus, the equations in this model, expressed in terms of mass air flow and pressure inside the pipe, are written as:

$$G = C_{d,\text{exh}} A\, p_t^* \sqrt{\frac{7}{RT_t}\left[\left(\frac{p_{\text{atm}}^*}{p_t^*}\right)^{1.4286} - \left(\frac{p_{\text{atm}}^*}{p_t^*}\right)^{1.714}\right]}$$

$$\text{si} \quad p_t^* \le 1.8929 \cdot p_{\text{atm}}^* \quad \text{(subsonic flow)}$$

$$G = C_{d,\text{exh}} A\, \frac{0.686}{\sqrt{RT_p}} p_t^*$$

$$\text{si} \quad p_t^* > 1.8929 \cdot p_{\text{atm}}^* \quad \text{(supersonic flow)} \qquad (2)$$

The equations for air intake are:

$$G = C_{d,\text{int}}\ A \sqrt{7 p_{\text{atm}}^* \rho_{\text{atm}} \left[\left(\frac{p_t^*}{p_{\text{atm}}^*}\right)^{1.4286} - \left(\frac{p_t^*}{p_{\text{atm}}^*}\right)^{1.714}\right]}$$

$$\text{si} \quad p_t^* \le 1.8929 \cdot p_{\text{atm}}^* \quad \text{(subsonic flow)}$$

$$G = C_{d,\text{int}}\ A \frac{0.686}{\sqrt{RT_{\text{atm}}}} p_{\text{atm}}^* = \text{constant}$$

$$\text{si} \quad p_t^* > 1.8929 \cdot p_{\text{atm}}^* \quad \text{(supersonic flow)} \qquad (3)$$

In the above equations, G is the mass flow through the air valve; p_t^* is the absolute pressure in the pipe; p_{atm}* is the absolute atmospheric pressure; R is the constant characteristic of the gases when considered to be an ideal gas; ρ_{atm} is the air density at atmospheric pressure; T_t is the air temperature inside the pipe; A is the cross-section of the outlet and $C_{d,int}$ y $C_{d,exh}$ represent the discharge coefficient values for the intake and exhaust flows.

An alternative approach to the mathematical representation of the behavior of a valve is to consider a reference value for density and assume incompressible air flow (Fuertes-Miquel, Iglesias-Rey, García-Mares, & Mora-Meliá, 2009). This premise is based on the premise that air compressibility has a minor effect on the normal operating range of a valve (Fuertes-Miquel, Iglesias-Rey, López-Jiménez, Martínez-Solano, & López-Patiño, 2011). Under these conditions, considering the effects of compressibility to be negligible and including incompressible flow, the equations for the behavior of the valve (Fuertes, 2001) can be written as:

$$G = C_{v,exh}\sqrt{\Delta p \cdot p_t^*} \quad \text{Air exhaust}$$

$$G = C_{v,int}\sqrt{\Delta p \cdot p_{atm}^*} \quad \text{Air intake} \qquad (4)$$

In equation (4), $C_{v,exh}$ and $C_{v,int}$ are the coefficients characteristic of the valve for exhaust and intake, respectively, while Δp is the differential pressure. The characteristic coefficients C_d in equation (2) and (3) are dimensionless when using international units for all the variables. Otherwise, the coefficients in equation (4) would be calculated by including the absolute pressure as well as the differential pressure, expressed in bars, with the maximum flow G measured in m^3/h under atmospheric pressure conditions

The objective of the work herein focused on validating the models that represent the behavior of the valves, shown in equations (2), (3) and (4). To this end, different commercial valves were analyzed, their pneumatic characteristics were determined and the validity of each of the models presented previously were studied.

Experimental Conditions for the Valve Tests

The main problem related to testing the ventilation characteristics of valves is the volume of air required to flow into the test system. Consider the possibility that sonic speed conditions could be reached when testing a valve. Under these circumstances, an 80 mm (3-inch) diameter valve can require a flow of approximately 6 200 m^3/h, measured under standard conditions. This mass flow greatly increases as the size increases. Thus, a 100 mm air valve could require 9 700 m^3/h, standard conditions, while a 300 mm could require a flow of over 87 000 m^3/h, standard.

Two primary techniques currently exist to test the pneumatic characteristics of a valve. The first involves the storage of large amounts of air in high-pressure air deposits. This air is then gradually released through a system that reduces the pressure to the operating pressure of the air valve. The minimum volume required by these tests is large, even when assuming a minimum time for each test of approximately 1 minute. With a storage pressure of 9 bars, the minimum volume needed to test a 4-inch air valve would be approximately 32 m^3. In the case of a 12-inch air valve, the minimum volume would exceed 290 m^3. These values are determined only by calculating the air volume that needs to be stored to obtain a maximum flow discharge with these valves for 1 minute.

An alternative is to acquire an air compressor with a large enough capacity to supply the air flow needed for the tests. The problem with this is related to the compressor's size

and power. This can be estimated based on the power transmitted to the fluid and an approximate compressor performance of 85%. Under these conditions, a 12-inch valve would require one compressor with the capacity to generate at least 24 m^3/s, and a manometric pressure of 0.9 bar, which corresponds to an approximate power of 1.4 MW.

When appropriately using both of these technologies, they are very effective to validate the behavior of the valve for exhaust air flow. Nevertheless, the former methodology is very inefficient when testing the functioning of valves during the air intake stage, since pressures below atmospheric values are needed.

A Bermad valve test bank was used (Figure 1) for the experimental phase of this work. This was built by the company Bermad CS at its Evron plant, Israel. It has a 314 kW compressor and a maximum exhaust air flow capacity of 16.320 m^3/h standard (at 20° Celsius), with a pressure of 52 kPa. Although its indicated power was lower than that described in the previous paragraphs, it was possible to use this bank to perform the tests for this work, given that the reference size used for this study was 3 inches (80 mm). Nevertheless, when limiting the operating range of the valves not to the sonic limit but rather to a maximum differential pressure of 0.5 bar for both exhaust and intake, it was possible to test the majority of the commercial valves that measured between 2 and 12 inches.

In brief, the test bank used complied with European regulations (Figure 2), including the minimum distance between elements. The pressure source consisted of a compressor and a set of control valves to connect it to the system, a test line with an air valve, a pressure transducer and a thermal mass air flow meter. The pressure transducer and the thermal mass flow meter were both calibrated prior to the test by certified laboratories. The configuration of the test bank was different for the air exhaust and intake tests. For the air exhaust test, the compressor was placed at the beginning of the installation and the valve to be tested was at the other end, at the outlet. For the intake test, the valve to be tested was at the air intake end of the assembly and the compressor was at the other end, at the outlet.

The air valves had three clearly different functions:

- Air intake. The introduction of large amounts of air when the pressure inside the pipe is lower than atmospheric pressure, in the case of draining the pipes.
- Air exhaust. The elimination of large amounts of air when the pressure inside the pipe is higher than atmospheric pressure, in the case of filling the pipes.
- Purging. The elimination of small amounts of air that accumulate at high points, produced during the normal operations of the system.

For this work, 19 different valve models were selected from 13 manufacturers in 10 countries (Germany, Austria, Belgium, France, Israel, Italy, Spain, United Kingdom and United States). A common reference size was needed in order to compare the

Figure 1. Test bank with Bermad valves.

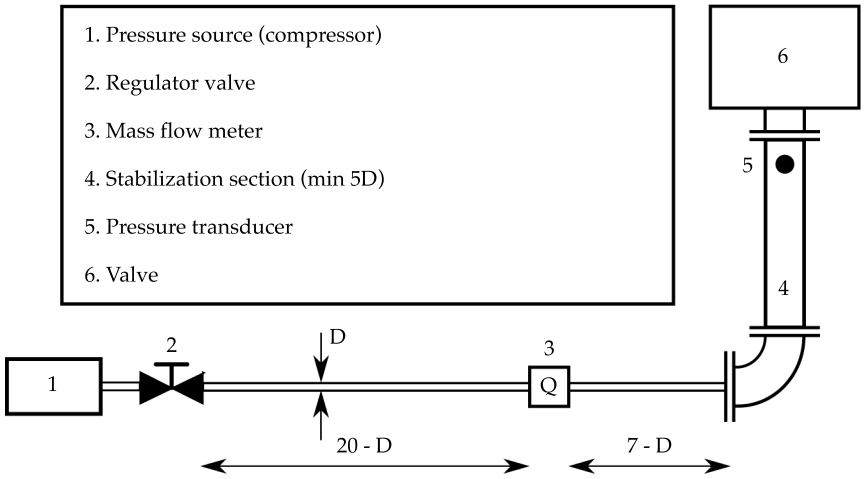

Figure 2. Layout of the experiment using tests in accordance with CEN regulations.

different valves. Some preliminary studies (García-Mares, Iglesias-Rey, Fuertes-Miquel, Mora-Meliá, & López-Jiménez, 2009) used a nominal diameter of 50 mm as the initial reference value. Nevertheless, according to the preliminary results (Fuertes *et al*., 2009), it is recommended that the study size be increased to 80 mm (3 inches) and a wider range of manufacturers be included. During this work, only intake and exhaust functions were considered, not purging.

Results from the Analysis

The comparative analysis of the behavior of the different valves involved running 194 tests with over 1 600 measuring points. Although the number of models considered in the study was 19, each model was tested several times in order to verify the reproducibility of the results.

Given the particularities of the system, certain limits were established to test the different valve models. These were determined based on some of the restrictions of the system, such as its maximum operating pressure limit, the compressor's maximum operating power and the maximum torque of the electric motor that starts the compressor. Nevertheless, a detailed analysis of the normal functioning of the valves analyzed was possible with the defined range. The installation's operating limits were established for maximum possible intake flow, exhaust flow and differential pressure. The maximum flow was set at 3 000 m3/h, measured under standard conditions and the maximum differential pressure was 0.5 bar for both the air intake and exhaust tests.

In this work, the comparative and numerical analysis of the functioning of the different valves focused on the following:

- Differences between the manufacturers' data with regard to the ventilation capacity of the valves, as specified by the technical product sheet, versus the data obtained experimentally.
- A comparison of the extreme functioning of the different models, obtained by analyzing the maximum intake and outlet air flows and identifying the kinetic closure point of the valves.

- The effect of the use of different types of valve covers on the characteristic curves of valve behavior.
- The validity of the mathematical models for representing the behavior of the valves.

Differences between Manufacturer and Experimental Data

The analysis of the results show a large difference between the manufacturer and experimental data for many of the cases analyzed. These differences were highly significant with some models (Figure 3, manufacturer R). In these cases, taking the data provided directly by the manufacturer as valid could result in significant design errors. As can be seen in Figure 3, the differences between the manufacturers' data and those obtained from the tests were greater for air intake than for exhaust. Even some of the manufacturers who had a good representation of exhaust (Figure 3, manufacturers E and M) had some discrepancies in terms of drainage.

Valve Functioning under Extreme Conditions

The extreme functioning conditions of a valve are given by two primary factors —maximum air intake and exhaust flow and the point that produces the kinetic closure of the valve. Table 1 shows the values of the maximum air intake and exhaust flows for each of the models tested, along with the kinetic closure point. In the column corresponding to kinetic closure in Table 1, "No" means that the valve did not close within the defined operating range (maximum flow of 3 000 m^3/h, standard conditions, maximum pressure of 0.5 bar). That is, it is not possible to say whether kinetic closure occurs with the valves labeled as "No." It is only possible to indicate that the closure did not occur within the defined operating range. In any case, the last available point before falling out of the operating

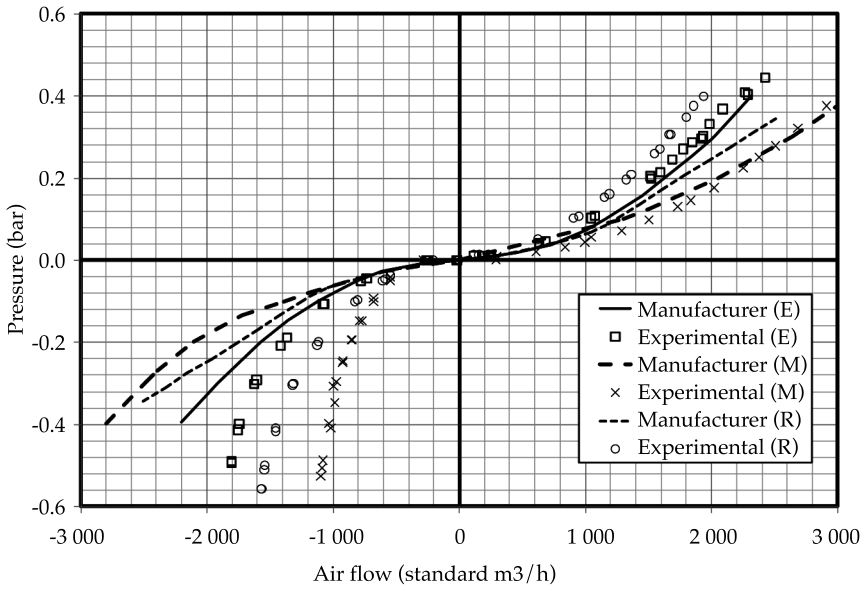

Figure 3. Differences between the manufacturer's curves and experimental data.

range was always collected. This point was either close to 0.5 bar or 3 000 m^3/h.

The results presented in Table 1 show the wide operating ranges of the valves. Kinetic closure occurred in a significant number of valves with low air flows and differential pressures (B, H, I, N, P).

For the case of air intake, the results from the maximum air flow at -0.5 bar ranged from 435 to 2 490, nearly a 6-fold difference. For example, an engineer who bases a design on the need for the system to have an air intake of 1 500 m^3/h , standard, could only use eight of the valves tested. Furthermore, if the designer recommends a specific valve model to satisfy the air control requirement, this could not be replaced by another one without checking the actual specifications related to its behavior. Even if two valves have the same nominal intake diameter, there is a risk that the system will not be protected as indicated by the design requirements (since the new air valve may not have the air flow capacity required).

Effect of Different Covers on the Characteristics of a Valve

One of the effects that was specifically studied by the present work was how a mechanical closure on the top of a valve may affect the valve's behavior. The manufacturers often supply their valves with different air exhaust systems, each adapted for the best diffusion. In this case, the characteristic curves of a single valve model with five different mechanical closure systems were compared: side outlet (SIDE), down outlet (DOWN), two mushroom outlets (MUSHROOM and MUSHROOM2)

Table 1. Extreme results with the air valves tested.

Model	Air exhaust (kinetic closure point)			Air intake (draining)
	Pressure (bar)	Mass flow (std m^3/h)	Kinetic closure?	Max. flow at -0.5 bar (std m^3/h)
A	0.30	880	Yes	- 435
B	0.07	915	Yes	- 1 473
C	0.46	2 231	No	- 1 719
D	0.29	1 955	Yes	- 1 825
E	0.45	2 417	Yes	- 1 812
F	0.46	2 345	No	- 825
G	0.53	972	No	- 1 359
H	0.11	1 015	Yes	- 1 493
I	0.14	1 135	Yes	- 1 648
J	0.51	846	No	- 830
K	0.27	3 493	No	- 2 128
L	0.52	900	Yes	- 688
M	0.38	2 912	No	- 1 096
N	0.02	420	Yes	- 1 242
O	0.31	1 300	Yes	- 1 000
P	0.01	780	Yes	- 2 490
Q	0.48	1 178	No	- 650
R	0.40	1 938	Yes	- 1 568
S	0.33	3 168	No	- 2 260

and a case in which the valve did not have an air direction mechanism installed.

Although the results obtained (Figure 4) show slightly different behaviors in terms of the intake and exhaust capacities, the point that produces a dynamic closure of the valve occurs more or less at the same flow level. It could be stated that, in this case, the dynamic closure occurs at a somewhat fixed flow regardless of the cover. Nevertheless, this closure point varies according to the differential pressure, since the resistance in the device changes with the different cover combinations.

The most significant result from the analysis of the different types of closures is that none of the manufacturers analyzed provide different curves for the different covers used. That is, in the technical information provided by the manufacturer, the characteristics of the valves are independent of the covers used. This represents a significant source of error which should be taken into account by engineers when designing these systems.

Validation of the Mathematical Model

After experimentally analyzing all the models, the different mathematical models representing the behavior of the valves were validated. To this end, the characteristic coefficients of each model were adjusted by least square regression. For the Wylie and Streeter model, the parameters that were adjusted were the discharge coefficients for air exhaust and intake coefficients ($C_{d,\text{exh}}$ and $C_{d,\text{int}}$). For the incompressible flow model, the parameters adjusted were the characteristic coefficients $C_{v,\text{exh}}$ and $C_{v,\text{int}}$.

The statistical analyses and errors are shown in Table 2. This table presents the maximum relative error obtained with the adjusted parameters. In the Wylie and Streeter model, there is a large difference between the discharge coefficients values for air exhaust and air intake. That is, this coefficient cannot be considered to be the same for any case. The results show that the Wylie and Streeter model works well for a few of the models

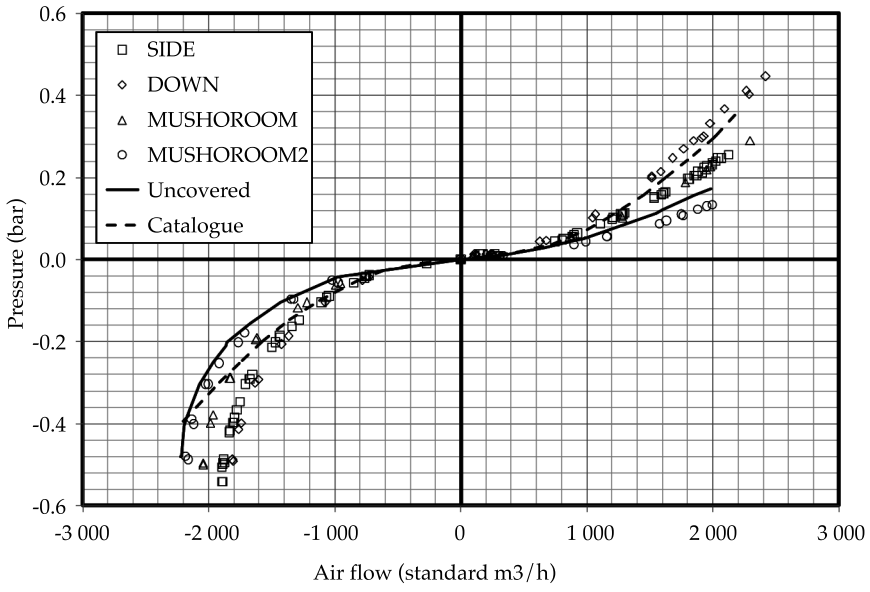

Figure 4. Effect of the cover on the characteristic curve.

tested, but only for air intake flow. For air exhaust flow, the model generates significant errors for a large number of the models tested

The discrepancies that appear with the Wylie and Streeter model may be due to the premise behind its very design. This model considers the flow in a valve to be similar to flow in an adiabatic convergent-divergent nozzle. Many of the models tested undoubtedly cannot simulate this situation, and therefore the model cannot adequately represent the behavior.

The results with the incompressible flow model were significantly different. While the errors in the air exhaust flow were significantly lower, they were slightly higher than those in the Streeter and Wylie model. The compressibility of the fluid needs to be considered in order to obtain the best fit of the data for air exhaust and intake. Variations in the air density in the exhaust section are much lower with differential pressures under 0.5 bar than for those with depressions of -0.5 bar. Therefore, the incompressible flow hypothesis is more suitable for exhaust than for intake.

Conclusions

Given the analysis of the results and the mathematical methods applied to them, a series of important conclusions can be drawn from the work performed herein:

Table 2. Validity of the mathematical models for air valves.

	Wylie & Streeter Model				Incompressible model proposed			
	Air outlet		Air intake		Air outlet		Air intake	
	$C_{d,exh}$	Error (%)	$C_{d,int}$	Error (%)	$C_{v,exh}$	Error (%)	$C_{v,int}$	Error (%)
A	0.21	9.7	0.11	11.3	1 358	6.2	641	13.8
B	0.49	34.6	0.37	12.4	3 534	33.7	2 071	13.9
C	0.35	71.9	0.40	64.8	2 294	66.9	2 348	52.6
D	0.48	10.6	0.49	4.3	3 209	7.8	2 827	14.4
E	0.47	20.9	0.49	3.6	2 997	17.2	2 834	13.7
F	0.42	46.8	0.22	11.2	2 919	44.3	1 246	21.5
G	0.17	35.3	0.36	7.2	1 079	41.8	2 065	13.6
H	0.37	26.6	0.39	9.0	2 579	24.8	2 159	12.1
I	0.41	11.2	0.44	7.5	2 904	9.4	2 406	11.6
J	0.14	139.8	0.22	8.3	969	149.7	1 211	13.1
K	0.93	10.0	0.58	1.9	6 183	9.2	3 415	18.8
L	0.14	47.7	0.17	23.3	966	58.1	996	31.1
M	0.65	7.4	0.30	11.4	4 259	9.7	1 717	21.2
N	0.36	40.3	0.34	2.1	2 606	40.2	1 892	16.8
O	0.31	18.8	0.26	11.3	2 023	15.7	1 426	11.4
P	0.81	23.3	0.70	3.0	5 896	23.2	4 122	13.0
Q	0.18	39.5	0.17	8.0	1 214	34.6	980	14.6
R	0.41	19.1	0.41	10.4	2 646	15.7	2 250	11.0
S	0.76	26.6	0.62	3.5	4 976	23.5	3 616	14.1

- Even though the air valves included in this investigation had the same nominal intake size (3 inches/80 mm), their intake and exhaust capacities varied greatly. This clearly demonstrates that the nominal diameter is not sufficient information to correctly define a valve. When indicating the specifications for projects, engineers should include not only the size of the valve but also its design characteristics (mass air flow and differential pressure). Therefore, the problem of characterizing the valves does not only depend on the manufacturer but also on the engineers responsible for the design and installation.
- Kinetic closure is a key parameter in the selection of valves. The models analyzed have presented very different kinetic closure behaviors. Some models present kinetic closures at extremely low values, which can affect a system's filling conditions. The selection of a valve with a low kinetic closure can create large and abrupt increases in pressure when filling pipes. In any case, engineers need to know this parameter for their projects, though it is generally not included in the information provided by the manufacturer.
- It is increasingly necessary to carefully review the information that manufacturers provide about their valves. Discrepancies are frequently found (sometimes significant) between the technical data from the manufacture and the actual behavior. In addition, the technical documentation from many manufacturers does not include information about kinetic closure or different behaviors with different covers.
- The Wylie and Streeter mathematical model to represent the behavior of the valves did not effectively represented their behavior, especially for air exhaust. The incompressible flow model much more effectively represents the behavior of air exhaust, but is less effective for air intake.
- The characteristic coefficients $C_{d,\text{exh}}$ and $C_{d,\text{int}}$ vary greatly. As a general rule, it can be stated that the value of $C_{d,\text{exh}}$ is generally slightly higher than the values of $C_{d,\text{int}}$. Nevertheless, specific cases exist in which this does not occur because of the particularities of the device's air exhaust. In addition, somewhat over 25% of the manufacturers have $C_{d,\text{exh}}$ values of 0.15 – 0.2, more than 50% have values between 0.35-0.5, and only 20% have values over 0.6. Three clearly differentiated groups of valves can be established in function of their exhaust capacity. Nevertheless, the analysis is different for the discharge coefficients, where $C_{d,\text{int}}$ ranges from 0.11 to 0.7 with no clear classification of intake capacities, and the same would occur for air exhaust capacities. The operating ranges for the coefficients $C_{d,\text{exh}}$ and $C_{d,\text{int}}$ are similar to the coefficients $C_{v,\text{exh}}$ and $C_{v,\text{int}}$.

This work definitely provides an important basis with which to improve the techniques used to characterize valves, which undoubtedly will enable and increase their use and optimization in water distribution networks. The experimental results obtained not only make the investigation of this subject easier but also can serve as notice to engineers responsible for the design and operations of water distribution networks.

Acknowledgements

This work was supported by project DPI2009-13674 (OPERAGUA), by the General Research Department and the National Management Plan I + D + I, Ministry of Science and Innovation, Spain.

References

AWWA (2004). *AWWA, C512-04: AWWA Standard for Air-Release, Air/Vacuum, and Combination Air Valves for Waterworks Service*. Catalog No. STC_0060331. Denver: American Water Works Association.

Boulos, P. F., Karney, B. W., Wood, D. J., & Lingireddy, S. (2005). Hydraulic Transient Guidelines for Protecting Water Distribution Systems. *Journal of American Water Works Association. Vol 97:5 (May, 2005)*. pp. 111-124.

Cabrera-Béjar, J. A., & Tzatchkov, V. G. (abril-junio, 2012). Modelación de redes de distribución de agua con suministro intermitente. *Tecnología y Ciencias del Agua, antes Ingeniería hidráulica en México*, *3*(2), 5-25.

Cambel, A. B., & Jennings, B. H. (1967). *Gas Dynamics*. New York: Dover Publications.

Carmona, R., & Aguilar, L. (enero-abril, 1987). Transitorios hidráulicos en conductos a presión. *Ingeniería Hidráulica en México*, *3*(1), 29-52.

Carmona, R. (septiembre-diciembre, 1987). Transitorios por corte de bombeo. *Ingeniería Hidráulica en México*, *3*(3), 53-61.

Cervantes-Osornio, R., Arteaga-Ramírez, R., Vázquez-Peña, M. A., Ojeda-Bustamante, W., Quevedo-Nolasco, A. (abril-junio, 2013). Comparación de modelos para estimar la presión real de vapor de agua. *Tecnología y Ciencias del Agua*, *4*(2), 51-68.

Chaudhry, M. H. (1987). *Applied Hydraulic Transients*. New York: Van Nostrand Reinhold Company.

CEN (2001). *EN 1074-4:2000. Valves for Water Supply. Fitness for Purpose Requirements and Appropriate Verification Tests. Air Valves*. Bruselas: European Committee for Standarization.

Fuertes, V. S. (2001). *Hydraulic Transients with Entrapped Air Pockets*. PhD Thesis. Valencia: Department of Hydraulic Engineering, Polytechnic University of Valencia, Editorial Universitat Politècnica de València.

Fuertes-Miquel, V. S., Iglesias-Rey, P. L., García-Mares, F. J. & Mora-Meliá, D. (2009). Air Valves Behavior. Comparison between Compressible and Incompressible Modelling. Environmental Hydraulics - Theoretical, Experimental and Computational Solutions (pp. 293-296; doi: 10.1201/b10999-79). *Proceedings of the International Workshop on Environmental Hydraulics*, Valencia, España.

Fuertes-Miquel, V. S., Iglesias-Rey, P. L., López-Jiménez, P. A., Martínez-Solano, F. J., & López-Patiño, G. (enero-marzo, 2011). Utilización de las ventosas para la expulsión del aire durante el llenado de las tuberías. Comportamiento adiabático frente a isotermo. *Tecnología y Ciencias del Agua*, *2*(1), 33-50.

García-Mares, F. J., Iglesias-Rey, P. L., Fuertes-Miquel, V. S., Mora-Meliá, D., & López-Jiménez, P. A. (2009). Comparison of Air Valve Behavior by using CFD Techniques. Environmental Hydraulics - Theoretical, Experimental and Computational Solutions (pp. 319-322; doi: 10.1201/b10999-79). *Proceedings of the International Workshop on Environmental Hydraulics*, Valencia, España.

Lingireddy, S., Wood, D. J., & Zloczower, N. (July, 2004). Pressure Surges in Pipeline Systems Resulting from Air Releases. *Journal of American Water Works Association*, *96*(7), 88-94.

Vázquez, G., & Aguirre, S. (enero-abril, 1986). Análisis de fenómenos transitorios en el acueducto Cutzamala. *Ingeniería Hidráulica en México*, *2*(1), 44-51.

Wylie, E. B., & Streeter, V. L. (1993). *Fluid Transients in Systems*. New Jersey: Prentice Hall, Englewood Cliffs.

Zhou, F., Hicks, F. E., & Steffler, P. M. (2002). Transient Flow in a Rapidly Filling Horizontal Pipe Containing Trapped Air. *Journal of Hydraulic Engineering*, 128(6), 625-634, doi: 10.1061/(ASCE)0733-9429(2002)128:6(625).

Institutional Address of the Authors

Dr. Pedro L. Iglesias-Rey
Dr. Vicente S. Fuertes-Miquel
M.I. Francisco J. García-Mares
Dr. F. Javier Martínez-Solano

Universitat Politècnica de València
Departamento de Ingeniería Hidráulica y Medio Ambiente
Camino de Vera s/n
46022 Valencia, España
Teléfono: +34 (98) 3877 000, extensiones 86111, 86103, 86105 y 86104
piglesia@upv.es
vfuertes@upv.es
fjgarcia@upv.es
jmsolano@upv.es

Click here to write the autor

Non-Stationary Frequency Analysis of Annual Rainfall

• Gabriela Álvarez-Olguín* •
Universidad Tecnológica de la Mixteca, México
*Corresponding Author

• Carlos Agustín Escalante-Sandoval •
Universidad Nacional Autónoma de México

Abstract

Álvarez-Olguín, G., & Escalante-Sandoval, C. A. (January-February, 2016). Non-Stationary Frequency Analysis of Annual Rainfall. *Water Technology and Sciences* (in Spanish), 7(1), 69-86.

In northwestern Mexico, where water stress is high, strategies to address periods of water scarcity could fail if availability is evaluated based on mean runoff or precipitation values without considering changes in the behavior of these variables. The objective of this work was to estimate accumulated annual rainfall events in northwestern Mexico based on different return periods and future scenarios. Three non-stationary models were proposed for seven probability functions related to minimum values. The models were validated for series with statistical characteristics that change over time. A total of 221 accumulated annual rainfall series were evaluated, of which 36 (16%) were determined to be non-stationary. For these series, non-stationary models better represented the variability of the data than conventional models. A decrease in annual mean rainfall under 20% is predicted by the year 2044 at stations located on the California peninsula (Sonora and Sinaloa). The results suggest that these areas will be more vulnerable to future droughts.

Keywords: Frequency analysis, non-stationary series, water scarcity, drought, water availability, climate change, Northwestern Mexico.

Resumen

Álvarez-Olguín, G., & Escalante-Sandoval, C. A. (enero-febrero, 2016). Análisis de frecuencias no estacionario de series de lluvia anual. Tecnología y Ciencias del Agua, *7(1), 69-86.*

En las zonas del noroeste de México, donde existe una alta presión sobre el agua, las estrategias para afrontar periodos de escasez de este recurso podrían fallar si la disponibilidad se evalúa a través de valores medios de escurrimientos o precipitación, sin considerar el cambio en el comportamiento de tales variables. El objetivo de este trabajo fue estimar eventos de lluvia acumulada anual del noroeste de la república mexicana, asociados con diferentes periodos de retorno y escenarios futuros. Para siete funciones de probabilidad de valores mínimos se propusieron tres modelos no estacionarios válidos para series cuyas características estadísticas se han modificado a través del tiempo. Se analizaron 221 series de lluvia acumulada anual, de las cuales se determinó que 36 (16%) no son estacionarias; para 30 de éstas, los modelos no estacionarios representan mejor la variabilidad de los datos que los modelos convencionales. Se predice para el año 2044 una disminución menor que 20% de la lluvia media anual, en estaciones ubicadas en la península de California, Sonora y Sinaloa. Los resultados sugieren que estas zonas serán más susceptibles a sequías en el futuro.

Palabras clave: *análisis de frecuencias, series no estacionarias, escasez de agua, sequías, disponibilidad de agua, cambio climático, noroeste de México.*

Received: 10/02/2015
Accepted: 21/09/2015

Introduction

The use of frequency analyses to predict rainfall events is highly important to various engineering studies, such as the design of hydraulic works to control runoff, adequate land use planning and the evaluation of water availability. Furthermore, because of their economic and social implications, frequency analyses should be performed with a high

degree of accuracy, since the underestimation of the availability of water could lead to faulty strategies to allocate water to users, particularly during prolonged droughts.

The classical methodology used to analyze and predict events involving hydrological variables is based on the theory of extreme values in non-stationary series. Under stationary conditions, the distribution of the variable of interest does not vary over time, it has no trends, changes or periodicities (Villarini & Smith, 2010). Nevertheless, because of climate change the validity of the stationarity of time series is being called into question by the scientific community (Milly et al., 2008; Gleick, 1989; Voss, May & Roeckner, 2002; Held & Soden, 2006; Webster, Holland, Curry, & Chang, 2005). According to the Intergovernmental Panel on Climate Change (IPCC, 2007), human activities are causing a warming of the planet, in which many long-term changes in the climate have been registered. These include possible increases in the intensity of tropical cyclones and heat waves as well as in the intensity and frequency of extreme events such as droughts and torrential rains. Climate change is expected to increase the current stress on water resources resulting from population growth, economic changes and land use changes, particularly urbanization (IPCC, 2007). Therefore, identifying water availability is key to create strategies to address periods of scarcity, although the process of allocating water to users could be inefficient if availability is evaluated based on mean runoff or precipitation values without including seasonal changes in the behavior of these variables. Better strategies to distribute water could be created if availability is estimated based on rainfall events associated with a certain probability and scenarios that consider a decrease in rainfall.

The climate scenarios that have been generated for Mexico suggest a possible decrease in precipitation in many regions of the country. Therefore, under a climate change scenario with prolonged drought conditions, the ongoing development of society would be at risk (Magaña-Rueda & Gay-García, 2002), primarily in northwestern Mexico where water resources are under a high degree of stress (Conagua, 2012). Given this context, the objective of the work herein was to estimate accumulated annual rainfall events in northwestern Mexico based on different return periods and future scenarios. The estimations were performed using valid probabilistic models with non-stationary time series. The results obtained could be used as a basis to adequately evaluate the availability of water in the region.

Materials and Methods

The study area includes the states of Baja California Norte, Baja California Sur, Sonora, Sinaloa, Chihuahua and Durango, located in northwestern Mexico (Figure 1). These states were selected due to the high stress on water resources in this area (Conagua, 2012) and its high vulnerability to droughts.

This work used rain gauge data from daily records registered by conventional weather stations located in the study area, obtained from the *CLICOM* database (Climate Computing Project) produced by the National Weather Service, part of the National Water Commission (Conagua). The stations selected were those having at least 90% of records with complete data between 1950 and 2013. The Grubbs and Beck test (1972) was used to identify the annual rainfall values that considerably deviated from the distribution of the data. These were compared to records from neighboring stations to corroborate their magnitude. Clearly erroneous values were eliminated and inverse distance weighted interpolation was applied (Shepard, 1968) to deduce missing data, which included two support stations and a distance exponent of 2. Relative information criteria (I) as defined by Escalante-Sandoval and Reyes-Chávez (2002) was used to verify whether the es-

Figure 1. Location of the study area.

timation of the mean and the variance of the expanded samples improved. This is represented by:

$$I = \frac{Var\left(S^2_{y_1}\right)}{Var\left(S^2_{y}\right)} \quad (1)$$

Where $Var\left(S^2_{y_1}\right)$ is the variance of the variance of the original series and $Var\left(S^2_{y_2}\right)$ is the variance of the variance of the expanded series.

If $I > 1$, then the variance of the variance of the expanded series does not exceed the original variance, and therefore the expansion of the registries is adequate. Based on the above, reliable daily rainfall data were obtained from 221 stations.

To spatially compare the changes that occurred in the rainfall series, monthly rainfall was regionalized based on a principal component analysis (PCA) in S-mode (Richman, 1986). The first five components that explained 73% of the variance of the precipitation were selected. Direct oblique rotation was performed with the remaining components, with an obliqueness parameter δ = 0. To delimit homogenous regions, each station was assigned the principal component with the largest absolute weight, considering only those with values over 0.4. The regions were defined according to the area of influence corresponding to each station, obtained using the Thiessen polygon method.

The next step was to verify the presence of gradual changes (trends) in the series or abrupt changing points in the mean and/or variance of the distribution of the variable of interest (Villarini et al., 2009). The Pettitt test (Pettitt, 1979) was applied in order to detect significant changes in the mean (median) of the series when the changing point was unknown. The trends in the series were analyzed by empirical mode decomposition (EMD), developed by Huang et al. (1998), which is an intuitive and direct method adaptable to non-linear and non-stationary processes. Recent studies have demonstrated its effectiveness for analyzing long-term trends and signs (Qian, Wu, Fu, & Zhou, 2010; Carmona,

2010; Wu, Huang, Long, & Peng, 2007). To determine the significance of the trends, the residuals obtained by the EMD were analyzed with the Mann-Kendall test (Kendall, 1975).

Of the large-scale phenomena that influence climate variability in Mexico, Pacific Decadal Oscillation (PDO) was chosen for inclusion in the frequency analysis of rainfall, given the association between persistent episodes with negative PDO values and severe and prolonged drought conditions throughout the west-central portion of North America (Cook, Woodhouse, Eakin, Meko, & Stahle, 2004). Thus, the correlation between regional annual accumulated rainfall and the PDO index was analyzed based on the correlation coefficient ϱ (rho) proposed by Spearman (1904), a non-parametric test that measures the association between two discrete variables, as defined by equation (2):

$$\rho = 1 - \left[\frac{6\sum d^2}{N\left(N^2 - 1\right)} \right] \tag{2}$$

Where the values of ρ vary on the interval [-1, 1]; d is the difference of the values x-y; N, the number of pairs which for $N > 20$, follows a Student-t distribution (3):

$$t = \frac{\rho}{\sqrt{\frac{\left(1-\rho^2\right)}{\left(n-2\right)}}} \tag{3}$$

In the analysis, to consider the lack of stationarity in the series, the parameters of the distributions can be associated with more than one covariable. The inclusion of covariables has made it possible to incorporate large-scale atmospheric circulation trends or indices —such as ENSO (El Niño-Southern Oscillation), PDO (Pacific Decadal Oscillation) and NAO (North Atlantic Oscillation)— in the modeling of extreme precipitation data (Katz, Parlange, & Naveau, 2002; El Adlouni, Ouarda, Zhang, Roy, & Bobée, 2007; Villarini, Smith, & Napolitano, 2010; Vovoras & Tsokos, 2009; Ouarda & El Adlouni, 2011), maximum temperatures (Villarini et al., 2010), maximum flows (Villarini et al., 2009; Towler et al., 2010; Vogel, Yaindl, & Walter, 2011), extreme sea levels (Coles, 2001) and hurricane intensity (Mestre & Hallegatte, 2009).

Since a general theory has not been established for non-stationary processes, it is common to use standard and expanded models of extreme values as a basis (Coles, 2001). For example, the log-normal distribution (*LN*3) with parameters x_0, μ and σ (location, scale and shape, respectively) can be used to obtain a suitable model to estimate the variable xt in function of time, as follows:

$$x_t \sim LN3\left(x_0(t), \mu(t), \sigma(t)\right) \tag{4}$$

where each parameter $x_0(t)$, $\mu(t)$ and $\sigma(t)$ has an expression in terms of time. The parameter $\mu(t)$ can be expressed by equation (5):

$$\mu(t) = \mu_0 + \mu_1 t \tag{5}$$

where t corresponds to the annual rate of change over time. Thus, observed variations in the processes over time are modeled with a linear trend in the location parameter of a distribution.

The maximum likelihood method (Katz et al., 2002) can be used to estimate the parameters of a model in function of time or of another covariable. This is considered to be the most efficient method since it is the one that results in the parameters with the smallest sampling variances, and therefore, the smallest variances in the estimated events. It also has the advantage of being adaptable to structural changes in the model.

For a proposed non-stationary model of the *LN*3 function, the likelihood function is

$$l = -\left\{ \sum_{t=1}^{n} \left(\ln\left(x - x_0(t)\right) + \ln\left(\sigma(t)\right)\right) + \frac{1}{2}\left(\frac{\ln\left(x - x_0(t)\right) - \mu(t)}{\sigma(t)} \right)^2 \right\} \tag{6}$$

Where $x_0(t)$, $\mu(t)$ and $\sigma(t)$ are location, scale and shape parameters, respectively, in function of time or of another covariable.

In terms of the analysis of accumulated annual rainfall in northwestern Mexico, it is of interest to know which future scenarios reflect the most adverse water scarcity. Although rainfall events should be predicted based on probability functions of minimum values, non-stationary probabilistic models for distribution functions of minimum values do not exist. Therefore, the models described in Table 1 were proposed, where model M_0 corresponds to the conventional frequency analysis and M_1, M_2 and M_3 to non-stationarity. Their parameters are expressed in terms of time and the PDO index. The average annual PDO series was obtained based on monthly values from the period 1950 to 2013, downloaded from the United States National Climatic Data Center (NCDC, 2013).

For each station, the estimators of the functions' parameters were obtained after maximizing the respective logarithmic likelihood functions. The models that best describe the variability of the data were selected according to the Akaike Information Criterion (*AIC*) (1974), for which expression (7) was used. The best model is the one with the smallest *AIC* value. In the case of having similar AIC values, the model with the fewest parameters was selected:

$$AIC = -2(l) + 2K \qquad (7)$$

Where l is the maximum value of the likelihood function and K is the number of parameters estimated.

The method described by Coles (2001) was used to compare the validity of an M_1 model against another M_0, such that $M_0 \subset M_1$, which uses the discordance measurement defined by expression (8).

$$D = 2\left\{l_1\left(M_1\right) - l_0\left(M_0\right)\right\} \qquad (8)$$

Where $L(M_i)$ is the maximum value of the logarithmic likelihood function of model M_i.

The D statistic is distributed according to the chi-square distribution (χ^2_v). The parameter v is the difference between the number of parameters in models M1 and M_0. The values of D that are larger than the χ^2_v distribution are considered significant at a particular confidence level. Therefore, M_0 is rejected in favor of model M_1.

After selecting the best model, it is necessary to verify whether it will result in a good fit with the observed data. Given that the data in a non-stationary series are not identically distributed, they can be transformed (Coles, 2001; Katz *et al*., 2002). The transformation of the data consisted of their normalization, a process which Krzysztofowicz (1997) called a normal quantile transformation. This normalization was performed according to expression (9), in which a random variable X with a determined probability distribution F is transformed into a variable Y, with a standard normal distribution G:

$$Y = G^{-1}\left(F\left(X\right)\right) \qquad (9)$$

Where G^{-1} is the inverse function of the standard normal distribution defined by equation (10):

$$G\left(z\right) = \frac{1}{\sqrt{2\pi}} \int e^{\frac{-z^2}{2}} dz \qquad (10)$$

After arranging the standardized values and associating them with the corresponding Weibull empirical distribution values, the following data pairs are obtained:

$$\left\{\hat{Y}_{(m)}, G^{-1}\left(1 - \frac{m}{N+1}\right)\right\}; m = 1, \ldots, N \qquad (11)$$

Quantile-quantile (Q-Q) graphs and "worm plots" (Buuren & Fredriks, 2001) were generated with the above data pairs. In

Water Technology and Sciences. Vol. VII, No. 1, January-February, 2016, pp. 69-86

Table 1. Models proposed for the probability density functions for the minimum values used in the analysis of annual accumulated rainfall.

Distribution	Probability density function	Restrictions	Stationary	Non-stationary		
			M_0	M_1	M_2	M_3
Log normal 3p (*LN*3)	$f(x)=\frac{1}{(x-x_0)\sigma\sqrt{2\pi}}e^{-\frac{1}{2}\left(\frac{\ln(x-x_0)-\mu}{\sigma}\right)^2}$	$x>x_0$	$\mu(t)=\mu_0$ $\sigma(t)=\sigma$ $x_0(t)=x_0$	$\mu(t)=\mu_0+\mu_1 t$ $\sigma(t)=\sigma$ $x_0(t)=x_0$	$\mu(t)=\mu_0+\mu_1 PDO_t$ $\sigma(t)=\sigma$ $x_0(t)=x_0$	$\mu(t)=\mu_0+\mu_1 t+\mu_2 PDO_t$ $\sigma(t)=\sigma$ $x_0(t)=x_0$
Gamma 3p (*GA*3)	$f(x)=\frac{1}{\alpha\Gamma(\beta)}\left(\frac{x-x_0}{\alpha}\right)^{\beta-1}e^{-\left(\frac{x-x_0}{\alpha}\right)}$	$x\geq x_0;\ \alpha>0;\ \beta>0$	$x_0(t)=\lambda_0$, $\alpha(t)=\alpha$, $\beta(t)=\beta$	$x_0(t)=\lambda_0+\lambda_1 t$ $\alpha(t)=\alpha$ $\beta(t)=\beta$	$x_0(t)=\lambda_0+\lambda_1 PDO_t$ $\alpha(t)=\alpha$ $\beta(t)=\beta$	$x_0(t)=\lambda_0+\lambda_1 t+\lambda_2 PDO_t$ $\alpha(t)=\alpha$ $\beta(t)=\beta$
Gumbel (*G*)	$f(x)=\frac{1}{\alpha}e^{-e^{-\left(\frac{\omega-x}{\alpha}\right)}}e^{-\left(\frac{\omega-x}{\alpha}\right)}$	$\alpha>0$	$\omega(t)=\omega_0\ \alpha(t)=\alpha$	$\omega(t)=\omega_0+\omega_1 t$ $\alpha(t)=\alpha$	$\omega(t)=\omega_0+\omega_1 PDO_t$ $\alpha(t)=\alpha$	$\omega(t)=\omega_0+\omega_1 t+\omega_1 PDO_t$ $\alpha(t)=\alpha$
Weibull (*W*3)	$f(x)=\frac{\alpha}{\beta-\gamma}\left(\frac{x-\gamma}{\beta-\gamma}\right)^{\alpha-1}e^{-\left(\frac{x-\gamma}{\beta-\gamma}\right)^{\alpha}}$	$x\geq\gamma;\ \beta>\gamma;\ \alpha>0$	$\gamma(t)=\gamma$ $\beta(t)=\beta$ $\alpha(t)=\alpha$	$\gamma(t)=\gamma_0+\gamma_1 t$ $\beta(t)=\beta$ $\alpha(t)=\alpha$	$\gamma(t)=\gamma_0+\gamma_1 PDO_t$ $\beta(t)=\beta$ $\alpha(t)=\alpha$	$\gamma(t)=\gamma_0+\gamma_1 t+\gamma_2 PDO_t$ $\beta(t)=\beta$ $\alpha(t)=\alpha$
Mixed Weibull (*WW*)	$f(x)=p\left(\frac{\alpha_1}{\beta_1-\gamma_1}\right)\left(\frac{x-\gamma_1}{\beta_1-\gamma_1}\right)^{\alpha_1-1}e^{\left(\frac{x-\gamma_1}{\beta_1-\gamma_1}\right)^{\alpha_1}}$ $+(1-p)\left(\frac{\alpha_2}{\beta_2-\gamma_2}\right)\left(\frac{x-\gamma_2}{\beta_2-\gamma_2}\right)^{\alpha_2-1}e^{\left(\frac{x-\gamma_2}{\beta_2-\gamma_2}\right)^{\alpha_2}}$	$x\geq\gamma_1;\ \beta_1>\gamma_1;\ \alpha_1>0,$ $x\geq\gamma_2;\ \beta_2>\gamma_2;\ \alpha_2>0,$ $0\leq p\leq 1$	$\gamma_1(t)=\varphi_0$ $\beta_1(t)=\beta_1$ $\alpha_1(t)=\alpha_1$ $\gamma_2(t)=\gamma_2$ $\beta_2(t)=\beta_2$ $\alpha_2(t)=\alpha_2$	$\gamma_1(t)=\varphi_0+\varphi_1 t$ $\beta_1(t)=\beta_1$ $\alpha_1(t)=\alpha_1$ $\gamma_2(t)=\upsilon_0+\upsilon_1 t$ $\beta_1(t)=\beta_2$ $\alpha_2(t)=\alpha_2$	$\gamma_1(t)=\varphi_0+\varphi_1 PDO_t$ $\beta_1(t)=\beta_1$ $\alpha_1(t)=\alpha_1$ $\gamma_2(t)=\upsilon_0+\upsilon_1 PDO_t$ $\beta_1(t)=\beta_2$ $\alpha_2(t)=\alpha_2$	$\gamma_1(t)=\varphi_0+\varphi_1 t+\varphi_2 PDO_t$ $\beta_1(t)=\beta$ $\alpha_1(t)=\alpha_1$ $\gamma_2(t)=\upsilon_0+\upsilon_1 t+\upsilon_2 PDO_t$ $\beta_1(t)=\beta_2$ $\alpha_2(t)=\alpha_2$
Mixed Gumbel (*GG*)	$f(x)=\frac{p}{\alpha_1}e^{-e^{-\left(\frac{\varpi_1-x}{\alpha_1}\right)}}e^{-\left(\frac{\varpi_1-x}{\alpha_1}\right)}$ $+\frac{(1-p)}{\alpha_2}e^{-e^{-\left(\frac{\varpi_2-x}{\alpha_2}\right)}}e^{-\left(\frac{\varpi_2-x}{\alpha_2}\right)}$	$x\geq 0;\ \alpha_1>0,\ \alpha_2>0,$ $0\leq p\leq 1$	$\omega_1(t)=\kappa_0\ \alpha_1(t)=\alpha_1$ $\omega_2(t)=\omega_2\ \alpha_2(t)=\alpha_2$	$\omega_1(t)=\kappa_0+\kappa_1 t$ $\alpha_1(t)=\alpha_1$ $\omega_2(t)=\eta_0+\eta_1 t$ $\alpha_2(t)=\alpha_2$	$\omega_1(t)=\kappa_0+\kappa_1 PDO_t$ $\alpha_1(t)=\alpha_1$ $\omega_2(t)=\eta_0+\eta_1 PDO_t$ $\alpha_2(t)=\alpha_2$	$\omega_1(t)=\kappa_0+\kappa_1 t+\kappa_2 PDO_t$ $\alpha_1(t)=\alpha_1$ $\omega_2(t)=\eta_0+\eta_1 t+\eta_2 PDO_t$ $\alpha_2(t)=\alpha_2$
Gumbel Weibull (*GW*)	$f(x)=\frac{p}{\alpha_1}e^{-e^{-\left(\frac{\varpi_1-x}{\alpha_1}\right)}}e^{-\left(\frac{\varpi_1-x}{\alpha_1}\right)}$ $+(1-p)\left(\frac{\alpha_2}{\beta_2-\gamma_2}\right)\left(\frac{x-\gamma_2}{\beta_2-\gamma_2}\right)^{\alpha_2-1}e^{-\left(\frac{x_2-\gamma_2}{\beta_2-\gamma_2}\right)^{\alpha_2}}$	$\alpha_1>0,\ x\geq\gamma_2;\ \beta_2>\gamma_2;$ $\alpha_2>0,\ 0\leq p\leq 1$	$\omega_1(t)=\kappa_0\ \alpha_1(t)=\alpha_1$ $\gamma_2(t)=\gamma_2$ $\beta_1(t)=\beta_2$ $\alpha_2(t)=\alpha_2$	$\omega_1(t)=\kappa_0+\kappa_1 t$ $\alpha_1(t)=\alpha_1$ $\gamma_2(t)=\upsilon_0+\upsilon_1 t$ $\beta_1(t)=\beta_2$ $\alpha_2(t)=\alpha_2$	$\omega_1(t)=\kappa_0+\kappa_1 PDO_t$ $\alpha_1(t)=\alpha_1$ $\gamma_2(t)=\upsilon_0+\upsilon_1 PDO_t$ $\beta_1(t)=\beta_2$ $\alpha_2(t)=\alpha_2$	$\omega_1(t)=\kappa_0+\kappa_1 t+\kappa_2 PDO_t$ $\alpha_1(t)=\alpha_1$ $\gamma_2(t)=\upsilon_0+\upsilon_1 t+\upsilon_2 PDO_t$ $\beta_1(t)=\beta_2$ $\alpha_2(t)=\alpha_2$

t : index that depends on time, for 1950, $t = 1$.
PDO_t: Annual value of the PDO index corresponding to t.

a "worm plot" graph, the vertical axis is the difference between the empirical and theoretical values, and contains the 95% confidence interval as in equation (12):

$$\mp 1.96 f(z)^{-1} \sqrt{\left(p(1-p)/n\right)} \qquad (12)$$

Where $f(z)$ is the normal density function; z is an event associated with a probability and n is the sample size.

Lastly, the design events $\hat{X}$, aassociated with different return periods were estimated. For the LN3 function, with the M_3 model, the design events were estimated by solving equation (13):

$$\hat{X} = \hat{x}_o + \exp\left\{F^{-1}\left(p/\hat{\mu}(t), \hat{\sigma}\right)\right\} \qquad (13)$$

$$\hat{\mu}(t) = \hat{\mu}_0 + \hat{\mu}_1 t_0 + \hat{\mu}_2 \widehat{PDO} \qquad (14)$$

$$p = F\left(x/\hat{\mu}(t), \hat{\sigma}\right) = \frac{1}{\sigma\sqrt{2\pi}} \int_{-\infty}^{x} e^{-\frac{1}{2}\left(\frac{z-\hat{\mu}(t)}{\sigma}\right)^2} \qquad (15)$$

Where $\hat{x}_0$ is the estimator of the location parameters; $\hat{\sigma}$ is the estimator of the shape parameters, and $\hat{\mu}(t)$ the scale parameter in function of the estimators $\hat{\mu}_0$, $\hat{\mu}_1$ and $\hat{\mu}_2$; t_0 is the value of the time index for a particular scenario (t_0= 65 for the scenario corresponding to the year 2014 and t_0 = 95 for the scenario corresponding to the year 2044); $\widehat{PDO}$ is the average value of the PDO index and $\hat{X}$ is the design event associated with a return period T and a future scenario t_0.

The analysis of the data included the period 1950 to 2013, and therefore t_0 = 1 for the first year (1950) and t_0 = 64 for the last year (2013). Thus, for later years, the values of the time index were consecutively increased one unit.

Due to the association between negative PDO values with periods of rainfall deficits, the value $\widehat{PDO}$ was estimated as the arithmetic mean of the PDO values corresponding to the period of anomalies with the largest annual accumulated rainfall deficit analyzed.

Results and Discussion

Figure 2 presents the spatial distribution of annual accumulated rainfall in the study area. The lowest values were found on the California peninsula, with under 200 mm per year, which was the area with the least precipitation nationwide. In contrast, values over 1 000 mm were obtained in Sonora, Sinaloa, Chihuahua and Durango.

The principal component analysis resulted in five components that explained 73% of the variance of the precipitation. After assigning the component with the greatest weight to the Thiessen polygon for each station, it was possible to spatially identify groups of polygons associated with the same component. Each group was considered to be a homogenous region. The five regions shown in Figure 2 were thereby generated.

Table 2 shows that 19% of the series analyzed was not stationary, 47% of which was located in region 1, which primarily includes the states of Sonora and Sinaloa. In addition, 73% of the total series with significant decreases in changing points correspond to region 1. Also located in this region are the three series with decreasing changing points and trends and two of the three series with declining trends.

A Spearman correlation of 0.43 was obtained for the PDO index and the accumulated rainfall series for region 3 —statistically significant at any level. The correlation was 0.2 for regions 4 and 5, significant at a level of 0.1. Since the correlation was positive for these three regions, and with the PDO in a persistent negative phase, periods with a rainfall deficit would occur, as seen in region 3 between 1950 and 1975 (Figure 3a). Cook *et al*. (2004) reported an association between prolonged episodes of negative PDO values and severe and prolonged drought conditions throughout the west and central portions of North America. Between 1977 and 1997, a

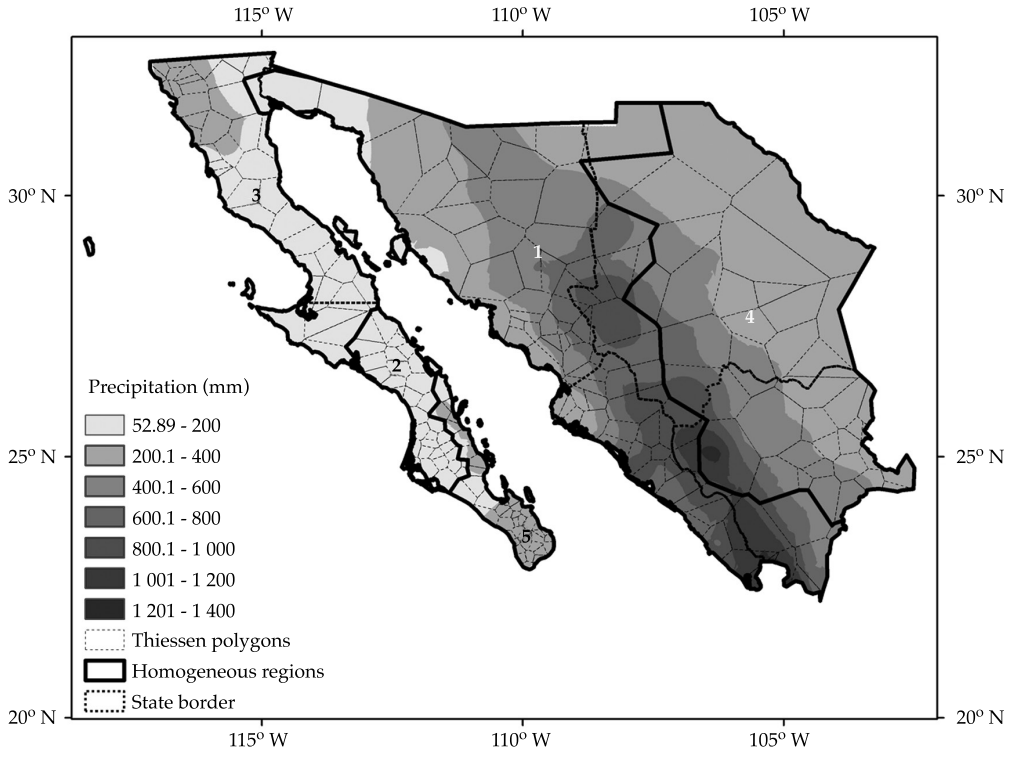

Figure 2. Homogeneous regions and distribution of annual accumulated rainfall.

Table 2. Number of annual accumulated rainfall series, acccording to the conditions determined by the Pettitt and Mann-Kendall tests, with a significance level of 0.05.

Region	Total	S	NS	IC	DC	IT	DT	IC & IT	DC & DT
1	72	55	17	2	8	0	2	2	3
2	33	27	6	1	0	3	1	1	0
3	43	38	5	2	3	0	0	0	0
4	34	28	6	0	0	2	0	4	0
5	39	37	2	1	0	0	0	1	0
Total	**221**	**185**	**36**	**6**	**11**	**5**	**3**	**8**	**3**

S: stationary; NS: non-stationary; IC: increasing change; DC: decreasing change; IT: increasing trend; DT: decreasing trend; IC & IT increeasing change and increasing trend; DC & DT decreasing change and decreasing trend.

positive PDO regime was present, and a trend towards a negative phase apparently began in 1998. Therefore, a change in polarity is very likely over the coming decades (Mantua, Hare, Zhang, Wallace & Francis, 1997; MacDonald & Case, 2005). Given what has been presented above, the loss in stationarity in the series corresponding to increased rainfall may be largely due to the influence of the positive PDO phase. Therefore, the persistence of negative PDO values that may cause prolonged droughts was considered in the analysis of the prediction of rainfall.

The goodness of fit tests of the frequency analysis of the 221 annual accumulated rainfall series indicate that statistically

non-stationary models better represent the variability of the data for 84 of these series (Table 3). In the case of the non-stationary series, non-stationary models better fit the data in 83% of these cases. For the remaining non-stationary series, while the *AIC* statistic indicated that the non-stationary models were better, the measurement of discordance (D) was under 3.85 χ^2_ν at a level of $\alpha = 0.05$), and therefore the use of models M_1, M_2, and M_3 instead of M_0 was not justified.

M_2 or M_3 were the majority (60%) of the non-stationary models selected for the *LN*3 function. The results obtained are consistent with the stationarity and correlation tests performed. For example, model M_2 was selected for 20 cases in region 3, which had the highest PDO correlation. Meanwhile, 22 M_3 models were selected for region 1, where 47% of the stations with non-stationary series was located. It is important to mention that for the GW distribution, model M_0 was selected for 61 of the stationary series. Therefore, mixed distributions better represent the variability of the data when they are stationary.

As an example of the procedure to select the best model, Tables 4 and 5 show the results from the goodness-of-fit tests and the estimators of the parameters of the models fitted with the series from stations 2060 ("Santa Cruz", Ensenada, Baja California) and 25082 ("San Blas", El Fuerte, Sinaloa), respectively. It is worth mentioning that the Pettitt test indicates that the series from station 2060 presented a significant breaking point in the year 2002, at a level of 0.05, with a decreasing change in the mean of the series (Figure 3b). Whereas for station 25082, the residual obtained with the EMD method (Figure 3c) indicates a monotonically decreasing trend (at a level of 0.05), according to the Mann-Kendall test.

For station 2060, the model with the lowest *AIC* value was M_2 for the function *LN*3, where the scale parameter was based on the PDO index. The value of the D statistic was over 3.84, which indicates that it is more suitable and better explains the variability of the data than model M_0. For the rainfall series from station 25082, M_1 for the *GA*3 function (which included a trend in the location parameter) better represented the variability of the data than the other models. The *AIC* value was lowest with model M_1, with a statistically significant D value of 5.0.

Figure 4 corresponds to the "worm plot" and quantile-quantile (Q-Q) graphs of stations 2060 and 25082 with the models mentioned. The data fall within the confidence limits and are near the unit diagonal in both cases. Therefore, it was determined that the models selected adequately fit the data.

For station 2060, a PDO index value of -0.86 was used to estimate design events, the average of the period from 2007 to 2013 characterized by the persistence of negative values and which included the largest rainfall deficit (Figure 3b). Therefore, for model M_2 for

Table 3. Number of models selected to predict annual accumulated rainfall events per region.

		Log normal 3p				Gamma 3p				Weibull	Gumbel-Weibull
Region	Total	M_0	M_1	M_2	M_3	M_0	M_1	M_2	M_3	M_0	M_0
1	72	4	0	0	10	10	2	0	12	7	27
2	33	6	2	5	2	3	0	1	2	6	6
3	43	3	0	16	9	4	0	4	0	2	5
4	34	7	4	0	0	8	1	0	3	2	9
5	39	3	0	6	2	5	0	2	1	6	14
Total	**221**	**23**	**6**	**27**	**23**	**30**	**3**	**7**	**18**	**23**	**61**

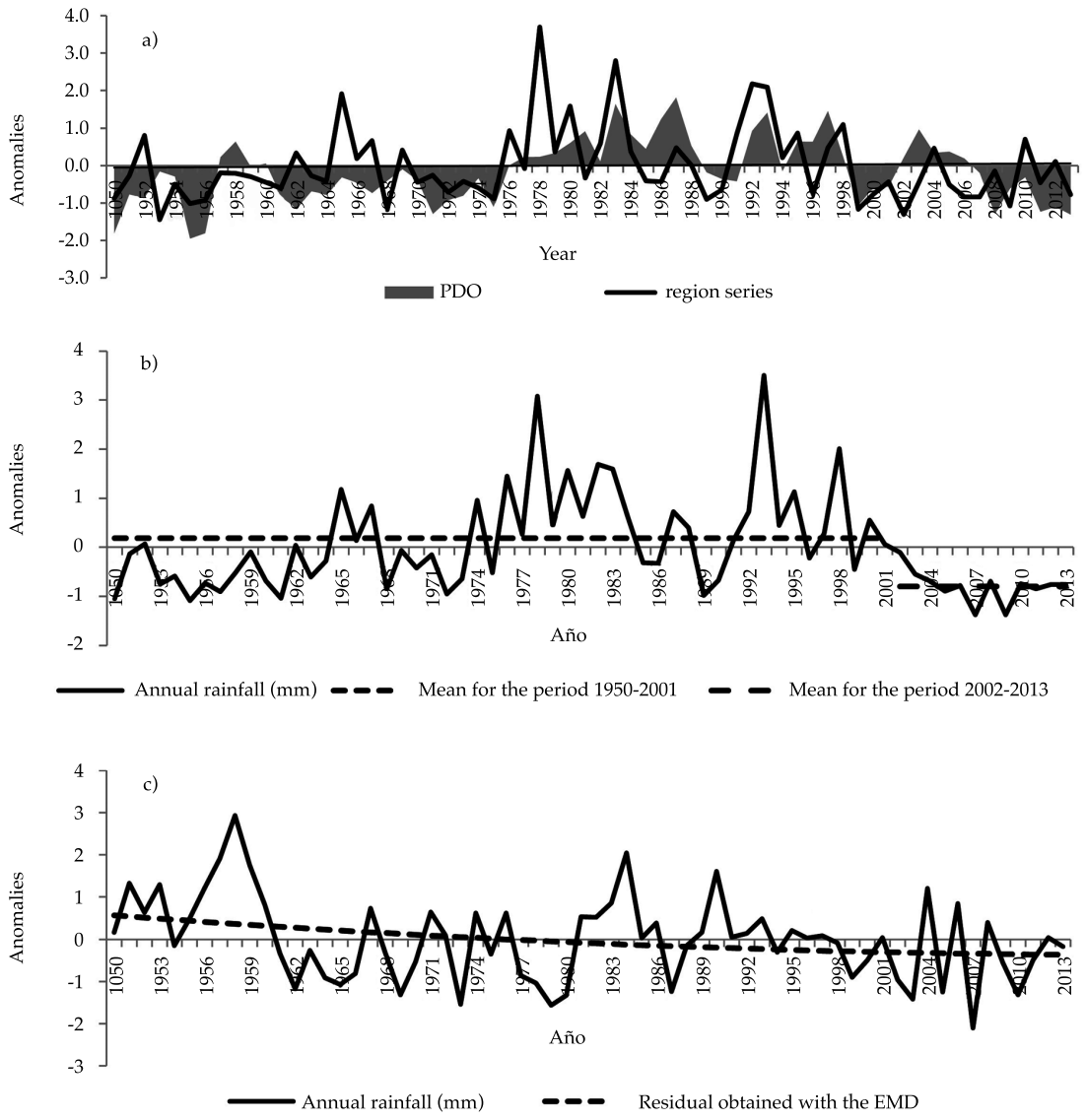

Figure 3. Temporal variation of annual series from northwestern Mexico: a) mean rainfall in region 3 and PDO index; b) Station 2060, "Santa Cruz", Ensenada, Baja California; c) station 25082, "San Blas", El Fuerte, Sinaloa.

the function *LN*3 (Table 4), the estimators of the parameters were:

$$\hat{\mu}(t) = \hat{\mu}_0 + \hat{\mu}_1 \widehat{PDO} = 5.65 + (0.29)(-0.86)$$

$$= 5.40, \hat{x}_0 = 0.05, \hat{\sigma} = 0.43$$

The values of the design events associated with different non-exceedance probabilities, p, were estimated by solving the following expression:

$$\hat{X} = 0.05 + \exp\left\{LN3^{-1}\left(p \middle| 5.40, 0.43\right)\right\}$$

Where $LN3^{-1}$ is the inverse log-normal probability distribution function.

Meanwhile, for station 25082 (Table 5), the parameters estimated for model M_1 with the *GA*3 were as follows:

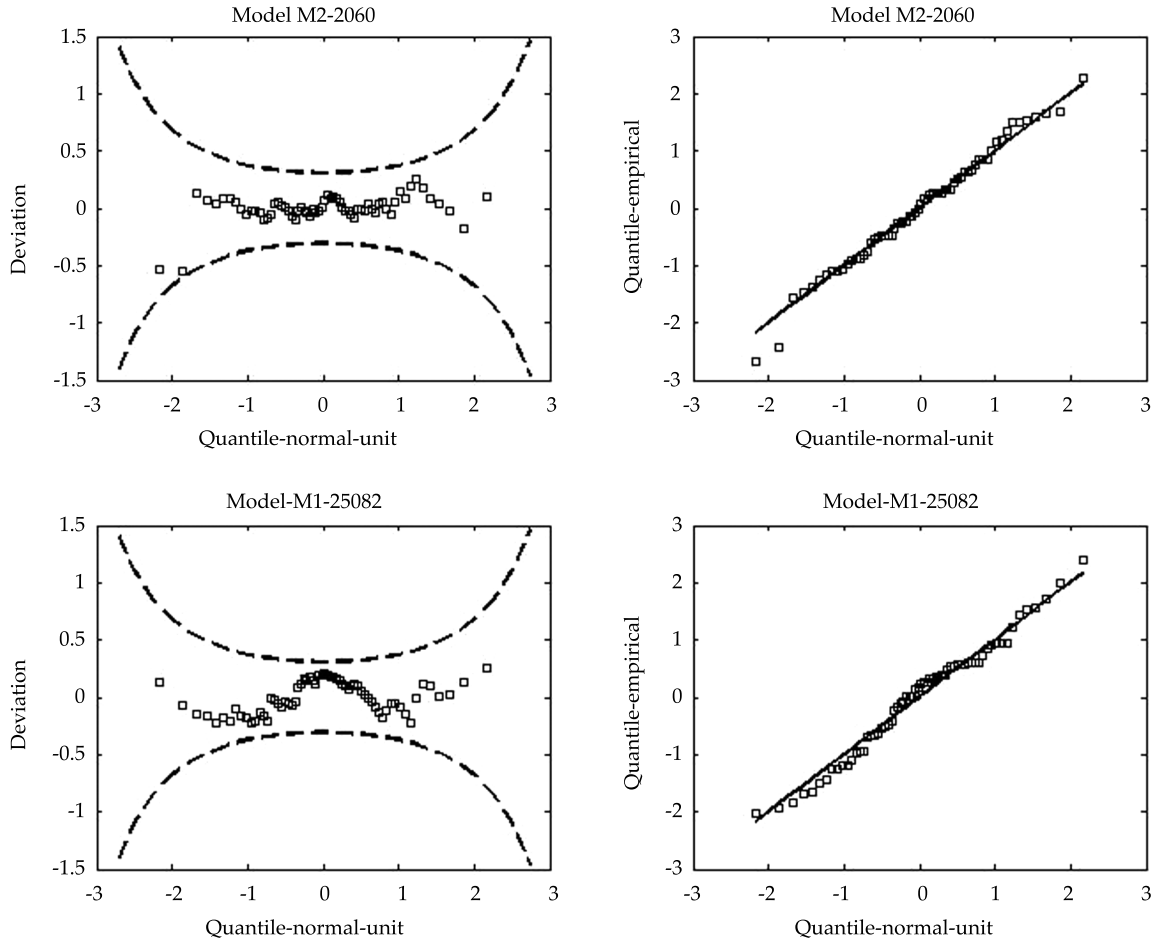

Figure 4. "Worm plot" (left) and Q-Q (right) for the visual analysis of the fit of the models selected; a) station 2060, "Santa Cruz", Ensenada, Baja California; b) station 25082, "San Blas", El Fuerte, Sinaloa.

For the scenario corresponding to the year 2014:

$$\hat{x}_0(t) = \hat{\lambda}_0 + \hat{\lambda}_1 t_o = -240.47 + (-2.59)(65) = -408.82, \ \hat{\alpha} = 33.17, \ \hat{\beta} = 26.43.$$

For the scenario corresponding to the year 2044:

$$\hat{x}_0(t) = \hat{\lambda}_0 + \hat{\lambda}_1 t_o = -240.47 + (-2.59)(95) = -486.52, \hat{\alpha} = 33.17, \hat{\beta} = 26.43.$$

The expressions used to estimate the design events were as follows:

For the scenario corresponding to the year 2014:

$$\hat{X} = -408.82 + GA3^{-1}(p|\, 26.43, 33.17)$$

For the scenario corresponding to the year 2044:

$$\hat{X} = -486.52 + GA3^{-1}(p|\, 26.43, 33.17)$$

Where $GA3^{-1}$ is the inverse gamma probability distribution function.

Figure 5 shows the graphic representation of the design events estimated for stations

Table 4. Results from the goodness-of-fit tests for station 2060 ("Santa Cruz", Ensenada, Baja California).

Station	Function	AIC	D	Estimators of the parameters										
				$\hat{\mu}_0$	$\hat{\mu}_1$	$\hat{\mu}_2$	$\hat{x}_0$	$\hat{\sigma}$						
2060	*LN*3 (M_0)	815.3	-	5.61	-	-	0.00	0.50	-	-	-	-	-	-
2060	*LN*3 (M_1)	817.3	0.0	5.63	0.00	-	0.00	0.50	-	-	-	-	-	-
2060	*LN*3 (M_2)	799.8	17.5	5.65	0.29	-	0.05	0.43	-	-	-	-	-	-
2060	*LN*3 (M_3)	799.9	1.9	5.79	0.00	0.31	0.02	0.43	-	-	-	-	-	-
				λ_0	λ_1	λ_2	$\hat{\alpha}$	β						
2060	*GA*3 (M_0)	815.6	-	64.50	-	-	102.56	2.37	-	-	-	-	-	-
2060	*GA*3 (M_1)	816.0	1.6	84.02	-0.42	-	103.77	2.29	-	-	-	-	-	-
2060	*GA*3 (M2)	810.3	7.3	-19.71	56.74	-	54.17	6.21	-	-	-	-	-	-
2060	*GA*3 (M3)	811.0	1.3	5.87	-0.81	59.58	52.71	6.40	-	-	-	-	-	-
				$\hat{\gamma}_0$	$\hat{\gamma}_1$	$\hat{\gamma}_2$	β	$\hat{\alpha}$						
2060	*W*3 (M_0)	816.5	-	77.14	-	-	332.28	1.48	-	-	-	-	-	-
2060	*W*3 (M_1)	812.0	6.5	133.29	-0.91	-	318.37	1.22	-	-	-	-	-	-
2060	*W*3 (M_2)	818.3	0.2	72.00	-10.2	-	326.85	1.49	-	-	-	-	-	-
2060	*W*3 (M_3)	808.1	12.2	168.09	-1.40	16.57	323.54	0.98	-	-	-	-	-	-
				$\hat{\omega}_0$	$\hat{\omega}_1$	$\hat{\omega}_2$	$\hat{\alpha}$							
2060	*G* (M_0)	870.0	-	397.17	-	-	207.06	-	-	-	-	-	-	-
2060	*G* (M_1)	870.9	1.1	334.58	1.93	-	203.70	-	-	-	-	-	-	-
2060	*G* (M_2)	846.2	25.8	407.61	146.91	-	162.28	-	-	-	-	-	-	-
2060	*G* (M_3)	847.5	0.7	445.44	-1.14	154.50	161.04	-	-	-	-	-	-	-
				$\hat{\varphi}_0$	$\hat{\varphi}_1$	$\hat{\varphi}_2$	β_1	$\hat{\alpha}_1$	$\hat{\upsilon}_0$	$\hat{\upsilon}_1$	$\hat{\upsilon}_2$	β_2	$\hat{\alpha}_2$	$\hat{p}$
2060	*WW* (M_0)	822.2		77.2	-	-	328.7	48.2	77.3	-	-	332.2	1.5	0.0
2060	*WW* (M_1)	807.1	19.1	133.2	-0.9	-	318.4	1.6	134.5	-0.9	-	318.3	0.7	0.7
2060	*WW* (M_2)	816.6	9.6	72.5	-10.5	-	327.1	2.2	83.4	-0.3	-	325.2	0.5	0.8
2060	*WW* (M_3)	829.7	-9.1	167.5	-2.4	17.3	323.4	1.0	167.5	-1.4	16.3	323.4	1.0	0.6
				$\hat{\kappa}_0$	$\hat{\kappa}_1$	$\hat{\kappa}_2$	$\hat{\alpha}_1$		$\hat{\eta}_0$	$\hat{\eta}_1$	$\hat{\eta}_2$	$\hat{\alpha}_2$		$\hat{p}$
2060	*GG* (M_0)	839.4	-	526.8	-	-	192.9	-	254.1	-	-	65.4	-	0.4
2060	*GG* (M_1)	839.7	3.7	244.0	11.1	-	152.3	-	285.3	0.2	-	89.5	-	0.3
2060	*GG* (M_2)	816.2	27.2	578.0	247.7	-	104.5	-	309.6	84.1	-	77.6	-	0.2
2060	*GG* (M_3)	817.9	2.3	624.1	-2.6	230.0	123.0	-	318.5	-0.7	67.3	66.0	-	0.3
				$\hat{\kappa}_0$	$\hat{\kappa}_1$	$\hat{\kappa}_2$	$\hat{\alpha}_1$		$\hat{\upsilon}_0$	$\hat{\upsilon}_1$	$\hat{\upsilon}_2$	β_2	$\hat{\alpha}_2$	$\hat{p}$
2060	*GW* (M_0)	822.5	-	397.2	-	-	207.0	-	77.1	-	-	332.3	1.5	0.0
2060	*GW* (M_1)	818.7	7.8	234.3	14.9	-	120.1	-	130.7	-0.9	-	304.2	1.3	0.1
2060	*GW* (M_2)	820.1	6.4	574.3	245.4	-	118.3	-	65.9	-8.6	-	291.5	1.8	0.2
2060	*GW* (M_3)	818.3	5.8	445.4	-1.1	154.5	154.5	-	168.1	-1.4	16.6	323.5	1.0	0.1

AIC: Akaike information criterion (1974) (dimensionless); D: measurement of discordance (dimensionless)

Table 5 Results from the goodness-of-fit tests for station 25082("San Blas", El Fuerte, Sinaloa).

Station	Function	AIC	D	Estimators of the parameters										
				$\hat{\mu}_0$	$\hat{\mu}_1$	$\hat{\mu}_2$	$\hat{x}_0$	$\hat{\sigma}$						
25082	*LN*3 (M_0)	852.1		6.26	-	-	0.00	0.34	-	-	-	-	-	-
25082	*LN*3 (M_1)	848.9	5.1	6.43	-0.01	-	-0.01	0.33	-	-	-	-	-	-
25082	*LN*3 (M_2)	854.0	0.0	6.26	0.00	-	0.00	0.34	-	-	-	-	-	-
25082	*LN*3 (M_3)	850.5	0.4	6.44	-0.01	0.03	0.02	0.33	-	-	-	-	-	-
				λ_0	λ_1	λ_2	$\hat{\alpha}$	β						
25082	*GA*3 (M_0)	848.7		-241.20	-	-	39.94	19.86	-	-	-	-	-	-
25082	*GA*3 (M_1)	845.8	5.0	-240.47	-2.59	-	33.17	26.43	-	-	-	-	-	-
25082	*GA*3 (M_2)	850.7	0.0	-241.20	-0.88	-	39.95	19.85	-	-	-	-	-	-
25082	*GA*3 (M_3)	847.2	0.6	-990.42	-2.98	21.56	17.22	95.36	-	-	-	-	-	-
				$\hat{\gamma}_0$	$\hat{\gamma}_1$	$\hat{\gamma}_2$	β	$\hat{\alpha}$						
25082	*W*3 (M_0)	848.4		125.68	-	-	605.57	2.57	-	-	-	-	-	-
25082	*W*3 (M_1)	850.2	0.2	197.18	-1.10	-	607.81	2.33	-	-	-	-	-	-
25082	*W*3 (M_2)	847.4	3.0	89.13	-110.0	-	603.24	2.72	-	-	-	-	-	-
25082	*W*3 (M_3)	849.3	3.0	9.01	1.16	-133.4	600.10	2.96	-	-	-	-	-	-
				$\hat{\omega}_0$	$\hat{\omega}_1$	$\hat{\omega}_2$	$\hat{\alpha}$							
25082	*G* (M_0)	866.0		643.63	-	-	191.84	-	-	-	-	-	-	-
25082	*G* (M_1)	857.2	10.8	768.42	-4.01	-	172.22	-	-	-	-	-	-	-
25082	*G* (M_2)	865.5	2.5	650.44	44.64	-	185.02	-	-	-	-	-	-	-
25082	*G* (M_3)	854.2	4.9	776.41	-4.03	56.49	162.50	-	-	-	-	-	-	-
				$\hat{\varphi}_0$	$\hat{\varphi}_1$	$\hat{\varphi}_2$	β_1	$\hat{\alpha}_1$	$\hat{\upsilon}_0$	$\hat{\upsilon}_1$	$\hat{\upsilon}_2$	β_2	$\hat{\alpha}_2$	$\hat{p}$
25082	*WW* (M_0)	852.9		124.9	-	-	622.4	8.5	139.5	-	-	595.3	2.2	0.2
25082	*WW* (M_1)	856.3	0.6	194.3	-0.3	-	621.7	7.3	207.2	-1.1	-	593.2	2.0	0.2
25082	*WW* (M_2)	855.4	1.5	89.1	-	-109.8	603.2	2.7	89.1	-	-110.0	603.2	2.7	0.2
25082	*WW* (M_3)	858.9	1.3	6.5	2.5	-127.8	593.9	3.0	11.5	0.4	-134.8	597.2	2.8	0.6
				$\hat{\kappa}_0$	$\hat{\kappa}_1$	$\hat{\kappa}_2$	$\hat{\alpha}_1$		$\hat{\eta}_0$	$\hat{\eta}_1$	$\hat{\eta}_2$	$\hat{\alpha}_2$		$\hat{p}$
25082	*GG* (M_0)	854.7		810.4	-	-	171.4	-	561.7	-	-	114.9	-	0.2
25082	*GG* (M_1)	863.2	-4.5	768.4	-3.9	-	172.2	-	768.4	-4.0	-	172.2	-	0.1
25082	*GG*(M_2)	853.3	5.4	886.1	-	187.2	65.8	-	578.2	-	-4.4	126.7	-	0.1
25082	*GG*(M_3)	847.6	19.5	979.8	-4.1	116.3	63.0	-	675.8	-3.2	16.8	111.1	-	0.2
				$\hat{\kappa}_0$	$\hat{\kappa}_1$	$\hat{\kappa}_2$	$\hat{\alpha}_1$		$\hat{\upsilon}_0$	$\hat{\upsilon}_1$	$\hat{\upsilon}_2$	β_2	$\hat{\alpha}_2$	$\hat{p}$
25082	*GW* (M_0)	850.9		625.2	-	-	59.5	-	139.4	-	-	596.0	2.2	0.2
25082	*GW*(M_1)	852.2	2.7	632.2	7.5	-	57.2	-	106.5	-109.0	-	594.5	2.4	0.2
25082	*GW* (M_2)	852.2	2.7	632.2	-	7.5	57.2	-	106.5	-	-109.0	594.5	2.4	0.2
25082	*GW* (M_3)	855.8	0.4	630.7	-8.0	-1.5	49.2	-	109.9	0.8	-95.6	604.8	2.6	0.0

AIC: Akaike information criterion (1974) (dimensionless); D: measurement of discordance (dimensionless)

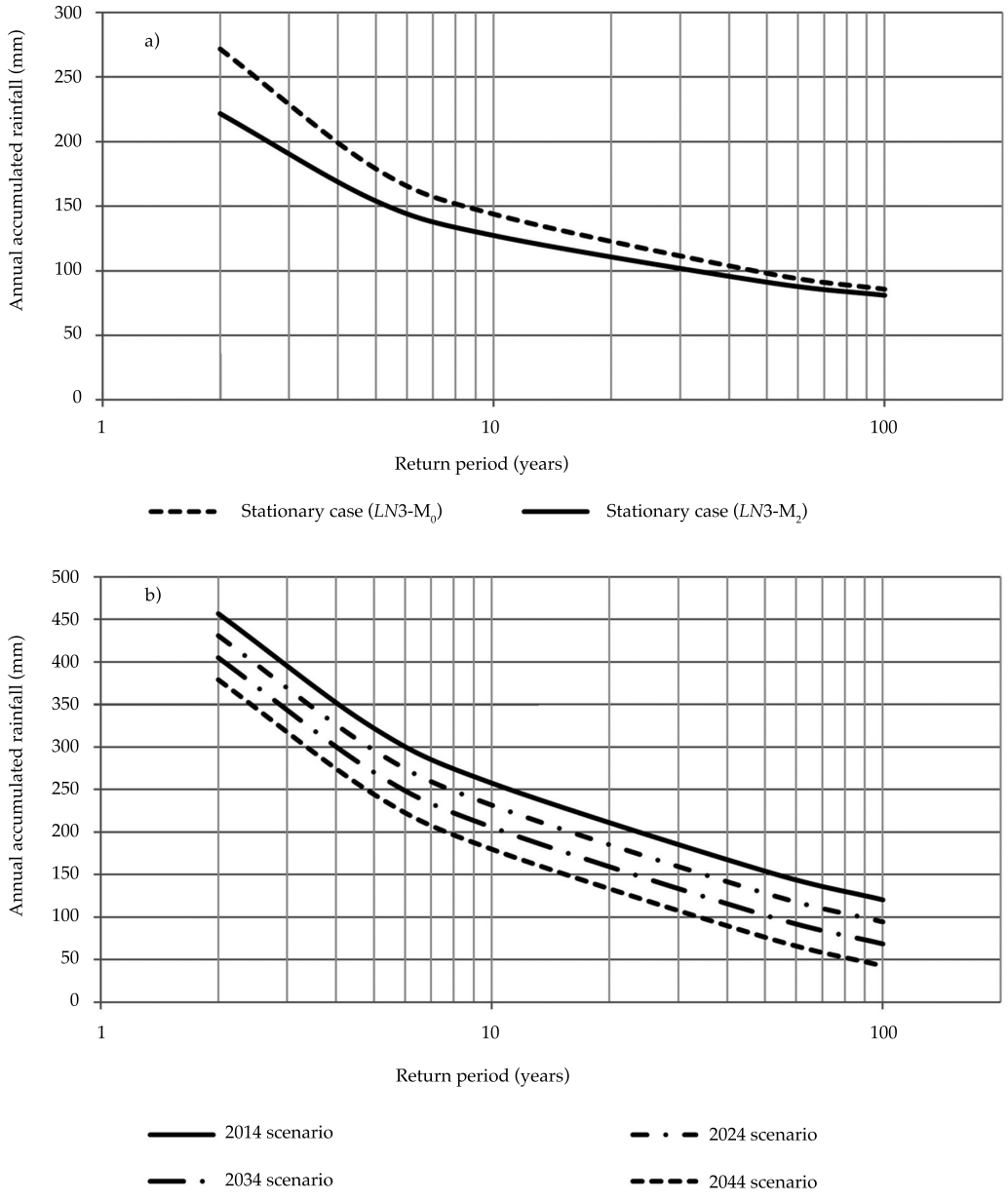

Figure 5. Design events for annual accumulated rainfall: a) station 2060, "Santa Cruz", Ensenada, Baja California; b) station 25082, "San Blas", El Fuerte, Sinaloa.

2060 and 25082, based on the above expressions.

For station 2060, the events with an estimated probability of occurrence of 50% (return period of 2 years) were 271.8 mm with the stationary model and 266.8 mm with the non-stationary model. While events were overestimated with the traditional approach, with the non-stationary analysis the rainfall values predicted reflected the most adverse historical drought conditions associated with the persistence of negative PDO values.

When taking into account a decreasing trend in rainfall at station 25082, it was possi-

ble to simulate the decrease in the magnitude of the design events for future scenarios. For example, a decrease in rainfall of 77 mm is predicted for the year 2044 with respect to rainfall for the 2014 scenario, for a return period of two years. Given that the statistical tests applied to the series from this station showed a significant decreasing trend, the prediction of the decrease in rainfall for the 2044 scenario is consistent with the behavior of the series.

For the remaining stations whose selected models (M_1 or M_3) were a function of time, the increase/decrease in rainfall for the year 2044 with respect to the year 2014 was estimated for a return period of 2 years. This return period corresponds to median rainfall (rainfall associated with a 50% probability of occurrence).

Figure 6 shows the spatial variation of the increase/decrease in rainfall as a percentage of annual mean rainfall. For the stations that did not present changes, the design events were obtained with models M_0 or M_2, which do not depend on time. A decrease of less than 20% in annual mean rainfall is predicted for 29 stations in regions 1,2, 3 and 5, located in the California peninsula, Sonora and Sinaloa, (Table 6). It is worth mentioning that this region has the lowest annual mean rainfall values in the country, and therefore these results suggest that it will be more vulnerable to future droughts. In contrast, increases of up to 30% in mean rainfall are expected in eight stations in region 4.

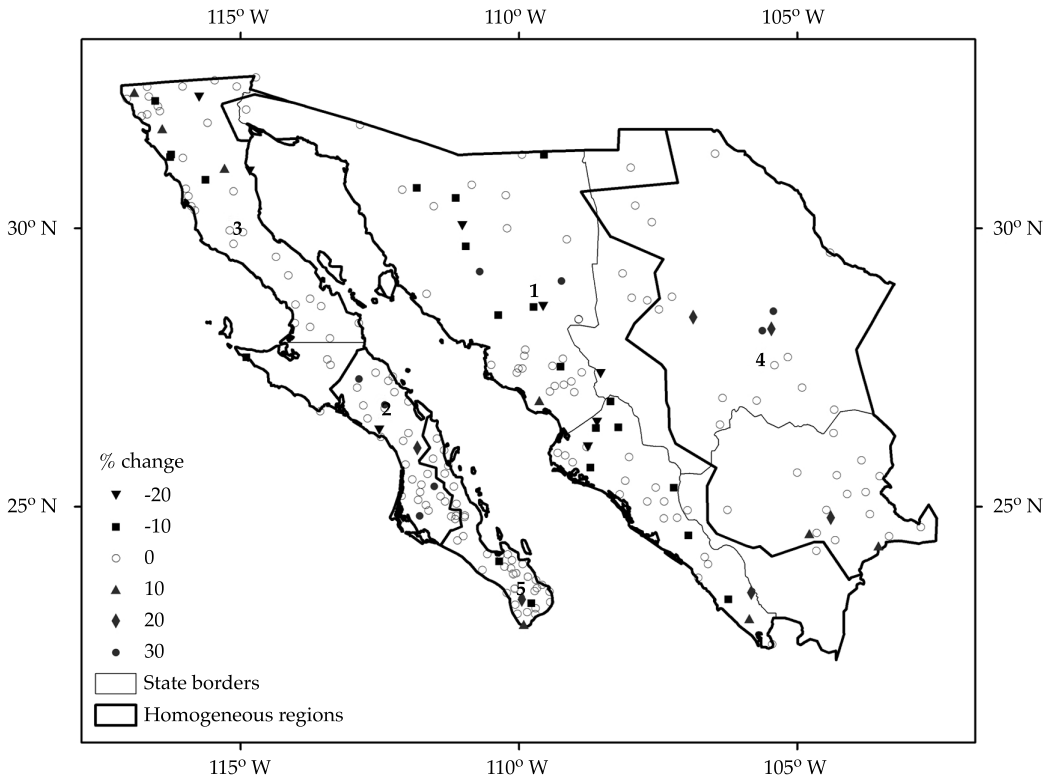

Figure 6. Increase/decrease in rainfall between scenario 2014 and 2044, with respect to annual mean rainfall for a return period of 2 years.

Table 6. Number of stations according to the percentage range of increase/decrease in rainfall between the 2014 and 2044 scenarios, with respect to annual mean rainfall for a return period of 2 years.

% Increase/Decrease	Region					
	1	2	3	4	5	Total
-20 a -10	5	1	2	0	0	8
-10 a -0	14	0	5	0	2	21
0	48	27	33	26	35	169
0-10	2	1	3	2	1	9
10-20	1	1	0	3	1	6
20-30	2	2	0	1	0	5
30-40	0	1	0	2	0	3
Total	72	33	43	34	39	221

Conclusion

In 83% of the non-stationary series analyzed, the models selected to estimate accumulated rainfall design events in northwestern Mexico included a linear trend and the PDO index as a covariable. Therefore, given the lack of stationarity in the rainfall series, it was determined that the non-stationary models proposed better explain the variability of the data than conventional models. The non-stationary models were better for the remaining non-stationary series. Nevertheless, the measurement of discordance indicates that the use of a non-stationary model instead of a conventional one is not justified at a significance level of 0.05. Thus, the change in the temporal behavior of rainfall is not a condition at all of the stations.

Non-stationary models make it possible to estimate design events associated with the most adverse PDO index conditions that have affected historical periods with the most severe rainfall deficits. The coming decades may again present a persistent period of drought, considering that a trend towards a negative PDO phase apparently began in 1998. Therefore, the persistence of negative PDO values should be included in the analysis of rainfall predictions.

By including a trend in the frequency analysis, design events associated with different return periods and future scenarios were obtained. Based on these, a decrease of less than 20% in annual mean rainfall is predicted for the year 2044 for 29 stations located on the California peninsula, Sonora and Sinaloa. Since this region has the lowest annual mean rainfall nationwide, these results suggest that it will be more vulnerable to future droughts.

References

Akaike, H. (1974). A New Look at Statistical-Model Identification. *Automatic Control, IEEE Transactions on*, *19*(6), 716-723.

Buuren, S. V., & Fredriks, M. (2001). Worm Plot: A Simple Diagnostic Device for Modelling Growth Reference Curves. *Statistics in Medicine*, *20*(8), 1259-1277.

Carmona, D. A. M. (2010). *Identificación de modos principales de variabilidad hidroclimática en Colombia y la Cuenca Amazónica mediante la transformada de Hilbert-Huang*. Tesis de doctorado. Medellín: Universidad Nacional de Colombia-Sede Medellín.

Coles, G. S. (2001). *An Introduction to Statistical Modeling of Extreme Values*. New York: Springer.

Conagua (2012). *Estadísticas del agua en México*. México, DF: Comisión Nacional del Agua.

Cook, E. R., Woodhouse, C. A., Eakin, C. M., Meko, D. M., & Stahle, D. W. (2004). Long-Term Aridity Changes in the Western United States. *Science*, *306*, 1015-1018.

El Adlouni, S., Ouarda, T. B. M. J., Zhang, X., Roy, R., & Bobée, B. (2007). Generalized Maximum Likelihood Estimators for the Nonstationary Generalized Extreme Value Model. *Water Resources Research*, *43*(3), W03410, doi:10.1029/2005WR004545.

Escalante-Sandoval, C., & Reyes-Chávez, L. (2002). *Técnicas estadísticas en hidrología*. México, DF: Facultad de Ingeniería, Universidad Nacional Autónoma de México.

Gleick, P. H. (1989). Climate Change, Hydrology and Water Resources. *Reviews of Geophysics*, *27*(3), 329-344.

Grubbs, F. E., & Beck, G. (1972). Extension of Sample Sizes and Percentage Points for Significance Tests of Outlying Observations. *Technometrics*, *14*(4), 847-854.

Held, I. M., & Soden, B. J. (2006). Robust Responses of the Hydrological Cycle to Global Warming. *Journal of Climate*, *19*, 5686-5699.

Huang, N. E., Shen, Z., Long, S. R., Wu, M. C., Shih, H. H., Zheng, Q, Tung, C. C., & Liu, H. H. (1998). The Empirical Mode Decomposition and the Hilbert Spectrum for Nonlinear and Non-Stationary Time Series Analysis. *Proceedings of the Royal Society of London. Series A: Mathematical, Physical and Engineering Sciences*, *454*(1971), 903-995.

IPCC (2007). *Climate Change 2007: The Physical Science Basis. Contribution of Working Group I to the Fourth Assessment Report of the Intergovernmental Panel on Climate Change*. In S. Solomon, D. Qin, M. Manning, Z. Chen, M. Marquis, K. B. Averyt, M. Tignor, & H. L. Miller (Eds.). Cambridge: Cambridge University Press, Intergovernmental Panel on Climate Change.

Katz, R. W., Parlange M. B., & Naveau P. (2002). Statistics of Extremes in Hydrology. *Advances in Water Resources*, *25*, 1287-1304.

Kendall, M. G. (1975). *Rank Correlation Methods* (4a ed). London: Charles Griffin.

Krzysztofowicz, R. (1997). Transformation and Normalization of Variates with Specified Distributions. *Journal of Hydrology*, *197*, 286-292.

MacDonald, G. M., & Case, R. A. (2005). Variations in the Pacific Decadal Oscillation over the Past Millennium. *Geophysical Research Letters*, *32*(8), L08703, doi:10.1029/2005GL022478.

Magaña-Rueda, V., & Gay-García, C. (2002). Vulnerabilidad y adaptación regional ante el cambio climático y sus impactos ambientales, sociales y económicos. *Gaceta Ecológica*, *65*, 7-23.

Mantua, N. J., Hare, S. R., Zhang, Y., Wallace, J. M., & Francis, R. C. (1997). A Pacific Interdecadal Climate Oscillation with Impacts on Salmon Production. *Bulletin of the American Meteorological Society*, *78*(6), 1069-1079.

Mestre, O., & Hallegatte, S. (2009). Predictors of Tropical Cyclone Numbers and Extreme Hurricane Intensities over the North Atlantic Using Generalized Additive and Linear Models. *Journal of Climate*, *22*, 633-648.

Milly, P. C. D., Betancourt, J., Falkenmark, M., Hirsch, R. M., Kundzewicz, Z. W., Lettenmaier, D. P., & Stouffer, R. J. (2008). Stationarity is Dead: Whither Water Management? *Science*, *319*, 573-574.

NCDC (2013). *Teleconnections* [en línea]. National Climatic Data Center. Recuperado en 1 de noviembre de 2013 de http://www.ncdc.noaa.gov/teleconnections.

Ouarda T. B. M. J., & El-Adlouni, S. (2011). Bayesian Nonstationary Frequency Analysis of Hydrological Variables. *Journal of the American Water Resources Association*, *47*(3), 496-505.

Pettitt, A. N. (1979). A Non-Parametric Approach to the Change-Point Problem. *Journal of the Royal Statistical Society. Series C, Applied Statistics*, *28*(2), 126-135.

Qian, C., Wu, Z., Fu, C., & Zhou, T. (2010). On Multi-Timescale Variability of Temperature in China in Modulated Annual Cycle Reference Frame. *Advances in Atmospheric Sciences*, *27*, 1169-1182.

Richman, M. B. (1986). Review Article: Rotation of Principal Components. *Journal of Climatology*, *6*, 293-335.

Shepard, D. (1968). A Two-Dimensional Interpolation Function for Irregularly-Spaced Data. A*CM '68 Proceedings of the 1968 23rd ACM National conference*, New York, USA.

Spearman, C. (1904). The Proof and Measurement of Association between Two Things. *The American Journal of Psychology*, *15*(1), 72-101.

Towler, E., Rajagopalan, B., Gilleland, E., Summers, R. S., Yates, D., & Katz, R. W. (2010). Modeling Hydrologic and Water Quality Extremes in a Changing Climate: A Statistical Approach Based on Extreme Value Theory. *Water Resources Research*, *46*(11), W11504, doi:10.1029/2009WR008876.

Villarini, G., Smith, J. A., Francesco, S., Bales, J., Bates, P. D., & Krajewski, W. F. (2009). Flood Frequency Analysis for Nonstationary Annual Peak Records in an Urban Drainage Basin. *Advances in Water Resources*, *32*, 1255-1266.

Villarini, G., & Smith, J. A. (2010). Flood Peak Distributions for the Eastern United States. *Water Resources Research*, *46*(6), W06504, doi:10.1029/2009WR008395.

Villarini, G., Smith, J. A., & Napolitano, F. (2010). Nonstationary Modeling of a Long Record of Rainfall and Temperature over Rome. *Advances in Water Resources*, *33*, 1256-1267.

Vogel, R. M., Yaindl C., & Walter M. (2011). Nonstationarity: Flood Magnification and Recurrence Reduction Factors in the United States. *Journal of the American Water Resources Association*, *47*(3), 464-474.

Voss, R., May, W., & Roeckner, E. (2002). Enhanced Resolution Modeling Study on Anthropogenic Climate Change: Changes in Extremes of the Hydrological Cycle. *International Journal of Climatology*, *22*, 755-777.

Vovoras, D., & Tsokos, C. P. (2009). Statistical Analysis and Modeling of Precipitation Data. *Nonlinear Analysis*, *71*, e1169-e1177.

Webster, P. J., Holland, G. J., Curry, J. A., & Chang, H. R. (2005). Changes in Tropical Cyclone Number, Duration, and Intensity in a Warming Environment. *Science*, *309*(5742), 1844-1846.

Wu, Z., Huang, N. E., Long, S. R., & Peng, C. K. (2007). On the Trend, Detrending, and Variability of Nonlinear and Nonstationary Time Series. *Proceedings of the National Academy of Sciences*, *104*(38), 14889-14894.

Institutional Address of the Authors

Dra. Gabriela Álvarez-Olguín

Universidad Tecnológica de la Mixteca
Instituto de Hidrología
69000 Huajuapan de León, Oaxaca, México
Teléfono: +52 (953) 5320 399, extensión 550
galvarez@mixteco.utm.mx
g_alvarez_o@yahoo.com.mx
Dr. Carlos Agustín Escalante-Sandoval

Universidad Nacional Autónoma de México (UNAM)
Facultad de Ingeniería
Departamento de Ingeniería Hidráulica
Circuito Exterior, Ciudad Universitaria
Coyoacán, 04510 México, D. F., México
Teléfono: +52 (55) 5622 3279
caes@servidor.unam.mx

Click here to write the autor

The Universality of State Functions that Guide the Dynamics of Solutes in Natural Rivers in "Dynamic Equilibrium": A New Method using Tracers to Calculate Slope

• Alfredo Constaín* •
Hydrocloro Technologies SAS, Colombia
*Corresponding Author

• Jorge Corredor •
Universidad Militar Nueva Granada, Colombia

Abstract

Constaín, A., & Corredor, J. (January-February, 2016). The Universality of State Functions that Guide the Dynamics of Solutes in Natural Rivers in "Dynamic Equilibrium": A New Method using Tracers to Calculate Slope. *Water Technology and Sciences* (in Spanish), 7(1), 89-103.

Ever since evidence has existed of a state function φ(t) that guides the evolution of solute plumes in natural flows, the nature of this function has been analyzed from diverse perspectives (Constaín, 2012). This article shows that φ(t) is universal for all flows that meet the "dynamic equilibrium" condition. At the same time, the validity of the Elder in function of φ(t) is demonstrated, which describes the relationship between dispersive transport and the geomorphology, making it possible to calculate the slope of a flow in a "steady state." This methodology is applied to a medium-sized river in Colombia, verifying that the graph of the peak concentration of the tracer is quite consistent with the expected data when applying the principles described herein.

Keywords: Water quality studies, hydraulics, dispersion, geomorphology.

Resumen

Constaín, A., & Corredor, J. (enero-febrero, 2016). Universalidad de la función de estado que guía la dinámica de los solutos en los cauces naturales en "equilibrio dinámico": un nuevo método de cálculo de la pendiente mediante trazadores. Tecnología y Ciencias del Agua, *7(1), 89-103.*

Desde que se ha hecho evidente que existe una función de estado φ(t) que guía la evolución de las plumas de solutos en los flujos naturales, la naturaleza de esta función ha sido analizada desde diversos puntos de vista (Constaín, 2012). En este artículo se muestra cómo φ(t) es universal para todo el flujo en tanto éstos cumplan la condición de "equilibrio dinámico". Al mismo tiempo se muestra la validez simultánea de la ecuación de Elder en función de φ(t), que relaciona el transporte dispersivo con la geomorfología y por lo tanto pudiendo calcularse la pendiente de un flujo en "estado estable". Se aplica esta metodología a un cauce mediano en Colombia, verificándose que la gráfica de la concentración pico para el trazador es bastante congruente con los datos esperados si se aplican los principios aquí desarrollados.

Palabras clave: *estudios de calidad de agua, hidráulica, dispersión, geomorfología.*

Received: 02/03/2015
Accepted: 21/09/2015

Introduction

In fluvial processes, the existence of an evident relationship has been observed between the forces that carve out natural rivers and the shape and proportions of their beds. For example, in a narrow channel, the force of the water will mainly carve out the lateral walls (A) to gain more width. Meanwhile, in wide channels, this force tends to deepen the channel (B). This is how processes that "cut" in one direction or the other dynamically end up finding a balancing point (C) (Figure 1).

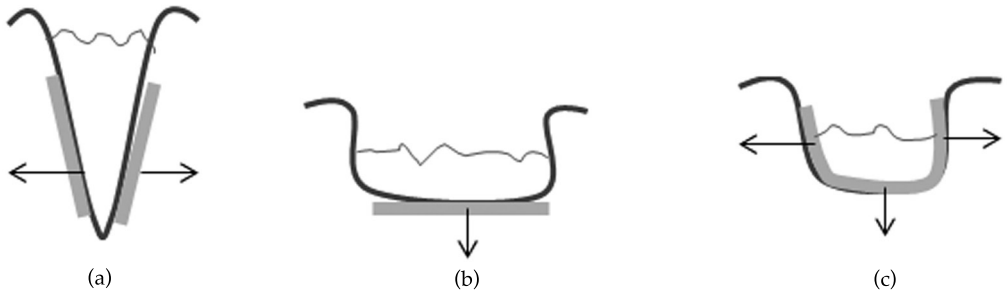

Figure 1. Process of "carving out" in beds.

"Dynamic equilibrium" then occurs when the cross-section of the channel reaches a point at which none of the forces that "cut" in different directions dominate the others, and the geomorphology of the flow remains roughly the same over time (Leopold & Maddock, 1954).

This "dynamic equilibrium" state which is reached as the channel is shaped by the continuous movement of water is interpreted not only in terms of changes in the effective areas of the resistant walls of the bed (effect) but undoubtedly by the flow velocity, slope and surface roughness (causes) as well. The final result of this stabilization process in opposite directions affects both the lateral and longitudinal directions. Thus, in terms of the longitudinal profile of the bed, the deposit of sediments will try to "soften" the profile in areas where the slope is greater, and where the slope is "softer," scouring will try to "steepen" the profile, where Sb is the slope (Figure 2).

"Dynamic equilibrium" in channels can therefore be seen as a trend towards a balance in the sediment "deposit" and "scouring" rates of the bed, in both the lateral and longitudinal profiles. Since the mean velocity of the fluid is the agent that directly controls these two opposite processes, this parameter of course does not take arbitrary values but rather those which are compatible with explicit trends towards equilibrium.

For a given degree of bed resistance, or "roughness" (depending on the physical characteristics of the particles in the bed), as a driving force of the movement of fluid the slope will have a certain value that accordingly adjusts the velocity-deposit-scouring interaction (Hack, 1957).

Therefore, the "dynamic equilibrium" mentioned is reflected in the mass transport rates inside the system. This is analyzed next.

Mass transport rates inside a natural channel system under "dynamic equilibrium" conditions

Consider a closed system evolving in a completely irreversible manner, Ω, according to the conservation of energy principle, in which the entering mechanical energy completely converts into thermal energy through degradation. We have:

$$\Delta U = \Delta Q \qquad (1)$$

In this case, the slope *Sb* contributes an initial potential gravitational energy component, $\Delta U(Z)$, which is transformed into kinetic energy, ΔK (movement of water). This

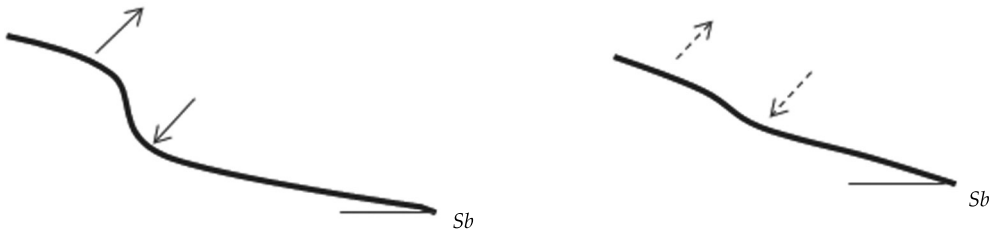

Figure 2. Process of leveling the profile.

is then completely transformed into heat, ΔQ (Figure 3).

In hydrological systems in which changes in the geomorphology have been studied, the importance of applying a second principle of thermodynamics, or entropy, has also been demonstrated. Under these conditions, for an irreversibly closed isothermal system in which all the potential energy, U, is transformed into heat, Q, the entropy can then be shown to be constant (Leopold & Langbein, 1962).

Therefore, the internal entropy (from irreversibility), Si, expulsed at the edge of the system, with T as the absolute temperature, can be written as:

$$\Delta Si = -\frac{\Delta Q}{T} = -\frac{\Delta U}{T} \qquad (2)$$

SBased on the definition of the ideal gas for a tracer cloud $PV = nRT$, where P is the pressure, V is the volume, n the number of moles and $R = 8.31$ J/(K*mol) is the universal constant for gas, substituting the temperature in the previous equations, we get:

$$\Delta Si = -\frac{(nR)\,\Delta U}{PV} \qquad (3)$$

Now considering pressure $P = f/A$, f as a force, area as $A = \Delta Y * \Delta X$, and volume as $V = \Delta Y * \Delta X * \Delta Z$, with Y = width, X = length and Z = depth of the fluid, we get:

$$\Delta Si = -\frac{(nR)\,\Delta U}{\frac{f}{A}\times V} = \frac{(nR)\,\Delta U}{(\frac{f}{\Delta y\times\Delta x})\times\Delta y\times\Delta z\times\Delta x}$$

$$= \frac{(nR)\,\Delta U}{f\times\Delta z} = \frac{(nR)\,\Delta U}{U} \qquad (4)$$

Lastly, dividing each member by the volume and knowing that $\Delta V = q * \Delta t$, where q is the flow, we get:

$$\frac{\left(\frac{\Delta Si}{\Delta t}\right)}{q} = -(nR)\frac{\left(\frac{\Delta U}{U}\right)}{\Delta V} \qquad (5)$$

This implies that the production of internal entropy per unit of flow contributes to the continuous *decrease in relative available energy per unit of volume*. The increasing entropy inside the system generates an increasingly uniform energy distribution in the volume of Ω.

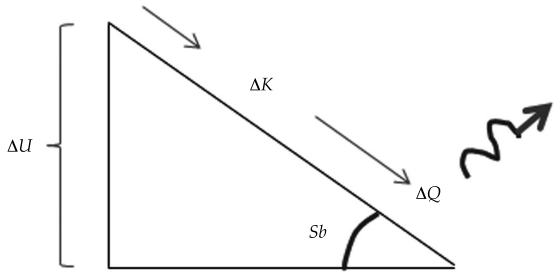

Figura 3. Transformaciones de energía en el flujo.

Therefore, the right side of this equation can be interpreted as the description of the most probable energy distribution in the system, which is constant according to Boltzmann's statistical interpretation (Leopold & Langbein, 1962) in which the different energy events in control volume Ω are equiprobable:

$$Si = k \times \sum_{\Omega} p_i \times \ln(p_i) = \text{maximum} \quad (6)$$

And

$$p_1 = p_2 = p_3 = p_4 = \ldots = p_i \quad (7)$$

"Dynamic equilibrium" (steady-state) in natural channels will therefore mean that not only is the net mass flow at the edges of the system virtually null —given the balance between scouring and depositing (conservation of mass)— but also, the individual internal events described by the exchange of energy in the control volume will be equivalent, uniform or indistinguishable due to equiprobability.

Calculation of the different mass transport rates in a flow system in "dynamic equilibrium"

It is now of interest to study the concrete consequences of the "equiprobability" for different energy exchange events in a system —in this case, the movement of different portions of mass within the system, whether it be a dissolved or suspended mass in the hydric system.

It is necessary to begin with the fact that, in a natural flow, the potential energy will be represented as follows:

$$U = m \times g \times h \quad (8)$$

Suppose that, because of its "location," a certain basic energy exchange in a system is associated with an increase of mass rather than an increase in height:

$$\Delta U = \Delta m \times g \times h \quad (9)$$

If the system is stationary (in dynamic equilibrium), then the different energy exchanges resulting from the mass exchange of similar solute particles will have the same probability. Then the exchanges of mass themselves, as a statistical distribution over time, will also be "equalized " by this principle.

This corresponds to a constant statistical distribution similar to that of equation (5), except that instead of the "potential energy" value, U, there is the mass variable M. It is also of interest to determine the distribution over time.

To analyze the distribution over time, the movement of a mass element Δmj through space is defined for time Δtj. The mass transport rate is then equal to the ratio of the mass differential mobilized at a point during the time differential in which this event occurs (Figure 4).

Mathematically, this is defined as:

$$Ttm_j = \frac{\Delta m_j}{\Delta t_j} \quad (10)$$

The "general" mass transport rate for the section under study, statistically defined by its representative value, is the mathematical expectation of the individual transport components (Spiridonov & Lopatkin, 1973). Therefore, its representative definition for the entire control volume domain, Ω, will be:

$$< Ttm > = \frac{1}{j} \sum_{j} \frac{\Delta m_j}{\Delta t_j} \quad (11)$$

But since the discrete elements of the transported mass are equal (equiprobable), then:

$$< Ttm > = \frac{1}{j} \times (j \times Ttm_j) \quad (12)$$

Lastly:

$$< Ttm > \approx Ttm_j \quad (13)$$

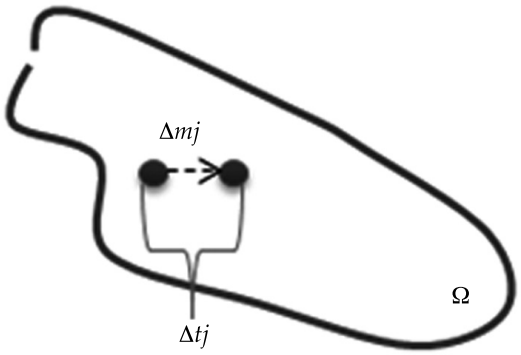

Figure 4. Mobilization of a mass element in Ω.

That is, the "general" mass transport rate converges with the "local" mass transport rates in a channel under "steady-state" conditions, which are considered indistinguishable (equal). In this case, the general replicates the particular.

Calculation of the Different Mass Transport Rates in a Flow System in "Dynamic Equilibrium": the case of dissolved mass

Although the mass transported in the flow could be suspended or dissolved, in a steady-state it is possible to perform a "detailed balance" (Prigogine & Kondepudi, 1998) of both types of masses based on the concept of the equivalence of "local transport rates" and the "general transport rate." This results from dynamic equilibrium, in which each elemental transformation is balanced by its specific counterpart, under the concrete scheme in which they have been described.

Then, if:

$$< Ttm > (\text{dissolved} + \text{suspended}) \approx Ttm_j\,(\text{dissolved} + \text{suspended}) \quad (14)$$

It follows that:

$$< Ttm > (\text{dissolved}) \approx Ttm_j\,(\text{dissolved}) \quad (15)$$

And:

$$< Ttm > (\text{suspended}) \approx Ttm_j\,(\text{suspended}) \quad (16)$$

Therefore, the principle of equivalence between "local" transport rates and "general" rates will be applied to the dissolved component, which makes it possible to analyze using tracers.

Calculation of the "general" dissolved mass transport rate in the system

In steady-state conditions in a natural flow, the addition of solutes to the current is a characteristic of the channel itself and of the flow to which these substances are added. If "Co" is the baseline concentration of this addition and "q" is the corresponding flow, the typical relationship is a hyperbolic curve (Hem,1985) (Figure 5).

This relationship takes this form as long as larger flows of a given addition of solutes in a bed correspond to larger volumes to be dissolved, that is, a lower concentration::

$$q \times C_o \approx k(Cte) \quad (17)$$

In terms of the dimensional part, the "constant" k is in milligrams per second, that is, the mass transport rate.

"Local" dissolved mass transport rate measured with tracers

One way to measure "local" mass transport rates in natural flows is with tracers. These were nearly instantaneously poured into the channel at a point in the study section. They can be considered local "witnesses" of the "individual" movement of mass in a system Ω (Figure 6).

To properly understand how the tracer can accomplish the objective of measuring the

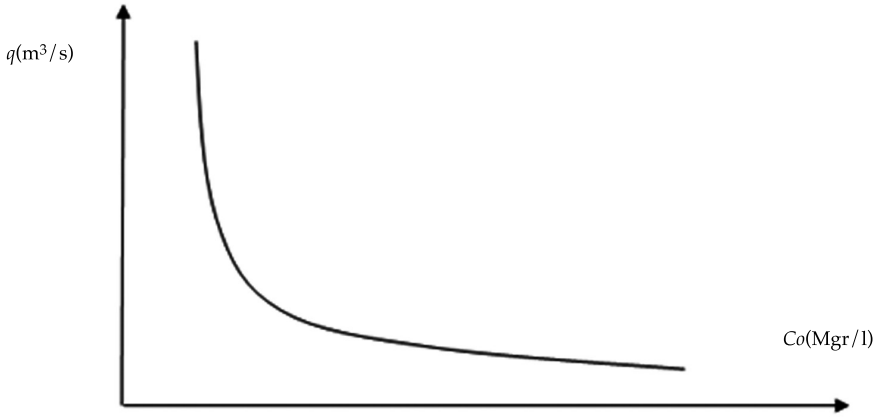

Figure 5. Relation between base concentration and flow.

Figure 6. Tracer as a local "witness" of flow.

local mass transport rate, it is necessary to review certain aspects of their dynamics.

Mean Flow Velocity in Function of Dispersive Transport Data

In previous articles, the authors have defined this function as the relationship between two velocities. One is the irreversible dispersion of the tracer, Vdisp, as measured by "random walk." The other is advection, U, which should not be confused with potential energy, is an integrating factor. Here, Δ and τ are parameters which are characteristic of movement and the Gaussian one-dimensional motion of the tracer plume (Constaín & Lemos, 2011; Constaín, 2013):

$$\varphi = \frac{V_{disp}}{U} = \frac{\left(\frac{\Delta}{\tau}\right)}{U} = \frac{\left(\frac{\sqrt{2E\tau}}{\tau}\right)}{U} = \frac{\left(\sqrt{\frac{2E}{\tau}}\right)}{U} \qquad (18)$$

However V_{disp} measures the speed at which the tracer particles distance themselves from each other, it is a function that represents the reaction of the system to a sudden break from chemical equilibrium, and is therefore a thermodynamic potential. The special nature of $\varphi(t)$ can be characterized by saying that it is a state function of the state of the system, defined by the following equation:

$$\oint_C d\varphi = 0 \qquad (19)$$

As already explained in other articles by the authors (Constaín & Corredor, 2013), the theoretical calculation of the function $\varphi(t)$, is performed based on the measurement of the time between the two inflexion points on the experimental Gaussian curve, divided by the transport time and multiplied by a constant.

A definition for the mean advective velocity can be established with equation (20):

$$U = \frac{1}{\varphi}\sqrt{\frac{2E}{\tau}} \qquad (20)$$

Solving for E:

$$E(t) = \frac{\varphi^2 U^2 \tau}{2} \qquad (21)$$

It should be noted here that the characteristic Gaussian time τ is different than the independent variable t —the former refers to the time in which the random separation of the particles occur while this average distance is Δ, whereas the general temporal scale is associated with the advective effect of U. The relationship between both times can be established by a Poisson-Svedberg dynamic (Constaín, Peña, Mesa, & Acevedo, 2014):

$$\beta = \frac{\tau}{t} = e^{-1.54} \approx 0.215 \qquad (22)$$

The State Function $\varphi(t)$

Since $\varphi(t)$ is a thermodynamic potential and in accordance with equation (19), its initial and final values are the same. Therefore, it is a single mode curve, with its peak at "a" and its usable part always after $t = a$ (Figure 7). The ascending side corresponds to transient and very rapid phenomena that occur when the conservative solute mixes with the liquid.

Since the velocity V_{disp} vcontinues to decrease as the system irreversibly tends towards equilibrium, after $t = a$, then $\varphi(t)$ is descending at its outermost end. It is necessary to take into account the maximum value of $\varphi(t \approx 0) \approx 2.16$.

Description of the Solute Plume as seen by Different Observers

The Galilean transformation to transform from one inertial system into another is partially included in the exponential argument represented by the classic Fick equation, where M is the solute mass and A is the flow cross-section of (Fischer, 1967):

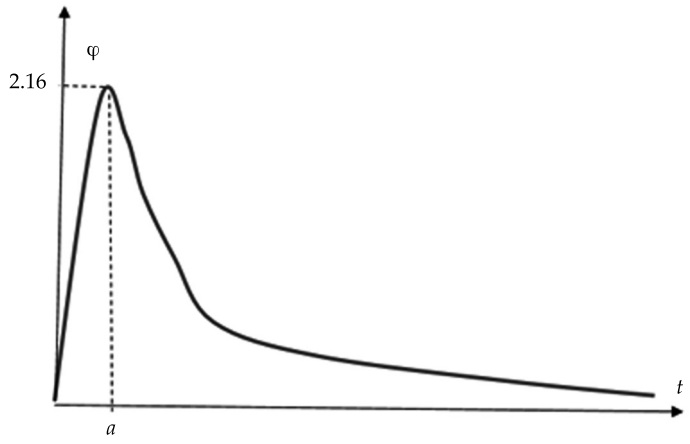

Figura 7. $\varphi(t)$ as a single mode state function.

$$C(x,t) = \frac{M}{A\sqrt{4\pi E t}} e^{-\frac{(X-Ut)^2}{4Et}} \quad (23)$$

Nevertheless, this transformation is complete only when coefficient E is a function of time, as described in equation (21). Now substituting in equation (23): $\sqrt{2\pi\beta} \approx 1.16$:

$$C(x,t) = \frac{M}{q_l \varphi t\, 1.16} e^{-\frac{(X-U_x t)^2}{2\beta\varphi^2 U_x^2 t^2}} \quad (24)$$

This particular equation (modified Fick formula) reproduced the experimental tracer curves very well, as will be shown in the section "IDF Measurement Screens." Suppose that a tracer is injected laterally at the edge of a turbulent flow, as shown in Figure6 by the tracer plume evolving in the section. In this case, the flow composed of the "current tube" which restricts the tracer plume, q_1, is a "local" value as long as, in principle, the tracer has not covered the entire actual flow volume, nor has it reached the full flow velocity ($U_l < U$) nor is its effective width that of the total flow ($W_l < W$) or its depth (at the edge) that of the channel ($hl < h$):

$$q_l \approx W_l \times h \times U_l \quad (25)$$

It should also be remembered that in a natural turbulent channel a transverse velocity distribution can be applied (dotted line), as shown in Figure 8. This graph also presents the "local" width of the tracer plume (red line). The depth is assumed to be the mean value of the entire channel (to simplify, $hl = h$).

Model of the Evolution of the Peak Tracer Concentration over Time, Cp(t)

The peak tracer concentration, as defined by equation (26), is very important because it will enable verifying the overall validity of the principles proposed herein:

$$C_p(t) = \frac{M}{q_l \varphi t\, 1.16} \quad (26)$$

Its evolution over time can now be defined more succinctly using the following empirical equation:

$$C_p(t) \approx \alpha(t) \times t^{-\frac{2}{3}} \quad (27)$$

The multiplier factor "α" is a function of time that should be adjusted based on the experimental data at different moments. It is convenient to use a simple descending exponential model of the type:

$$\alpha(t) \approx \alpha_o\, e^{-k t} \quad (28)$$

Definition of the Local Mass Transport Rate using the Modified Fick Equation

It is now possible to use tracer experiments to define the "local mass transport rate" based on the concepts developed above. At the measuring point in equation (33), the local mass transport

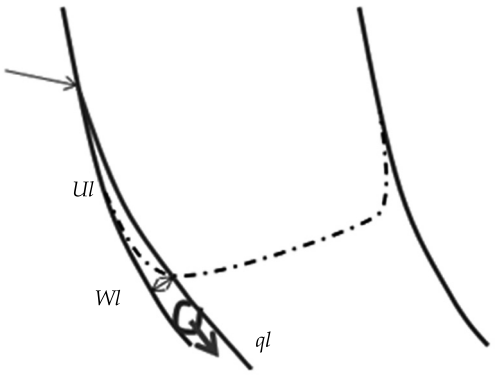

Figure 8. Local velocity and width of the tracer, defining the local flow.

rate is roughly equal to the following equation, where *Cp* is the peak tracer concentration, considered conservative in that its decrease throughout the section is only due to the effect of dispersion:

$$Ttm_j = \frac{\Delta M_j}{\Delta t_j} \approx \frac{M}{t} \approx C_p \times \varphi \times q_l \times 1.16 \qquad (29)$$

Equalization of the "general" and "local" mass transport rates in a flow in "dynamic equilibrium"

With respect to what was established in section 4 —equation (15) for the "generally" and "locally" observed dissolved mass in a natural channel— a flow in dynamic equilibrium can roughly be described as:

$$q \times C_o \approx C_p \times \varphi \times q_l \times 1.16 \qquad (30)$$

That is:

$$\varphi \approx \frac{\left(\frac{q}{q_l}\right)}{\left(\frac{C_p}{C_0}\right) \times 1.16} \qquad (31)$$

This equation is highly significant as long as $\varphi(t)$ is a state function, as mentioned, and its thermodynamic significance is very special in that it reflects "general" properties of the system in which it evolves, even though it is measured in "local" zones. Thus, it contains information about the particular state of the advance of the tracer plume (q_l and C_p) as well as general processes in a channel in dynamic equilibrium (such as *q* and *Co*). Therefore, equation (31) can be considered a universal definition for that function, that is, it is valid for the entire scope of the flow in the study section. Now, since q_l and C_p are parameters of the time function associated with the plume, equation (31) should be calculated for a particular time, which we have called "mixing time" (*mt*). At this instant, given the predominantly steady-state thermodynamic conditions, one single calculation reflects the information for the *entire* process. This information will naturally contain the slope as a driving force of the process.

Role of "mixing time" (mt) in the formation of the solute plume

Given what was explained in the previous paragraphs (equation (31) and the principle on which it is based) it is important to understand the mechanisms involved in the formation of tracer plumes once the conservative solute enters the water. In this regard, the peak initial concentration of the solute is dependent on the baseline concentration in the physical environment and the general flow value. It is as if, during the time the plume is forming, its evolution were predetermined by general flow parameters, whose information in a certain sense is transferred to that flow element. The nature of that transmission is likely electrochemical. The baseline concentration of *Co* is "constant," in principle, and therefore the adjustment needed to obtain the appropriate peak concentration is a function of time. This means that its adjusted value should be calculated for a particular time period, as previously mentioned.

Slope as a Key Datum about the "Dynamic Equilibrium" Condition

The introduction described the dominant role of the flow's slope as a key agent in the transformation of energy in channels, and thus in conditions that establish "dynamic equilibrium" involving the balance of scouring and depositing of mass in the study section. A careful examination of this suggests that $\varphi(t)$) is dependent on the mechanism through which the flow establishes a precise and specific slope value, *Sb*, in the process of the channel's formation.

It is important to mention that this physical process of establishing the slope —which specifically involves the mean velocity, flow and roughness conditions— is similar to the analytical process to establish the tracer's longitudinal dispersion coefficient (function of the slope), which is really applicable to the entire section. Given this similarity, it can be said that the state function used to apply the principle of the equivalence of transport rates is the same for the determination of the slope.

To demonstrate this, it is necessary to refer to the Elder equation and its most recent interpretation according to the theory of tracers.

Calculation of the Slope of a Flow in Dynamic Equilibrium according to Elder

In 1959, Elder proposed his now well-known definition of the longitudinal dispersion coefficient, E (Elder, 1959), where h is the mean depth of the flow, *Sb* is the slope as a gravitational driving force of the motion of flow and g is the acceleration of gravity:

$$E \approx 5.93 \times h \times \sqrt{h \times g \times S_b} \qquad (32)$$

Of course, if equation (21) is equated with equation (32), then it must be accepted that the definition by Elder is also a function of time. That is, it can move along the same curve (Figure 9).

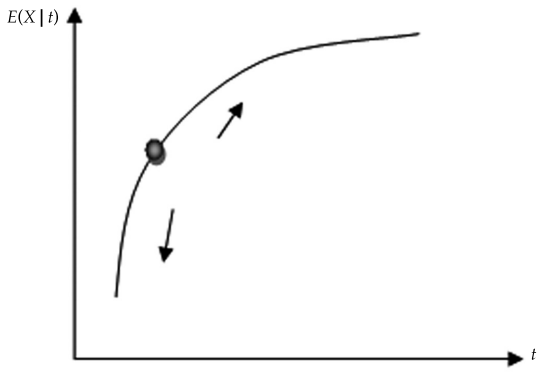

Figure 9. E as a function of time

Specific Location of the Longitudinal Dispersion Coefficient on the Time Function Curve

It is actually not sufficient to state that the definition of the Elder slope is a function of time, but rather, it is necessary to determine the concrete point at which the corresponding value is located on the curve (black dot on the curve in Figure 9). To determine this, the approximate time frame to be explored must first be estimated (Constaín, 2014).

Estimation of mt

This is estimated based on equation (31), which provides a very direct panorama of the different relationships among the parameters of interest. Thus, for example, if the maximum value of φ is 2.16, then the numerator and the denominator must be of the same order. In addition, $q >> q_l$, for the initial trajectory of the tracer in large rivers, which means that $C_p >> Co$.

Calculating the Slope, Chezy Coefficient and Estimation Function

The slope of the Elder equation can be solved after estimating the probable time value, which is applied to the relation between transport rates. To this end, a "trial and error" process should be used with several values of E to determine the best fit. This is done using an estimation function, *F*, which will be described next. It is advisable to begin by applying the initial value found with tracers, according to equation (21). If this first attempt does not fit, then different values are used until the best fit is obtained, as will be seen later in the experimental application:

$$S_b \approx \frac{E^2}{35.2 \times h^3 \times g} \qquad (33)$$

The estimation function is determined by equalizing the two definitions of mean flow

velocity —the new one represented in equation (20) and the Chezy classic definition of uniform flow, where *R* is the hydraulic radius and *Ch* is the Chezy coefficient:

$$\frac{1}{\varphi}\sqrt{\frac{2E}{\tau}} \approx C\sqrt{RS_b} \tag{34}$$

Based on this, the estimation function F is determined, which will measure the goodness of the estimation of the slope according to different values of *E*. The fit is "ideal" when function *F* is equal to the numerical coefficient of the Elder equation:

$$F \approx \varphi^2 \times 0.215 \times t_o \times \left(\frac{C_h^2}{2}\right) \times \left(\frac{R}{h}\right) \times \sqrt{\frac{S_b}{h \times g}} \rightarrow 5.93 \tag{35}$$

And, therefore, in ideal condition:

$$\varphi \approx \sqrt{\frac{37.2 \times h^{\frac{3}{2}}}{t_c \times C_h^2 \times R \times \sqrt{S_b}}} \tag{36}$$

Therefore, the state functions $\varphi(t)$ that appear in equations (31) and (36) have the same value, thereby ensuring the validity of the concept of "dynamic equilibrium" in the study section of the natural channel, adequately adjusted for slope. The slope simultaneously adjusts the dispersion and the equivalence of the transport rates.

When several "trial and error" processes need to be performed, equation (21) should be used again to obtain other values of E in order to determine the slope with the best value.

Application of the Method to Determine Slope in a Medium-Sized Mountain River in Colombia

Aspects of the Channel

The application was based on experimental results obtained with a saline tracer in the year 2007, used in the Pance River in the Valley of Cauca, southwestern Colombia. Figure 10 presents different aspects of the study section.

Instrumentation Used and Aspects Related to the Injection of the Ionic Tracer

An ionic tracer (common salt) was measured with an Inirida Deep Flow device developed in Colombia for real-time operations. This device contains a powerful graphic interface

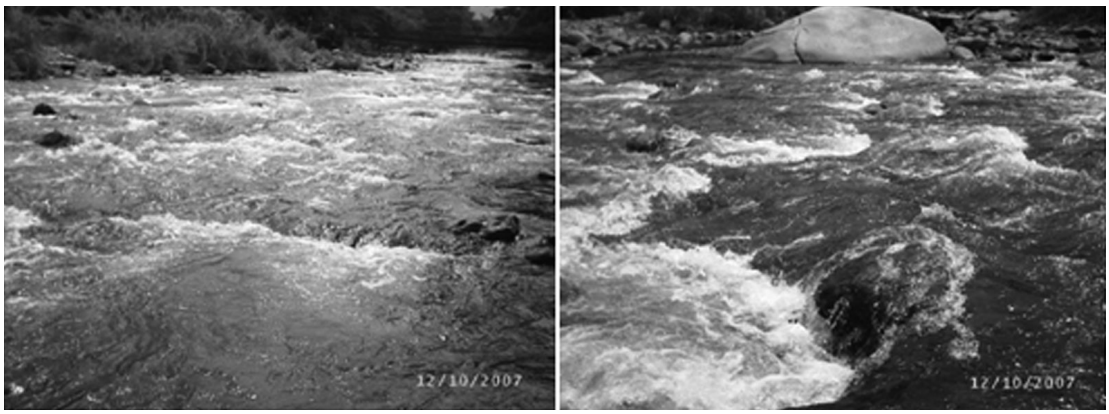

Figure 10. Characteristics of the channel in the study section.

in order to function interactively, and saves the measurements in its memory. Figure 11 shows some of the characteristics of the instrumentation and the injection of the tracer "upstream." In the experiment described, 9 060 grams of common salt were initially dissolved in water contained in a 20-liter bucket.

IDF Equipment Measurement Screens

Figure 12 shows photographs of the device's screens which display the measurement data.

The first photograph (upper left) shows the experimental curve (unsymmetrical line), and superimposed with the theoretical model obtained using equation (33), based on the data in Table 1. The close fit between the theoretical model and the experimental curve ensures the certainty of the data obtained with the instrument.

The upper right photo corresponds to the calculation of flow based on the conservation of mass principle (area under the tracer curve). The lower left photo corresponds to the instrument's screen which displays the calculation of the state function $\varphi(t)$ for the measurement $X = 400$ m. The lower right photo shows some of the data calculated using the equipment's software.

Numerical Data Table

Table 1 summarizes the information collected by the IDF related to the measurements of the channel. It is based on the distance of the tracer injection and the measurement $X = 400$ m for an estimated width of 20 meters.

Figure 11. Aspects of the IDF instrument and the injection of the tracer.

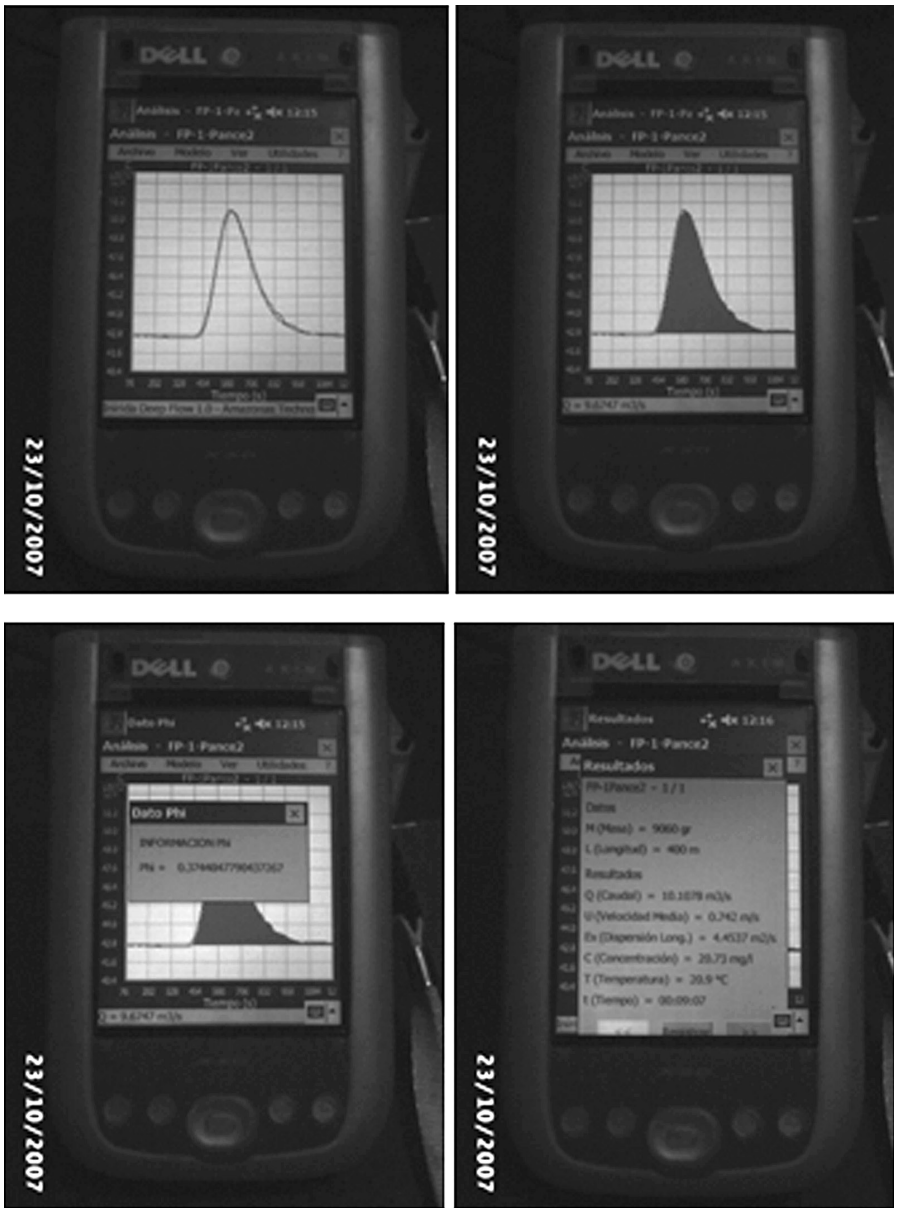

Figure 12. Aspects of the IDF's measurement screens.

Development of the Study

Study of mt based on the Elder Relation

Having conducted several experiments at times very close to the moment at which the tracer was injected, the correct dynamic after injection can now be characterized by an *mt* of 2.6 s, that is, $X = 1.9$ m, if a mean velocity of $U = 0.74$ m/s is considered. The detailed calculations to determine that this is correct will be shown next.

Elder Calculation for the slope when mt = 2.6 s

The process begins by calculating the longitudinal dispersion coefficient, assuming that the state function φ is 2.16 this point in time very close to the injection:

Table 1. Results from the Tracer

Injection	Base concentration, Co Mgr/l	Mass, M K	Mean velocity, Ux m/s	Φ	Flow, Q m^3/s	Peak concentration, Cp, Mgr/l	Time t s	Depth H m
X = 400 m	29.4	9.060	0.742	0.37	11.7	3.9	539	0.80

$$E(t=2.6\,s) \approx \frac{\varphi^2 \times U^2 \times 0.215 \times t}{2}$$

$$\approx \frac{2.16^2 \times 0.74^2 \times 0.215 \times 2.6}{2} \approx 0.71\ m^2/s \quad (37)$$

Then the probable slope is calculated, assuming that the mean depth remains the same throughout the study section:

$$S \approx \frac{E^2}{35.2 \times h^3 \times 9.81}$$

$$\approx \frac{0.71^2}{35.2 \times 0.8^3 \times 9.81} \approx 0.0029 \quad (38)$$

The approximate Chezy coefficient is then calculated:

$$Ch \approx \frac{U}{\sqrt{RS}} \approx \frac{0.74}{\sqrt{0.8 \times 0.0029}} \approx 15.4\ m^{1/2}/s \quad (39)$$

Then the estimation function F is determined:

$$F \approx \varphi^2 \times 0.215 \times t \times \frac{Ch^2}{2} \times \sqrt{\frac{S}{h \times g}}$$

$$\approx 2.16^2 \times 0.215 \times 2.6 \times \frac{15.4^2}{2} \times \sqrt{\frac{0.0029}{0.8 \times 9.81}} \approx 5.93 \quad (40)$$

This value is considered satisfactory when it is the ideal Elder coefficient, 5.93, and then the approximate values calculated previously can be considered correct. This is estimated to be the correct time to calculate the equivalence of transport rates.

Calculation of the Transport Rate Ratio with $mt = 2.6$ s

The calculation begins with an approximate calculation of the lateral diffusion coefficient —the local width of the plume— to thereafter estimate local flow:

$$\varepsilon_y \approx 0.23 \times h \times \sqrt{h \times g \times S} \approx 0.23 \times 0.8$$

$$\times \sqrt{0.8 \times 9.81 \times 0.0029} \approx 0.028\ m^2/s \quad (41)$$

$$W_l \approx \sqrt{3.22 \times \varepsilon_y \times t} \approx \sqrt{3.22 \times 0.028 \times 2.6}$$

$$\approx 0.48\ m \quad (42)$$

$$Q_l \approx W_l \times U \times h \approx 0.48 \times 0.74 \times 0.8$$

$$\approx 0.284\ m^3/s \approx 284\ l/s \quad (43)$$

Therefore, the flow ratio is:

$$\frac{q}{q_l} \approx \frac{11\,700}{284} \approx 41.2 \quad (44)$$

And thus the concentration ratio in a stable state with mixing time = 2.6 s is:

$$\frac{C_p}{C_0} \approx \frac{\left(\frac{q}{q_l}\right)}{2.16 \times 1.16} \approx \frac{41.2}{2.51} \approx 16.4 \quad (45)$$

The peak tracer concentration at $mt = 2.6$ s after the injection, with 9.06 kg of solute, is:

$$C_p \approx 16.4 \times 29.4 \approx 483\ Mgr/l \quad (46)$$

Verification of the Calculations based on the General Determination of the Peak Concentration Curve, Cp(t)

The function $Cp(t)$ now needs to be constructed in function of the different data at two different moments: A, the measuring point at t = 539 s and B, the mixing point at mt = 2.6 s.

At the moment of injection, $t \approx 0$ s. To completely perform this task, it is necessary to begin with what was explained in the section "Model for the evolution of the peak tracer concentration over time, $Cp(t)$". This begins by identifying the different experimental values of "α":

A. Measuring point at t = 539 s:

$$\alpha_M \approx \frac{C_p}{t^{-\frac{2}{3}}} \approx \frac{3.9}{539^{-\frac{2}{3}}} \approx 258 \qquad (47)$$

B. Calculation for the mixing point at t = 2.6 s:

$$\alpha_I \approx \frac{C_p}{t^{-\frac{2}{3}}} \approx \frac{483}{2.6^{-\frac{2}{3}}} \approx 913.3 \qquad (48)$$

As was mentioned, it is possible to demonstrate that, as in the case of $\varphi(t)$, α is a function of time. Therefore, it is necessary to propose a descending exponential model for this parameter, such that the model coincides with the experimental data:

$$C_p(t) \approx 913.3\, e^{-0.00234\ t} \times t^{-\frac{2}{3}} \qquad (49)$$

For the fitting of the expression, it can be shown that the constant k is 0.00234, and then the peak concentration $C_p(t)$ approximately reproduces the experimental data for the mixing time and measurement (Figure 13a and b).

Verifying the Congruency of the Calculation

It is very helpful to have the general model for $C_p(t)$ since the peak tracer concentration can be found approximately at the very moment of the injection ("slug" type).

It is reasonable to say that the initial peak concentration should be the same as the concentration of the initial mixture at the instant at which it is injected, that is, the ratio of the mass of the injected tracer (9.060 kg) and the approximate volume of the bucket of water used, which was 20 liters:

$$C_p(t \approx 0\ s) \approx \frac{9\ 060\ 000\ \text{Mgr}}{20\,\text{l}} \approx 453\ 000\ \text{Mgr/l} \qquad (50)$$

According to equation (49), at time very near to zero, the peak tracer concentration is:

$$C_p(t \approx 0.0001\,\text{s}) \approx 913.3\, e^{-0.00234\ t} \times t^{-\frac{2}{3}} \approx 424\,651\ \text{Mgr/l} \qquad (51)$$

That is, a value very close to the expected value, with a percentage error of 7%. This can be graphically seen in Figure 14.

Conclusions

Based on the analysis presented in this article, the following can be stated with respect to the application of the ionic tracer experiment in the study section of the Pance River:

1. The experimental application of the theoretical guidelines presented herein were successful in the sense that the different data were highly congruent. They are accepted as a reliable description of the evolution of the tracer and its relationships with the geomorphological and hydraulic parameters —within the scope of the approaches and simplifications used.

2. The basic concept presented herein is that of the "equivalence of transport rates" in

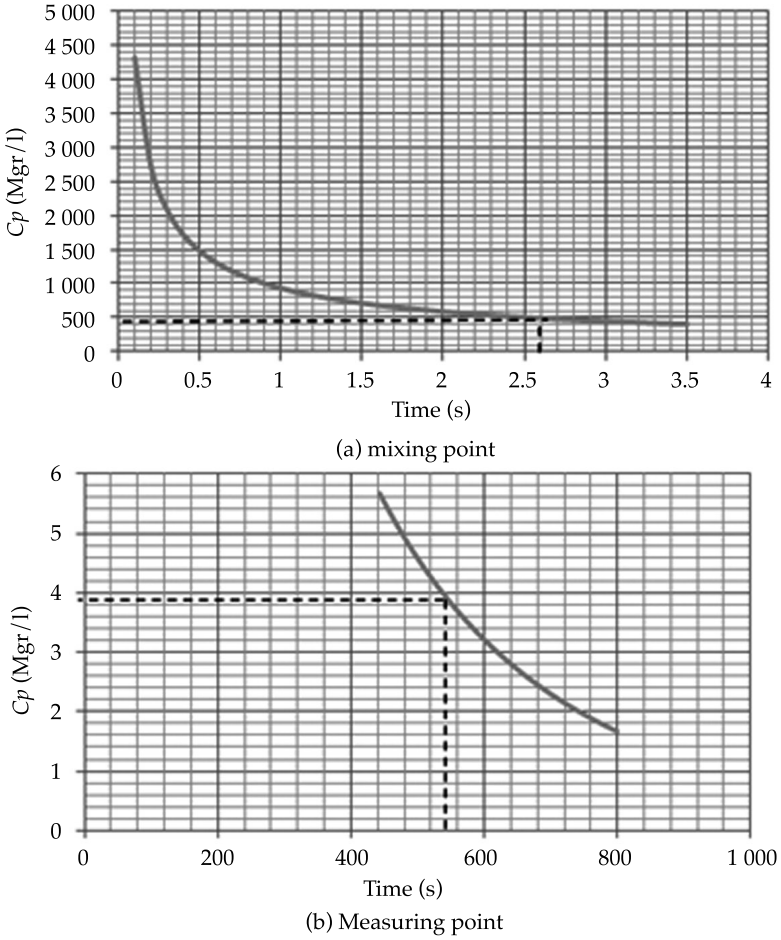

Figure 13. Curve of Cp(t) replicating the experimental data.

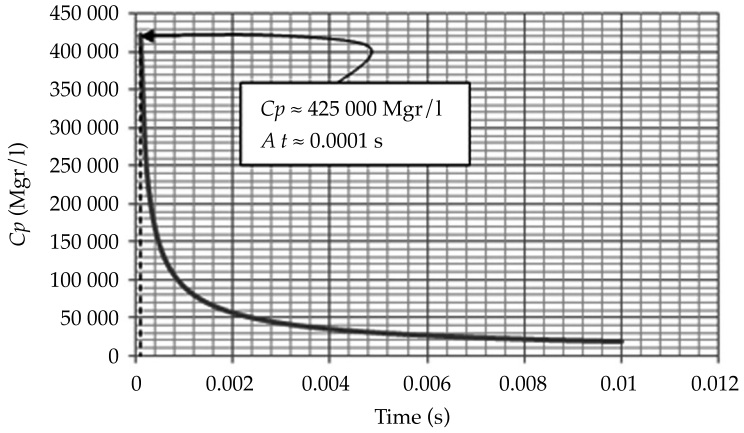

Figure 14. Approximate verification for Cp(t = 0) at the injection point.

natural channels —locally and generally. This is due to statistical flow properties in steady-state conditions that are approaching "dynamical equilibrium," which had been analyzed in-depth by several authors in the 1900s, particularly Luna B. Leopold. In a closed fluvial system with an irreversible evolution, the mass is conserved not only at its edges but the transport rates are also equal at each interior point. This is a process in which global information is incorporated in individual phenomena.

3. This equivalence makes it possible to precisely define the mechanisms involved in the formation of tracer plumes in natural channels, and is therefore of interest to specialists who conduct water quality studies related to pollution processes. Having congruent hydraulic, dispersive transport and geomorphological information greatly helps to calibrate the models to be used later.

References

Constaín, A. J. (2012). Definición y análisis de una función de evolución de solutos en flujos naturales. *Revista DYNA*, *79*(175), 173-181.

Constaín, A. J. (2013). Aplicación de una ecuación de velocidad media en régimen no uniforme: análisis detallado del transporte en el canal Caltech. *Revista Ingeniería Civil*, CEDEX, *170*, 103-122.

Constaín, A. J. (2014). Revalidación de la ecuación de Elder para la medición precisa de los coeficientes de dispersión en flujos naturales. *Revista DYNA*, *81*(186), 19-27.

Constaín, A., & Corredor, J. (2013). Evolution of Conservative Tracer Plumes in Turbulent Flows: A Thermodynamic Description. *IJESIT Journal*, *2*(5), 185-197.

Constaín, A. J., & Lemos, R. A. (2011). Una ecuación de velocidad media del flujo en régimen no uniforme, su relación con el fenómeno de dispersión como función del tiempo y su aplicación a los estudios de calidad de agua. *Revista Ingeniería Civil*, CEDEX, 164, 114-135.

Constaín, A., Peña, C., Mesa, D., & Acevedo, P. (2014). *Svedberg´s Number in Diffusion Processes*. 2014 International Conference in Hydraulic Resources, Santorini.

Elder, W. J. (May, 1959).The Dispersion of Marked Fluid in Turbulent Shear Flow. *Journal of Fluid Mechanics*, *5*(4), 544-560.

Fischer, H. B. (November, 1967). The Mechanics of Dispersion in Natural Streams. *Journal of the Hydraulics Division*, *93*(6), 187-216.

Hack, J. T. (1957). *Studies of Longitudinal Stream Profiles in Virginia and Maryland* (pp. 46-94). Paper 294-B. Washington, DC: USGS.

Hem, J. (1985). *Study and Interpretation of the Chemical Characteristics of Natural Water*. Water Supply Paper 2254. Washington, DC: U.S. Geological Survey.

Leopold, L. B., & Langbein, W. B. (1962). *The Concept of Entropy in Landscape Evolution*. Paper 500-A. Washington, DC: USGS.

Leopold L.B & Maddock T. *The hydraulic geometryof streams channels and some physiographic impications*. G.S Proffesional paper 252, US gov. printing office, Washington 1953, pp 1-57.

Prigogine, I., & Kondepudi, D. (1998). *Modern Thermodynamics*. Chichester, USA: Wiley.

Spiridonov, V. P., & Lopatkin, A. (1973). *Tratamiento matemático de datos fisicoquímicos*. Moscú: Editorial Mir.

Institutional Address of the Authors

Ing. Alfredo Constaín

Gerente I+D Hydrocloro Tech.
Carrera 19B 166-37, Of. 101
Bogotá, Colombia
Teléfono: +57 (1) 7031 695
alfredo.constain@gmail.com

Ing. Jorge Corredor

Director Programa de Ingeniería Civil
Universidad Militar Nueva Granada
Campus Calle 100
Bogotá, Colombia
Teléfono: +57 (1) 6500 000
jorge.corredor@unimilitar.edu.co

Click here to write the autor

Glass of the Francisco Zarco Dam, Cuencamé, Durango, Mexico.

Photo: Gerardo Esquivel Arriaga.

Huella hídrica del cultivo de la papa en Cuba

• Juan José Cabello* • Alexis Sagastume •
Universidad de La Costa, Colombia
*Autor de correspondencia

• Eduardo López-Bastida •
Universidad de Cienfuegos, Cuba

• Carlo Vandecasteele •
University of Leuven, Belgium

• Luc Hens •
Flemish Institute for Technological Research, Belgium

Resumen

Cabello, J. J., Sagastume, A., López-Bastida, E., Vandecasteele, C., & Hens, L. (enero-febrero, 2016). Huella hídrica del cultivo de la papa en Cuba. *Tecnología y Ciencias del Agua,* 7(1), 105-114.

En el artículo se determina la huella hídrica de la cosecha de la papa en Cuba entre los años 2009 y 2012 utilizando el modelo CROPWAT. Los datos climáticos, de rendimiento y de fertilización son específicos de cada una de las áreas donde se realiza la cosecha y los resultados obtenidos se comparan con los de trabajos anteriores realizados en otros países de América Latina y el Caribe. En el caso de Cuba los resultados muestran diferencias de un 25% respecto a los obtenidos en reportes internacionales elaborados a partir de datos climáticos y de la cosecha promedios del país. Respecto a otros países de la región tienen niveles similares aunque con menor componente gris y mayor componente verde. También se compara la Huella Hídrica de la cosecha de la papa con la de otros cultivos en Cuba estableciéndose que la papa ocupa el cuarto lugar en demanda de agua.

Palabras clave: huella hídrica, agricultura cubana, cosecha de la papa, cosecha de papas en el Caribe.

Abstract

Cabello, J. J., Sagastume, A., López-Bastida, E., Vandecasteele, C., & Hens, L. (January-February, 2016). Water Footprint from Growing Potato Crops in Cuba. Water Technology and Sciences *(in Spanish), 7(1), 105-114.*

This article determines the water footprint from the potato crop in Cuba between the years 2009 and 2012 using the CROPWAT model. Climate, yields and fertilization data are specific to each of the areas where the crops were grown. The results are compared with previous works in other countries in Latin America and the Caribbean. In the case of Cuba, the results show a difference of 25% with respect to international reports developed with data related to climate and average crops in the country. Other countries in the region have similar levels, although with a smaller gray component and a larger green component. The water footprint from potato crops is also compared with other crops in Cuba, finding that potatoes represent the fourth largest water demand.

Keywords*: *Water foot print, Cuban agriculture, potatoes crop, water use in agriculture, potatoes crop in Caribbean.

Recibido: 12/02/2014
Aceptado: 26/08/2015

Introducción

A nivel mundial la demanda de agua para producir alimentos, abastecer industrias y sostener a las poblaciones urbana y rural crece en forma continua desde hace muchos años. Además, un número creciente de regiones en el mundo enfrenta la escasez de agua dulce (Hoekstra, Mekonnen, Chapagain, Mathews y Richter, 2012).

La agricultura utiliza aproximadamente 86% del agua dulce mundial. Uno de los principales retos de la sustentabilidad planetaria es lograr un

equilibrio entre la demanda creciente de agua para la producción de alimentos y sus impactos sociales y ambientales (Chapagain y Orr, 2009).

También en Cuba la agricultura es el principal consumidor de agua con 55% del total de las extracciones de agua dulce, 63% de las aguas superficiales y 47% de las aguas subterráneas (Onei, 2013a). La planificación del uso del agua está centrada en la satisfacción de su demanda, aumentando simplemente el suministro.

La huella hídrica (*HH*) es un indicador amplio del uso del agua: "la huella hídrica es un indicador del uso de agua dulce que no solo se fija en el uso directo del agua de un consumidor o productor, sino también en el uso indirecto del agua" (Hoekstra, Chapagain, Aldaya y Mekonnen, 2011). Las evaluaciones de *HH* se han utilizado para buscar soluciones y contribuir a una mejor gestión de los recursos hídricos (Aldaya y Hoekstra, 2010).

El uso de los indicadores de la *HH* en Cuba contribuye a la evaluación y el análisis del suministro de agua en el país (García y Cantero, 2008). La importancia de utilizar indicadores para los países latinoamericanos fue señalada por Vázquez y Buenfil (2012).

La papa representa alrededor del 10 por ciento de la producción cubana de tubérculos y raíces y es el único cultivo totalmente de regadío durante la temporada seca. La papa se cultiva en áreas particulares y limitadas, lo que facilita el cálculo de su *HH*.

Este estudio tiene como objetivo calcular las *HH* verde, azul y gris de la producción de papa en Cuba y su comparación con otros cultivos en dicho país, así como con la *HH* de las papas cultivadas en otros países caribeños y latinoamericanos con el fin de identificar su importancia ambiental para el país.

Materiales y métodos

Huella hídrica

La *HH* proporciona un marco de referencia para analizar la relación entre el consumo humano y la apropiación del agua dulce. Incluye tres componentes: agua azul (Mekonnen y Hoekstra, 2010), la cual corresponde al volumen de las aguas superficiales y subterráneas consumidas como resultado de la producción de un bien o servicio. El agua verde, que corresponde al volumen del agua evaporada a partir de los recursos de agua verde mundiales (el agua de lluvia almacenada en el suelo como humedad del mismo). Las aguas grises, las cuales corresponden al volumen de agua dulce requerido para asimilar la carga de contaminantes con base en los estándares de calidad del agua ambiental.

Mekonnen y Hoekstra (2011) clasificaron a los países en función de su *HH* durante el período 1996-2005. Los países industrializados tienen una *HH* per cápita que oscila entre 1 250 y 3550 m^3/año. El Reino Unido muestra la *HH* más baja con 1 255 m^3/año, mientras que los Estados Unidos son los mayores consumidores de agua con una *HH* calculada de 2 842 m^3/año. La *HH* de los países en desarrollo varía ampliamente: 550 a 3 500 m^3/año per cápita. La República Democrática del Congo con 552 m^3/año muestra la HH más baja, mientras que Bolivia, con 3 500 m^3/año muestra el valor más alto. La *HH* cubana se estima en 1 687 m^3/año per cápita. En consecuencia Cuba ocupa el número 36 entre 208 países estudiados. La *HH* cubana es 21% superior al promedio global, lo cual es sorprendentemente alto. Entre los 19 países latinoamericanos, Cuba ocupa el séptimo lugar (Vázquez y Buenfil, 2012).

El componente principal de la *HH* cubana es la producción agrícola que representa 1 519 m^3/año, 90% del total; 85% de este total (1 305 m^3/año) es interno y el resultado de los recursos cubanos. Los componentes de la *HH* interna agrícola incluyen: 1 189 m^3/año per cápita de verde (91%), así como 74.9 y 41.4 m^3/año per cápita de azul y gris, respectivamente (Mekonnen y Hoekstra, 2011a y 2011b).

García y Cantero (2008) y González (2012) vinculan la alta *HH* en Cuba con los siguientes hechos: 60% del agua es para el riego, la tecnología ineficiente para el riego, la planificación inadecuada de sistemas de riego y factores climáticos de los trópicos (la precipitación abundante y alta evaporación, así como la

evapotranspiración y el rendimiento del cultivo limitado).

Huella de agua de los cultivos

La *HH* de una cosecha es la suma de las cantidades verde, azul y gris de agua utilizadas para su producción. Aplicado a las papas en Cuba se utiliza el cálculo siguiente (Hoekstra et al., 2011).

$$HH = HH_A + HH_V + HH_G \quad (1)$$

Dónde: *HH* es la huella hídrica total del cultivo de papa (m^3/t). HH_A es la *HH* azul del cultivo de papa (m^3/t) y HH_V es la *HH* verde del cultivo de la papa (m^3/t). HH_G es la *HH* gris del cultivo de la papa (m^3/t).

Los valores de las *HH* azul y verde se calculan por medio de:

$$HH_A = \frac{AAU_U}{Y_P} \quad (2)$$

$$HH_V = \frac{AAU_V}{Y_P} \quad (3)$$

Dónde: AAU_A corresponde al agua azul utilizada (m^3/ha). AAU_V es el agua verde utilizada (m^3/ha). Y_P es el rendimiento de la cosecha de papa (t/ha).

El agua verde y azul que se utilizan para el cultivo de papas se calcula integrando la evapotranspiración diaria (*ET*, mm/día) sobre el período de crecimiento:

$$AAU_A = 10 \bullet \sum_{i=1}^{lgp} E_{TA} \quad (4)$$

$$AAU_V = 10 \bullet \sum_{i=1}^{lgp} E_{TV} \quad (5)$$

Dónde: E_{TA} es la evapotranspiración azul diaria (mm/día); E_{TV} es la evapotranspiración verde diaria (mm/día); y *lgp* corresponde a la duración del período de crecimiento (días).

Para convertir la profundidad del agua en milímetros en volumen de agua por unidad de tierra (m^3/ha) se utiliza un factor de 10. La evapotranspiración se estima utilizando el modelo CROPWAT (Allen, Pereira, Raes y Smith, 1998), el cual proporciona dos maneras: los requerimientos de agua del cultivo (RAC), asumiendo condiciones óptimas, y el programa de riego (PR), incluyendo la posibilidad de especificar el suministro de riego real en el tiempo (Hoekstra *et al*., 2011). El RAC es menos preciso y más simple que el PR y se usa más a menudo (Chapagain y Hoekstra, 2011).

Las "condiciones óptimas" requieren que la evapotranspiración de los cultivos (ET_C) sea igual a la RAC, que la cosecha esté libre de enfermedad, que los cultivos estén bien fertilizados, crezcan bajo condiciones óptimas de suelo y agua, Y alcancen una máxima producción (Allen *et al*., 1998), rendimiento máximo y el valor más bajo de HH_G. El cálculo del RAC solo necesita datos de clima y de la cosecha.

La evapotranspiración se calcula como:

$$ET_C = Cc \times ET_O \quad (6)$$

Donde: *Cc* es el coeficiente de cultivo, que incorpora las características del cultivo y efectos promediados de la evaporación del suelo. ET_O es la evapotranspiración de una hierba de referencia hipotética crecida en condiciones de suficiente disponibilidad de agua (mm/día).

La ET_C se estima con un intervalo de diez días y durante la temporada de crecimiento, utilizando la precipitación efectiva (Hoekstra *et al*., 2011).

El requerimiento de riego (RR) de la cosecha es la diferencia entre el RAC y la precipitación efectiva (P_{ef}). El *RR* es cero si la P_{ef} supera el RAC; de otro modo es la diferencia entre el RAC y la P_{ef} que se utiliza:

$$RR = \max(0, \text{RAC-}P_{ef}), \text{ mm} \quad (7)$$

En caso de que el RAC se cumpla plenamente por medio de la lluvia (*RR* = 0), entonces su valor es igual a la ET_C. Por lo tanto, ET_V será igual al valor mínimo de ET_C, y P_{ef} y ET_A serán iguales a cero:

$$ET_C = \text{RAC (mm/día)} \quad (8)$$

$$ET_V = \min (ET_C, P_{ef}) \text{ (mm/día)} \quad (9)$$

En caso de que el RAC no se cumpla plenamente por medio de la lluvia ($RR > 0$), ET_A es la diferencia entre el RAC P_{ef}.

$$ET_A = \max (0, \text{RAC} - P_{ef}) \quad (10)$$

La P_{ef} se calcula utilizando el método recomendado por Hoekstra *et al.* (2011):

$$P_{ef} = Pt \cdot (1.25 - 0.2\, Pt\, /125) \quad \text{si } Pt < 250 \text{ mm} \quad (11)$$

$$P_{ef} = 1.25 + 0.1 \cdot Pt \text{ si } Pt > 250 \text{ mm} \quad (12)$$

Donde: Pt es la precipitación acumulada mensual: (mm).

El *Cc* considera la evaporación del suelo y los principales factores que la afectan son la variedad del cultivo, el clima y la etapa de crecimiento. Debido a diferencias en la evaporación durante las etapas de crecimiento, el *Cc* para un cultivo dado varía durante el período de producción (Chapagain y Orr, 2009). Las tendencias del Cc durante el período de crecimiento se muestran en la curva del coeficiente de cultivo: la etapa inicial (*Cc* ini = 0.5), la etapa de mediados de temporada (*Cc* media = 1.15) y el final del crecimiento de la papa (*Cc* final = 0.75).

La Organización de las Naciones Unidas para la Alimentación y la Agricultura (FAO) define la duración de estos períodos (días) para una serie de cultivos (Allen *et al.*, 1998). Para las papas son: Etapa inicial (*L*ini = 25 días), la etapa de desarrollo (*L*dev = 30 días), etapa media (*L*mid = 30 a 45 días) y la etapa final (*L*final = 30 días). Esto proporciona un período de crecimiento total de 115 a 130 días. Un periodo ordinario para cultivar papas en Cuba es de alrededor de 100 días, y las etapas coinciden respectivamente con: *L*ini = 20, *L*dev = 25, *L*mid = 30 y *L*final = 25 (González, 2012).

La curva del *Cc* para las papas cosechadas en Cuba se compara con los datos de la FAO en la figura 1, el periodo del ciclo de cultivo de papa

Cuadro 1. Valores del coeficiente de cultivo (Cc) para papas cosechadas en Cuba. Fuente de datos: producción propia.

Periodo	Días (di)	*Cc (coeficiente de cultivo)*
Inicial	1 a 20	0.5
Desarrollo	21 a 45	0.5 + 0.04 (di – 20)
Medio	46 a 75	1.5
Fin	76 a 100	1.5 – 0.03 (di – 75)

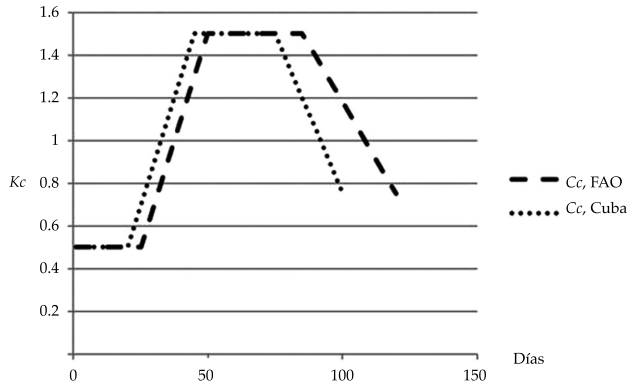

Figura 1. Curva de coeficiente de cultivo. Fuente de datos: Allen *et al*. (1998), González (2012).

Figura 2. Promedio de la distribución de la ETo en Cuba. Año 2005. Fuente de datos: Mendez et al. (2012).

en Cuba es más corto que la de la reportada por la FAO y los valores del *Cc* son diferentes en el desarrollo y el final. En el cuadro 1 se muestran los valores del *Cc* para el cultivo de papas en Cuba.

Los valores de evapotranspiración del cultivo de referencia (ET_O) se han tomado de Méndez, Solano y Ponce (2012). En Cuba la ET_O anual muestra una distribución normal, lo cual es común en zonas tropicales y subtropicales. La ET_O se comporta como en la zona subárida durante la mitad del año y durante la otra mitad como en las zonas subtropicales áridas.

La figura 2 muestra que la distribución media anual de la ET_O en Cuba no se comportar de forma homogénea en todo el país y disminuye de este a oeste. El cuadro 2 muestra los valores promedio mensuales de la ET_O en las regiones occidental y central de Cuba, estimados mediante las ecuaciones de Penman-Monteith.

La HH_G es un indicador de la contaminación de agua dulce causada por el cultivo de papas, y corresponde al agua necesaria para diluir la contaminación por fertilizantes y pesticidas, hasta que las concentraciones no excedan los niveles máximos permisibles definidos de la regulación (Hoekstra et al., 2011).

El componente gris en la HH_G se calcula como:

$$HH_V = \frac{1}{Y} \cdot \left(\frac{\alpha \cdot AR}{C_{max} - C_{nat}} \right) \left(m^3/t \right) \qquad (13)$$

Donde: *AR* es la tasa de aplicación química de fertilizantes o pesticidas (kg/ha); α ies la fracción de lixiviación-escorrentía; $C_{máx}$ es la concentración máxima aceptable (kg/m^3); C_{nat} es la concentración natural del contaminante (kg/m^3); Y_p el rendimiento del cultivo (t/ha).

Los cultivos de papa en Cuba

La papa se cultiva en Cuba en las regiones occidental y central del país (figura 3). Estas áreas se

Cuadro 2. Promedio mensual por región en Cuba, 1960-2000. Fuente de datos: Pacheco, Domínguez y Lamadrid (2006).

Mes	ET_o (mm/day)		Mes	ET_o (mm/day)	
	Oeste	Central		Oeste	Central
Enero	2.9	2.5	Julio	5.1	4.5
Febrero	3.6	3.1	Agosto	5.3	4.1
Marzo	5.0	4.0	Septiembre	4.4	3.9
Abril	6.3	4.5	Octubre	4.1	3.1
Mayo	6.2	4.3	Noviembre	3.7	2.7
Junio	5.5	4.2	Diciembre	3.7	2.2

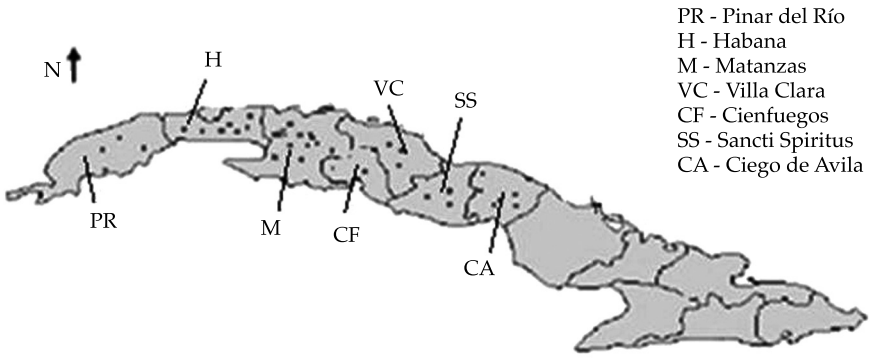

Figura 3. Distribución de cosechas de papas en Cuba. Fuente de datos: Gonzalez (2012).

Cuadro 3. Producción anual y rendimiento de las papas en Cuba por provincia. Fuente de datos: ONEI (2013a).

Provincia		Años				
		2009	2010	2011	2012	Promedio
Pinar del Río	Producción (t)	5 900	3 700	2 200	-	3 933
	Rendimiento(t/ha)	24.1	18.7	20.2	-	21
Habana	Producción (t)	125 900	87 100	69 700	64 400	94 233
	Rendimiento(t/ha)	20.6	19.1	18.6	20.1	19
Matanzas	Producción (t)	52 100	42 900	36 300	26 600	43 767
	Rendimiento(t/ha)	21.0	12.5	17.1	18.6	17
Villa Clara	Producción (t)	19 100	15 900	13 600	10 000	16 200
	Rendimiento(t/ha)	24.6	11.8	21.2	22.2	19
Cienfuegos	Producción (t)	19 000	10 100	10 500	6 300	13 200
	Rendimiento(t/ha)	23.9	16.8	21.1	22.4	21
Sancti Spiritus	Producción (t)	7 000	3 400	3 300	3 200	4 567
	Rendimiento(t/ha)	26.8	16.2	19.8	19.2	21
Ciego de Avila	Producción (t)	53 400	32 000	31 700	20 200	39 033
	Rendimiento(t/ha)	20.3	14.4	17.6	21.9	17
Total	Producción (t)	282 400	195 100	167 300	130 700	214 933
	Rendimiento(t/ha)	23.0	15.6	19.4	17.8	19

caracterizan por temperaturas que oscilan entre 18 y 28 °C durante la temporada seca, que es el período de crecimiento para este cultivo. En consecuencia, su producción requiere de riego (González, 2012).

El cuadro 3 muestra la producción y el rendimiento de la papa en Cuba durante el período 2009-2012.

El rendimiento anual de papas en Cuba promedia 19 t/ha, lo que supera el promedio mundial de 16 t/ha, pero está lejos de las producciones más altas: Países Bajos (45.8 t/ha), Estados Unidos (40.6 t/ha), Alemania (40.5 t/ha) y el Reino Unido (40 t/ha) (Infoagro System SL, 2011).

Cuba tiene dos temporadas: una seca de noviembre a mayo y una lluviosa de mayo a octubre. Las papas se siembran entre noviembre 20 y diciembre 30. Se recolectan en marzo. El cuadro 4 muestra el promedio mensual de lluvia

Cuadro 4. Precipitación mensual promedio en la temporada de la papa en Cuba. Fuente de datos: ONEI (2013b).

Provincia	Precipitación mensual promedio (mm)			
	Enero	Febrero	Noviembre	Diciembre
Pinar del Río	46.95	39.35	67.95	42.83
Habana	130.35	53.30	71.25	70.70
Matanzas	43.30	47.83	39.55	14.75
Villa Clara	65.30	76.03	110.65	53.23
Cienfuegos	78.18	41.20	39.60	51.93
Sancti Spiritus	40.90	59.65	87.63	58.93
Ciego de Avila	13.08	44.88	50.30	20.13

para las diferentes provincias donde se cultivan las papas.

Resultados y discusión

En este estudio se ha elegido diciembre 10 como la fecha en que se plantan las papas. El 10 de diciembre es la mediana entre el 20 noviembre y el 30 de diciembre. Se estima que las papas se recolectan 100 días después: el 20 de marzo (González, 2012).

Huellas hídricas azul y verde

La evaporación se calcula sobre una base día a día, mientras que la precipitación se calcula en períodos más largos. El modelo CROPWAT (Allen *et al.*,1998) supone que la precipitación media mensual se produce durante eventos de un intervalo de seis días y que la lluvia se distribuye uniformemente a lo largo del mes. En varios estudios se utilizan intervalos de diez días para calcular la precipitación efectiva y las necesidades de riego (Hoekstra et al., 2011). En este estudio se utiliza un intervalo de 5 días, en analogía con el trabajo de Aldaya y Hoekstra (2010).

Los resultados de las HH_A y HH_V promedio durante los últimos cuatro años en las diferentes provincias cubanas, se muestran en el cuadro 5. El valor promedio de la HH_V es 104.45 t/m^3, 30% más alta que la HH_A, pero tiene menos variabilidad en las provincias con una desviación estándar media de 22.12 contra 32.5 de HH_A.

A pesar de que la papa se cultiva durante la temporada seca (invierno), la lluvia promedio contribuye 64% a la RAC. La HH_V es aproximadamente 30% mayor que la HH_A.

Cuadro 5. HHV y HHA de cosechas de papas en Cuba por provincia. Promedio 2009-2012.

Provincia	Et_c	P_{ef}	RR	ET_V	ET_A	HH_V m^3/t	HH_A m^3/t
	mm/periodo	mm/periodo	mm/periodo	mm/periodo	mm/periodo		
Pinar del Río	392.9	198.8	194.1	198.8	194.1	94.6	92.4
Habana	392.9	344.3	48.5	246.4	116.4	145.5	61.3
Matanzas	392.8	150.9	241.9	150.1	241.1	88.8	142.3
Villa Clara	320.5	303.3	17.2	263.8	56.7	138.8	29.8
Cienfuegos	320.5	224.9	125.1	195.4	125.1	93.0	59.6
Sancti Spiritus	320.5	244.3	108.7	211.8	108.7	100.9	51.7
Ciego de Avila	320.5	125	195.5	124.9	195.5	73.5	115.0
Cuba	351.5	242.9	130.9	204.3	147.2	104.5	78.6

Huella hídrica gris

El nitrógeno se utiliza como un indicador del impacto de fertilizantes y pesticidas en la evaluación de la HH_G (Chapagain y Hoekstra, 2011). La cantidad de nitrógeno que llega a los cuerpos de agua se supone que es 10% de la cantidad de fertilizante aplicado. El valor máximo recomendado de nitrato (NO_3) por litro en aguas superficiales y subterráneas, de acuerdo con la Organización Mundial de la Salud y la Unión Europea, es de 50 mg de nitrato por litro, y de acuerdo con la EPA de los EUA, de 10 mg por litro (Mekonnen y Hoekstra, 2010). En Cuba existe una norma admisible de 50 mg de NO_3 por litro (González, 2012). En este estudio se utilizó una concentración natural de 4 mg de nitrato por litro (Betancourt, Suárez y Jorge, 2012).

Para cultivar papas en Cuba se recomiendan entre 120 y160 kg de fertilizante por hectárea (González, 2012). Esta investigación utiliza un valor de140 kg/ha.

El cuadro 6 muestra los valores de la HH_G durante los últimos cuatro años en las provincias donde se cultiva la papa.

Los valores HH_G tienen una baja variabilidad debido a que la aplicación de fertilizantes se lleva a cabo de acuerdo con las recomendaciones de la planificación nacional.

Comparación de la HH de la papa con la HH de otros cultivos en Cuba

El valor medio de la HH de los cultivos de papas para el periodo 2009-2012 en Cuba es de 202 m^3/t. El cuadro 7 muestra la comparación entre los resultados obtenidos en este estudio y los reportados por Mekonnen y Hoekstra (2011) para los cultivos de papas y otros cultivos seleccionados en Cuba. También se presenta el resultado reportado por Carmona (2010) acerca de la HHG para papas cultivadas en Cuba.

La diferencia entre los valores confirma la cuestión planteada por Herath (2013) acerca de la necesidad de cálculos y medidas más precisos de la *HH* antes de su uso como una herramienta eficaz para gestionar la sustentabilidad a nivel local.

La *HH* de las papas en Cuba es menor que la de la mayoría de otros cultivos reportados por Mekonnen y Hoekstra (2011a y 2011b). Las diferencias ascienden a un factor de 15 en comparación con la caña de azúcar. Esto se relaciona principalmente con los valores más bajos de la HH_G porque las papas son un cultivo de tempo-

Cuadro 6. HHG promedio de papa, 2009-2012.

Provincia	PR	H	M	VC	Cf	SS	CA	Cuba
HH_G (m^3/t)	16.56	17.90	20.62	18.12	16.88	16.62	19.95	17.99

Cuadro 7. Comparación entre las HH de la de papa y otros cultivos en Cuba.

Cultivo	HH_V[1] (m^3/t)	HH_A[2] (m^3/t)	HH_G[3] (m^3/t)	HH[4] (m^3/t)
Papa (este estudio)	105	79	18	202
Papa(Carmona, 2010)	-	-	47.9	-
(Mekonnen Y Hoekstra, 2011)				
Papa	70	75	5	150
Arroz	2 235	214	152	2 601
Camote	943	9	0	952
Caña	2 814	394	17	3 225
Soya beans	1 998	55	17	2 409
Tomate	310	88	250	648
Otras raíces	857	1	0	858

Cuadro 8. Comparación del rendimiento y la HHA de la papa en algunos países. Fuente de datos: FAO (2012); Mekonnen y Hoekstra (2011a y 2011b).

País	HH_V (m³/ha)	HH_A[2] (m³/ha)	HH_G (m³/ha)	HH (m³/ha)	Rendimiento (t/ha)	HH_S[6] (m³/t)
México	128	102	32	150	27.8	5.4
Costa Rica	193	5	54	262	24.9	10.5
República Dominicana	152	8	27	252	22.3	11.3
Cuba (este estudio)	105	79	18	202	19.0	10.6
Jamaica	114	25	93	232	14.2	16.3
Haití	131	2	6	139	12.5	25.4

rada seca. Por el contrario, las papas muestran mayores valores del agua azul que la mitad de los otros cultivos, debido principalmente a que todas las áreas de producción son irrigadas. Las papas también muestran altos valores de aguas grises que destacan la importancia ambiental de esta evaluación. La agricultura cubana está sujeta a la sobrefertilización, a pesar de los problemas financieros del país y la transición hacia una agricultura ecológica.

El cuadro 8 muestra que los valores de la HH_V son similares en estos países con climas similares. También la HH_A debe mostrar valores similares, pero este tipo de agua se consume más en Jamaica, Cuba y México. La HH_G muestra el valor más alto en Jamaica, donde hay una gran cantidad de fertilizantes (1.5 t/ha), mientras que el valor más bajo se registra en Haití, donde el uso de fertilizantes es mínimo (una tasa de aplicación de 1.5 t /ha) (Carmona, 2010). Sin embargo, ambos países obtienen rendimientos similares. Los otros países en el cuadro 8 muestran valores de la HH_G entre los de Jamaica y Haití, mientras que alcanza producciones más altas. Por último, los valores de la HH_S muestran que México consume la menor cantidad de agua por tonelada, y que Costa Rica, República Dominicana y Cuba consumen cantidades similares de agua, en tanto que Jamaica y Haití presentan el mayor consumo.

Conclusiones

Este estudio, que evaluó la *HH* de la papa en Cuba, muestra que a pesar de que las papas se cosechan en la temporada seca y se cultivan exclusivamente en las zonas de riego, la lluvia podría alcanzar un promedio de más de 60% de la demanda de los cultivos. También es el cultivo con la menor diferencia entre la HH_V y la HH_A.

La *HH* de la papa en Cuba es menor que en países como Costa Rica y la República Dominicana, a pesar de las HH_S son similares, la HH_G es mucho más pequeña y con ella se logra una mayor eficiencia en el uso de fertilizantes.

Las diferencias significativas entre los resultados de la *HH* basados en datos locales cubanos reportados en estudios internacionales ponen de relieve la importancia de los estudios locales para la puesta en práctica de una gestión más sustentable de la agricultura.

Referencias

Aldaya, M., & Hoekstra, A. (2010). The Water Needed for Italians to Eat Pasta and Pizza. *Agricultural Systems*, *103*, 351-360.

Allen, R., Pereira, L., Raes, D., & Smith, M. (1998). *Crop Evapotranspiration: Guidelines for Computing Crop Water Requirements*. Irrigation and Drainage Paper 56. Available at: http://www.fao.org/docrep/x0490e/x0490e00.htm. Accessed: June 2014.

Betancourt, C., Suarez, R., & Jorge, F. (2012). Influencia de los procesos naturales y antrópicos sobre la calidad del agua en cuatro embalses cubanos. *Limnetica*, *31*(2), 193-204.

Carmona, L. (2010). *Estimación de la huella gris de la agricultura teniendo en cuenta el efecto de fertilizantes y pesticidas*. Master Thesis. Barcelona: Polytechnic University of Cataluña.

Chapagain, A., & Orr, S. (2009). An Improved Water Footprint Methodology Linking Global Consumption to Local Water Resources: A Case of Spanish Tomatoes. *Journal of Environmental Management*, *90*(2), 1219-1228.

Chapagain, A., & Hoekstra, A. (2011). The Blue, Green and Grey Water Footprint of Rice from Production and

Consumption Perspectives. *Ecological Economics*, *70*(4), 749-758.

FAO (2012). *FAOSTAT*. Food Agriculture Organization. Available at: http://193.43.36.221/site/339/default.aspx. Accessed: June 2014.

Garcia, J., & Cantero, L. (2008). Indicadores globales para el uso sostenible del agua: caso cubano. *Revista Voluntad Hidráulica*, *100*, 12-19.

González, L. (2012). *Cálculo de la huella hídrica en un cultivo de papa en la Empresa Cultivos Varios Horquita*. Master Thesis. Cienfuegos, Cuba: University of Cienfuegos.

Herath, I. (2013). *The Water Footprint of Agricultural Products in New Zealand: The Impact of Primary Production on Water Resources*. PhD Thesis. Palmerston North, New Zealand: Institute of Agriculture and Environment, Massey University.

Hoekstra, A., Chapagain, A., Aldaya, M., & Mekonnen, M. (2011). *The Water Footprint Assessment Manual. Setting the Global Standard*. London: Earthscan.

Hoekstra, Y., Mekonnen, M., Chapagain, A., Mathews, R. & Richter, B. (2012). Global Monthly Water Scarcity: Blue Water Footprints *versus* Blue Water Availability. *Plus One*, *7*(2), 1-9.

Infoagro System SL. (2011). *El cultivo de la patata*. 1ra parte, Madrid, 2014. Available at: http://www.infoagro.com/hortalizas/patata.htm. Accessed: June 2014.

Mekonnen, M., & Hoekstra, A. (2010). A Global and High-Resolution Assessment of the Green, Blue and Grey Water Footprint of Wheat. *Hydrology and Earth System Sciences*, *14*(7), 1259-1276.

Mekonnen, M., & Hoekstra, A. (2011). The Green, Blue and Grey Water Footprint of Crops and Derived Crop Products. *Hydrology and Earth System Sciences*, *15*(5), 1577-1600.

Mekonnen, M., & Hoekstra, A. (2011a). *National Water Footprint Accounts: The Green, Blue and Grey Water Footprint of Production and Consumption*. Volume 1. Delft: UNESCO-IHE Institute for Water Education.

Mekonnen, M., & Hoekstra A. (2011b). *National Water Footprint Accounts: The Green, Blue and Grey Water Footprint of Production and Consumption*. Volume 2. Delft: UNESCO-IHE Institute for Water Education.

Mendez, A., Solano, O., & Ponce, D. (2012). Valoración de las incertidumbres en la estimación de la evapotranspiración de referencia en Cuba. *Revista Ciencias Técnicas Agropecuarias*, *21*(2), 53-61.

ONEI (2013a). *Sector agropecuario. Indicadores seleccionados*. National Office of Statistic and Information. Available at: http://www.one.cu/publicaciones/05agropecuario/ppalesindsectoragrop/ppales_inddic12.pdf. Accessed: June 2014.

ONEI (2013b). *Panorama ambiental de Cuba*. National Office of Statistic and Information. Available at: http://www.one.cu/publicaciones/04industria/medioambientecifras/medioamb2012.pdf. Accessed: June 2014.

Pacheco, J., Domínguez, I., & Lamadrid, O. (2006). Lluvia y evapotranspiración de referencia en cuatro puntos representativos de la provincia de Villa Clara, Cuba. *Centro Agrícola*, *33* (4), 67-72.

Vázquez, R., & Buenfil, M. (March, 2012). Huella hídrica de América Latina: retos y oportunidades. *Aqua-LAC*, *4*(1), 41-48.

Dirección institucional de los autores

Dr. Juan José Cabello

Universidad de La Costa
Facultad de Ingeniería
Calle 58 # 5566
Barranquilla, Colombia
Tel.: +57 (310) 4705 210
jcabello2@cuc.edu.co

Dr. Alexis Sagastume

Universidad de La Costa
Facultad de Ingeniería
Calle 58 # 5566
Barranquilla, Colombia
Tel.: +57 (310) 4705 210
asagastume2@cuc.edu.co

Dr. Eduardo López Bastida

Universidad de Cienfuegos
Centro de Producción más Limpia
Facultad de Ingeniería
Carretera a Rodad, km 2
Cienfuegos, Cuba
Tel.: +53 (4) 3500 138
kuten@ucf.edu.cu

Dr. Carlo Vandecasteele

University of Leuven
Department of Chemical Engineering
De Croylaan 46, B-3001
Heverlee, Belgium
Carlo.Vandecasteele@cit.kuleuven.be

Dr. Luc Hens

Flemish Institute for Technological Research (VITO)
Mol, Antwerp, Flanders
Belgium.luchens51@gmail.com

Click here to write the autor

Use of Saint-Venant and Green and Ampt Equations to Estimate Infiltration Parameters based on Measurements of the Water Front Advance in Border Irrigation

• Heber Saucedo* •
Instituto Mexicano de Tecnología del Agua
*Corresponding Author

• Manuel Zavala •
Universidad Autónoma de Zacatecas, México

• Carlos Fuentes •
Instituto Mexicano de Tecnología del Agua

Abstract

Saucedo, H., Zavala, M., Fuentes, C. (January-February, 2016). Use of Saint-Venant and Green and Ampt Equations to Estimate Infiltration Parameters based on Measurements of the Water Front Advance in Border Irrigation. *Water Technology and Sciences* (in Spanish), 7(1), 115-122.

A method is presented to estimate infiltration parameters using the Saint-Venant equations to describe the flow of water over soil and the Green and Ampt equations to represent flow of water in the soil. The Levenberg-Marquardt method was applied to estimate the hydrodynamic parameters, namely saturated hydraulic conductivity and pressure in the wet front. By obtaining the model in this manner, the hydrodynamic parameters can be adjusted based on tests of the advance of the water front in border irrigation and the texture of the soil.

Keywords: Saint-Venant equations, Green & Ampt equation, Levenberg-Marquardt method.

Resumen

Saucedo, H., Zavala, M., Fuentes, C. (enero-febrero, 2016). Estimación de parámetros de infiltración a partir de mediciones de avance de riego por melgas empleando las ecuaciones de Saint-Venant, y Green y Ampt. Tecnología y Ciencias del Agua, 7(1), 115-122.

Se presenta un método para realizar la estimación de parámetros de infiltración con base en el empleo de las ecuaciones de Saint-Venant para describir el flujo del agua sobre el suelo, y la ecuación de Green y Ampt para representar el flujo del agua en el suelo. La estimación de los parámetros hidrodinámicos de conductividad hidráulica a saturación y presión en el frente de humedad, se realiza aplicando el método Levenberg-Marquardt. El modelo así obtenido, permite el ajuste de los parámetros hidrodinámicos a partir de datos de pruebas de avance de riego por melgas y de la textura del suelo.

***Palabras clave**: ecuaciones de Saint-Venant, ecuación de Green y Ampt, método Levenberg-Marquardt.*

Received: 17/11/2014
Accepted: 27/08/2015

Introduction

The objective of border irrigation design is to obtain the most uniform application of water possible, as required by the crop, maintaining high application efficiency. Irrigation design consists of determining the supply flow and the time during which this flow needs to be applied to a border head in order to achieve the highest uniformity possible —that is, the determination of optimal flow for the specific length of a given border and the hydrodynamics of a particular soil. One method for this hydrodynamic characterization is based on information from tests of the advance of the wetting front, which involve adjusting and

optimizing parameters to minimize the error between the observed and the simulated advance of the wetting front in gravity fed irrigation systems.

The objective of the present study was to develop a model which can be used to automatically optimize the hydraulic conductivity of soil at saturation and the pressure in the wetting front parameters. This is based on precisely modeling the flow of water on a free surface using Saint-Venant equations, while the flow of water in the soil is described using Green and Ampt equation, which is a simple way to model the phenomenon while maintaining the physical-mathematical bases in the representation.

Flow of Water Over a Soil Surface

The flow of water over a free surface is modeled with the Saint-Venant equations resulting from the application of the laws for the conservation of mass and momentum. Given the relationship between the width of a border and the water depth, equations for runoff over a surface with an infinite width can be considered (Woolhiser, 1975). The continuity equation is written as:

$$\frac{\partial h}{\partial t}+\frac{\partial q}{\partial x}+\frac{\partial I}{\partial t}=0 \qquad (1)$$

and the momentum equation is written according to the form recommended by Saucedo, Fuentes and Zavala (2005):

$$\frac{1}{h}\frac{\partial q}{\partial t}+\frac{2q}{h^2}\frac{\partial q}{\partial x}+\left(g-\frac{q^2}{h^3}\right)\frac{\partial h}{\partial x}+g(J-J_o)+\beta\frac{q}{h^2}\frac{\partial I}{\partial t}=0 \qquad (2)$$

where $q(x,t)=U(x,t)h(x,t)$is the flow per unit width of the border [L^2T^{-1}]; x is the spatial coordinate in the main direction of the movement of the water through the border [L]; t is time [T]; U is the mean velocity, h is the water depth [L]; J_o is the topographic slope of the border [LL^{-1}]; J is the slope of friction [LL^{-1}]; $V_I=\partial I/\partial t$, the flow of infiltration [LT^{-1}], that is, the volume of water infiltrated over a unit of time per a border's unit width and unit length; I is infiltration depth [L]; g gravitational acceleration [LT^{-2}]; the dimensionless parameter $\beta=U_{Ix}/U$, with $\alpha=1-U_{Ix}/U$, where U_{Ix} is the projection in the direction of the movement of the water mass' outflow velocity from infiltration.

The relationship between the slope of friction (hydraulic resistance) and the hydraulic variables q and h is based on Fuentes, De León, Saucedo, Parlange and Antonino (2004), using a law of potential resistance:

$$q=k\nu\left(\frac{h^3gJ}{\nu^2}\right)^d \qquad (3)$$

where ν is the kinematic viscosity coefficient of the water [L^2T^{-1}] and k is a dimensionless factor; d is the dimensionless parameter with a range of $1/2\le d\le 1$ in function of the type of flow; the extreme values $d=1/2$ y $d=1$ correspond to Chezy and Poiseuille flow, respectively.

The initial and border conditions to be applied to the Saint-Venant equations to model the water front advance are:

$$q(x,0)=0 \quad \text{y} \quad h(x,0)=0 \qquad (4)$$

$$q(0,t)=q_o, \quad q(x_f,t)=0 \quad \text{y} \quad h(x_f,t)=0 \qquad (5)$$

where $x_f(t)$ is the position of the wave front for time t and q_o is the flow of the water supply at the border's inlet.

To close the system, it is necessary to know how the infiltrated depth evolves over time throughout the border, that is, the law of infiltration.

Water Flow in Soil

The Green and Ampt model (1911) is established based on the continuity equation and Darcy's

Law, with the following premise: a) the initial moisture profile in a soil column is uniform $\theta = \theta_o$; b) the water pressure on the surface of the soil is hydrostatic, $\psi = h \geq 0$, where h is the water depth; c) a well-defined moisture front exists, characterized by a negative pressure, $\psi = -h_f < 0$,
where h_f is the suction head at the wetting front; d) the region between the soil surface and the wetting front is completely saturated (piston flow): $\theta = \theta_s$ and $K = K_s$, where K_s is the hydraulic conductivity at saturation, that is, the hydraulic conductivity value from Darcy's Law corresponding to the volumetric water content at saturation. The resulting ordinary differential equation is:

$$V_I = \frac{dI}{dt} = K_s\left[1 + \frac{(h_f + h)\Delta\theta}{I}\right] \qquad (6)$$

where $\Delta\theta = \theta_s - \theta_o$ is the accumulated infiltration volume per unit of soil surface or infiltration depth.

Numerical Solution

The model developed by Saucedo, Zavala and Fuentes (2011) is used to simulate the advance of the wetting front in border irrigation. The discrete continuity equation for the advance stage is written as:

$$\begin{aligned}
&\left[\omega q_\ell + (1-\omega)q_j\right]\delta t - (x_\ell - x_j)\begin{bmatrix}\omega(h_\ell + I_\ell)\\ +(1-\omega)(h_j + I_j)\end{bmatrix}\\
&-\left[\omega q_r + (1-\omega)q_m\right]\delta t + (x_r - x_m)\begin{bmatrix}\omega(h_r + I_r)\\ +(1-\omega)(h_m + I_m)\end{bmatrix}\\
&-\left[\varphi h_\ell + (1-\varphi)h_r + \varphi I_\ell + (1-\varphi)I_r\right](x_r - x_\ell)\\
&+\left[\varphi h_j + (1-\varphi)h_m + \varphi I_j + (1-\varphi)I_m\right](x_m - x_j) = 0 \qquad (7)
\end{aligned}$$

The momentum equation has the same discrete form for the four irrigation stages:

$$\begin{aligned}
&2\bar{q}\bar{h}(q_r - q_\ell)\delta t + \left(g\bar{h}^3 - \bar{q}^2\right)(h_r - h_\ell)\delta t\\
&+\bar{h}^2(x_r - x_\ell)\left[\omega q_r + (1-\omega)q_\ell - \omega q_m - (1-\omega)q_j\right]\\
&+g\,\delta t\,\bar{h}^3(x_r - x_\ell)\left[\omega J_r + (1-\omega)J_\ell - J_o\right] \qquad (8)\\
&+\beta\,\delta t\,\bar{q}\bar{h}(x_r - x_\ell)\left[\omega I_r + (1-\omega)I_\ell - \omega I_m - (1-\omega)I_j\right] = 0
\end{aligned}$$

In equations (7) and (8), δt is the passage of time, ω and ϕ sare weight factors in space and time. The coefficients are calculated based on the values from the previous time step $\bar{q} = (1-\phi)q_m + \phi q_j$, $\bar{h} = (1-\phi)h_m + \phi h_j$ (Saucedo *et al.*, 2005). The small variables are introduced (Strelkoff & Katopodes, 1977) —δh_r, δq_r, δh_ℓ and δq_ℓ— such that $h_\ell = h_j + \delta h_\ell$, $h_r = h_m + \delta h_r$, $q_\ell = q_j + \delta q_\ell$ y $q_r = q_m + \delta q_r$ for the interior cells. Substituting in the discrete continuity and momentum equations, a system of algebraic equations is obtained whose solution enables advancing the values of the hydraulic variables over time. The details regarding the inputs for the matrix system can be consulted in Saucedo *et al.* (2011).

The Green and Ampt equation (equation (6)) is numerically solved using a finite differences method. This procedure is well-documented in the literature and can be consulted in Burden and Faires (1985), for example.

A constant time step was used, $\Delta t = 1.0$ s to couple the Saint-Venant and Green and Ampt equations. The discretization used to completely solve the Saint-Venant equations was similar to those reported by the literature: $\Delta t_{min} = 5$ s, as per Katopodes and Strelkoff (1977), $\Delta t_{max} = 1$ s, as per Akanbi and Katopodes (1988), $\Delta t_{min} = 2.12$ s as per Playán, Walker and Merkley (1994)..

Optimization of Parameters

The Levenberg-Marquardt method can be used to calculate the hydrodynamic parameters K_s and h_f, based on the data recorded during a test of the advance of the wetting front, in which the value of the parameters

estimated by a given iteration is calculated according to the expression with the following form:

$$\left[J(p)^T J(p) + \lambda I\right]\Delta p = -J(p)^T K(p) \qquad (9)$$

where $J(p)$ is the Jacobian matrix of the variations of the position function of the wetting front $x_f = x_f(t)$ with respect to each one of the parameters to be optimized (K_s y h_f); I is the identity matrix; $K(p)$, is the vector of differences between the positions of the wetting front observed in the field and those obtained by the prior iteration of the Levenberg-Marquardt method; λ is the damping parameter and is important for the convergence of the method. Its value can be determined with one of the procedures suggested by Griva, Nash and Sofer (2009), for example.

The Jacobian matrix $J(p)$ is calculated as:

$$J(p) = \begin{bmatrix} \frac{\partial x_{f1}}{\partial K_{s1}} & \frac{\partial x_{f2}}{\partial h_{f1}} \\ \frac{\partial x_{f1}}{\partial K_{s2}} & \frac{\partial x_{f2}}{\partial h_{f2}} \\ \vdots & \vdots \\ \frac{\partial x_{f1}}{\partial K_{sn}} & \frac{\partial x_{f2}}{\partial h_{fn}} \end{bmatrix} \qquad (10)$$

In this equation, $i = 1, 2, \ldots, n$ n is the number of points recorded during the test of the advance of the wetting front. A maximum of 10 points is recommended to reduce computing effort. The position function of the wetting front $x_f = x_f(t)$ is the result of the internal numerical coupling of the Saint-Venant and the Green and Ampt equations. The derivatives are numerically calculated with the function $x_f = x_f(t)$ calculada para dos valores cercanos de los parámetros a optimar.

By way of example, consider a case in the literature involving a test of the water front advance, performed by Fuentes (1992) with loam soil from Montecillo. The following information is available: unit flow $q_o = 0.0032$ $m^3/s/m$; topographical slope $J_o = 0.002$ m/m; border length $L = 100$ m; parameters $d = 1$ y $k = 1/54$; from the law of resistance; parameter $\beta = 2$; from the momentum equation; initial volumetric water contents $\theta_o = 0.2749$ cm^3/cm^3. The value of the porosity is assimilated in the volumetric water content at saturation, such that $\theta_s = 0.4865$ cm^3/cm^3. Figure 1 shows the graph of the recorded values of the advance of the front.

Figures 2 through 4 present the results from the first, third and seventh iterations of the Levenberg-Marquardt method. Figure 5 shows the evolution of the mean squared error as the iterations advanced. The values of the parameters $h_f = 40.4$ cm and $K_s = 1.35$ cm/h were obtained by applying the optimization procedure to reproduce the data from the irrigation test performed with the experiment mentioned.

While a relatively low number of iterations was performed to reach convergence, it should be taken into account that the largest computing effort involves the estimation of the Jacobian matrix which appears in equations (9) and (10).

Conclusions

A method was developed to estimate infiltration parameters based on the use of Saint-Venant equations to describe the flow of water over soil and the Green and Ampt equation to represent the flow of water in the soil. The hydrodynamic hydraulic conductivity at saturation and pressure in the water front were estimated based on the Levenberg-Marquardt method. The resulting model makes it possible to adjust the hydrodynamic parameters based on test data related to the advance of the wetting front in border irrigation and the texture of the soil.

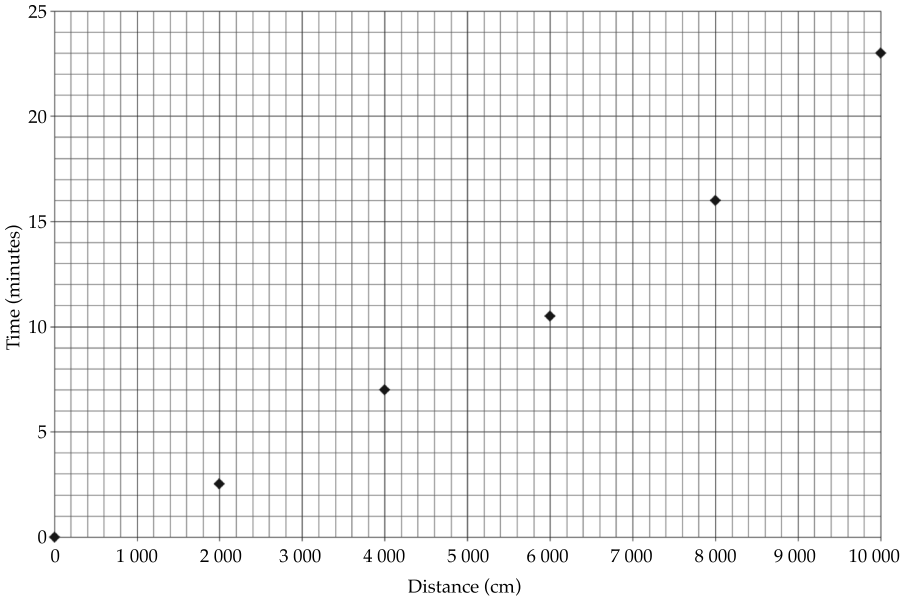

Figure 1. Observed values from a test of the water front advance reported in the literature.

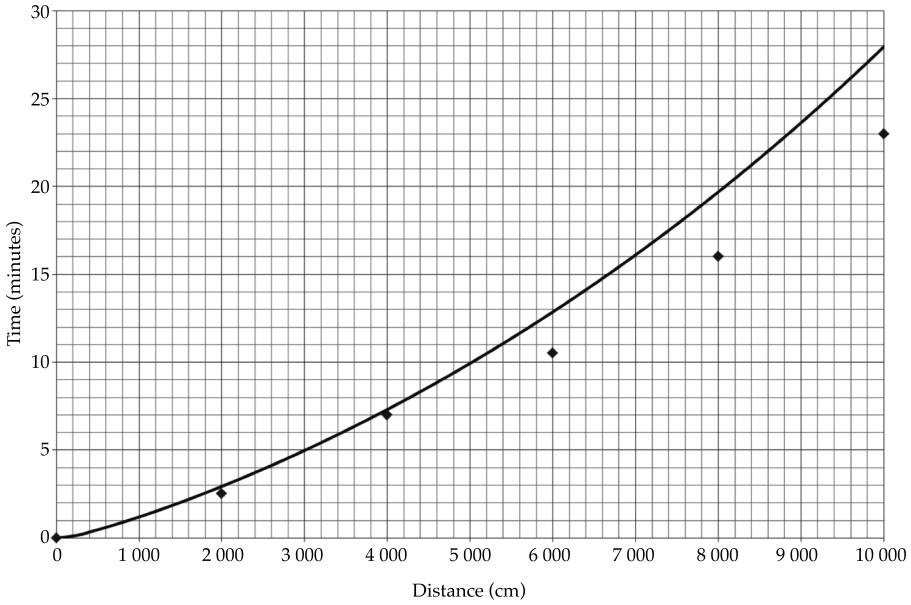

Figure 2. Results from the first iteration with the Levenberg-Marquard method, $h_f = 33.4$ cm and $K_s = 1.58$ cm/h.

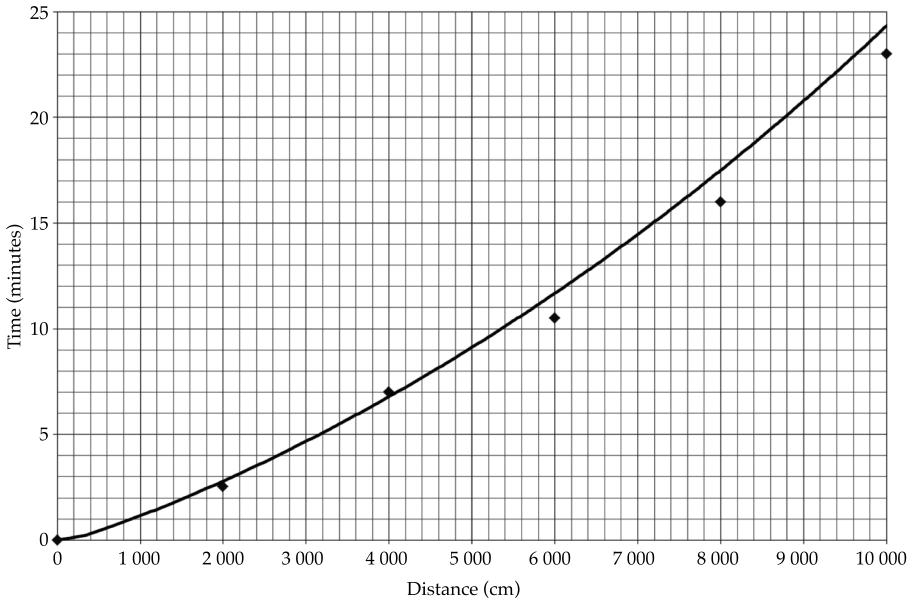

Figure 3. Results from the third iteration with the Levenberg-Marquard method, $h_f = 38.3$ cm y $K_s = 1.49$ cm/h.

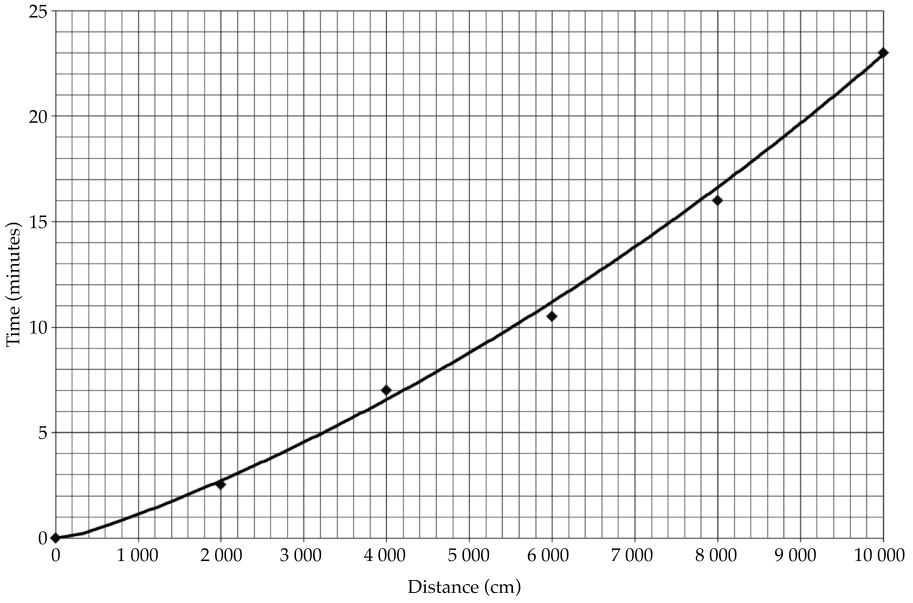

Figure 2. Results from the seventh iteration with the Levenberg-Marquard method, $R^2 = 0.997$, $h_f = 40.4$ cm y $K_s = 1.35$ cm/h.

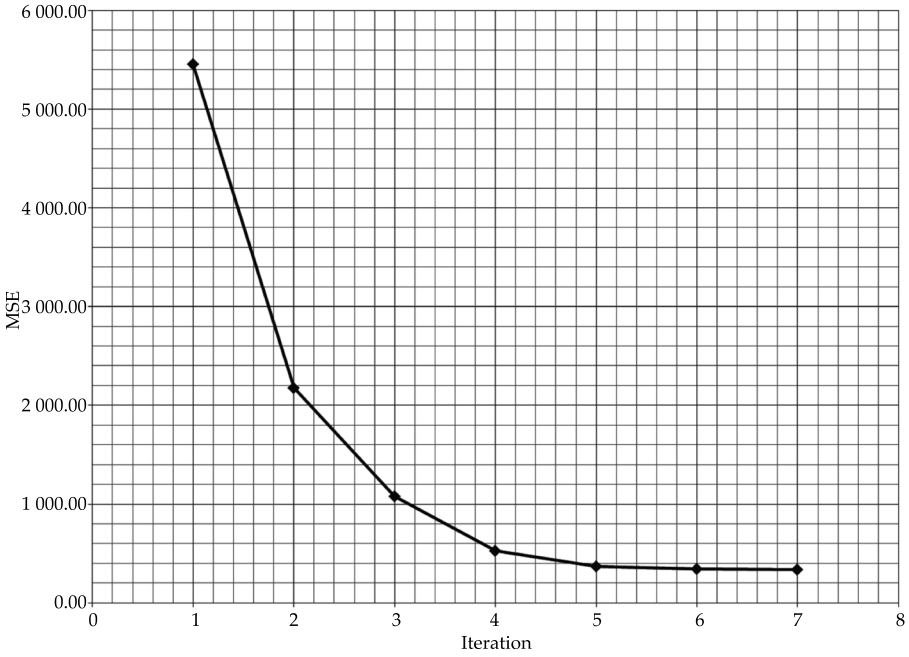

Figure 5. Evolution of the mean squared error during the application of the Levenberg-Marquardt method.

References

Akanbi, A., & Katopodes, N. (1988). Model for Flow Propagation on Initially Dry Land. *Journal of Hydraulic Engineering*, *114*(7), 689-706.

Burden, R. L., & Faires, J. D. (1985). *Análisis numérico* (721 pp.). México. DF: Grupo Editorial Iberoamérica.

Fuentes, C. (1992). *Approche fractale des transferts hydriques dans les sols non saturès* (267 pp.). Tesis de Doctorado. Grenoble, Francia: Universidad Joseph Fourier.

Fuentes, C., De León, B., Saucedo, H., Parlange, J. Y., & Antonino, A. (2004). El sistema de ecuaciones de Saint-Venant y Richards del riego por gravedad: 1. La ley potencial de resistencia hidráulica. *Ingeniería Hidráulica en México*, *18*(2), 121-131.

Green, W. H., & Ampt, G. A. (1911). Studies in Soil Physics, I: The Flow of Air and Water through Soils. *J. Agric. Sci.*, *4*, 1-24.

Griva, I., Nash, S., & Sofer, A. (2009). *Linear and nonlinear optimization* (pp. 765). USA: Ed. Society for Industrial and Applied Mathematics (SIAM).

Katopodes, N., & Strelkoff, T. (1977). Hydrodinamics of Border Irrigation, Complete Model. *Journal of the Irrigation and Drainage Division*, *IR3*, 13188, 309-324.

Playán, E., Walker, W. R., & Merkley, G. P. (1994). Two-Dimensional Simulation of Basin Irrigation. I. Theory. *Journal of Irrigation and Drainage Engineering*, *120*(5), 837-856.

Saucedo, H., Fuentes, C., & Zavala, M. (abril-junio, 2005). El sistema de ecuaciones de Saint-Venant y Richards del riego por gravedad: 2. Acoplamiento numérico para la fase de avance en el riego por melgas. *Ingeniería Hidráulica en México*, *20*(2), 109-119.

Saucedo, H., Zavala, M., & Fuentes, C. (abril-junio, 2011). Modelo hidrodinámico completo para riego por melgas. *Tecnología y Ciencias del Agua, antes Ingeniería Hidráulica en México*, 2(2), 23-38.

Strelkoff, T., & Katopodes, N. (1977). Border Irrigation Hydraulics with Zero Inertia. *Journal of the Irrigation and Drainage Division*, *IR3*, 325-342.

Woolhiser, D. A. (1975). *Simulation of Unsteady Overland Flow* (pp. 485-508). In K. Mahmood & V. Yevjevich (Eds.). *Unsteady Flow in Open Channels*. Vol II. Fort Collins, Colorado, USA: Water Resources Publications.

Institutional Address of the Authors

Dr. Heber Saucedo

Instituto Mexicano de Tecnología del Agua
Paseo Cuauhnáhuac 8532, Progreso
62550 Jiutepec, Morelos, México
Teléfono. +52 (777) 3293 600
hsaucedo@tlaloc.imta.mx

Dr. Manuel Zavala

Universidad Autónoma de Zacatecas
Av. Ramón López Velarde # 801, Centro
98000 Zacatecas, Zacatecas, México
Teléfono. +52 (492) 9239 407
mzavala73@yahoo.com.mx

Dr. Carlos Fuentes

Instituto Mexicano de Tecnología del Agua
Paseo Cuauhnáhuac 8532, Progreso
62550 Jiutepec, Morelos, México
Teléfono. +52 (777) 3293 600
cfuentes@tlaloc.imta.mx

Tecnical Note

Identificación y caracterización de sequías hidrológicas en Argentina

• Erica Díaz* • Andrés Rodríguez • Oscar Dölling •
• Juan Carlos Bertoni • Marcelo Smrekar •
Universidad Nacional de Córdoba, Argentina
*Corresponding Author

Abstract

Díaz, E., Rodríguez, A., Dölling, O., Bertoni, J. C., & Smrekar, M. (January-February, 2016). Identification and Characterization of Hydrological Drought in Argentina. *Water Technology and Sciences* (in Spanish), 7(1), 123-131.

The temporal and spatial distribution of water resources need to be determined for adequate water planning and management. Droughts are highly complex and extreme hydrological phenomena which affect the development and use of water resources in a single region. In this work, droughts were identified and characterized from the hydrological perspective, with the largest spatial area and time period possible given the available flow data. The study area includes 14 hydrographic basins in Argentina (Colorado, Mendoza, San Juan, Atuel, Ctalamochita, Anisacate, Xanaes, Suquía, Dulce, Juramento, Salado, Paraná, Bermejo and Pilcomayo rivers). The objective was to spatially and temporally identify and characterize hydrological droughts to evaluate the regional water availability, which is an essential component in water planning. This work defines a hydrological drought as an event in which water flow (annual mean) in unregulated natural basins is lower than the flow value that occurs over 70% of the time. The simultaneous occurrence of multi-year droughts in spatially large areas is a result of climate variability. This information is relevant to the management of water resources given that the supply of water for human, irrigation and energy production uses, among others, may be seriously affected by a simultaneously occurrence of severe droughts in basins that supply a particular region or neighboring areas.

Keywords: Hydrological drought, annual flows, management.

Resumen

Díaz, E., Rodríguez, A., Dölling, O., Bertoni, J. C., & Smrekar, M. (enero-febrero, 2016). Identificación y caracterización de sequías hidrológicas en Argentina. Tecnología y Ciencias del Agua, *7(1), 123-131.*

Para una adecuada planificación y gestión de los recursos hídricos es clave conocer la distribución temporal y espacial de éstos. La sequía es un fenómeno hidrológico extremo de gran complejidad que afecta el desarrollo y aprovechamiento de los recursos hídricos en una misma región. En este trabajo se abordó la identificación y caracterización de sequías desde el punto de vista hidrológico, abarcando la mayor ventana de tiempo y espacio en función de los datos de caudales disponibles. Este estudio comprende un área de 14 cuencas hidrográficas argentinas (los ríos Colorado, Mendoza, San Juan, Atuel, Ctalamochita, Anisacate, Xanaes, Suquía, Dulce, Juramento, Salado, Paraná, Bermejo y Pilcomayo). El objetivo del presente trabajo ha sido identificar y caracterizar, temporal y espacialmente, sequías hidrológicas para evaluar la disponibilidad hídrica regional, que es una componente esencial en la planificación del agua. En este trabajo se define como sequía hidrológica aquel suceso en el cual la oferta de caudal (medio anual) en cuencas naturales no reguladas sea inferior al valor del caudal excedido el 70% de tiempo. Se observó la ocurrencia de sequías plurianuales simultáneas en áreas de gran extensión espacial, producto de la variabilidad climática. Esta información es de relevancia para la gestión de los recursos hídricos, pues usos tales como el abastecimiento humano, riego y producción energética, entre otros, pueden ser seriamente afectados por la ocurrencia de manera simultánea de sequías severas en cuencas que aportan a una región y zonas vecinas.

Palabras clave: *sequías hidrológicas, caudales anuales, gestión.*

Received: 12/03/2015
Accepted: 03/09/2015

Introduction

Droughts are extreme and complex natural phenomena, about which much less is known than flooding events. The impacts have significant social, political and economic costs that affect large areas. Given that they are intrinsic natural conditions that cannot be prevented, and considering that there has been much talk about these events but little is known, the study of droughts is necessary in order to base planning on the availability of water and thereby better respond to these events when they occur. A lack of hydrological and meteorological data is one of the reasons why knowledge about these events is still limited. Therefore, this work is aimed at identifying and characterizing droughts from the hydrological perspective in order to maximize the use of information about annual supplies, which generally covers a large time frame and spatial area.

The temporal and spatial identification and characterization of streamflow droughts makes it possible to evaluate regional and local water availability, which is an essential component of water resource planning.

Study Zone

The present work encompasses an area containing 14 hydrographic basins in Argentina. The following river basins were selected: Colorado (CO), Mendoza (ME), San Juan (SJ), Atuel (AT), Ctalamochita (CT), Anisacate (AN), Xanaes (XA), Suquía (SU), Dulce (DU), Juramento (JU), Salado (SA), Paraná (PA), Bermejo (BE) and Pilcomayo (PI) (Figure 1).

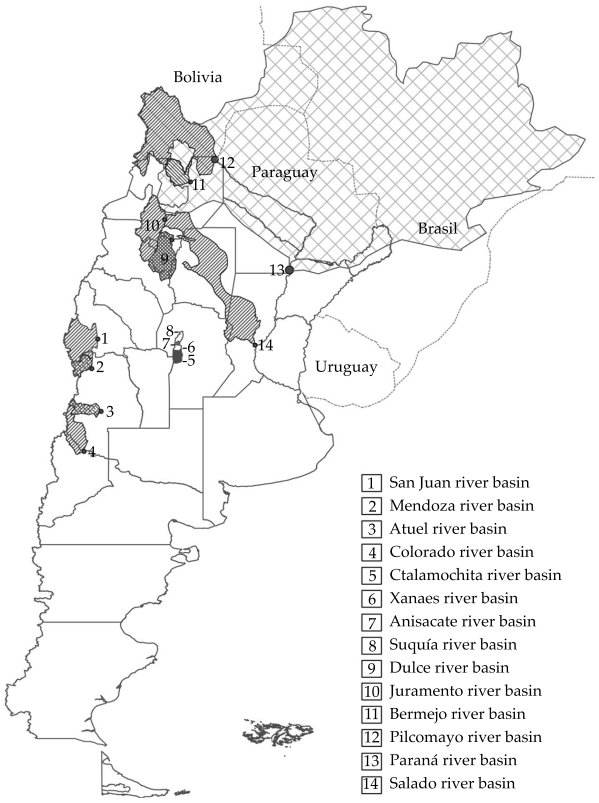

Figure 1. Location of the basins analyzed by this study.

The rivers had different characteristics in terms of their locations in the basin, modules, supply areas and annual supply volume (Table 1). These basins were selected because they contained sufficiently large flow series (over 50 years) and they represented the largest hydrographic systems in Argentina. The points chosen for data collection were the headwaters of the basins where there was no influence from control systems or significant changes in land use, with the exception of the Parana River (for which that information was not available). The series corresponded to flow data measured in the study sections in the San Juan, Atuel, Mendoza, Salado, Paraná, Colorado, Anisacate, Ctalamochita, Bermejo and Pilcomayo river basins. In the Dulce, Suquía, Xanaes and Juramento river basins, the flow data were measured until the control dams were built, and afterwards the series were calculated based on the balance in the reservoir. The sections were the same and the reservoir did not affect the series since they included the flows that reached the reservoir and not those that were diverted.

Information Processing

All the series used by this work were subjected to different statistical analyses to verify their reliability and identify their characteristics. First, a visual inspection was performed in order to detect outliers, through an analysis of questionable data proposed by Chow, Maidment and Mays, 1994. Homogeneity was then verified (with the Wilcoxon and Arch Annual Scale) as well as stationarity (using the Mann-Kendall and Dickey-Fuller methods). The application Arch and Dickey-Fuller method to the series did not verify homogeneity and the application of Wilcoxon and Mann-Kendall did not verify stationarity, since these tests are based on the independence of the data. A temporal dependency may exist in the case of annual flows (see results shown in Table 2).

Analysis of Maximum Historical Droughts

The present work characterized streamflow droughts in terms of annual supply deficits,

Table 1. Summary of hydrological and geographical characterisitcs of the basins analyzed.

River basin	Station			Altitude (masl)	Supply area (km²)	Module (m³/s)	Period
	Name	Latitude	Longitude				
Colorado	Buta Ranquil	37° 04′ 34.4″	69° 44′ 48.1″	850	15 300	148	1940-2013
Mendoza	Guido	32° 54′ 55.0″	69° 14′ 16″	1 408	8 180	45.6	1956-2013
San Juan	San Juan - km 47.3	31° 30′ 59.7″	68° 56′ 24.6″	934	25 660	65	1909-2013
Ctalamochita	Embalse	32° 10′ 00.0″	64° 23′ 00″	650	3 300	27.1	1914-1982
Xanaes	Los Molinos	31° 05′ 00.0″	64°30′00″	770	980	9.5	1936-2008
Anisacate	Santa Ana	31° 40′ 00.0″	64° 34′ 00″	900	465	4.83	1925-1979
Suquía	San Roque	31° 22′ 00.0″	64° 27′ 00″	650	1 350	10	1926-2010
Dulce	La Escuela	27° 30′ 00.0″	64° 51′ 00.0″	265	19 700	82.2	1926-2013
Salado	Ruta Provincial 70	31° 29′ 28.4″	60°46′50,0″	17	29700	137	1954-2013
Juramento	Cabra Corral	25° 16′ 19.0″	65° 19′ 47.0″	945	32 885	29.5	1934-2013
Bermejo	Pozo Sarmiento	23° 13′ 00.0″	64° 12′ 00″	296	25 000	446	1941-2013
Pilcomayo	La Paz	22° 22′ 41.0″	62° 31′ 21″	230	96 000	237	1961-2013
Paraná	Corrientes	27° 28′ 30″	58° 49′ 60″	52	1 950 000	17 189	1906-2013
Atuel	La Angostura	35° 05′ 56.80″	68° 52′ 25.80″	1 302	3 800	35.4	1906-2013

Note: module refers to the annual mean flow.

Table 2. Summary of the homogeneity and stationarity analysis for the complete series.

Basin	Series	Homogeneity		Stationarity		Questionable data
		Wilcoxon	Arch	Kendall	Dickey-Fuller	
Suquía	1926-2010	$p = 0.000216$	$p = 0.5909$	$p = 0.0869$	$p = 0$	0
Xanaes	1936-2008	$p = 0.000283$	$p = 0.3206$	$p = 0.0277$	$p = 0$	1
Anisacate	1925-1979	$p = 0.561$		$p = 0.896$		1
Ctalamochita	1914-1982	$p = 0.256$		$p = 0.768$		0
Dulce	1926-2013	$p = 0.00197$	$p = 0.8119$	$p = 0.0108$	$p = 0$	1
Colorado	1940-2013	$p = 0.214$		$p = 0.815$		0
Juramento	1934-2013	$p = 0.940$		$p = 0.581$		0
Paraná	1906-2013	$p = 0.00440$	$p = 0.9903$	$p = 0.0101$	$p = 0$	0
Bermejo	1941-2013	$p = 3.36E\text{-}006$	$p = 0.6261$	$p = 6.44E\text{-}007$	$p = 0$	0
Pilcomayo	1961-2013	$p = 0.793$		$p = 0.0762$		0
Salado	1954-2013	$p = 0.0630$		$p = 0.241$		0
San Juan	1909-2013	$p = 0.499$		$p = 0.310$		0
Mendoza	1956-2013	$p = 0.0735$		$p = 0.0364$		0
Atuel	1906-2013	$p = 0.441$		$p = 0.886$		0

following a methodology for the analysis of time series known as succession analysis. The use of succession analyses has been proposed as an objective method to identify periods of drought and to evaluate their statistical properties. This methodology has been used for the stochastic analysis and characterization of droughts ever since Yevjevich (1967) proposed the definition of a drought event as the period during which the variable that indicates water availability, *Xt* (supply, rainfall, soil moisture, etc.), is below a particular threshold, *Xo*. This threshold, or cut-off level, may be a fixed value in the case of annual time series or a periodic value in the case of periodic time series (Salas *et al.*, 1980). It may also be the mean or median of the hydrological data series used, a fraction of the mean (Coastal, Clausen, & Pearson, 1995), a defined level (such as the mean less the standard deviation) or the value of a given exceedance probability (Fernández-Larrañaga, 1997). In any case, the threshold should be selected in such a way that it is representative of water demand (Tsakiris et al., 2007).

For the present study, an exceedance probability of 70% was chosen as the threshold value. This criterion has been adopted by several authors worldwide (Hisdal et al., 2001; Fernández-Larrañaga, 1997; Rivera & Penalba, 2013). The use of similar criteria as those applied to other basins in other regions enables comparing the results, given that droughts in regions with different climates can be characterized based on an exceedance probability (Fernández-Larrañaga, 1997). Using a successions analysis, parameters that are useful to quantify droughts can be obtained, including: length (*L*), severity or magnitude (*M*)(accumulated sum of the differences between the threshold and the supply flows), specific point in time (beginning and end); maximum intensity (I_{max} defined as the maximum of the differences between the threshold and the supply flows that comprise the event), and mean intensity (I_{mean}, the relationship between magnitude and length). These parameters are seen in Figure 2.

Figure 3 shows each of the variables (that characterize droughts) divided by the an-

nual mean supply [x] in each basin, thereby identifying the years with the most severe droughts for each basin and their magnitudes (with respect to the annual mean supply) for an exceedance probability threshold of 70%.

The graph of their lengths and magnitudes shows that the most critical droughts in each basin were registered in the mid 1940s and 1960s (except for the Juramento River, which was registered in 1991). The most severe

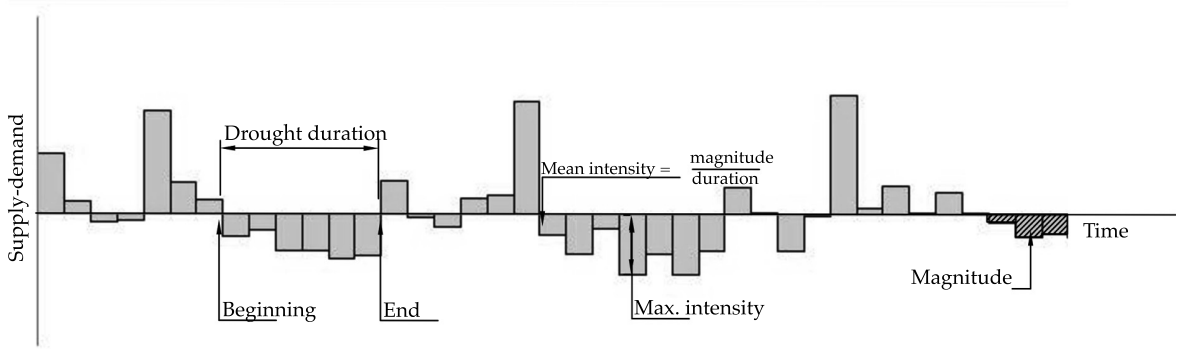

Figure 2. Chronological series of supply minus a threshold representing the demand in a region to identify and characterize droughts according to the successive method. Source: adapted from Fernández-Larrañaga (1997).

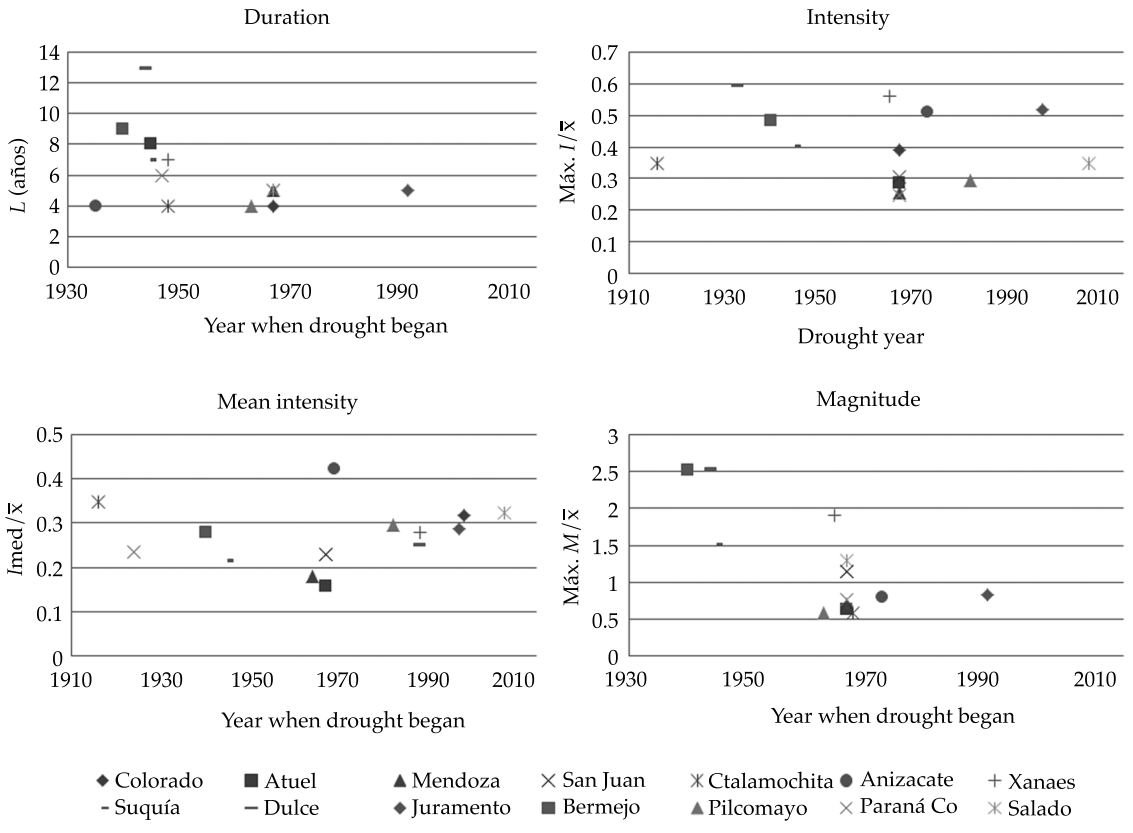

Figure 3. Maximum parameters for characterizing droughts divided by the mean annual supply.

drought in terms of magnitude began in 1967 in the majority of the basins (Colorado, Atuel, Mendoza, San Juan, Ctalamochita, Xanaes, Pilcomayo, Paraná Co, Salado). This result coincides with studies by Ravelo, Da Porta and Zanvettor (1999), Mauas, Buccino and Flamenco (2008), Rivera and Penalba (2013), and with the most severe drought identified in Chile (Fernández-Larrañaga, 1997). The longest droughts lasted 4 to 13 years and the magnitudes were 0.6 to 2.5 times the mean. In terms of the maximum intensities of the droughts, these were recorded before 1970 in the majority of the basins (except Juramento, Pilcomayo and Salado). The graph of the mean intensity shows the basins that have had droughts over recent decades with shorter lengths but larger magnitudes, such as those in the Colorado (1998), Juramento (1997) and Salado (2007) basins.

Spatial and Temporal Analysis of Streamflow droughts

The spatial and temporal analysis of droughts is supported by a matrix containing rows corresponding to the geographic location of the basins (from south to north) and columns arranged chronologically. A color scale identifies different drought thresholds. The values for each unit in the matrix are obtained by calculating the exceedance probability corresponding to the annual mean supply registered for each year in the chronological series of the available water supply:

$$\text{Probability}\ (X_{jt} > x_{jt}) = \alpha \quad (1)$$

Where:

X_{jt}: available water series.

x_{jt}: numerical value of the annual supply observed for year t in basin *j*.

α: probability thresholds.

The matrix was generated with the following thresholds, according to the study by Fernández- Larrañaga (1997), which makes it possible to compare the present results in Argentina with those from Chilean basins.

$0.00 < \alpha < 0.40$	Rainy
$0.40 < \alpha < 0.60$	Normal
$0.60 < \alpha < 1.00$	Dry

The following can be identified based on the resulting characterization matrix (Figure 4):

1. Multi-annual droughts occurred during the periods 1967-1971, 1945-1952 and 1936-1939 in all the basins (that contained data). The drought identified in 1967-1971 coincided with one in Chile in the late 1960s (1968-1972), which had a large impact on farming activities in central Chile, particularly affecting its north-central region (Fernández-Larrañaga, 1997).
2. A notable break between dry and rainy periods occurred in 1975. This break (in 1975/1976) in the trends in the annual supply and loss of water volumes coincides with a change in the mean temperature of the central equatorial Pacific in 1976/1977 and changes in the climate that affect over 40 bioenvironmental variables in the Pacific and the Americas, reflecting an ENSO (El Niño Southern Oscillation) type of variability (Compagnucci &Agosta, 2008; Díaz, 2013).
3. Regions with similar behavior the majority of the time. These regions coincide with those presented in the study of hydrological families (Dölling,Lopez, Calizalla, & Marquez, 2013). They include the Colorado, Mendoza, San Juan and Atuel rivers, with common years between 1956-1976 during which inter-annual and multi-annual droughts occurred (1956-1957, 1960, 1962, 1964,1967-1970, 1976), 1990-2014 (1990, 1996,1998-1999, 2004, 2010-2013). Droughts in the region of Ctalamochita, Xanaes, Anisacate and Suquía

Figure 4. Matrix of the characterization of streamflow droughts in the Republic of Argentina.

occurred between 1937-1938, 1948- 1951 and 1973-1975. The Xanaes and Suquia river basins (those containing data for those dates) experienced simultaneous droughts during the years 1988-1989 and 1994. Over the past decade, the flows have been characterized as normal-to-dry. In Juramento, Bermejo, Pilcomayo and Dulce droughts occurred between 1962 and 1973 (1962, 1967, 1970-1973), 1989-1996 (1989, 1990, 1994, 1996). And Paraná and Salado had common years with multi-annual droughts between 1954 and 1971 (1954-1955, 1961-1963, 1967-1971). All the regions experienced a severe drought in 2008.

Conclusions

The results obtained from the identification and characterization of streamflow droughts indicate that multi-annual and simultaneous streamflow droughts occurred in all the basins in the study area (14 basis in central, northern and the Cuyo region of Argentina). These were registered during the periods 1967-1971, 1945-1952 and 1936- 1939 and is highly relevant to planning for energy deficit scenarios and preventing them, given that 6-year droughts compromise four large hydro-energy systems in Argentina (in the Paraná, Juramento, Ctalamochita and Colorado river basins). The drought identified in 1967-1971 coincided with one in Chile in the late 1960s (1968-1972), which had significant consequences for agricultural activities in central Chile, primarily affecting the north-central region (Fernández-Larrañaga, 1997). In this regard, the size of the territory that can undergo a streamflow drought such as those detected is notable. Rainy periods in the mid 1970s were also simultaneously observed in all the study basins. And a break between a dry and rainy period was seen (1977-1987), which coincided with three other events: a rainy decade detected in Chile (1977-1987) by Fernández-Larrañaga (1997), a change in mean temperature in the central equatorial Pacific from 1976 – 1977 and changes in the climate that affected over 40 bio-environmen-

tal variables in the Pacific and America, which are expressions of an ENSO (El Niño Southern Oscillation) type of variability (Compagnucci & Agosta, 2008).

At the spatial level, groupings among the basins was observed in which simultaneous droughts occurred the majority of time analyzed. Specifically:

1) The Colorado, Mendoza, San Juan and Atuel rivers; 2) Ctalamochita, Xanaes, Anisacate and Suquía rivers; 3) Juramento, Bermejo, Pilcomayo and Dulce rivers; 4) Salado and Paraná rivers. This information is relevant to the management of water resources given that human, irrigation and energy production usages, among others, can be seriously affected by the simultaneous occurrence of severe droughts in basins that supply a region and neighboring areas.

Over the past decade, water deficit events have impacted society with economic losses related to soil productivity, affects on engineering works that supply water and reductions in the capacity of hydroelectric plants to generate energy (due to lower reservoir levels). The droughts that have created these effects have not reached the magnitude of those recorded before 1970 (which were most critical in terms of their duration, magnitude and intensity).

References

Chow, V. T., Maidment, D., & Mays, L. (1994). *Hidrología aplicada*. Bogotá: McGraw Hill.

Coastal, E., Clausen, B., & Pearson, C. P. (1995). Regional Frequency Analysis of Annual Maximum Streamflow Drought. *Journal of Hydrology*, *173*, 111-130.

Compagnucci, R. H., & Agosta, E. A. (2008). La precipitación de verano en el centro-oeste de Argentina y los fenómenos interanuales El Niño/Oscilación Sur (ENOS) e Interdecádico "Tipo" Enos. *Geoacta*, *33*, 97-103.

Díaz, E. (2013). *Identificación y Caracterización de Sequías Hidrologías en el centro y norte de Argentina*. Tesis de Maestría en Recursos Hídricos. Córdoba, Argentina: FCEFyN-UNC.

Dölling, O., Lopez, G., Calizalla, G., & Marquez, L. (diciembre, 2013). Una herramienta para optimizar el uso del agua. *Hydria, 50*, 8.

Fernández-Larrañaga, B. (1997). Identificación y caracterización de sequías hidrológicas en Chile Central. *Ingeniería del Agua en España*, *4*, 37-46.

Hisdal, H., Stahl, K., Tallaksen, L., & Demuth, S. (2001). Have Streamflow Droughts in Europe become More Severe or Frequent? *International Journal of Climatology*, 21, 317-333.

Mauas, P., Buccino, A., & Flamenco, E. (octubre, 2008). Solar Forcing of the Streamflow of a Continental Scale South American River. *Physical Review Letters, PRL 101*, 168501.

Ravelo, A., Da Porta, W., & Zanvettor, R. (1999). *Evaluación de las sequías extremas en la región pampeana Argentina durante el período 1930-1990*. XI Congreso Brasileiro de Agrometeorología y II Reunión Latino-Americana de Agrometeorología, Florianopolis, SC, Brasil, del 19 al 22 de julio de 1999.

Rivera, J., & Penalba, C. (2013). Identificación de los periodos de déficit en los caudales de los ríos de los andes argentinos. Análisis de sus variabilidades temporales. *Actas del XXIV Congreso Nacional del Agua*, San Juan, Argentina.

Salas, J., Delleur, J., Yevjevich, V., & Lane, W. (1980). *Applied Modeling of Hydrologic Time Series*. Littleton, USA: Water Resources Publications.

Tsakiris, G., Loukas, D., Pangalou, H., Vangelis, H., Tigkas, D., Rossi, G., & Cancelliere, A. (2007). Drought Characterization. *Options Méditerranéennes, Series B*, 58, 85-102.

Yevjevich, V. (1967) An Objective Approach to Definition and Investigation of Continental Droughts. *Hydrology Paper 23*. Fort Collins, USA: Colorado State University.

Yevjevich, V. (1972). *Stochastic Processes in Hydrology*. Littleton, USA: WRP.

Institutional Address of the Authors

M.C. Erica Betiana Díaz

Universidad Nacional de Córdoba
Laboratorio de Hidráulica de la Facultad de Ciencias Exactas, Físicas y Naturales
Consejo Nacional de Investigaciones Científicas y Técnicas (CONICET)
Av. Filloy s/n, Ciudad Universitaria
Córdoba, República Argentina
Teléfono y fax: +54 (0351) 4334 446
erica.b.diaz@gmail.com

Dr. Andrés Rodríguez

Universidad Nacional de Córdoba
Laboratorio de Hidráulica de la Facultad de Ciencias Exactas, Físicas y Naturales
Consejo Nacional de Investigaciones Científicas y Técnicas (CONICET)
Av. Filloy s/n, Ciudad Universitaria
Córdoba, República Argentina
Teléfono y fax: +54 (0351) 4334 446
arodrig@efn.uncor.edu

Dr. Oscar Raúl Dölling

Universidad Nacional de San Juan
Subsecretaría de Recursos Hídricos-MINPLAN-Nación
Olegario V. Andrade 50 Sur
5400 San Juan Capital, República Argentina
Teléfono y fax: +54 (264) 15671 6378
odolling@gmail.com

Dr. Juan Carlos Bertoni

Universidad Nacional de Córdoba
Facultad de Ciencias Exactas, Físicas y Naturales
Av. Filloy s/n, Ciudad Universitaria
Córdoba, República Argentina
Teléfono y fax: +54 (0351) 4334 446
jcbertoni@gmail.com

Dr. Marcelo Smrekar

Universidad Nacional de Córdoba
Facultad de Ciencias Exactas, Físicas y Naturales
Laboratorio de Ingeniería y Mantenimiento Industrial
Av. Filloy s/n, Ciudad Universitaria
Córdoba, República Argentina
Teléfono y fax: +54 (0351) 4334 446
marcelosmrekar@gmail.com

Click here to write the autor

Cattle grazing in wetlands of Pátzcuaro, Michoacán, Mexico, without control of the same.

Photo: Lenin Medina Orozco.

Discussion

Technical notes and technical articles are open to discussion according to the following guidelines:

- The discussion will be written in the third person.
- The writer of the discussion shall use the term "commentator" when referring to oneself and the term "author" when referring to the one responsible for the technical note or article.
- The discussion shall be sent within 12 months of the last day of the quarter in which the a technical article or note was published.
- The length of the discussion may be extended by written request from the commentator.
- The discussion is to be presented according to the Guide for Collaborators published in this journal (omitting data referring to the length and abstract). In addition, the bibliographical citation of the technical notes or articles to which the discussion refers shall be included.
- The maximum length of the discussion is 4 journal pages (approximately 10 cuartillas, including figures and tables).
- The figures and tables presented by the commentator shall be progressively marked with Roman numbers and when citing those generated by the author the original numeration should be respected.
- The editors will suppress data that does not pertain to the subject of the discussion.
- The discussion will be rejected if it contains topics addressed by other sources, promotes personal interests, is carelessly prepared, raises controversy involving already established facts, is purely speculative or falls outside the purpose of the journal.
- The discussion will be published along with commentaries from the author or authors to which it refers.
- The discussion will be directed by the editor in chief.

It is observed a typical fluvial island pertaining to the system of the middle Paraná river in the province of Entre Ríos, Argentina. The predominant ecosystem is the forests in gallery, denominated thus by the presence of a great abundance of climbing plants that are developed on the trees of the forest. The natural ecosystem of the Paraná River is a great source of natural resources for man.

Photo: Hernán R. Hadad.

Guide for Collaborators

The journal ***Water Technology and Sciences*** invites specialists to collaborate with original, unpublished technical articles or notes **related to water, resulting from investigations and provide original contributions**, based on the disciplines of hydrology, hydraulics, water management, water and energy, water quality, and physical, biological and chemical sciences as well as political and social sciences, among other disciplines, according to the guidelines stated below.

PREPARATION OF THE ARTICLE

FORMAT

Font: Palatino throughout the entire document (body of text, tables and figures).

Font Size: Use 8, 9, 10 and 20 points, according to the following table:

8 points (Palatino)	9 points (Palatino)
• Tables. • Figures. • Acknowledgements.	• Name of authors. • Institution of authors. • Abstract. • *Abstract* and *keywords*. • Institutional address of the authors.
10 points (Palatino)	**20 points capital letters (Palatino)**
• Body of the text. • Title of the work in Spanish.	• Title of the work in English.

Line Spacing: double-spaced.

Page Numbers: all pages shall be numbered.

Length

Technical article: **30 pages** (numbered), including figures and tables.

Technical note: **10 pages** (numbered), including figures and tables.

CONTENS

Title

The article shall present significant contributions to scientific and technological knowledge pertaining to the specialty. It shall be based on finished works or those that have completed a development cycle. It shall show results from a series of experiences over 1 year or more of investigations and be supported by an adequate bibliographical review. **The basic structure of the text shall contain an introduction, the development and the conclusions**. The classic layout is preferable: abstract, introduction, methodology, results, discussion, conclusion and references.

Title

The title, **written in Spanish and English**, shall be informative and not exceed 12 words.

Abstract

The abstract, **written in Spanish and English**, shall be concise and provide a broad overview of the investigation (objective, method, results and conclusions) without exceeding 250 words.

Key Words

Eight words or key phrases (maximum) shall be provided **in Spanish and English** that facilitate the identification of the information.

Footnotes

Not admitted. The information is to be incorporated into the text.

Acknowledgements

To be included after the text and before the references.

Tables

- One page for each table.
- A list of all the tables cited shall be presented after the references.

Figures

- One page for each figure.
- All the names of the figures shall be included after the tables.
- They should be high-resolution (300 dpi).

Note: When the article is approved by the publication, the author shall send each figure in JPG format with high-resolution (300 dpi).

References

- The entire bibliography must be referenced in the main body of the text.
- In the case of addressing scientific and technological topics that are common domain, works that denote the knowledge of the authors about the state-of-art shall be cited.
- Avoid self-citations to the extent possible
- APA format shall be used as a basis.

Some examples of references in APA format are:

Complete Books

Last name, A. A. (Year). Title of work. city published: Publisher.
Last name, A. A. (Year). Title of work. Consulted at http://www.xxxxx
Last name, A. A. (Year). Title of work. doi:xxxxx
Last name, A. A. (Ed.). (year).City published: Publisher.

Book Chapters

Last Name, A. A., & Last Name, B. B. (Year).. Title of chapter or entry. In A. Last Name, B. Last Name & C. Last Name (Eds.), Title of book (pp. xxx-xxx). Place: Publisher.
Last Name, A. A., & Last Name, B. B. (Year).. Title of chapter or entry. In A. Last Name, B. Last Name & C. Last Name (Eds.), Title of book (pp. xxx-xxx). Consulted at http://www.xxxxxxx

Newspaper Article or Note Consulted Online

Last Name, A. A., & Last Name, B. B. (Year). Title of article. Title of publication, issue (number), pp. Consulted at http://www.xxxxxxx

That is: Last Name, A. A., & Last Name, B. B. (Year). Title of article. Title of publication, 1(2), 5-17, pp. Consulted at http://www.xxxxxxx

Printed Newspaper Article or Note

Last Name, A. A., & Last Name, B. B. (Year). Article Title. Title of publication, 8(1), 73-82.

Newspaper Article Publication with DOI

Last Name, A. A., & Last Name, B. B. (Year). Article Title. Title of publication, 8(1), 73-82, doi:xxxxxx

Conferences or Symposiums

Collaborator, A. A., Collaborator, B. B., Collaborator, C. C., & Collaborator, D. D. (Month, year). Title of collaboration. In E. E. President (Presidency), Title of symposium. Symposium held at the conference by Name of Organization, Place.

Citations within the body of the text

Type of citation	First appearance in text	Subsequent appearances	Format in parenthesis, first citation in text	Format in parenthesis, subsequent citing in text
Work by one author	Last name (Year)	Last name (Year)	(Last name, year)	(Last name, year)
Work by two authors	Last name and Last name (Year)	Last name and Last name (Year)	(Last name & Last name, Year)	(Last name & Last name, Year)
Work by three authors	Last name, Last name and Last name (Year)	Last name *et al*. (Year)	(Last name, Last name, & Last name, year)	(Last name of first author *et al*., year)
Work by four authors	Last name, Last name, Last name and Last name (Year)	Last name *et al*. (Year)	(Last name, Last name, Last name, & Last name, year)	(Last name of first author *et al*., year)
Work by five authors	Last name, Last name, Last name, Last name and Last name (Year)	Last name *et al*. (Year)	(Last name, Last name, Last name, Last name, & Last name, year)	(Last name of first author *et al*., 2008)
Work by six or more authors	Last name of first author *et al*. (Year)	Last name of first author *et al*. (Year)	(Last name of first author *et al*., Year)	(Last name of first author *et al*., year)
Groups (easily identified with abbreviations) such as authors	Complete name of institution (Acronym, year)	Acronym (Year)	(Complete name of institution [acronym], year)	(Institution, year)
Groups (without abbreviations) such as authors	Complete name of institution (year)	Complete name of institution (year)	(Complete name of institution, year)	

Language

Spanish or English

Separation of numbers and use of decimal points

In *Tecnología and Ciencias del Agua*, the separation between thousands is denoted with a blank space. A decimal point is used to separate whole numbers from fractions. In this regard, refer to Diccionario panhispánico de dudas, edited by the Real Academia Espyearla and the Asociación de Academias de la Lengua Espyearla, in 2005, with respect to numeric expressions: "**the Anglo-Saxon use of the period is accepted, normal in some Hispano-American countries…: π = 3.1416.".**

Delivery of Article

Send the article in *Word* with the name of the authors and institutional address to **revista.tyca@gmail.com**, with copy to Elizabeth Peña Montiel, elipena@tlaloc.imta.mx.

General Information

The review process will begin once the material is received, during which time the manuscript could be rejected. If the text is suitable for review, having fulfilled the Editorial Policy and the Editorial Committee having determined so, it will proceed to the review stage.

Depending on the review process, the text may be accepted without changes, with minor changes, with extensive changes or rejected.

Once a work is published, the main author has the right to two journals and ten offprints free of charge.

In there are any questions, please write to Helena Rivas López, hrivas@tlaloc.imta.mx or Elizabeth Peña Montiel, elipena@tlaloc.imta.mx

Editorial Policy

Mission

Disseminate scientific and technical knowledge and advances related to water through the publication of previously unpublished articles and technical notes that provide original contributions.

Our Principles

- Impartiality
- Objectivity
- Honesty

Our Values

- Knowledge
- Experience
- Thematic expertise

Contents

Interdisciplinary, composed of previously unpublished articles and technical notes related to water, that result from research and provide original scientific and technological contributions or innovations, developed based on the fields of knowledge of diverse disciplines.

Topics Covered

Interdisciplinary, related to water, with priority topics in the following knowledge areas:

- Water and energy
- Water quality
- Physical, biological and chemical sciences
- Hydro-agricultural sciences
- Political and social sciences
- Scientific and technological development and innovation
- Water management
- Hydrology
- Hydraulics

Type of Contributions

Technical article: scientific document that addresses and communicates, for the first time, results from a successful investigation or innovation, whose contributions provide and increase current knowledge about the topic of water.

Technical note: text that addresses advances in the field of hydraulic engineering and professional practices in the field of water, while not necessarily making an original contribution in every case it must be a previously unpublished work.

Some of the articles submitted to the review process can result in being published as notes and vice versa. This will occur through a proposal and process of mutual agreement between the authors and the editor responsible for the topic. The article and the note have nearly the same structure (abstract, introduction, methodology, results, discussion, conclusion, references).

Review Process

The journal is governed by a rigorous review process which establishes that each article be analyzed separately by three reviewers who recommend its acceptance, acceptance with minor changes, acceptance with extensive changes, rejection or acceptance as a technical note with the required changes.

At least one of three reviewers will be sought from a foreign institution.

The reviewers may not belong to the same institution as the authors proposing the article for publication.

When the decisions are opposing or inconsistent, the involvement of other reviewers or the members of the Editorial Committee may be requested.

On occasion, the approval of an article will be decided by two reviewers in addition to the opinion of the editor of the corresponding topic or, the editor in chief.

A rejected article will not be accepted for a new review process.

The review process will be performed in such a way that neither the authors nor the reviewers know the names of the other party.

The review process is performed by high-level specialists and experts who are national and internationally renowned in their professional fields and have the ability to reliably evaluate, in a timely manner, the quality as well as the originality of contributions, in addition to the degree of scientific and technological innovation in the topic under which it is submitted for possible publication.

This participation is considered a professional contribution and will be performed as a courtesy.

The reviews have a "Guide for the Reviewer" provided by the journal's Editorial Department.

Final Ruling

The ruling resulting from the review process is not subject to appeal.

Authors

Works are published from authors of any nationality who present their contributions in Spanish; nevertheless, we all accept works in Spanish or English.

Responsibility of the Authors

Submitting a proposal for the publication of an article commits the author not to simultaneously submit it for consideration by other publications. In the event an article has been submitted to another media for eventual publication, the author agrees to do so with the knowledge of the Editorial Department, which will suspend the review process and inform the Editorial Committee of the decision by the authors.

Collaborators whose articles have been accepted will formally cede the copyright to ***Tecnología y Ciencias del Agua***.

The authors are responsible for the contents of the articles.

The author is responsible for the quality of the Spanish used. If the writing is deficient the work will be rejected. ***Water Technology and Sciences*** will only be responsible for the editorial management.

The author commits to making the changes indicated by the editor of the topic in the time frame establish by the editor. In the event these indications are not met, the article will be removed from the review process and be classified as rejected.

The author shall be attentive to resolving the questions and proposals presented by the editors and the editorial coordinator.

Each author shall approve the final printed proofs of their texts.

It is suggested that authors consult the "Guide for Collaborators."

Readers

Academics, investigators, specialists and professionals interested in the analysis, investigation and search for knowledge and solutions to problems related to water.

Reception of Articles

The reception of articles and notes is ongoing.

Time period

Bimonthly, appearing in the second month of the period.

Subscription and Distribution

The journal is distributed through paid and courtesy subscriptions.

Open Access

Water Technology and Sciences, previously ***Hydraulic Engineering in Mexico***, provides a digital version of all the material published since 1985.

Special editions and issues

Water Technology and Sciences will publish special numbers independently or in collaboration with other journals, professional associations or editorial houses with renowned prestige and related to water resources.

In addition, it will publish articles by invitation, acknowledging the professional advances of prominent investigators.

In both cases, the quality of the technical continents and scientific contributions will be reviewed.

Water Technology and Sciences is registered in the following national and international indices and abstracts:

• Thomson Reuters Science Citation Index® (ISI) • Expanded Thomson Reuters Research Alert® (ISI) • Índice de revistas mexicanas de investigación científica y tecnológica del Consejo Nacional de Ciencia y Tecnología (Conacyt) (2013-2018) • Sistema de Información Científica Redalyc (Red de Revistas Científicas de América Latina y El Caribe, España y Portugal), Universidad Autónoma del Estado de México • EBSCO (Fuente Académica Premier NISC; Geosystems, como Marine, Oceanographic and Freshwater Resources) • ProQuest (Cambridge Scientific Abstracts) • Elsevier (Fluid Abstracts: Process Engineering; Fluid Abstracts: Civil Engineering) • CAB Abstracts, CAB International • Latindex (Sistema Regional de Información en Línea para Revistas Científicas de América Latina, el Caribe, España y Portugal), Universidad Nacional Autónoma de México • Periódica (Índice de Revistas Latinoamericanas en Ciencias), Universidad Nacional Autónoma de México • Catálogo Hela (Hemeroteca Latinoamericana), Universidad Nacional Autónoma de México • Actualidad Iberoamericana, CIT-III, Instituto Iberoamericano de Información en Ciencia y Tecnología.

Other Sources

The journal can also be found archived in Google scholar.

Contents

Technical articles

Technical notes

Contenido

Artículos técnicos

Notas técnicas

IMTA
Instituto Mexicano de Tecnología del Agua

http://www.imta.gob.mx/tyca